

THE RAMAN SPECTROSCOPY OF SOME HALOGEN-BRIDGED,
LINEAR-CHAIN INORGANIC COMPLEXES

David James Michael

A thesis submitted to the University of London in partial
fulfilment of the requirements for the Degree of Doctor
of Philosophy in the Faculty of Science.

Christopher Ingold Laboratories
University College London

September, 1991

ProQuest Number: 10609553

All rights reserved

INFORMATION TO ALL USERS

The quality of this reproduction is dependent upon the quality of the copy submitted.

In the unlikely event that the author did not send a complete manuscript and there are missing pages, these will be noted. Also, if material had to be removed, a note will indicate the deletion.



ProQuest 10609553

Published by ProQuest LLC (2017). Copyright of the Dissertation is held by the Author.

All rights reserved.

This work is protected against unauthorized copying under Title 17, United States Code
Microform Edition © ProQuest LLC.

ProQuest LLC.
789 East Eisenhower Parkway
P.O. Box 1346
Ann Arbor, MI 48106 – 1346

Acknowledgements

I would like to thank my supervisor, Professor R. J. H. Clark for his help with this work. I would also like to thank Dr. S. P. Best and Mr. D. Oprescu for assistance with computer programming, Drs. M. Yamashita, K. Toriumi, F. P. Fanizzi and H. Toftlund for supplying complexes, Miss S. A. Ciniawsky for running infrared spectra, and numerous other colleagues and technical staff for expert help and guidance and useful discussions. I am grateful to the Science and Engineering Research Council and British Petroleum for funding and to Johnson Matthey Chemicals Ltd. for the loan of chemicals.

Abstract

Optical studies have been made of a number of halogen-bridged, mixed-valence complexes of platinum, palladium and nickel. These complexes all have a linear chain structure containing the repeat unit $\text{---X}\cdots\text{M}^{\text{II}}\text{L}\cdots\text{X}\text{---M}^{\text{IV}}\text{L}$, where M = Pt, Pd or Ni, L = equatorial ligand, usually amine and or halide and X = halogen.

Electronic spectra of the complexes show a strong, broad, and polarised band in the visible region, which is assigned to an $\text{M}^{\text{II}} - \text{M}^{\text{IV}}$ intervalence charge transfer (IVCT) transition. Raman spectra, when obtained using excitation wavelengths within the IVCT band, demonstrate long and intense progressions $\nu_1\nu_1$ in the band assigned to the symmetric $(\text{X-M}^{\text{IV}}\text{-X})$ stretch vibration. Weaker progressions $\nu_a + \nu_1\nu_1$ are also sometimes observed, where ν_a is a second vibrational mode, e.g. $\nu(\text{M}^{\text{IV}}\text{-L})$ or $\delta(\text{N-M}^{\text{IV}}\text{-N})$. This resonance enhancement occurs as a result of electron-phonon interaction between the IVCT transition and motion along the ν_1 normal coordinate, i.e. a Frank-Condon mechanism operates in the scattering.

The effects of changing the metal, the bridging halogen, the equatorial ligand and the counterion on the optical properties and, by inference, on the structure of the complexes have been investigated. The wavenumber of the IVCT transition and that of ν_1 are shown to increase on going from bidentate to quadridentate equatorial ligands, as a result of increased hydrogen bonding.

Studies of a variety of $\text{Ni}^{\text{II}}/\text{Ni}^{\text{IV}}$ complexes have revealed two distinct types, which differ markedly in their optical characteristics. In addition, the only known example of the more symmetric $\text{M}^{\text{III}}/\text{M}^{\text{III}}$ linear chain structure, $\{[\text{Ni}(\text{R},\text{R-chxn})_2\text{Br}]\text{Br}_2\}_\infty$, where R,R-chxn = 1R,2R-cyclohexanediamine, has been investigated and shown to have Raman characteristics utterly different to those of the II/IV variety of complex.

In a study of $[\text{Pt}(4\text{Me-dien})\text{I}][\text{Pt}(4\text{Me-dien})\text{I}_3]\text{I}_2$ and related complexes it is shown that a terdentate ligand may be stabilised in a high energy conformation, when incorporated in the linear chain structure.

Unusual features in the resonance Raman spectroscopy of $[\text{Pd}(\text{R,R-chxn})_2][\text{Pd}(\text{R,R-chxn})_2\text{Br}_2]\text{Br}_4$ are reported.

Investigations are reported of a mixed-metal complex, $[\text{Cu}_x\text{Pt}_{1-x}(\text{en})_2][\text{Pt}(\text{en})_2\text{Cl}_2](\text{ClO}_4)_4$, analogous to those described above. Change in x dramatically alters the optical spectra.

Finally, a discussion is given of the long observed dispersion in ν_1 with excitation wavelength. A further interpretation is offered of this phenomenon.

Contents

Abbreviations	4
I. <u>INTRODUCTION</u>	5
I.1. The Raman Effect	
I.2. The Resonance Raman Effect	
I.3. Mixed-valence Complexes	
I.4. Halogen-bridged, Mixed-valence Complexes of Platinum, Palladium and Nickel	
I.5. Discrete d-orbitals on the Metal Ions	
I.6. Resonance Raman Scattering versus Luminescence in Halogen-bridged, Mixed-valence Complexes	
I.7. Methods of Preparation of Halogen-bridged, Mixed-valence Complexes	
I.8. Copper (II)-Platinum (IV) Complexes	
I.9. Halogen-bridged, Non-mixed-valence, Linear- chain Complexes of Nickel	
I.10. Models of Halogen-bridged, Mixed-valence Complexes	
I.11. Excitons, Solitons, Polarons and Bipolarons in Halogen-bridged, Mixed-valence Complexes	
I.12. Aims of this Work	
II. <u>THE RAMAN EXPERIMENT</u>	37
II.1. Excitation Radiation	
II.2. Beam Steering	
II.3. Sample	
II.4. Scattered Light Collection	
II.5. Monochromator and Detector - Resolution and Sensitivity	
II.6. Output	
II.7. Spectral Response Measurement	
II.8. Fourier Transform Raman Spectroscopy	
II.9. Raman Microscopy	
II.10. Instrumentation used in this Work	
II.11. Measurements	

III.	<u>HALOGEN-BRIDGED, MIXED-VALENCE COMPLEXES WITH QUADRIDENTATE LIGANDS</u>	46
III.1.	Complexes of Platinum with Chain Quadridentate Ligands	
III.1.1.	Introduction	
III.1.2.	Results and Discussion	
III.2.	Complexes of Palladium with Chain Quadridentate Ligands	
III.2.1.	Introduction	
III.2.2.	Results and Discussion	
III.3.	Complexes of Palladium with Macrocyclic Quadridentate Ligands	
III.3.1.	Introduction	
III.3.2.	Results and Discussion	
IV.	<u>HALOGEN-BRIDGED, MIXED-VALENCE AND SINGLE VALENCE COMPLEXES OF NICKEL WITH QUADRIDENTATE AND BIDENTATE LIGANDS</u>	86
IV.1.	Introduction	
IV.2.	Mixed-valence Systems	
IV.2.1.	Ni ^{II} /Ni ^{IV} Chains with Quadridentate Ligands and Large Complex Counteranions	
IV.2.2.	Ni ^{II} /Ni ^{IV} Chains with Bidentate Ligands and Chloride Counteranion	
IV.3.	A Ni ^{III} /Ni ^{III} System	
IV.4.	Discussion	
V.	<u>A STUDY OF A HALOGEN-BRIDGED, MIXED-METAL, MIXED-VALENCE COMPLEX OF PLATINUM AND COPPER</u>	102
V.1.	Introduction	
V.2.	Synthesis	
V.3.	Results and Discussion	
VI.	<u>FURTHER STUDIES OF PLATINUM AND PALLADIUM COMPLEXES</u>	120

VI.1.	A Raman Study of the Terdentate Ligand 3-methyl-3-azapentane-1,5-diamine, in its Coordination to Pt ^{II} and Pt ^{IV} and in a Mixed-valence Chain	
VI.1.1.	Introduction	
VI.1.2.	Results and Discussion	
VI.2.	A Resonance Raman Study of [Pd(-chxn) ₂][Pd(-chxn) ₂ Br ₂]Br ₄	
VI.2.1.	Introduction	
VI.2.2.	Results and Discussion	
VII.	<u>EXCITATION LINE DEPENDENCE OF THE SYMMETRIC (X-M-X) STRETCH MODE IN THE RAMAN SPECTRA OF HALOGEN-BRIDGED MIXED-VALENCE COMPLEXES</u>	136
VII.1.	Introduction	
VII.2.	Further Discussion of the Chain Length Effect	
Appendix I.	<u>Raman and Resonance Raman Scattering Intensity and Selection</u>	142
Appendix II.	<u>Electronic Spectroscopy</u>	156
Appendix III.	<u>Syntheses of Complexes</u>	156
References		158

Abbreviations

A	Angstrom	i.r.	infra-red
ax	axial	IVCT	intervalence charge transfer
c	speed of light		
ca.	circa	K	Kelvin
chxn	1,2-cyclohexanediamine	kbar	kilobar
cm	centimetre	m	metre
cm ⁻¹	wavenumber	mW	milliwatt
dien	diethylenetriamine	nm	nanometre
E _g	band gap energy	p.m.t.	photomultiplier tube
e.p.	excitation profile		
eq	equatorial	RR	resonance Raman
eV	electronvolt	s	second
FT	Fourier Transform	uv	ultra-violet
h	Planck's constant	vis	visible

[14]aneN ₄	1,4,8,11-tetraazacyclotetradecane
[15]aneN ₄	1,4,8,12-tetraazacyclopentadecane
2,3,2-tet	3,7-diazanonane-1,9-diamine
3,2,3-tet	4,7-diazadecane-1,10-diamine
4Me-dien	3-Methyl-3-azapentane-1,5-diamine

A variable abbreviation commonly used, in this thesis and elsewhere, for halogen-bridged, mixed-valence, linear-chain complexes of the type described herein is [M-L-X-Y], where M is the metal, L is the equatorial ligand, X is the bridging halogen and Y is the counteranion (where applicable).

I. INTRODUCTION

I.1. The Raman Effect

The Raman effect is the scattering of electromagnetic radiation by matter with a change of frequency. When a beam of monochromatic radiation of frequency ν_0 and irradiance I_0 is incident upon a sample which does not absorb it significantly, a small proportion (about $10^{-5} I_0$) of the radiation is scattered in all directions at the same frequency. A smaller proportion (about $10^{-8} I_0$) is scattered at other frequencies $\nu_0 \pm \nu_i$, where ν_i are frequencies of transitions within the sample molecules; the transitions ν_i may be any combination of rotational, vibrational and electronic transitions allowed by the appropriate selection rules. A single Raman scattering event involves the destruction of a photon of the incident light, on interaction with the initial state of the scattering molecule, the latter being stimulated to a virtual intermediate state, followed by the creation of the scattered photon, leaving the molecule in its final state of energy. The observation of the scattering at the frequencies $\nu_0 \pm \nu_i$, first carried out by C. V. Raman in 1928, constitutes Raman spectroscopy.^{1,2} Use of this analytical tool yields substantial information about the structure and properties of molecules in the ground state.

Although the intensity of an observed Raman band is proportional to $(\nu_0 \pm \nu_i)^4$, the Stokes lines ($\nu_0 - \nu_i$) are stronger than the anti-Stokes lines ($\nu_0 + \nu_i$), because the molecular energies are distributed according to the Maxwell-Boltzmann equation (Appendix I).

The activity of a vibrational mode in Raman spectrum depends primarily on the polarizability of the bonds involved, which is required to change during the motion of the mode (Appendix I). Since a small fraction of scattered light is observed, a high intensity of incident radiation is desirable, a laser being outstandingly suitable.

As ν_0 may be chosen accordingly, Raman spectroscopy may be carried out on any sample without hindrance. Thus, for example, unlike infra-red absorption, the Raman method is straightforwardly applicable to aqueous solutions.

I.2. The Resonance Raman Effect

If the energy of excitation radiation ν_0 is allowed to approach that of an electronic transition in the sample, it is sometimes observed that the band attributed to a fundamental vibration of the appropriate symmetry is strongly enhanced, perhaps by several orders of magnitude, relative to other bands, and many overtones may appear.³ In addition, combination bands involving the same mode may be enhanced. Corresponding changes in the nature of the scattering process are illustrated in Figure 1, which shows types of Raman scattering. The most common type of resonance enhancement in the Raman spectrum occurs by the Franck-Condon mechanism (Appendix I) and generally applies only to totally symmetric normal modes, these usually being the modes which most effectively convert the molecule from its ground state to its excited state geometry.⁴

Where resonance enhancement of a band occurs, it is possible to determine an excitation profile showing the intensity of the band as a function of excitation wavenumber. This will indicate the extent to which the enhancement matches the electronic excitation being probed, and may, in favourable cases, show vibronic structure of the excited electronic state.⁴ Indeed, if the normal Raman spectrum and the absorption or fluorescence spectrum are already known, the excitation profile may be calculated from theory (Appendix I).

Where a significant number of overtones is observed, it is possible to determine by measurement the harmonic wavenumber and the anharmonicity of the (ground state) vibration involved (Appendix I). Where there is a

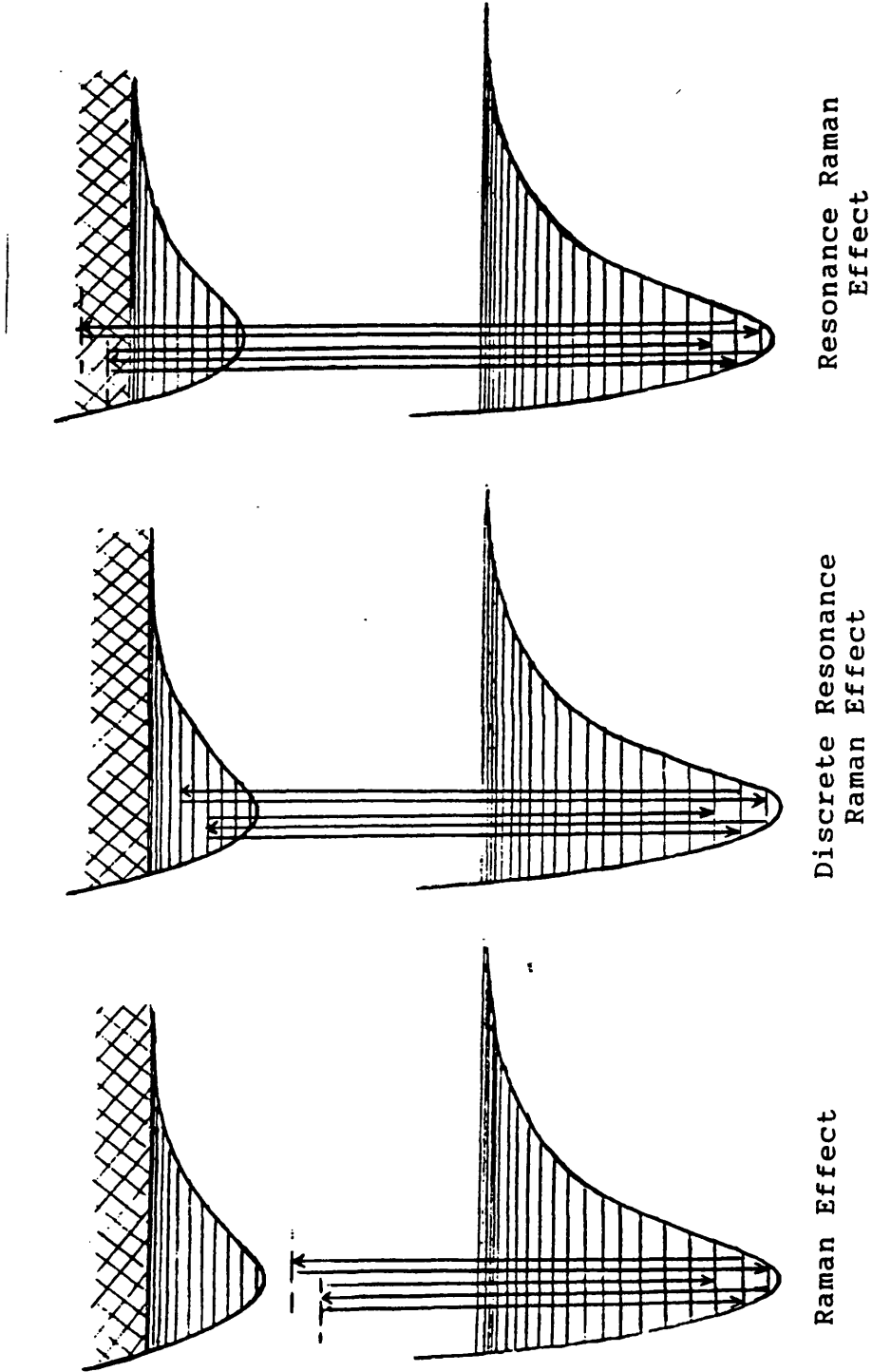


Figure 1. Types of Raman scattering.

combination of modes in the progression, further anharmonicity constants may be determined (Appendix I).

I.3. Mixed-valence Compounds

A mixed-valence compound may be defined as one containing an element in more than one oxidation state. About forty elements are known to form compounds of this type, perhaps the earliest to be known being Prussian Blue, $\text{Fe}^{\text{III}}_4[\text{Fe}^{\text{II}}(\text{CN})_6]_3 \cdot 14\text{H}_2\text{O}$. This latter is a Type II mixed-valence complex in the Robin-Day classification of such materials (1967)⁵, which is made according to the ease with which the sites (say, A and B) of different oxidation states may be interchanged in the structure. This depends on the strength of electronic interaction (Section I.10.1). Type I ("trapped valence") compounds contain sites A and B of different symmetry and ligand field strength, which can interchange only with great difficulty. They are generally insulators, with a very high intervalence transition energy, the valence electron delocalisation being minimal. Type II complexes contain sites A and B, which are similar but distinguishable. Generally they have strong visible intervalence transitions and are semiconductors, because of partial valence electron delocalisation. In Type III materials, A and B are identical sites, between which electron transfer can occur with no energy barrier to be overcome, i.e. valence electrons are completely delocalised, the corresponding molecular orbitals being delocalised into bands. Two subtypes are identifiable. Type IIIA lattices are non-continuous, in which electron delocalisation over A and B occurs within finite clusters. These structures are non-conducting and have intervalence transitions in the visible region. Type IIIB lattices are continuous and conducting. They are commonly opaque, having an infra-red absorption edge and metallic reflectivity.

In general the class of a mixed-valence complex may be

determined from its optical, magnetic and conductive properties as well as from its structure. Thus class I complexes have only the properties of the constituent species of different valence, while, at the other extreme, in class IIIB complexes much of the character of the discrete species is lost, while the valence delocalisation promotes the metallic nature.

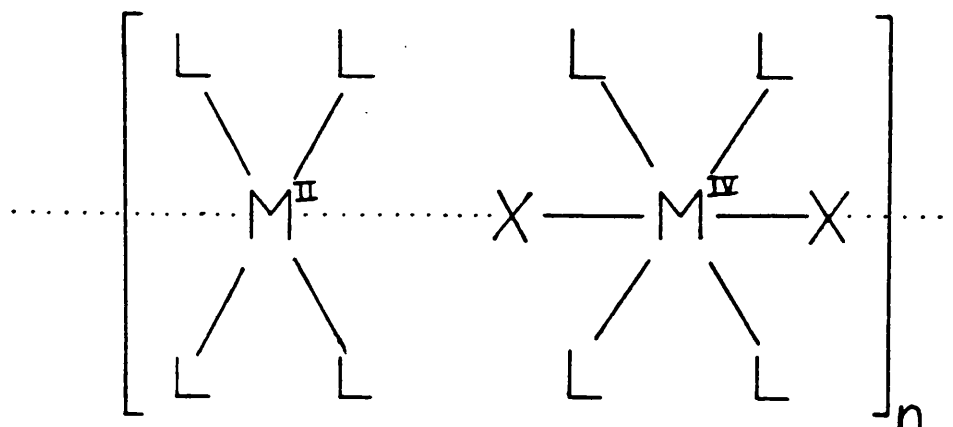
Many low-dimensional materials, in particular one-dimensional inorganic complexes, exhibit mixed-valence character.⁶ Of these, a large majority contain second or third row transition metals, which have large, diffuse outer electron orbitals commonly involving d_{z^2} electrons, which are suitable for the formation of a chain structure. In particular, palladium, platinum, iridium and gold easily form square planar complexes which stack in columns. They vary considerably in mixed-valence type and properties. Thus the tetracyanoplatinate $K_2Pt(CN)_4Br_{0.30} \cdot 3H_2O$ (KCP) is a Type IIIB complex, being metallic in the chain direction, while Wolfram's Red Salt, $[Pt(etn)_4][Pt(etn)_4Cl_2]Cl_4 \cdot 4H_2O$, where $etn =$ ethylamine, is a semiconducting Type II complex. The latter is one of a large group of one-dimensional complexes with similar structures, which are described in the next section.

I.4. Halogen-bridged, Mixed-valence Complexes of Platinum, Palladium and Nickel

Halogen-bridged mixed-valence metal complexes containing platinum, palladium and nickel⁷ have been synthesised and examined since the start of the twentieth century, the best known of them being Wolfram's Red Salt.⁸

Most of the complexes studied, particularly until the last decade, have been platinum complexes, but substantial work has now been done on palladium and nickel analogues and on the platinum/palladium/nickel mixed-metal analogues. The

linear chains which these compounds form have the structural formula shown below.



where M^{II}/M^{IV} is Pt^{II}/Pt^{IV} , Pd^{II}/Pd^{IV} ,
 Ni^{II}/Ni^{IV} , Pd^{II}/Pt^{IV} or
 Ni^{II}/Pt^{IV} (+2 and +4 being nominal
oxidation states),

X is Cl, Br, or I,

and L is equatorial ligand.

Thus all the complexes contain metal ions with alternately d^6 and d^8 electron configurations along the chain. The ligands L may be neutral or charged and uni- or multidentate, including macrocyclic.⁹⁻¹⁷ In work reported thus far the ligand arrangement has always been the same for both the M^{II} and the M^{IV} species. Depending on the ligands, the linear chain may have positive, zero or negative charge.^{8,18-21}

Examples of different charge types are given in Table 1.

Charge per Pt site	Example	Reference
+2	$[Pt(etn)_4][Pt(etn)_4Cl_2]Cl_4 \cdot 4H_2O$	8
+1	$[Pt(4Me-dien)I][Pt(4Me-dien)I_3]I_2$	18
0	$[Pt(trans-chxn)Cl_2][Pt(trans-chxn)Cl_4]$	19
-1	$Cs_2[Pt(NO_2)(NH_3)Br_2][Pt(NO_2)(NH_3)Br_4]$	20
-2	$K_4[PtI_4][PtI_6]$	21

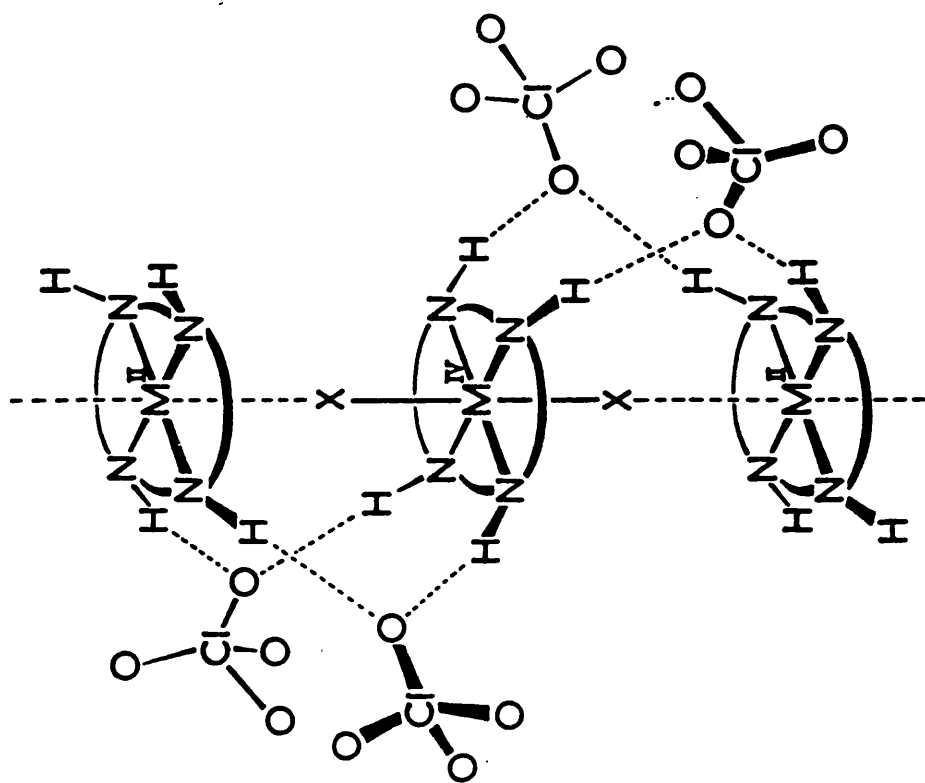
Table 1. Types of Halogen-bridged, Mixed-valence Complexes of Platinum.

Most commonly chains require counteranions with a charge of -4 per repeat unit of chain. A variety of anions has been used, including X^- , ClO_4^- , BF_4^- , HSO_4^- , SO_4^{2-} , CuX_4^- and $Cu_3Br_5^{2-}$.²²⁻²⁷ These are situated alongside the chains and generally midway between the ligands of adjacent metal centres. In the case of cationic chains hydrogen bonding is considered to play an important rôle in stabilising the linear chain structure. Hydrogen bonding exists between appropriately oriented hydrogen atoms on the equatorial ligands and the counteranions. The hydrogen bonding network differs markedly with different types of ligand, as illustrated in Figure 2 for bidentate and quadridentate ligands.²⁸⁻³⁰

Mixed-valence linear chains are examples of a quasi-one-dimensional charge density wave state, which exists as a result of Peierls-Hubbard dimerisation of the more symmetric chain structure in which the metal ions are all in oxidation state +3 and the bridging halogens are equidistant between them (see Sections I.10.3-4).

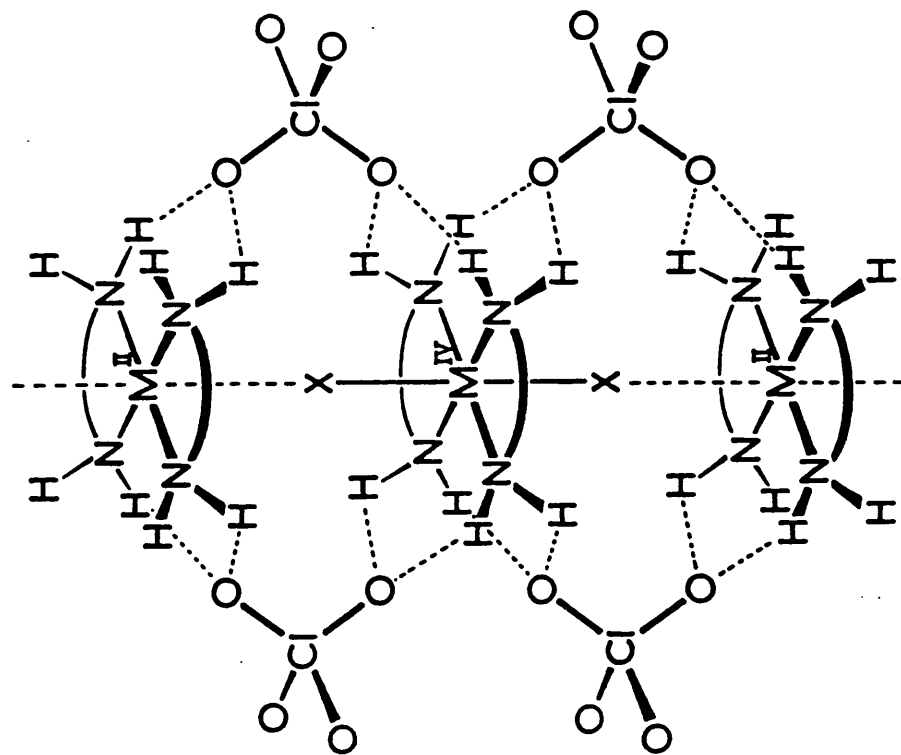
These complexes, which usually crystallise as needles with the long axis coinciding with the linear chain axis (occasionally as platelets), appear strongly coloured. On observing the polarisation of light transmitted by the crystals, they are found to be very dichroic; the strong colour arises from the absorption of light with the electric vector parallel to the needle (z) axis, while for light with the electric vector perpendicular to the needle axis, the crystal is colourless or yellow (like the constituent M^{II}/M^{IV} species).

Evidence that the structure of halogen-bridged mixed-valence complexes is as shown above has accumulated from the use of several techniques, some of which are listed below.



II. $[ML][MLX_2]Y_4$

L = macrocycle



I. $[ML_2][ML_2X_2]Y_4$

L = diamine

Figure 2. Schematic diagram of two general structures.

I.4.1. X-ray Diffractometry

Crystal structures have been determined by x-ray diffraction for a large number of halogen-bridged mixed-valence complexes, almost all of the $\text{Pt}^{\text{II}}/\text{Pt}^{\text{IV}}$ variety. Examples of x-ray structural information are given in Table 2. In all cases the non-equivalence of the two metal ion sites is indicated as well as the position of the bridging halogen atom closer to alternate metal centres. In addition many other features of the chain are clarified. Thus, in the majority of cases, the equatorial ligands L are eclipsed; while there is disorder in neighbouring chains because of 1/2-unit cell slippage, giving a crystallographically unique metal site and 50% occupancy at two bridging halogen sites. The $\text{M}^{\text{II}}\dots\text{M}^{\text{IV}}$ distance is a function of many parameters, but in general for bromide or iodide bridges it increases on going from a cationic to a neutral to an anionic chain. On changing the bridging halogen X, the bond distance $r(\text{M}^{\text{IV}}\text{-X})$ changes more than does the bond distance $r(\text{M}^{\text{II}}\text{-X})$, the trend being towards a more central position on going from Cl to Br to I. This implies decreased valence electron localisation on going from Cl to Br to I, which is in agreement with conductive and other experiments as outlined below. A correlation is observed between the bond distance ratio $r(\text{M}^{\text{IV}}\text{-X})/r(\text{M}^{\text{II}}\text{-X})$ and certain optical characteristics, such as the wavenumber of the visible intervalence electronic transition (Section I.4.4) and the symmetric stretch vibration $\nu_1(\text{X-M}^{\text{IV}}\text{-X})$ (Section I.4.6), described further below. In general, as the former increases in value, i.e. as X moves to a more central position, the latter two decrease. These changes are a function of the extent of valence delocalisation, which varies with metal, bridging halogen, equatorial ligand and counterion.

X-ray structures have indicated that the $\text{M}^{\text{II}}\dots\text{X-M}^{\text{IV}}$ angle can vary considerably from 180 degrees. For the complex $[\text{Pt}(\text{dien})\text{I}][\text{Pt}(\text{dien})\text{I}_3]\text{I}_2$, where dien is the terdentate ligand diethylenetriamine,

Table 2
X-ray structural information on mixed-valence complexes of platinum

Complex	r(Pt-Pt)/Å	r(Pt ^{IV} -X)/Å	r(Pt ^{II} -X)/Å	$\frac{r(\text{Pt}^{\text{IV}}-\text{X})}{r(\text{Pt}^{\text{II}}-\text{X})}$	Ref.
<u>X = Cl</u>					
[Pt(etn) ₄][Pt(etn) ₄ Cl ₂ Cl ₄ ·4H ₂ O]	5.39	2.26	3.13	0.72	31
[Pt(NH ₃) ₄][Pt(NH ₃) ₄ Cl ₂](HSO ₄) ₄	5.466	2.310	3.158	0.73	32
[Pt(en) ₂][Pt(en) ₂ Cl ₂](ClO ₄) ₄	5.403	2.318	3.085	0.75	23
{[Pt(en) ₂][Pt(en) ₂ Cl ₂]} ₃ (O ₃ Cl ₄) ₄	5.261	2.328	2.937	0.79	26
[Pt(pn) ₂][Pt(pn) ₂ Cl ₂](ClO ₄) ₄	5.512	2.29	3.22	0.71	23
		2.33	3.18	0.73	
[Pt(tn) ₂][Pt(tn) ₂ Cl ₂](BF ₄) ₄	5.395	2.299	3.096	0.74	24
[Pt(chxn) ₂][Pt(chxn) ₂ Cl ₂ Cl ₄]	5.158	2.324	2.834	0.83	22
<u>X = Br</u>					
[Pt(NH ₃) ₄][Pt(NH ₃) ₄ Br ₂](HSO ₄) ₄	5.489	2.467	3.026	0.82	33
[Pt(etn) ₄][Pt(etn) ₄ Br ₂ Br ₄ ·4H ₂ O]	5.586	2.447	3.139	0.79	34
[Pt(en) ₂][Pt(en) ₂ Br ₂](ClO ₄) ₄	5.470	2.71	2.76	0.98	35
[Pt(pn) ₂][Pt(pn) ₂ Br ₂](O ₃ Br ₅) ₂	5.617	2.55	3.07	0.83	27
[Pt(tn) ₂][Pt(tn) ₂ Br ₂](BF ₄) ₄	5.462	2.541	2.921	0.87	24
[Pt(tn) ₂][Pt(tn) ₂ Br ₂](ClO ₄) ₄	5.501	2.546	2.955	0.86	24
[Pt(en)Br ₂][Pt(en)Br ₄]	5.606	2.48	3.125	0.79	36
K ₂ [Pt(py)Br ₃][Pt(py)Br ₅]·2H ₂ O	5.606	2.481	3.126	0.79	37
CS ₂ [Pt(NO ₂)(NH ₃)Br ₂][Pt(NO ₂)(NH ₃)Br ₄]	5.820	2.492	3.341	0.75	20
<u>X = I</u>					
[Pt(en) ₂][Pt(en) ₂ I ₂](ClO ₄) ₄	5.827	2.791	3.036	0.92	38
	5.820	2.704	3.115	0.87	39
		2.726	3.039	0.90	
[Pt(pn) ₂][Pt(pn) ₂ I ₂](ClO ₄) ₄	5.726	2.770	2.956	0.94	40
[Pt(pn) ₂][Pt(pn) ₂ I ₂]I ₄	5.770	2.815	2.995	0.94	35
[Pt(dien)I][Pt(dien)I ₃]I ₂	5.805	2.705	3.234	0.84	15
K ₄ [PtI ₄][PtI ₆]	5.907	2.715	3.205	0.85	21
Rb ₄ [PtI ₄][PtI ₆]	5.941	2.702	3.252	0.83	21
CS ₂ [Pt(NO ₂)(NH ₃)I ₂][Pt(NO ₂)(NH ₃)I ₄]	6.063	2.711	3.362	0.81	20

this angle was determined¹⁵ to be alternately 153 and 158 degrees. Other x-ray determinations⁴¹ have indicated that, under pressures up to approximately 60 kbar, no phase changes occur, but that the c dimension of the unit cell decreases less than the a and b dimensions.

I.4.2. Photoelectron Spectroscopy

X-ray photoelectron spectroscopic studies⁴²⁻⁴⁶ have shown, for halogen-bridged, mixed-valence complexes of platinum, a pair of doublet peaks corresponding to spin-orbit components of platinum in two oxidation states. This is further evidence of the mixed-valence nature of the complexes. Furthermore, the difference in energy between the doublets decreases on going from Cl through Br to I as the bridging halogen,⁴⁴ in agreement with greater delocalisation of iodide-bridged chains. Such differences in doublet energies, both in the chains and in constituent monomer complexes, may be correlated with metal-halogen bond length ratios $r(M^{IV-X})/r(M^{II...X})$ in determining the extent of valence delocalisation.

I.4.3. Conductivity

Measurements have been made of the electrical conductivity of halogen-bridged, mixed-valence complexes of platinum, palladium and nickel under different conditions of temperature and pressure.^{41,47,48} Being of Type II mixed-valence nature, they are semiconducting, although some iodide-bridged chains, as they approach Type IIIB mixed-valence, come close to being conducting, especially under high pressure. Typically conductivity parallel to the chain axis is about 300 times greater than conductivity perpendicular to the chain.⁴⁷ Interrante et al.⁴¹ demonstrated that conductivity increases in the order $Cl < Br < I$ and $Pd^{II}/Pt^{IV} < Pt^{II}/Pt^{IV} < Pd^{II}/Pd^{IV}$. They further showed that increasing pressure could

dramatically increase the conductivity, but that a metallic state is not attained. Their proposed mechanism of electron movement along the chain is by electron hopping between adjacent metal sites. More recently, Hamaue et al.⁴⁹ have argued in terms of a band mechanism for the conductivity.

I.4.4. Electronic Spectroscopy

In addition to being strongly coloured, crystals of halogen-bridged, mixed-valence complexes of platinum, palladium and nickel are highly reflective, especially those which are bromide- or iodide-bridged. Thus, for example, bromide-bridged platinum complexes generally transmit blue or violet light, but appear a lustrous green or gold in reflected light.

Electronic spectra may therefore be obtained by transmission or diffuse reflectance or specular reflectance.

The transmission or diffuse reflectance electronic spectrum of a halogen-bridged mixed-valence complex shows, in addition to features seen for its constituent M^{II} and M^{IV} species, a broad, intense and unstructured peak at low energy (largely in the visible region), which is seen only with incoming light with its electric vector parallel to the chain axis (as determined by single crystal transmission^{25,50,51}). This absorption, which has typically a full width at half-maximum of $5000-6000\text{ cm}^{-1}$, causes the strong colour and dichroism observed and may be understood in terms of excitation of an M^{II}/M^{IV} pair (II/IV state) to an M^{III}/M^{III} pair (III/III state), by the intervalence charge transfer (IVCT) of one electron between adjacent metal ions via the intervening halogen. The absorption energy maximum is observed to decrease in the orders $Cl > Br > I$ and $Ni^{II}/Pt^{IV} > Pd^{II}/Pt^{IV} > Pt^{II}/Pt^{IV} > Pd^{II}/Pd^{IV} > Ni^{II}/Ni^{IV}$.^{14,46,52,53} It is also observed to increase with decreasing crystal size.⁵⁴⁻⁵⁶ These trends are in parallel with those observed in structure and conductivity. It is similarly

observed that, with increasing pressure, the absorption maximum moves to lower energy.⁴¹ However, it has not been observed to change substantially with temperature.

When the electronic spectrum is determined by means of specular reflectance at normal incidence,^{35,40,56-58} it is possible to gain more information than by transmission. As for transmission, the electric vector of the incident light is required to be parallel to the linear-chain axis for the IVCT band to be observed. Following a Kramers-Kronig transformation of the spectrum, it is possible⁵⁶ to determine the dielectric constant, the refractive index and the gap frequency of the crystal. The last of these has been shown to change in the same manner as the transmission/absorption maximum with different M^{II}/M^{IV} combinations or bridging halogen, in agreement with structural and conductive measurements.

Narrower and weaker bands, likewise polarised, are observed^{50,59} just below the absorption edge of the IVCT band. They are understood to be associated with excitons and chain defects and will be discussed later.

I.4.5. Vibrational Spectroscopy

The infra-red spectrum of a halogen-bridged, mixed-valence, linear-chain complex of platinum, palladium or nickel is almost entirely a superposition of those of the constituent M^{II} and M^{IV} complexes. Where there are no resonance effects, the same may be said of the Raman spectrum. This is because interchain interactions in these complexes are weak and, consequently, vibrations involving motion transverse to the chain are essentially unchanged with formation of the linear chain. However, the interactions between the M^{II} and M^{IV} units in the linear chain are sufficiently strong, for two of the vibrations of the individual M^{IV} complexes to be changed substantially in wavenumber on incorporation of M^{IV} in the linear chain,

and to be better considered as longitudinal optical modes of the lattice.⁶⁰ These are the symmetric and asymmetric (X-M^{IV}-X) stretch modes, ν_1 and ν_2 respectively. The latter is theoretically only infra-red active in the linear chain (although in fact it occurs in the Raman spectra also) and occurs at lower wavenumber than in the discrete complex. The former is Raman active, likewise occurring at lower wavenumber than in the discrete M^{IV} complex (it is lower by 40 - 50 cm⁻¹ for cases where M^{IV} = Pt^{IV}) and also displays strong resonance enhancement as described below. In addition to ν_1 and ν_2 , creation of the linear-chain complexes produces other phonon modes, which are not associated with any modes of the individual molecules. One of these is a third longitudinal optical mode ν_3 , in which the M^{IV}X₂ unit oscillates between adjacent M^{II} units. This is expected to be infra-red active and to appear at very low wavenumber, but has so far not been observed.

I.4.6. Resonance Raman Spectroscopy

Resonance Raman spectroscopy has been found to have a wide application in the study of halogen-bridged, linear-chain complexes.^{9,11,18,61,62} If excitation is within the IVCT band, a very strong enhancement (an intensity increase of several orders of magnitude) of the band assigned to the X-M^{IV}-X symmetric stretch, ν_1 , is observed, together with the appearance of many overtones $\nu_1\nu_1$ (ν_1 up to 17 has been observed⁶³) and, in some cases, weaker enhancement of combination bands involving $\nu_1\nu_1$. Maximum enhancement occurs at or near the electronic absorption edge E_g of the IVCT band, a commonly observed resonance Raman (RR) effect, which has been theoretically interpreted.^{64,65} The enhancement is observed primarily for light polarised parallel to the chain length, the scattered light being mostly likewise polarised. These observations indicate a strong coupling between the intervalence electronic transition and the ν_1 symmetric

stretch vibration. By consideration of some theory of one-dimensional complexes (section I.10), the spectra can be understood in terms of excitation from a mixed-valence ground state to a non-mixed-valence excited state.^{51,66,67}

The change in wavenumber of ν_1 on going from the discrete complex to the linear chain depends on the metal, the bridging halogen, the equatorial ligand and, where appropriate, the counterion. From a long RR overtone progression, a harmonic wavenumber ω_1 and an anharmonicity constant x_{11} may be calculated (Appendix I), which show this mode to be in most cases virtually harmonic.

In addition to the ν_1 progressions a weak, z-polarised luminescence (B band) is observed underlying the $\nu_1\nu_1$ bands, as is a strong, z-polarised luminescence (L band), several orders more intense than the RR scattering and with a full width at half maximum of around 2000 cm^{-1} , at a wavenumber corresponding to roughly half the IVCT band gap energy E_g .⁶⁸ The latter band, which increases in intensity with decreasing temperature, is ascribed to electron-hole recombination at the lowest vibrational level of the III/III state. The L and B bands will be discussed in Section I.6.

Tanaka et al. observed⁵⁹ that, for excitation of a $[\text{Pt}(\text{en})_2][\text{Pt}(\text{en})_2\text{Cl}_2](\text{ClO}_4)_4$ single crystal within the weaker bands (possibly excitonic) below the IVCT absorption edge, little RR scattering or luminescence occurred. They also concluded that the maximum of the excitation profile of the RR scattering occurred at exactly the absorption edge. Work on Wolfram's red salt⁶⁸ has indicated that, with increasing excitation frequency, the intensity of the weak luminescence B increases at the expense of the RR scattering, while the strong luminescence L is unchanged.

I.4.7. Solid State N. M. R. Spectroscopy

Solid state n. m. r. spectroscopy has recently been

shown to have useful application to the study of halogen-bridged, mixed-valence complexes of platinum and palladium. ^{13}C n. m. r. spectra of palladium complexes have indicated the feasibility of estimating the extent of valence delocalisation from the position of resonance of the α -carbons in ligands attached to the Pd^{II} and Pd^{IV} sites. ^{15}N n. m. r. spectroscopy is likely to be a better measure of delocalisation because the nitrogen nuclei are directly attached to the metal sites and (in the case of platinum complexes) because substantial coupling is likely between ^{15}N and ^{195}Pt nuclei, the coupling constants being correlated with the metal oxidation state.

I.5. Discrete d-orbitals on the Metal Ions

It is likely that, from data such as the ratio of $\text{M}^{\text{IV}}\text{-X}$ to $\text{M}^{\text{II}}\text{-X}$ distances, (i.e. relative to the ratio for isolated M^{IV} and M^{II} molecules) and the polarisation of the intervalence transition absorption, there is a considerable interaction between adjacent metal centres in the halogen-bridged chain, even in the ground state. This is also apparent from the decrease in the ν_1 wavenumber on going from the M^{IV} monomer to the mixed-valence complex.

If the metal centres are assigned the oxidation states of two and four alternately along the chain and considered as individual molecular entities, the molecular d-orbital energies and occupancies of those species will appear approximately as in Figure 3.⁹

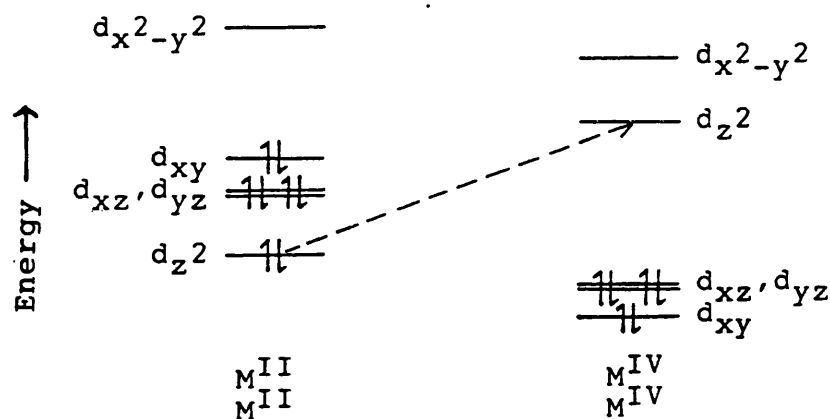


Figure 3. Qualitative d orbital energies of the M^{II} and M^{IV} sites, showing the intervalence transition.

Since the IVCT band is z-polarised, the most likely transition to be occurring is the transfer of one electron between d_z^2 orbitals, via the halogen p_z orbital,^{51,66,67} as indicated in Figure 3 and below:



The IVCT absorption edge energy, E_g , is found^{49,50,69} to be roughly related to the activation energy, ΔE , for electrical conductivity by a common equation for intrinsic, direct gap semiconductors ($E_g = 2\Delta E$), suggesting that the same electronic process is occurring. Since the electrical conduction rises rapidly when the activation barrier is overcome, it appears that a process of electron transfer along the whole chain is set off when the critical energy is reached. A similar electron transfer, within individual M--X--M units of the chain, probably occurs with optical excitation within the IVCT band. The origin of the great width of the band is not clear within this scheme.

Beyond the above explanation, it is not useful to consider the electronic excitation in terms of a separate d_z^2 orbital on each metal centre. Instead the d_z^2 electrons should be considered, as a whole, to occupy a band of orbitals, which span the whole chain of metal sites. The qualitative derivation of this band is outlined in Section I.10.3.

I.6. Resonance Raman Scattering versus Luminescence in Halogen-bridged Mixed-valence Complexes

Onset of the RR effect in halogen-bridged,

mixed-valence complexes occurs with excitation at or around the IVCT absorption edge. The scattering process is rapid, i.e. the lifetime of the excited state is of the order of 10^{-13} seconds. However, RR scattering is in competition with resonance fluorescence-type processes, which, by the following argument⁶⁸ may produce the luminescence bands seen. With excitation a free electron-hole pair is created. This pair will have one of two immediate fates. It may rapidly recombine and undergo a single energy transition to a vibrational level of the ground state. This would be RR scattering. Alternatively, whilst in close proximity in the excited state, the electron and hole could, prior to recombination, interact with the ν_1 phonon mode, such as to be partially deactivated. It has been proposed,⁶⁸ that this could occur via a phonon "cascade" down the k vector versus energy curve (giving the B band), with the average position of the halogen unchanged from the ground state equilibrium position. This would then be followed by the favourable displacement of the halogen to a position central between the M^{III} sites. This M^{III} pair is now trapped, i.e. the electron and hole are bound, both to each other and primarily to one site in the chain. They will ultimately fluoresce to the ground state (L band).

I.7. Methods of Preparation of Halogen-bridged, Mixed-valence Complexes of Platinum, Palladium and Nickel

There are essentially three methods of preparing these complexes, which are:

- (a) Partial oxidation of the M^{II} species,
 - (b) Partial reduction of the M^{IV} species,
 - (c) Separate preparation of M^{II} and M^{IV} species,
- followed by cocrystallisation.

Methods (a) and (c) are more commonly used than method (b). Partial oxidation of the M^{II} species is usually with halogen X_2 ,¹⁰ but other oxidising agents, such as

ammonium persulphate,⁷⁰ hydrogen peroxide,⁷ sulphuric acid, nitric and hydrochloric acid mixtures⁷¹ and copper(II) halides⁷² have been used in the past. Partial oxidation is necessary where M^{IV} is Pd^{IV} or Ni^{IV} , because these species are unstable, requiring that immediate crystallisation of the linear chain is effected. In the case of Pt^{II}/Pt^{IV} chains, method (c) is preferable for the creation of large, well-formed crystals at a governable rate.⁷³ Separate preparation of the Pt^{IV} complex by halogenation of the Pt^{II} species gives exclusively the trans-dihalogeno complex as required. Clearly, for the preparation of mixed-metal linear chains Ni^{II}/Pt^{IV} or Pd^{II}/Pt^{IV} , method (c) is necessary. In such a case, it is essential that the platinum is present exclusively as Pt^{IV} , i.e. that no reduction to Pt^{II} occurs; otherwise the product will be contaminated by Pt^{II}/Pt^{IV} mixed-valence complex.

It is possible to substitute the bridging halogen in a mixed-valence complex. Thus a chloride bridge may be replaced by bromide or iodide, and bromide by iodide, either by addition of a solution of the hydrohalic acid or alkali halide, or by grinding with alkali halide.⁷⁴ It should be noted, however, that in such a process substitution may occur not only at the bridging halogen site, but also (where appropriate) at the counteranion site.

I.8 Copper(II)-Platinum(IV) Complexes

The synthesis was reported⁷⁵ in 1988 of $[Cu(en)_2][Pt(en)_2X_2](ClO_4)_4$, where $X = Cl$ or Br . These are considered to be linear-chain complexes analogous to the mixed-metal mixed-valence complexes described above, in which the M^{II} site is occupied by Cu^{II} , which has the d^9 configuration, with a singly occupied $d_{x^2-y^2}$ orbital in the square planar geometry. This deviation from the usual d^6/d^8 configuration in the mixed-valence

complexes indicates the possibility of making a wide variety of compounds, which are structurally analogous to, but non-isoelectronic with, the Pt, Pd and Ni systems. In both the Cl- and the Br-bridged cases the Cu-Pt complex crystallises as red-brown needles, which are not strongly dichroic. That platinum and copper may not necessarily be present in equal amounts was indicated by x-ray data⁷⁵ which implied that the crystals contained Cu and Pt in the ratio 0.89:1.11, with some M^{II} sites occupied by Pt^{II}. Magnetic data⁷⁵ indicated only a weak antiferromagnetic coupling between Cu^{II} ions along the chain. From optical data Oshio et al.⁷⁶ concluded that there exists an intense, polarised, visible IVCT band in the electronic spectrum, and corresponding electron-phonon interaction leading to strong resonance enhancement of the $\nu_1(\text{Cl-Pt}^{\text{IV}}\text{-Cl})$ symmetric stretch band at 312 cm^{-1} in the Raman spectrum. Work reported herein shows the conclusions of Oshio et al. from their optical spectroscopic data to be erroneous. As will be shown, it is considered that the Pt^{II} content of their complexes was so high that optical spectra of the Cu^{II}/Pt^{IV} complex were masked by the more prominent features arising from Pt^{II}/Pt^{IV} impurities.

I.9. Halogen-bridged, Non-mixed-valence, Linear-chain Complexes of Nickel

Recent work by Toriumi et al.⁷⁷ has shown that a nickel complex may be made which is very similar to halogen-bridged Ni^{II}/Ni^{IV} complexes, but in which the nickel ions are of non-mixed-valence. The linear chain consists of halogen-bridged Ni^{III} ions and the halogen is equidistant between adjacent nickel sites. This complex appears to be stable against Peierls-Hubbard dimerisation to the Ni^{II}/Ni^{IV} state, the distortion due to electron-lattice interaction being outweighed by the electron-electron repulsion.

The appearance and properties of the $\text{Ni}^{\text{III}}/\text{Ni}^{\text{III}}$ complex^{77,78} are different from those of $\text{M}^{\text{II}}/\text{M}^{\text{IV}}$ complexes. The crystals are black-brown with no lustre. The position of the bridging halogen - the critical factor in ascertaining the valence of the Ni - has been determined from x-ray studies to be truly central between adjacent nickel sites. Reflectance data indicate that there is a low energy (deep red to infra-red) electronic band polarised parallel to the chain length. Magnetic data show the spins of the unpaired electrons to be antiferromagnetically coupled along the chain, so that a spin density wave exists in the chain (c.f. the charge density wave in a mixed-valence chain). It has been suggested⁷⁸ that counteranions to the chain play an important role in stabilising the $\text{Ni}^{\text{III}}/\text{Ni}^{\text{III}}$ state, and that planar structures are created by cross-linking via counteranions.

I.10. Models of Linear-chain, Halogen-bridged, Mixed-valence Complexes of Platinum, Palladium and Nickel

A number of theories have been developed to model the structures and properties of halogen-bridged, mixed-valence complexes. The Robin and Day classification and the PKS model are based on interactions between discrete complex units and may be applied to all mixed-valence complexes, of the linear-chain or other variety. The models of Nasu and Whangbo and Foshee, however, are based upon consideration of linear-chain structures in particular and view them as extended complexes. Each of these theories will be considered here in turn.

I.10.1. The Robin and Day model

The Robin and Day model⁵ is a static model of

discrete units enabling quick classification of mixed-valence materials into types I, II, IIIA and IIIB according to the degree of valence electron delocalisation. If wavefunction ψ_0 describes one state of mixed-valence in the complex and ψ_1 another, where valence exchange has occurred, of slightly different energy, then the ground state wavefunction ψ_g will be given by

$$\psi_g = (1 - \alpha^2)^{1/2} \psi_0 + \alpha \psi_1$$

where α is the valence delocalisation coefficient. The value of α determines the classification of a mixed-valence complex and may be correlated with conductive and spectroscopic measurements. Where α is small but not zero, the different valence sites are distinguishable but may be interchanged. Complexes of this type, of which halogen-bridged, mixed-valence complexes of Pt, Pd and Ni are examples, are in class II. The Robin and Day model serves as a quick means of approximate classification of mixed-valence complexes according to their conductive and spectroscopic properties.

I.10.2. The PKS model

The PKS (Piepho, Krausz and Schatz⁷⁹) model extends the Robin and Day model by considering the effect of vibronic coupling between two discrete units in the linear chain and enables predictions to be made of the IVCT band contour, the extent of and relative intensities in resonance Raman progressions and excitation profiles, all of which will depend on the degree of valence delocalisation. Three parameters ξ , λ and W are used to quantify the characteristic properties of mixed-valence complexes. ξ is the estimated strength of electron-electron interaction between the discrete valence sites. λ is a calculation of the vibronic interaction between the sites, determined from

the difference in equilibrium position of the appropriate normal coordinate in the two valence states. W measures the difference in zero-point energy of the two states. The relationship between these three parameters will determine the class of a mixed-valence complex. Thus for complex types I, II, and III, the approximate relations $|\epsilon| \ll (\lambda^2 + W)$, $|\epsilon| \lesssim (\lambda^2 + W)$ and $|\epsilon| > (\lambda^2 + W)$, respectively, hold true.

It is predicted that, on going from Type I through to Type III, the IVCT band will become sharper and more intense and the RR progression will become shorter. It is further predicted that electronic Raman bands may appear, as a result of the vibronic coupling of potential energy surfaces.

Wong and Schatz⁸⁰ have applied the PKS (two-site, one-electron) model to the case of Wolfram's Red, obtaining good agreement between theory and experiment in predicting the nature of the RR progression. However, their prediction of the location, intensity and shape of an electronic Raman band does not agree sufficiently well with experiment to be equated with the observed L band. Prassides et al.⁸¹ extended the model by considering the two-site, two-electron case (necessary where the mixed-valence moieties differ in oxidation number by two) and concluded that the L band should not be considered as electronic Raman scattering, but as luminescence from the III/III state, as suggested by Tanino and Kobayashi⁶⁸ (section I.6).

The PKS model considers only interactions between adjacent M^{II} and M^{IV} complexes and takes no account of possible interactions between non-adjacent units. For a fuller understanding, such interactions need to be taken into account. The Whangbo and Foshee model goes some way towards this.

Whangbo and Foshee^{67,82} use tight-binding calculations of the extended Hückel type to determine the energies of electron band orbitals derived from the mixing of orbitals of appropriate symmetry from all the ions in the linear chain. They begin by considering a more symmetric chain consisting of halogen-bridged M^{III} species, where the halogen X is equidistant between adjacent M^{III} . The relevant interacting orbitals of the ionic species are the outermost d orbitals of the metal and the outermost s and p orbitals of the halide. Of these, the d_{z^2} , p_z and s orbitals form a set of appropriate symmetry to mix. Mixing of the d_{z^2} with the p_z and s orbitals (at the limits $k = \pm\pi/a$ and $k = 0$ respectively of the first Brillouin zone, where a is the repeat distance in the chain) creates a band of orbitals, which are largely d_{z^2} -like in nature. This band shows energy dispersion across the Brillouin zone. The M^{III} sites upon which the derived band orbitals are based are d^7 ; hence the d_{z^2} band is half occupied (Fermi level $k_F = \pm\pi/2a$). This state is unstable with respect to a Peierls distortion, whereby the chain repeat distance is doubled, the Brillouin zone conversely halved in length and an energy gap appears at the Fermi level k_F between the two sections of the "folded" d_{z^2} energy dispersion. The effect of the Peierls distortion is depicted in Figure 4. It is seen that orbital degeneracy at the Brillouin zone edge is removed and the occupied orbitals near the edge are significantly lowered in energy.

A favourable distortion of this type would occur in the M^{III} chain if the halogens were displaced from their central positions towards alternate metal sites. Such a move will be accompanied by a shift in electron density towards the favoured metal ions, i.e. the oxidation states become $3+\delta$ and $3-\delta$ alternately, where $0 < \delta < 1$. These are the true oxidation states of the metal in halogen-bridged mixed-valence complexes. The halogen displacement can be regarded as a motion of the ν_1 symmetric stretch phonon. Thus we have electron-electron and electron-phonon

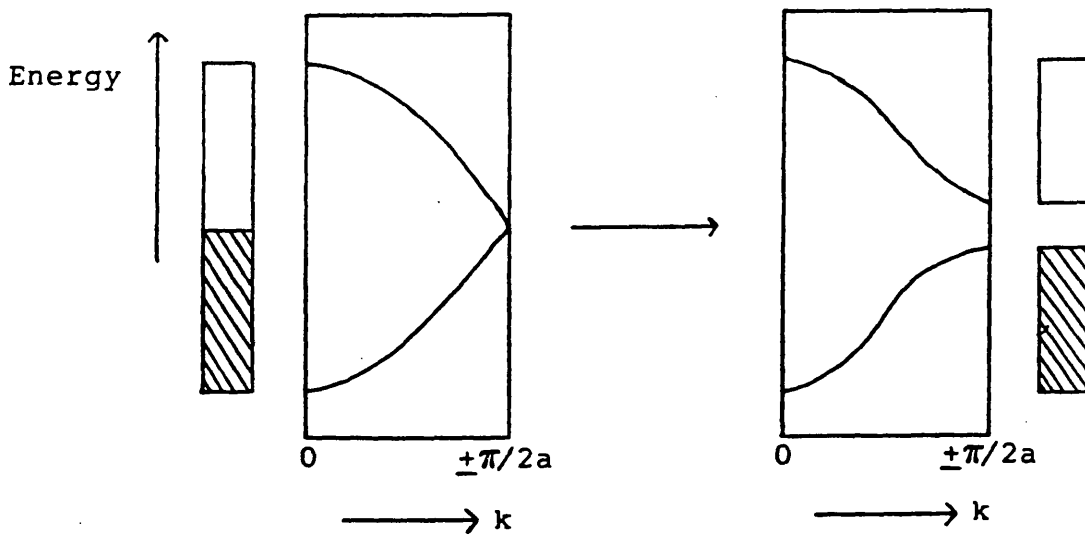


Figure 4. Splitting of the d_{z^2} band with Peierls distortion of the III/III lattice.

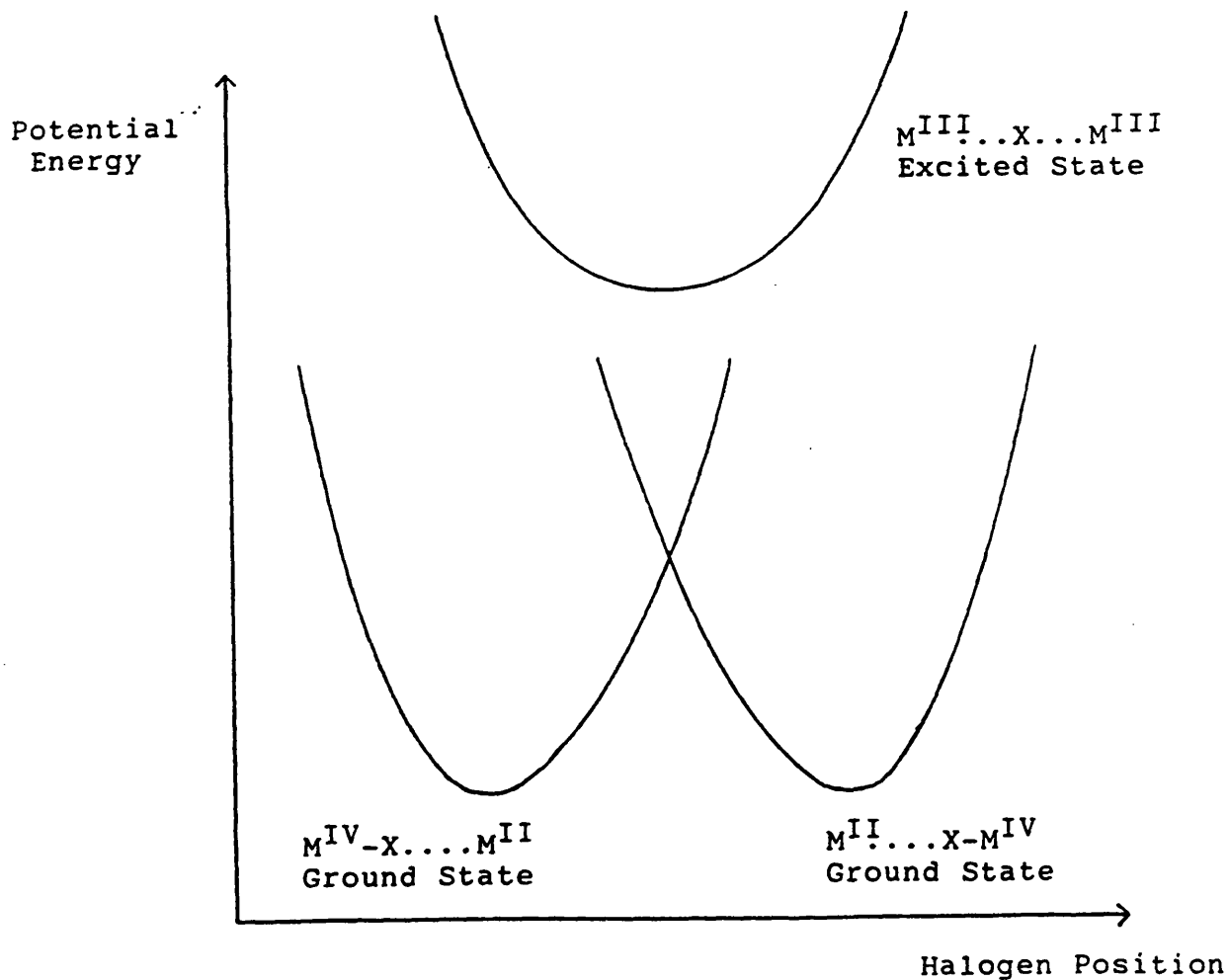


Figure 5. Variation of potential energy with halogen position on the chain axis, in the ground and excited states.

interactions occurring to give the Peierls distorted lattice and, in the process, produce a charge density wave (CDW) in the chain.

The lower, filled valence band has primarily $M^{III-\delta}$ (d_{z^2}) character, while the upper, empty conduction band has primarily $M^{III+\delta}$ (d_{z^2}) character.

In the band orbital scheme outlined above, the onset of conduction occurs with excitation from the valence to the conduction band and explains well the observed semiconductivity in the chain direction. Optical excitation within the IVCT band of the electronic spectrum is believed to involve similar transitions.

If electrons in the valence band are excited into the conduction band with their k values unchanged (as is theoretically required), the Peierls distorted lattice may have no energetic advantage over the more symmetric lattice. This will depend on whether the electrons remain spin paired in the vicinity of a given metal site and on how the intermetal site electron density varies along the chain. It is possible, therefore, that the excited state of the linear chain would, given enough time, take up the more symmetric lattice geometry. The qualitative features of the potential functions associated with the ground and (supposed) excited states are shown in Figure 5 for one X--M--X segment of the chain. The equilibrium position of X is well displaced by the excitation. It is therefore likely that, from a consideration of Franck-Condon factors, excitation will be to a high vibrational level of the excited state. Relaxation from this state to the ground electronic state could produce the long progression of vibrational overtones observed.

I.10.4. The Nasu Model or extended Peierls-Hubbard Model

Nasu⁸³⁻⁸⁵ has developed a model of linear-chain systems, which attempts to quantify the electron-electron and electron-phonon interactions, by the consideration of four parameters S , T , U and V . In application to

halogen-bridged, mixed-valence complexes, it begins by considering the more symmetric M^{III}/M^{III} chain, which, as was demonstrated via the Whangbo/Foshee model, is unstable with respect to Peierls dimerisation. S , the electron-phonon coupling energy, is determined from the change of electrostatic potential of an electron at the metal lattice site due to displacement of the halide ions X from the midpoints, and is approximately constant. T , the transfer energy of an electron between two neighbouring metal sites, increases with increasing size of bridging halogen, as it depends on the $d_{z^2}(M^{III}) - p_z(X)$ orbital overlap. U , the intra-site electron-electron repulsion energy depends primarily on the $d_{z^2}(M^{III})$ orbital and increases with decreasing atomic number of M . V , the inter-site electron-electron repulsion energy, is likewise dependent primarily on the d_{z^2} orbitals; as these do not extend to cover effectively the distance between neighbouring sites M^{III} , the value of V is much smaller than that of U .

When the electron-phonon interaction outweighs the electron-electron interaction, as in the halogen-bridged, mixed-valence complexes, a charge density wave (CDW) is created in the chain. When the opposite is the case, a spin density wave (SDW) is created, and such is the case in the non-Peierls distorted Ni^{III}/Ni^{III} chain (section I.9). The transition of ground state stability from one to the other occurs at the interface $U = S + 2V$. Variation in these parameters and T as a function of the metal and halide ions in the mixed-valence chains explains qualitatively the nature of the IVCT band gap. Measurements⁸⁵ have thus far indicated S , U and $2T$ each to be of the order of 1 eV.

It should be noted that this model verifies the concept that, although the metal sites are nominally in oxidation states +2 and +4, in reality they are in states $+3+\delta$ and $+3-\delta$, where $0 < \delta < 1$.

I.11. Excitons, Solitons, Polarons and Bipolarons in Halogen-bridged, Mixed-valence, Linear-chain Complexes of Platinum, Palladium and Nickel

The origins of the relatively weak A and B bands on the low energy side of the IVCT absorption edge (section I.4.4) have been the object of much debate and experiment in recent years. It is considered that they are the absorptions of defect states in the mixed-valence chain, which may have the character of polarons, solitons or bipolarons. These features are now considered.

With excitation truly within the IVCT transition, i.e. above the absorption edge, free electron-hole pairs are created.^{86,87} The electrons and holes are not correlated spatially and permeate the chain independently. Although in this excited state the electrons and holes are never fully localised on specific (different) metal sites, it is useful to associate an electron-hole pair primarily with two M^{III} sites in the chain at any one time. It is also reasonable, from the nature of the electron transfer occurring, to associate an electron-hole pair creation with the creation of two M^{III} sites adjacent in the chain. Thus we may visualise the creation of one electron-hole pair as follows.⁸⁸

Firstly, The M^{III} pair creation:



followed by a "dissociation" of the M^{III} pair, e.g.



to give



followed by movement of the independent M^{III} species throughout the chain.

The independent M^{III} sites have the nature of neutral solitons, having spin $\frac{1}{2}$ and no charge (relative to the average of the ions normally encountered in the M^{II}/M^{IV} sequence). Between a pair of neutral solitons (domain walls) the alternation of oxidation states is reversed.

The dissociation stage occurs only for excitation beyond the absorption edge. It does not occur with excitation below the absorption edge, in which case each electron-hole pair forms a spatially correlated pair (a Mott-Wannier exciton). An electron and hole of this type are not energetic enough to be fully independent and therefore must move around together. In the above depiction, The M^{III} pair movement would differ as follows.

Firstly the M^{III} creation:



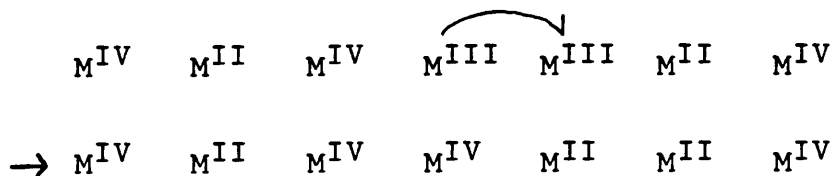
Dissociation does not occur; the M^{III} must move around together, e.g.



etc.

The bound M^{III} pair may possibly be separated by several metal sites, depending on the energy of the exciton.

If the excited M^{III}/M^{III} pair relaxes to a self-trapped charge transfer exciton (by B band emission, section I.6), it may subsequently relax to form an M^{IV}/M^{II} pair of reversed valence in the chain, by the following process.

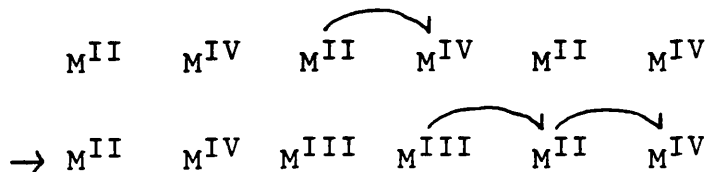


This mechanism has been proposed⁸⁹ for the creation of an S^+S^- soliton pair, S^+ and S^- having charge $+e$ and $-e$ respectively and no spin, responsible for the A band absorption below the absorption edge. Kurita et al.⁹⁰ have determined that, with irradiation within the charge transfer band, the absorption bands A and B grow, in proportion, in relative intensity. Such growth of A is consistent with electronic movement according to the above mechanism.

Thus a possibility is that the A band is due to S^+/S^- absorptions and the B band is due to S^0 absorptions, where S^+/S^- and S^0 are solitonic states derived as above.^{91,92} However, it has also been observed,^{93,94} that, with halogen doping of the linear chains, e.g. with I/I^- , the A and B bands are likewise enhanced, but the defects so produced have both spin and excess charge. Since solitons have either spin or charge, but not both, and since polarons have both spin and charge, there is a strong possibility that polarons rather than solitons are responsible for the A and B bands.^{90,95} A polaron is highly mobile lattice defect with spin and excess charge, positive (P^+) or negative (P^-), which does not alter the sequence of valence either side of it (unlike neutral solitons). In the case of halogen doping of mixed-valence complexes, the M^{III} ions could be produced by direct exchange:



In the case of photoexcitation, they could be produced by the following sequence:



(autodissociation - simultaneous 2-electron transfer)

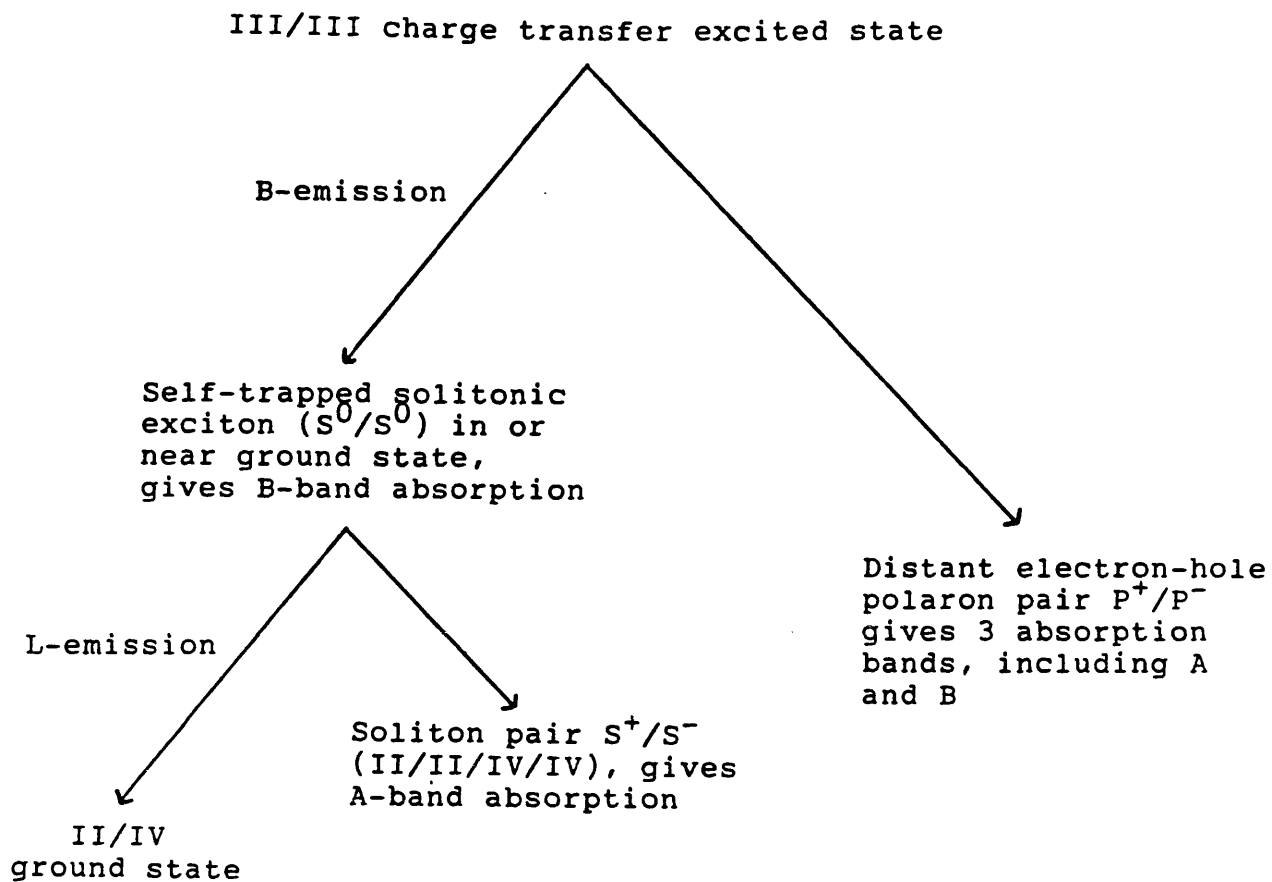
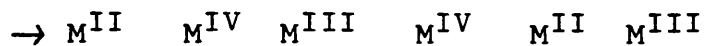


Figure 6. Possible means of non-linear relaxation of the III/III charge transfer excited state.



It is predicted⁹⁵ that three bands would appear below the absorption edge, if the polaron pair is produced. Two of these, at 70 and 80% of E_g , would correspond closely with the observed A and B bands, respectively.

In summary, there are three possible means of non-linear relaxation of the Franck-Condon III/III charge transfer excited state,⁹¹ as illustrated in Figure 6.

It is still unclear whether the soliton (S^+ , S^- and S^0) channel or the polaron (P^+ and P^-) channel is the cause of enhancement of the A and B bands, but experiment and calculation appear to favour the latter. However, it should be remembered that a variety of related processes may complicate the situation, e.g. $P^+ + P^+ \rightarrow S^+ + S^+$, or $P^+ + P^+ \rightarrow B^{2+}$, where B^{2+} = bipolaron (spin zero, charge $2e$), by heavy halogen doping; any band assignment may be more complex than the above schemes would suggest.

I.12. Aims of this Work

The principal aims of this work were to carry out optical studies, primarily by Raman and resonance Raman spectroscopy, of a variety of inorganic complexes, mostly of the halogen-bridged, mixed-valence type, and thereby to gain insight into the structure and properties of the complexes investigated.

II. THE RAMAN EXPERIMENT

A schematic diagram of a typical Raman experiment is shown in Figure 7.

II.1. Excitation Radiation

Whereas discharge lamps (e.g. the 'Toronto arc') were used in the past, lasers are now the exclusive means of excitation. For the bulk of Raman spectroscopy, inert gas ion ($\text{Ar}^+/\text{Ar}^{2+}$ and $\text{Kr}^+/\text{Kr}^{2+}$) lasers are used. Principal wavelengths obtainable with an Ar^+ laser are 1092.3, 528.7, 514.5, 501.7, 496.5, 488.0, 476.5, 472.7, 465.8, 457.9, 454.5, 363.8, 351.4, 351.1, 335.8, 334.5 and 333.6 nm, while those from a Kr^+ laser are 799.3, 793.1, 752.5, 676.4, 647.1, 568.2, 530.9, 520.8, 482.5, 476.2, 468.0, 415.4, 413.1, 406.7, 356.4, 350.7 and 337.5 nm. Thus they span the visible region and also extend into the infra-red and ultra-violet regions. The next most common type of laser used is the dye laser. A dye such as Rhodamine 6G, when irradiated with 514.5 nm excitation from an Ar^+ laser, will fluoresce strongly between 570 and 650 nm; when placed within an optical cavity, the dye may be made to lase at a wavelength tunable over part of the fluorescence range. Stilbene 1, when irradiated with near ultra-violet light, may act similarly as a laser dye in the blue - violet range. There are numerous other dyes. A third type of laser which is gaining in importance in Raman spectroscopy is the Nd/YAG laser with radiation at 1064 nm. This excitation is very suitable for the Fourier transform Raman experiment, which is described in Section II.8.

II.2. Beam Steering

The beam which emerges from the laser is coherent (all the photons are in phase), intense, virtually monochromatic and polarised in the vertical plane. These qualities make

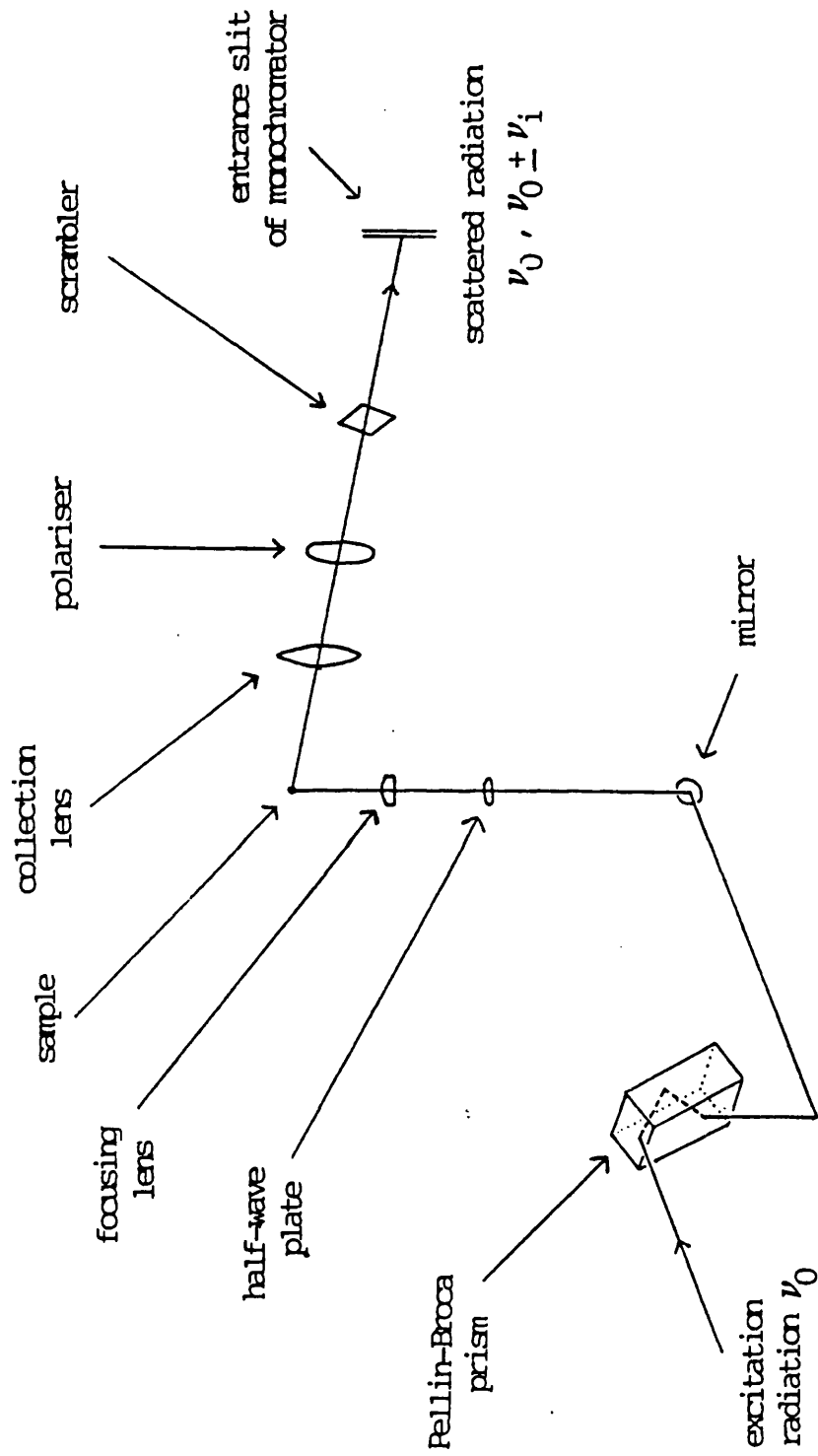


Figure 7. Schematic diagram of a typical Raman experiment.

the beam ideal for Raman excitation. However, it still requires for weak plasma lines to be filtered out. This may be done by means of a narrow band filter or a Pellin-Broca prism (total internal reflection followed by wide angle dispersion). To change the polarisation of the light incident on the sample, a half-wave plate or a scrambler may be used. At the sample, a lens focuses the beam to a point just microns across.

II.3. Sample

Samples in all states of matter may be probed.⁹⁶ All Raman spectra in this work are of solids, either as single crystals or as pressed discs of powder. Where a solid is easily decomposed by the laser beam (either thermally or photolytically), it is desirable to cool the sample to a low temperature. Cooling also improves the spectral quality, by reducing 'hot band' interference. With pressed discs decomposition may also be avoided by spinning the sample.

It is equally possible to heat samples to high temperature and to study them at high pressures.⁹⁷ For the latter, a diamond anvil cell is commonly used.

II.4. Scattered Light Collection

Depending on the nature of the sample, scattered light may be collected at all angles to the incident beam ν_0 . Most commonly the geometry of the experiment is such as to collect at 90° to ν_0 . Where (this work) the sample is a cooled pressed disc or non-transmitting crystal, it is mounted on a cold surface, such that ν_0 strikes at 30° (Figure 8). Scattered light is collected through a wide diameter collection lens, which focuses the light through a polarisation scrambler on to the entrance slit of the monochromator. Where specific polarisations of the incident and scattered light are being investigated, a rotatable polariser may be inserted between collection lens and scrambler.

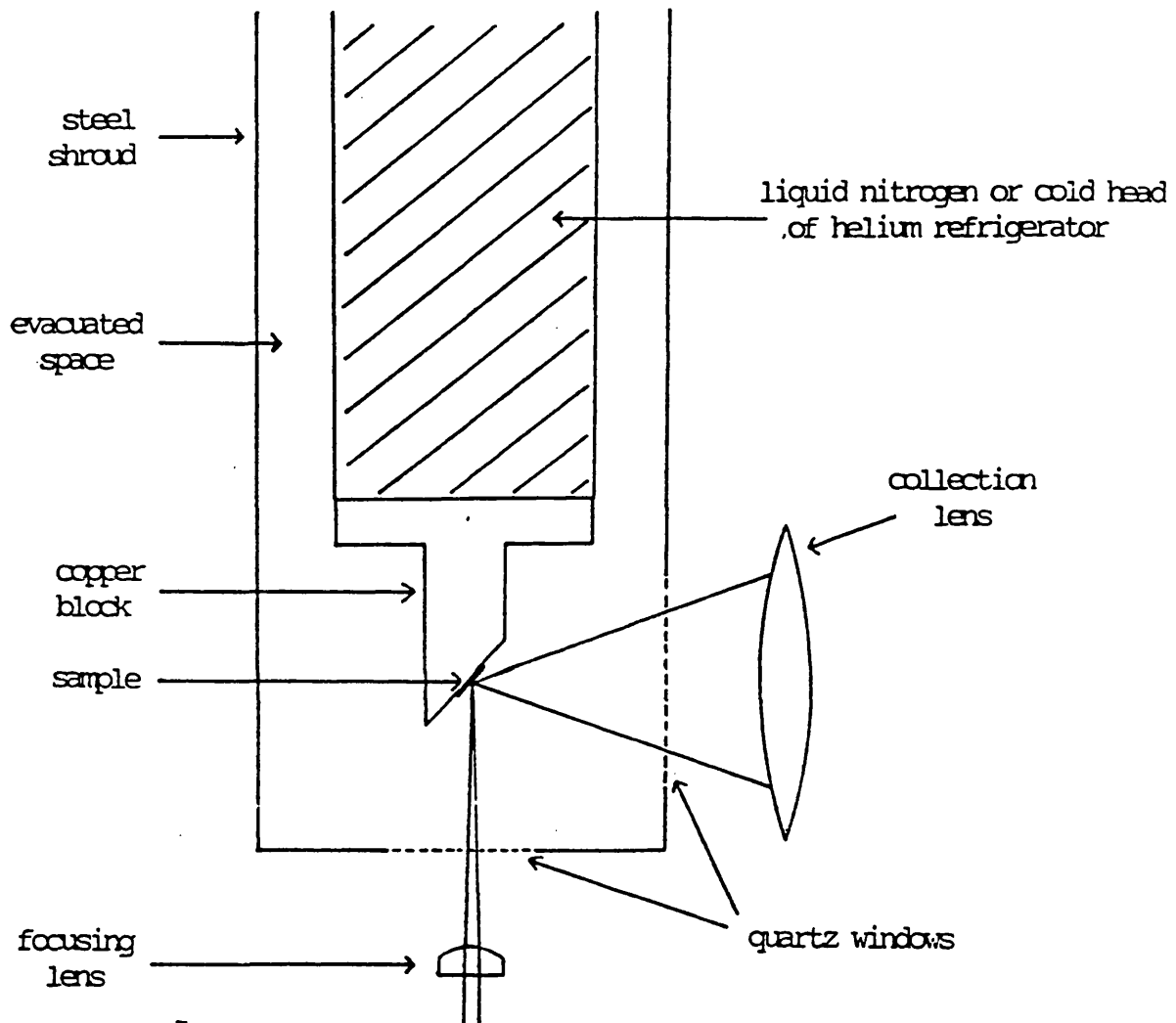


Figure 8. Cooled sample apparatus and Raman scattering arrangement.

II.5. Monochromator and Detector - Resolution and Sensitivity

A high resolution monochromator is used, commonly with a double or triple pass. As the inelastic scattering is a relatively weak optical effect, discrimination against high noise and background is essential. There must therefore be adequate resolution to exclude effectively the elastically scattered light - this is especially important for observing low wavenumber bands - while the signal-to-noise ratio is kept sufficiently high.

Two types of highly sensitive detector, the photomultiplier tube and the diode array, are commonly used. Where a photomultiplier tube is used, a 'floating' lens and a focusing lens just beyond the exit slit of the monochromator focus the light on to the light sensitive surface (e.g. GaAs) in the tube. In the case of a multichannel diode array, an exit slit is not utilised, as the array of photosensitive channels is situated within the monochromator to collect simultaneously into different channels light of different frequencies arriving in an arc of space. Whilst a diode array enables a wide spectral range to be collected simultaneously (and hence much quicker), it is inferior in resolution to collection by scanning, for a given signal-to-noise ratio.

A third type of detector gaining in importance, which is especially useful with very low light levels, is the charge coupled device (C.C.D.) which, like the diode array, simultaneously collects over a spectral range.

II.6. Output

The signal detected by a photomultiplier tube is relayed to a digital photometer, which registers a number of photon counts per unit time in proportion to the number hitting the detector. This information may be plotted on a

chart recorder or saved in computer memory for subsequent manipulation.

II.7. Spectral Response Measurement

Where a Raman spectrum is obtained over a large wavelength range, it is important to make corrections for variations in the throughput of the spectrometer and the response of the detector with wavelength. This may be achieved by measuring the spectral response of spectrometer and detector combined, by measuring the spectrum of a lamp of known emissivity across the wavelength range under predetermined conditions of current and voltage. Experiments of this type were carried out on instrumentation used for the bulk of this work. The spectrum of a tungsten filament lamp was obtained using the following procedure. The lamp (identification number 7BB89) was operated under conditions for which the emissivity was known (National Physical Laboratory calibration at a potential difference of 9.60 V and a direct current of 8.200 A, giving a colour temperature of 2924 K, with an ambient temperature of 20 ± 1 °C). To give a uniform irradiance of light at the entrance slit of the spectrometer (Spex 14018/R6), light from the lamp illuminated a BaSO₄ diffuser plate situated such as to reflect light approximately uniformly in the envelope of a collection lens on the optical axis of the spectrometer. Access of light by any other route to the entrance slit was blocked off. With a thermoelectrically cooled GaAs photomultiplier tube (type RCA31034) for detection, the lamp spectrum was obtained over the range 29000 - 11500 cm⁻¹ (approximately 345 - 870 nm). The emissivity data of the lamp over the same range were obtained in the form of a ninth order polynomial, which was then combined with the raw spectral data, to give a spectrum corrected for lamp emissivity, i.e. a spectral response curve for the combination of spectrometer and detector used.

II.8. Fourier Transform Raman Spectroscopy

The technique of Fourier Transform (FT) Raman spectroscopy has been developed in recent years to the extent that several machines are now commercially available. Because of the superior signal-to-noise ratios attainable compared with conventional scanning instruments, it is possible to use an excitation wavelength of much lower energy, e.g. the 1064 nm line from a Nd/YAG laser. FT Raman spectroscopy is expected to have widespread applications, particularly to organic materials which fluoresce strongly with u.v./visible excitation. F. T. Raman spectroscopy was not used for any of the work reported here, but it is expected to have application to some halogen-bridged, mixed-valence, linear-chain complexes having an IVCT band with the absorption edge in the near infra-red, especially nickel complexes and iodide-bridged complexes.

II.9. Raman Microscopy

Another significant development of the last decade is the Raman microscope, in which laser excitation is passed down the objective of a microscope to a sample point predetermined using coaxial white light. Scattered light is collected back through the objective (i.e. 180° scattering) and a Raman spectrum thereby obtained. This instrument is expected to have widespread application in the study of microscopic samples, e.g. fibres and geological specimens.

II.10. Instrumentation used in this Work

Figure 9 illustrates the plan of instrumentation used for the majority of the experiments in this work.

Excitation radiation was obtained using Coherent Radiation Kr⁺ ion (models CR3000K and 52) and Ar⁺ ion (18 and Innova 70) lasers.

Where samples were cooled to low temperature, an

evacuated liquid nitrogen cryostat (80 K) or a Displex closed-cycle helium refrigerator (40 - 50 K) was used.

To obtain the spectra a Spex 14018/R6 double monochromator was used with Jobin-Yvon holographic gratings (1800 lines/mm blazed at ca. 500 nm). Thermoelectrically cooled GaAs photomultiplier tubes (type RCA31034) were used to detect light, this signal being relayed to a DPC2 digital photometer. Spectral scans were programmed and saved on floppy disc using BBC Micro computers (software) programmes written by Dr. S. P. Best and Mr. D. Oprescu. Spectral response measurements on the spectrometer and detector have been made using a tungsten filament lamp.

II.11. Measurements

Wavenumbers of bands in the spectra (accurate to less than 1 cm^{-1}) were calibrated from neon emission lines or from the Rayleigh line ν_0 . Where appropriate, e.g. for excitation profiles, relative intensities were determined by measurement against an internal standard, e.g. K_2SO_4 (SO_4^{--} symmetric stretch at 985 cm^{-1}) or KClO_4 (ClO_4^- symmetric stretch at 938 cm^{-1}) in pressed discs. Where excitation profiles were measured, intensity corrections were made for the ν^4 factor and the variation in spectral response.

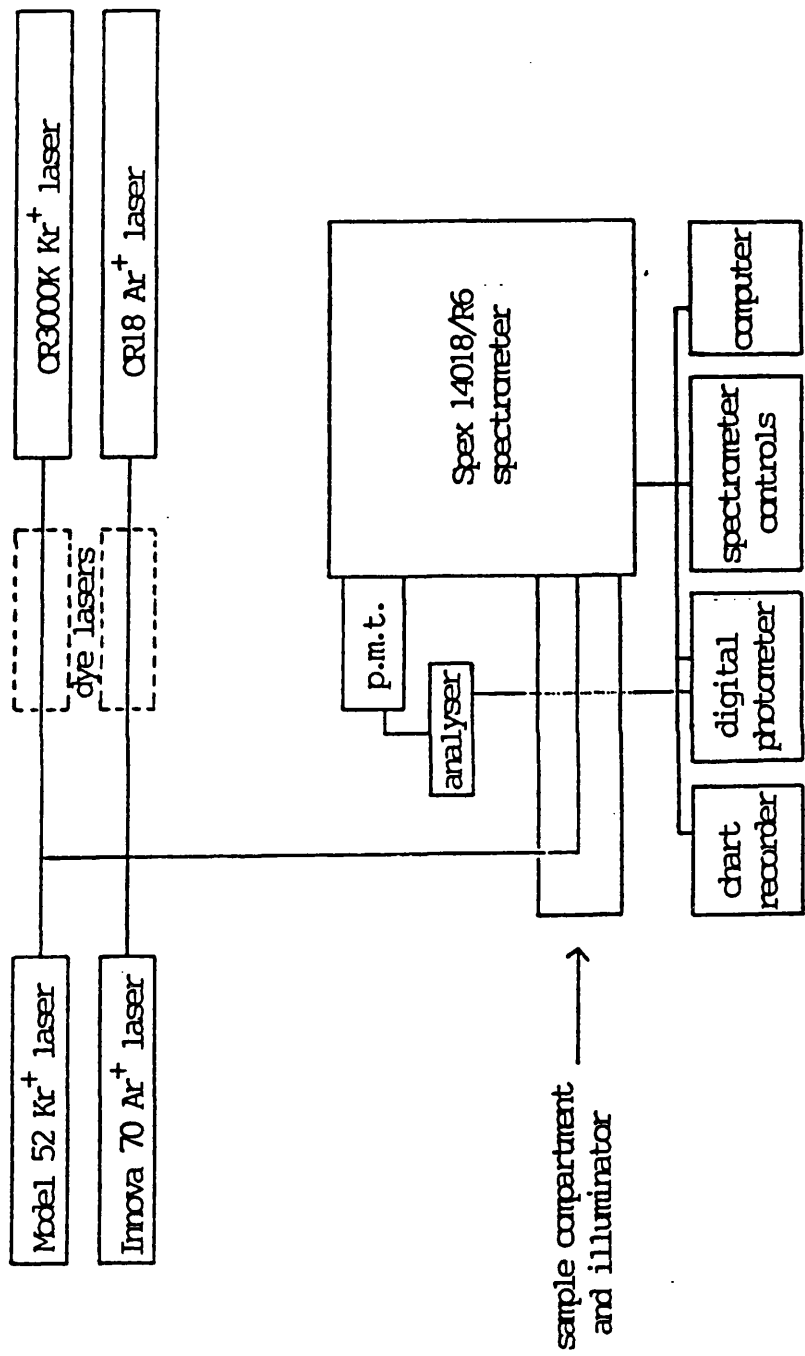


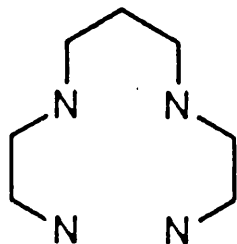
Figure 9. Plan of Raman instrumentation used.

III. HALOGEN-BRIDGED, MIXED-VALENCE COMPLEXES WITH QUADRIDENTATE LIGANDS

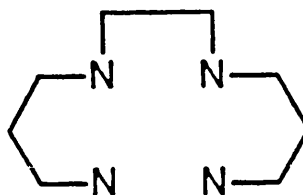
III.1. Complexes of Platinum with Chain Quadridentate Ligands

III.1.1. Introduction

The electronic and resonance Raman spectra were obtained of the series of complexes $[PtL][PtLX_2](ClO_4)_4$, where L = 3,7-diazanonane-1,9-diamine (henceforth referred to as 2,3,2-tet) or 4,7-diazadecane-1,10-diamine (henceforth referred to as 3,2,3-tet) and X = Cl, Br or I. The ligands L are illustrated below.



2,3,2-tet



3,2,3-tet

The general structure of these complexes is as described previously; they are of the +2 charge linear chain type and are believed to display the macrocycle-type hydrogen bonding structure (see Figure 2). They were prepared by Dr. M. Yamashita according to methods described in Appendix III. Electronic spectra were recorded at room temperature by transmission through pressed discs (X = Cl, Br) and by reflectance from powder (X = I), as described in Appendix II. Resonance Raman spectra were recorded from pressed discs at 80 K as described in Section II.

III.1.2. Results and discussion

These complexes show the expected dichroism. In the case of the powdered complexes, for light with its electric vector parallel to the chain axis, the chloride-bridged

complexes appear yellow or orange, the bromide-bridged complexes blue and the iodide-bridged complexes grey. As larger crystals, the bromide-bridged complexes are a lustrous green and the iodide-bridged complexes are metallic gold (transmitting, respectively, dark green to pale brown and brown-black to pale brown in polarised light). The electronic spectra are shown in Figure 10. and IVCT band maxima are given in Table 3. They show that, while there is little or no change in the IVCT maximum wavenumber with change of equatorial ligand (taking into account possible variations with particle size of the sample), there is an increase in wavenumber with change in halogen bridge in the order $I^- < Br^- < Cl^-$. This trend parallels the decrease in the degree of valence delocalisation on the metal atom sites, i.e. increased Peierls distortion from the III/III state to the II/IV state, which is reflected, in general for halogen-bridged mixed-valence complexes, in the ratio of the metal-halogen distances $r(M^{IV-X})/r(M^{II-X})$; these decrease, for constant M, from iodide to bromide to chloride.^{9,17,61,68,86,92,98}

Resonance Raman spectra are shown in Figures 11-16. Each spectrum is dominated by a long overtone progression $\nu_1\nu_1$, assigned to the symmetric $(X-Pt^{IV}-X)$ stretch, extending to $\nu_1=12$ for $X=Cl$, $\nu_1=9$ for $X=Br$ and $\nu_1=5$ for $X=I$. Measured values of ν_1 , $\nu_1(\max)$ and $I(2\nu_1)/I(\nu_1)$ and calculated values of harmonic wavenumber ω_1 and anharmonicity x_{11} are given in Table 3, while a full list of wavenumbers and assignments is given in Table 4. This shows that some further weak progressions $\nu_i+\nu_1\nu_1$ occur in some cases, where ν_i is an enabling mode, e.g. the $(N-Pt-N)$ bend at approximately 210-215 cm^{-1} , and ν_1 is the progression forming mode. The wavenumbers of ν_1 , at 313, 178.5 and 120 cm^{-1} for $X = Cl, Br$ and I , respectively ($L = 2,3,2$ -tet) are fairly typical of those observed for halogen-bridged mixed-valence complexes of platinum.⁶¹ The appearance of progressions involving ν_i indicates that the electron-phonon

interaction is not exclusively between the IVCT band and the symmetric (X-Pt^{IV}-X) stretch vibration. Nevertheless a clear relationship is shown between the electronic and the resonance Raman spectra, demonstrated with the change of X. An increase of valence delocalisation on going from Cl⁻ to Br⁻ to I⁻ occurs, which allows a lesser Peierls distortion, with a correspondingly smaller electron-phonon interaction; hence the degree of resonance enhancement decreases on going from Cl⁻ to Br⁻ to I⁻. An excitation profile for [Pt-2,3,2-tet-Cl-ClO₄] is shown in Figure 17, which indicates a maximum at approximately 22200 cm⁻¹ (approx. 450 nm). This is, as expected, at lower wavenumber than the maximum, at approx. 25000 cm⁻¹, in the electronic spectrum, probably occurring^{99,100} at a point determined by the combination of the chain length distribution and absorption edge energy factors.

Table 3

Summary of optical results from platinum complexes with linear quadridentate ligands

Complex	Crystal colour	Powder colour	λ_{max}^* nm	λ_{inf}' nm	ν_1 (max)	ω_1 cm ⁻¹	χ_1 cm	$I(2\nu_1)/I(\nu_1)$
[Pt(2,3,2-tet)][Pt(2,3,2-tet)Cl ₂] (ClO ₄) ₄	Yellow	Yellow	400 ± 20	488.0	10	315.8 ± 0.5	-1.43 ± 0.05	0.22
[Pt(3,2,3-tet)][Pt(3,2,3-tet)Cl ₂] (ClO ₄) ₄	Orange	Yellow	400 ± 20	488.0	12	315.2 ± 0.5	-1.23 ± 0.05	0.28
[Pt(2,3,2-tet)][Pt(2,3,2-tet)Br ₂] (ClO ₄) ₄	Green	Blue	545 ± 10	488.0	9	179.3 ± 0.5	-0.39 ± 0.05	0.25
[Pt(3,2,3-tet)][Pt(3,2,3-tet)Br ₂] (ClO ₄) ₄	Green	Blue	570 ± 10	488.0	9	181.5 ± 0.5	-0.58 ± 0.05	0.30
[Pt(2,3,2-tet)][Pt(2,3,2-tet)I ₂] (ClO ₄) ₄	Gold-brown	Grey	755 ± 20	676.4	5	121.9 ± 0.5	-1.09 ± 0.05	0.19
[Pt(3,2,3-tet)][Pt(3,2,3-tet)I ₂] (ClO ₄) ₄	Brown	Grey	740 ± 20	676.4	4	120.8 ± 0.5	-0.70 ± 0.05	0.23

* The spectra were obtained by transmission from a pressed disc using the corresponding alkali halide matrix, except for the iodide-bridged complexes, for which they were obtained by reflectance from a sample/KClO₄ powder.

Table 4. Wavenumbers $\tilde{\nu}$, relative intensities $I(\tilde{\nu})/I(\nu_1)$, full widths at half maximum $\Delta\tilde{\nu}_{1/2}$ and assignments of bands in the resonance Raman spectra of $[\text{PtL}][\text{PtLX}_2](\text{ClO}_4)_4$, where L = 2,3,2-tet or 3,2,3-tet and X = Cl, Br or I (excitation wavelengths as specified in Table 3). $\nu_1 = \nu(\text{X-Pt}^{\text{IV-X}})_{\text{sym}}$ and $\nu_2 = \nu(\text{X-Pt}^{\text{IV-X}})_{\text{asym}}$.

$\tilde{\nu}/\text{cm}^{-1}$	$I(\tilde{\nu})/I(\nu_1)$	$\Delta\tilde{\nu}_{1/2}/\text{cm}^{-1}$	Assignment
(a) $[\text{Pt}(2,3,2\text{-tet})][\text{Pt}(2,3,2\text{-tet})\text{Cl}_2](\text{ClO}_4)_4$			
182	0.03	9	
212	0.06	8	$\delta(\text{N-Pt-N})$
226	0.03	9	
313	1.00	13	ν_1
348.5	0.04	8	ν_2
398.5	< 0.01	8	
422.5	< 0.01	11	
490.5	< 0.01	8	
503.5	< 0.01	10	
540.5	0.01	11	
624	0.22	31	$2\nu_1$
657	< 0.01	11	$\nu_1 + \nu_2$
931	0.08	50	$3\nu_1$
1109	< 0.01	11	
1232	0.04	61	$4\nu_1$
1402	< 0.01	11	
1535	0.02	85	$5\nu_1$
1833.5	< 0.01	> 100	$6\nu_1$
2132	< 0.01	> 100	$7\nu_1$
2428	< 0.01	> 100	$8\nu_1$
2708	< 0.01	> 100	$9\nu_1$
2985	< 0.01	> 100	$10\nu_1$
(b) $[\text{Pt}(3,2,3\text{-tet})][\text{Pt}(3,2,3\text{-tet})\text{Cl}_2](\text{ClO}_4)_4$			
152	< 0.01	8	
172.5	< 0.01	6	
215.5	0.01	8	
267	< 0.01	8	

Table 4 continued.

$\tilde{\nu}/\text{cm}^{-1}$	$I(\tilde{\nu})/I(\nu_1)$	$\Delta\tilde{\nu}_{\frac{1}{2}}/\text{cm}^{-1}$	Assignment
(b) [Pt(3,2,3-tet)][Pt(3,2,3-tet)Cl ₂](ClO ₄) ₄ continued.			
312.5	1.00	11.5	ν_1
347.5	0.01	8	ν_2
380.5	< 0.01	3	
395	< 0.01	6	
408.5	< 0.01	6	
537	0.01	8	$\nu_1 + \delta(\text{N-Pt-N})$
623.5	0.28	23	$2\nu_1$
657	< 0.01	15	$\nu_1 + \nu_2$
849.5	< 0.01	15	$2\nu_1 + \delta(\text{N-Pt-N})$
931	0.12	35	$3\nu_1$
1108	< 0.01	11	
1237	0.07	42	$4\nu_1$
1333	< 0.01	8	
1414	< 0.01	8	
1541	0.04	69	$5\nu_1$
1643	< 0.01	11	
1727	< 0.01	15	
1840	0.02	85	$6\nu_1$
1952	< 0.01	15	
2040	< 0.01	12	
2140	0.01	100	$7\nu_1$
2432	< 0.01	> 100	$8\nu_1$
2728	< 0.01	> 100	$9\nu_1$
3016	< 0.01	> 100	$10\nu_1$
3288	< 0.01	> 100	$11\nu_1$
3572	< 0.01	> 100	$12\nu_1$

(c) [Pt(2,3,2-tet)][Pt(2,3,2-tet)Br₂](ClO₄)₄

178.5	1.00	11.8	ν_1
210.5	0.05	7	$\delta(\text{N-Pt-N})$
242	0.02	7	
304	< 0.01	7	
328.5	0.01	7	
356.5	0.25	23	$2\nu_1$

Table 4 continued.

$\tilde{\nu}/\text{cm}^{-1}$	$I(\tilde{\nu})/I(\nu_1)$	$\Delta\tilde{\nu}_{\frac{1}{2}}/\text{cm}^{-1}$	Assignment
(c) [Pt(2,3,2-tet)][Pt(2,3,2-tet)Br ₂](ClO ₄) ₄ contd.			
388	0.01	10	$\nu_1 + \delta(\text{N-Pt-N})$
533.5	0.09	35	$3\nu_1$
593.5	< 0.01	6	
709.5	0.03	59	$4\nu_1$
882.5	0.02	72	$5\nu_1$
1054	< 0.01	85	$6\nu_1$
1236	< 0.01	-	$7\nu_1$
1304	< 0.01	10	
1402	< 0.01	-	$8\nu_1$
1580	< 0.01	-	$9\nu_1$
(d) [Pt(3,2,3-tet)][Pt(3,2,3-tet)Br ₂](ClO ₄) ₄			
180.5	1.00	18	ν_1
232	< 0.01	4	
359.5	0.30	37	$2\nu_1$
410	< 0.01	3	
536	0.11	53	$3\nu_1$
711	0.05	67	$4\nu_1$
889	0.02	83	$5\nu_1$
1069	0.01	> 100	$6\nu_1$
1241	< 0.01	> 100	$7\nu_1$
1333	< 0.01	6	
1411	< 0.01	> 100	$8\nu_1$
1515	< 0.01	10	
1593	< 0.01	> 100	$9\nu_1$
(e) [Pt(2,3,2-tet)][Pt(2,3,2-tet)I ₂](ClO ₄) ₄			
120	1.00	16.6	ν_1
183	< 0.01	10	
237.5	0.19	33	$2\nu_1$
353	0.04	50	$3\nu_1$
467	< 0.01	75	$4\nu_1$
580	< 0.01	-	$5\nu_1$

Table 4 continued.

$\tilde{\nu}/\text{cm}^{-1}$	$I(\tilde{\nu})/I(\nu_1)$	$\Delta\tilde{\nu}_{\frac{1}{2}}/\text{cm}^{-1}$	Assignment
(f) [Pt(3,2,3-tet)][Pt(3,2,3-tet)I ₂](ClO ₄) ₄			
119.5	1.00	14.3	ν_1
238	0.23	28	$2\nu_1$
354.5	0.06	46	$3\nu_1$
468.5	0.02	65	$4\nu_1$

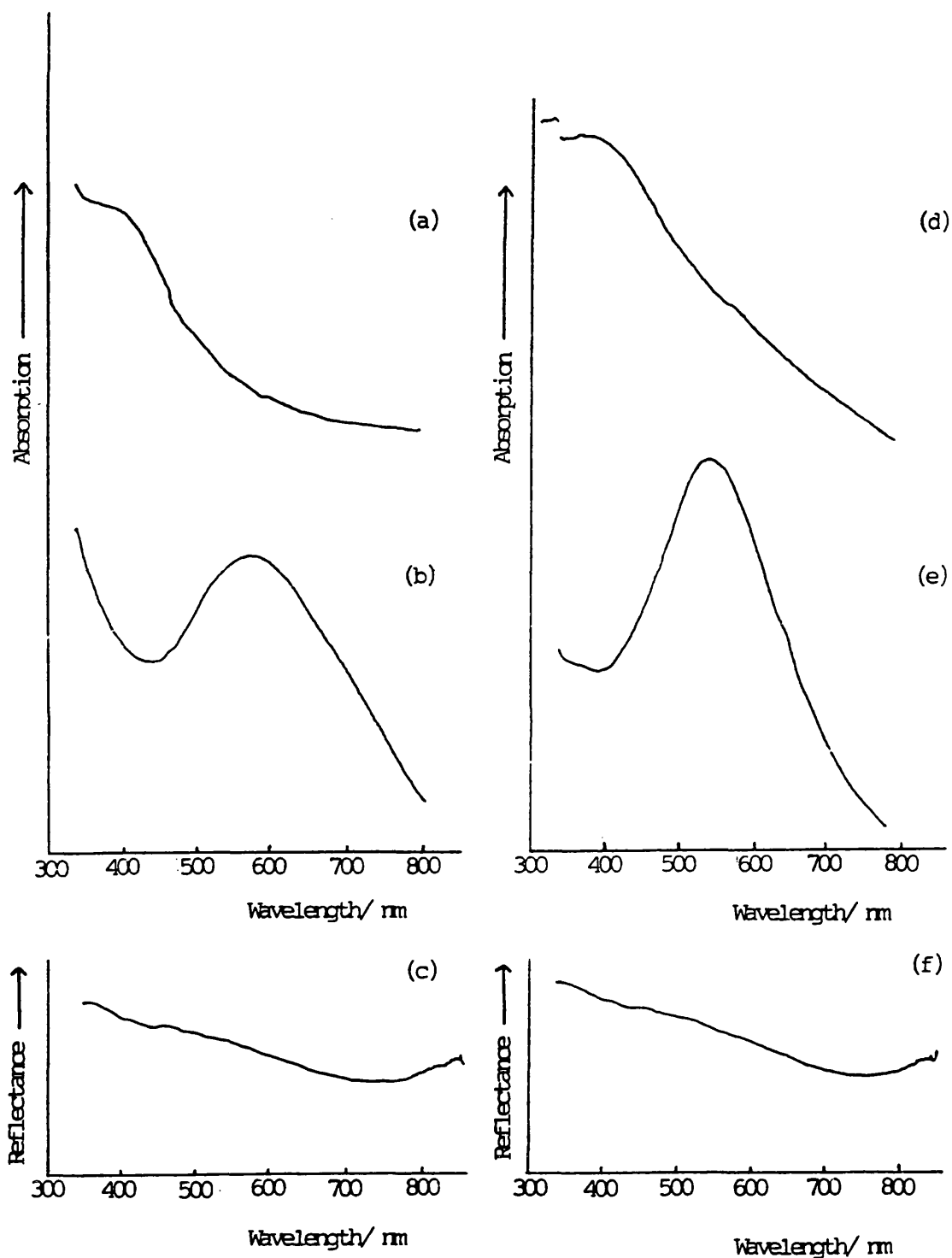


Figure 10. Electronic spectra of $[Pt-L-X-ClO_4]$, where $L = 2,3,2\text{-tet}$ and $X = Cl$ (a), Br (b) or I (c), or $L = 3,2,3\text{-tet}$ and $X = Cl$ (d), Br (e) or I (f). Obtained by transmission from a pressed disc using the corresponding alkali halide matrix ($X = Cl$ or Br) and by reflectance from a sample/ $KClO_4$ powder ($X = I$).

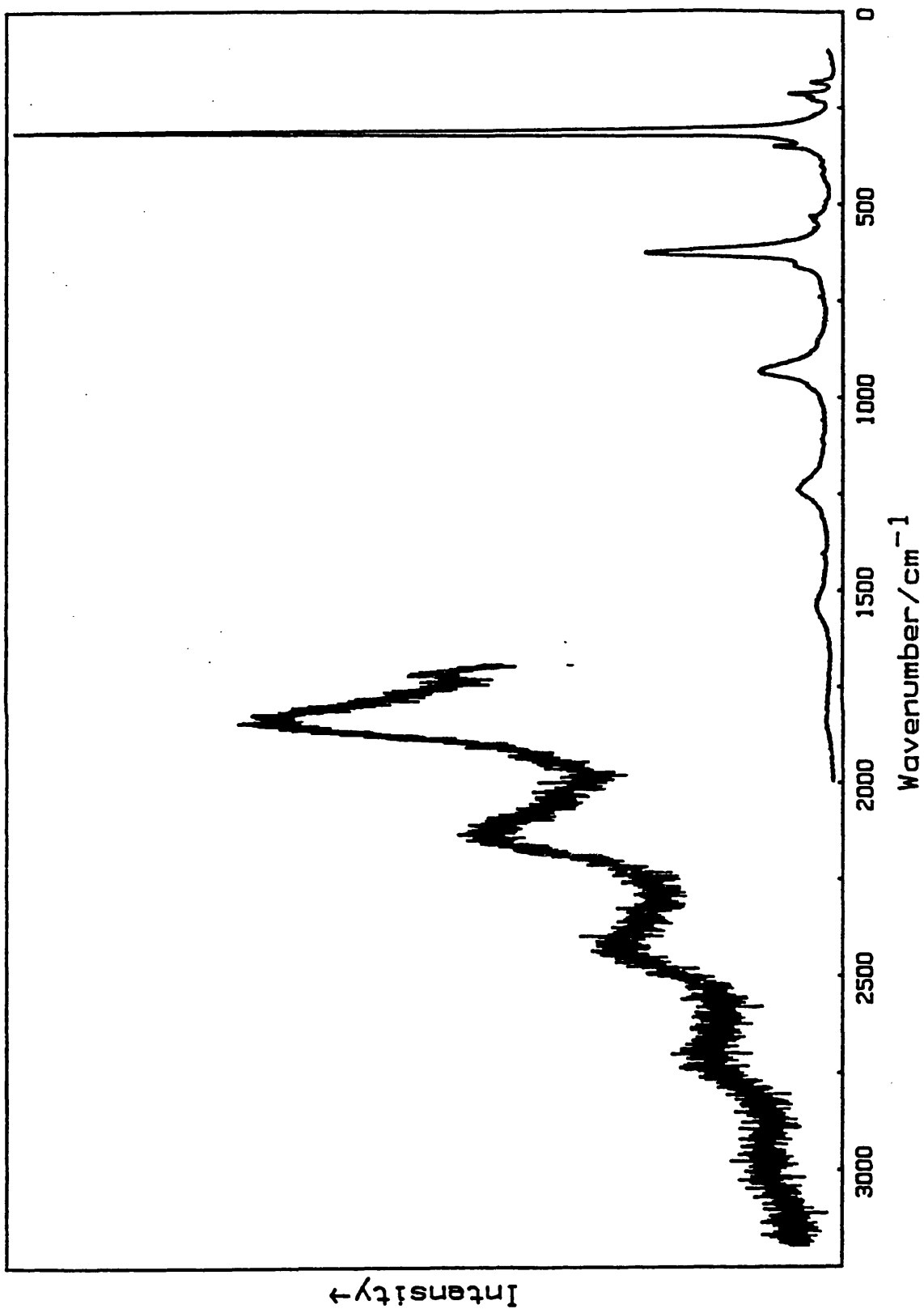


Figure 11. Resonance Raman spectrum of $[\text{Pt}(2,3,2\text{-tet})][\text{Pt}(2,3,2\text{-tet})\text{Cl}_2][\text{ClO}_4]_4$ (pure disc at ca. 80 K, $\lambda_0 = 488.0 \text{ nm}$).

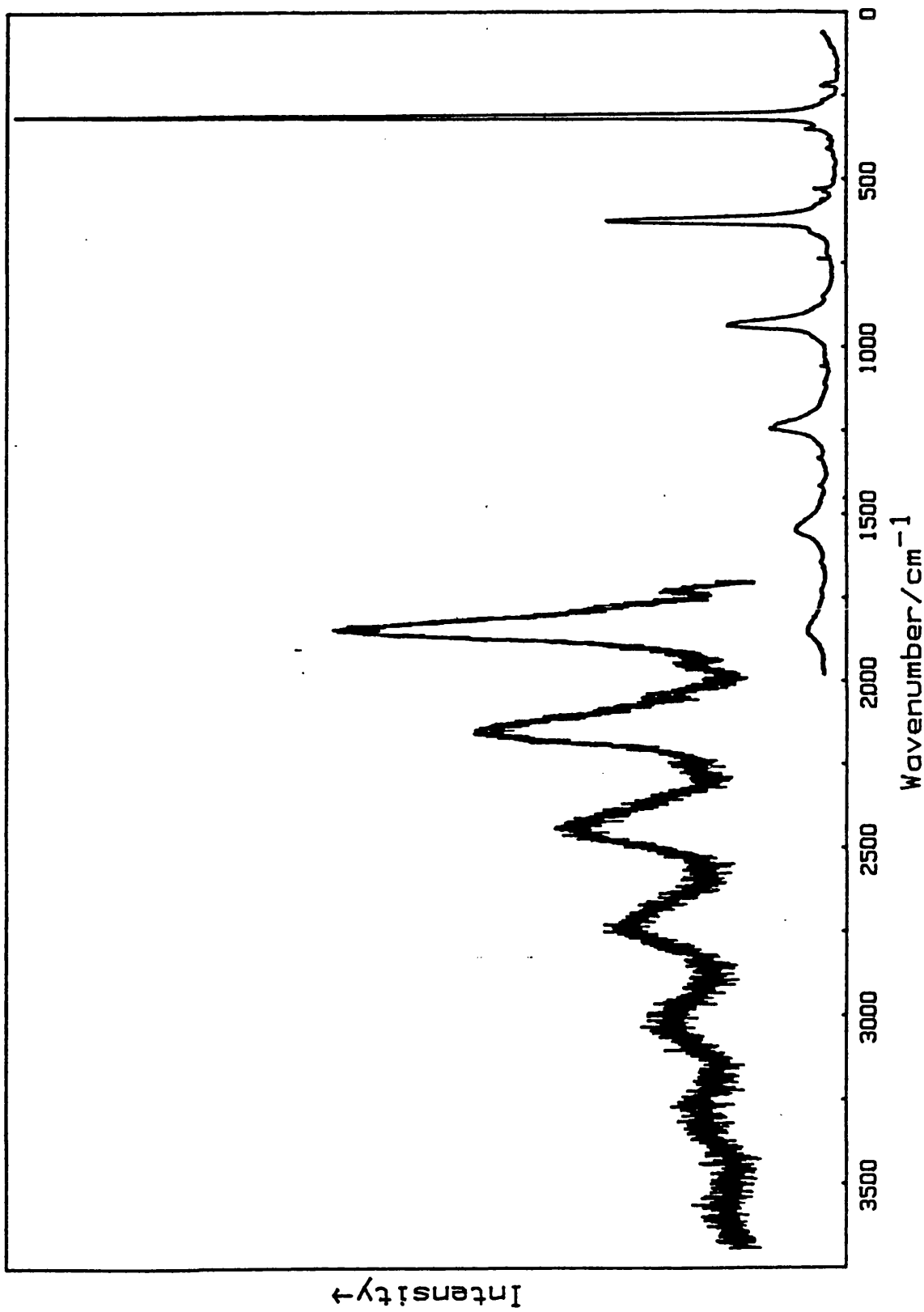


Figure 12. Resonance Raman spectrum of $[\text{Pt}(3,2,3\text{-tet})][\text{Pt}(3,2,3\text{-tet})\text{Cl}_2][\text{ClO}_4]_4$ (pure disc at ca. 80 K, $\lambda_0 = 488.0 \text{ nm}$).

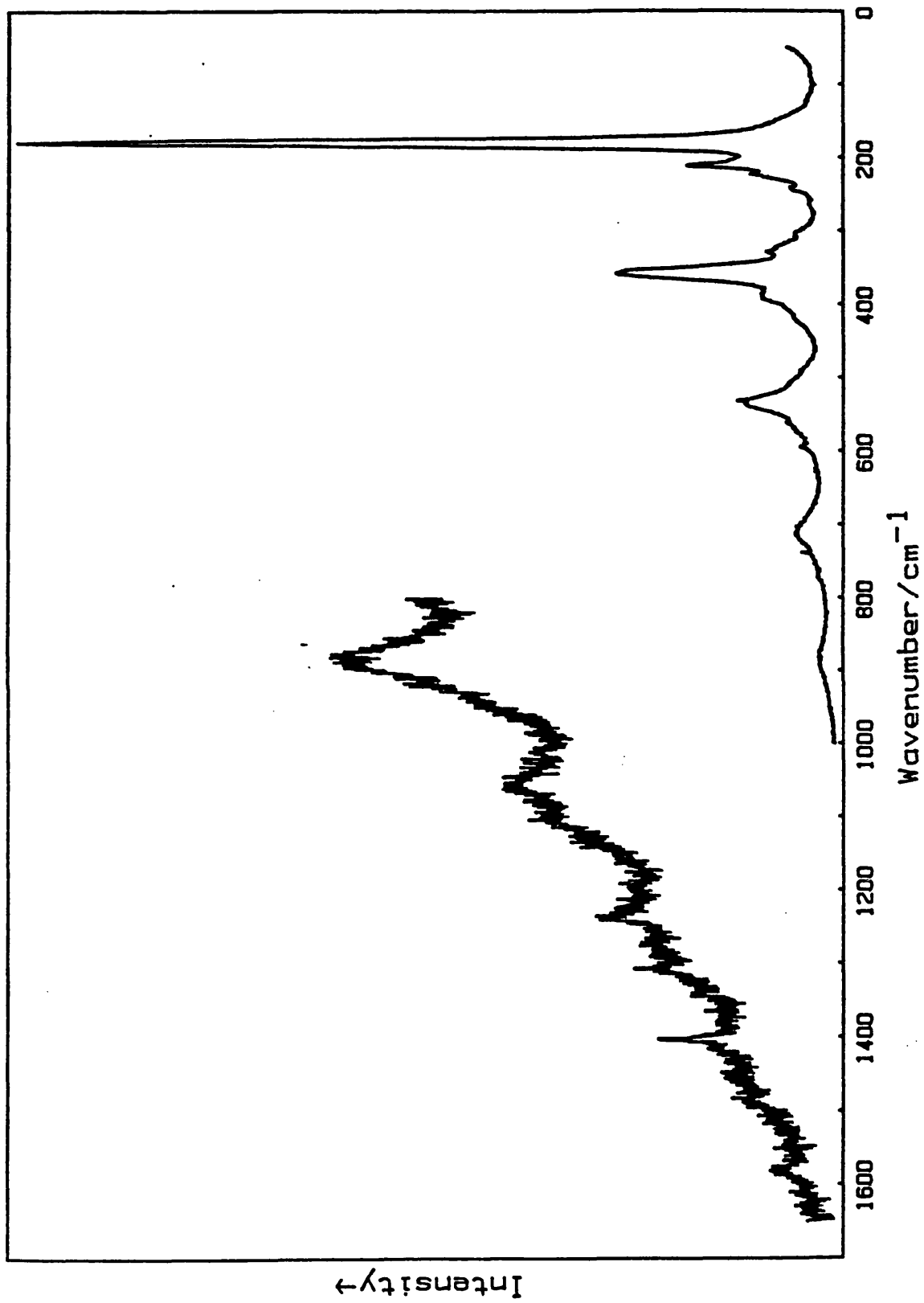


Figure 13. Resonance Raman spectrum of $[\text{Pt}(2,3,2\text{-tet})][\text{Pt}(2,3,2\text{-tet})\text{Br}_2][\text{ClO}_4]_4$ (pure disc at ca. 80 K, $\lambda_0 = 488.0 \text{ nm}$).

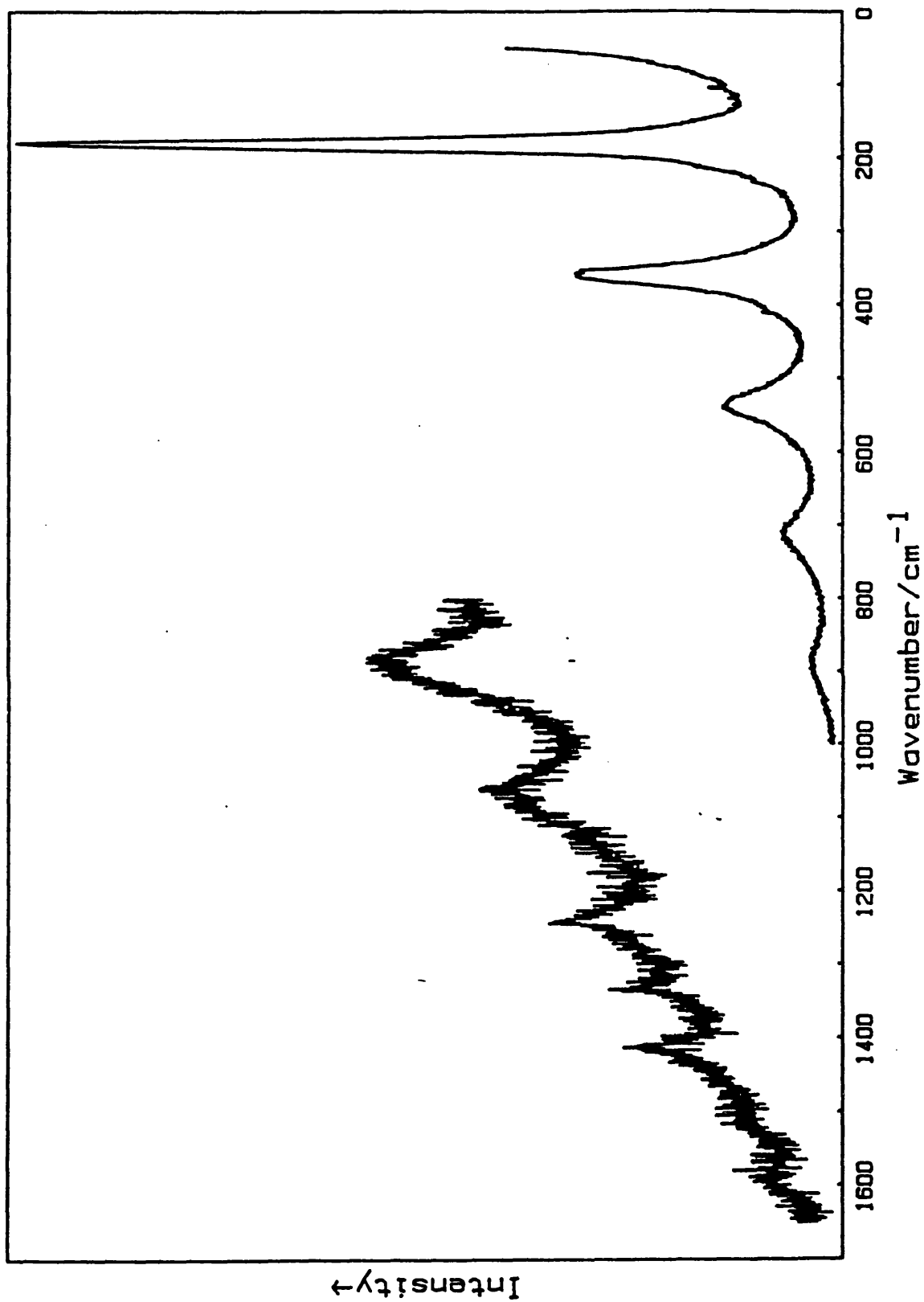


Figure 14. Resonance Raman spectrum of $[\text{Pt}(3,2,3\text{-tet})][\text{Pt}(3,2,3\text{-tet})\text{Br}_2][\text{ClO}_4]_4$ (pure disc at ca. 80 K, $\lambda_0 = 488.0 \text{ nm}$).

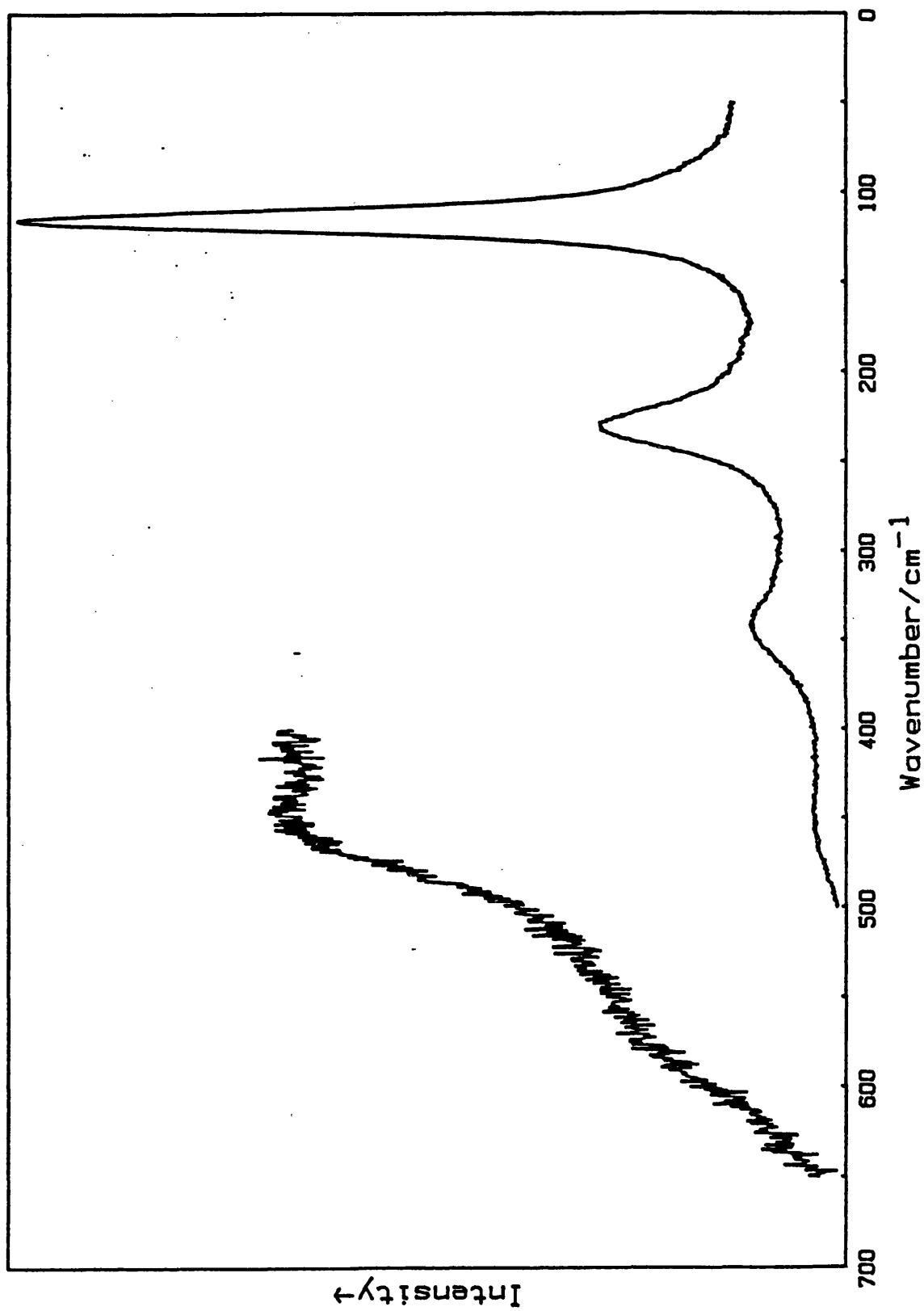


Figure 15. Resonance Raman spectrum of $[\text{Pt}(2,3,2\text{-tet})][\text{Pt}(2,3,2\text{-tet})\text{I}_2][\text{ClO}_4]_4$ (pure disc at ca. 80 K, $\lambda_0 = 676.4 \text{ nm}$).

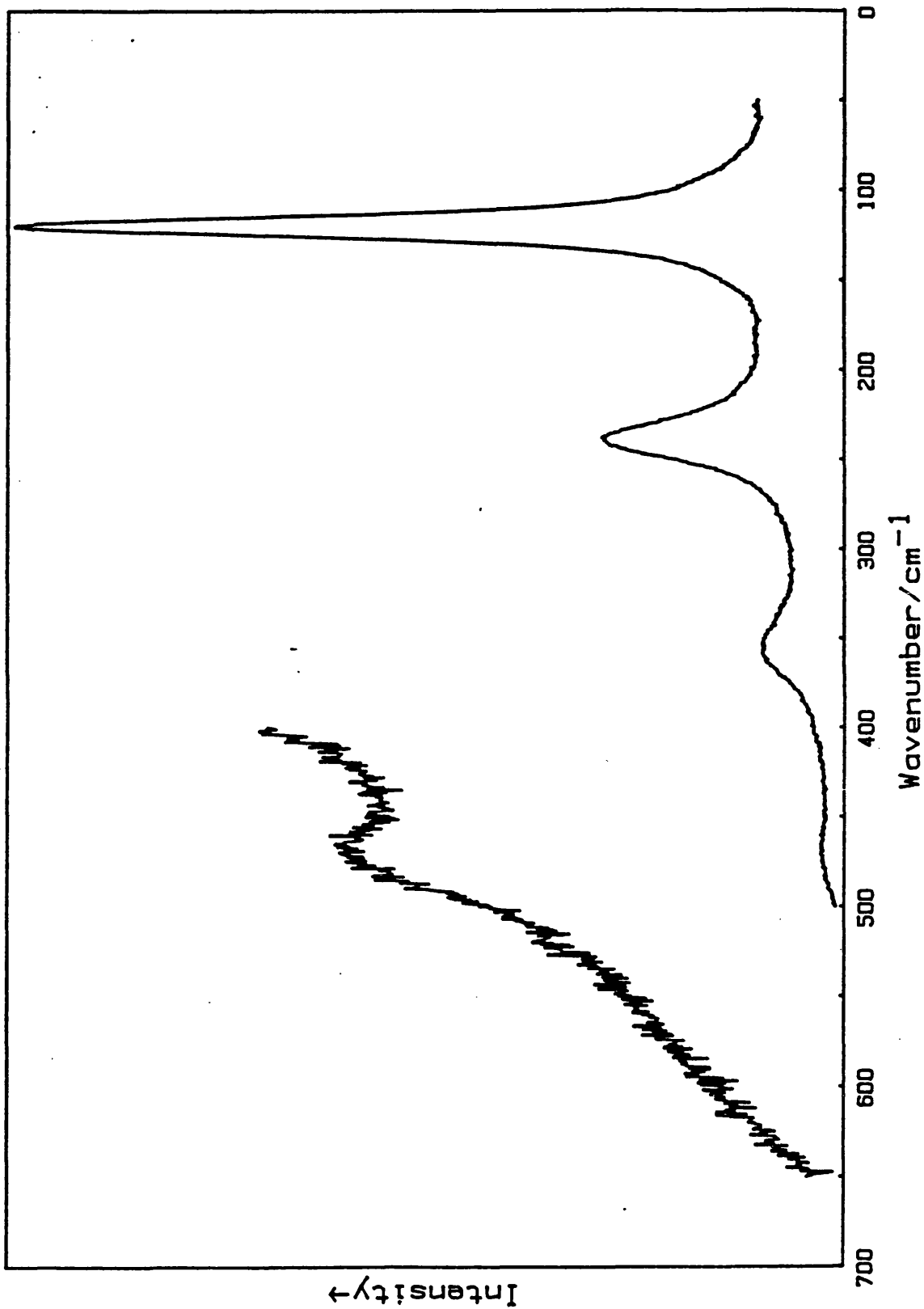


Figure 16. Resonance Raman spectrum of $[\text{Pt}(3,2,3\text{-tet})][\text{Pt}(3,2,3\text{-tet})\text{I}_2][\text{ClO}_4]_4$ (pure disc at ca. 80 K, $\lambda_0 = 676.4 \text{ nm}$).

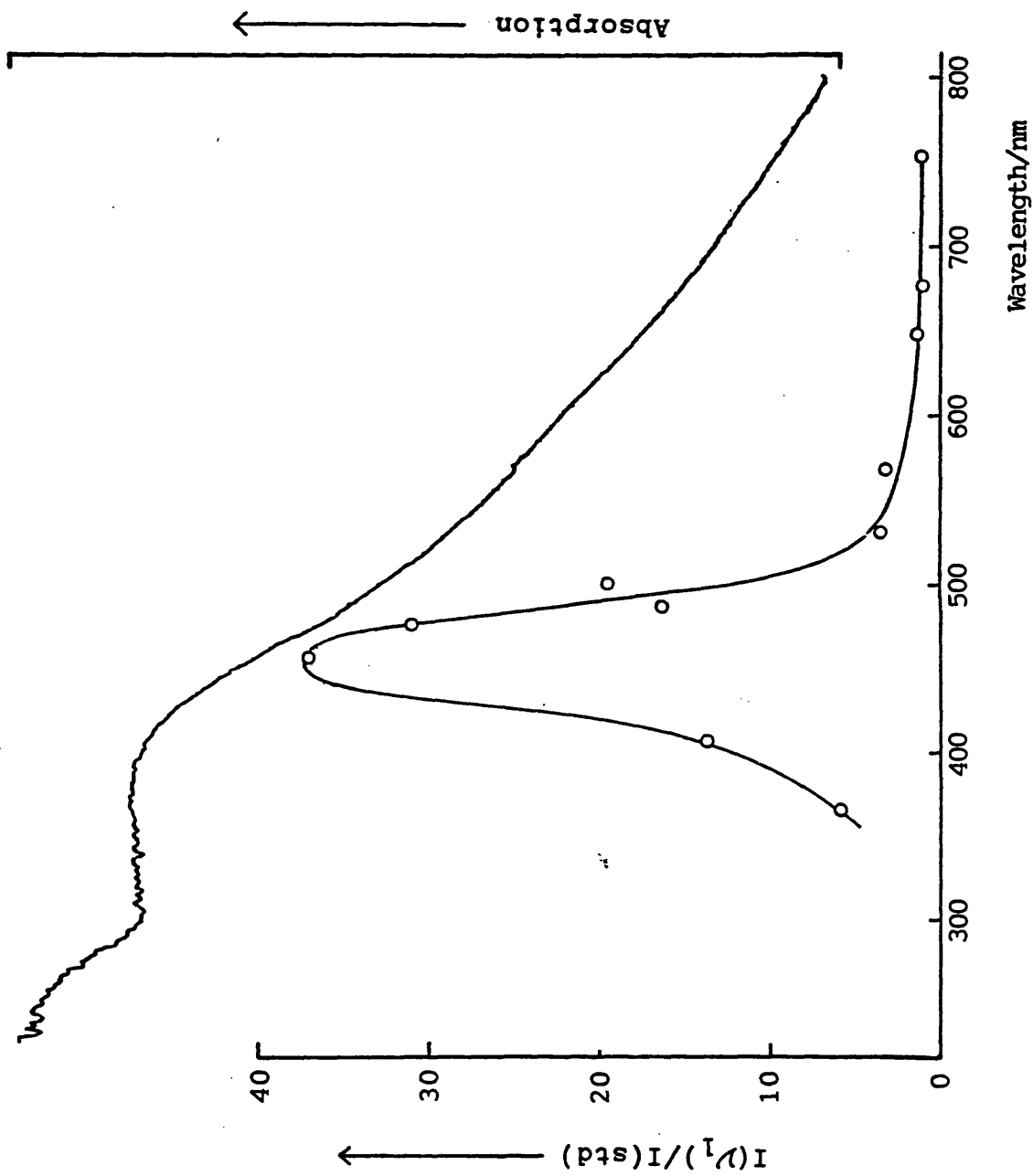


Figure 17. Excitation profile of the ν_1 band of $[\text{Pt}(2,3,2\text{-tet})][\text{Pt}(2,3,2\text{-tet})\text{Cl}_2][\text{ClO}_4]_4$ (obtained from a sample/ KClO_4 disc at ca. 80 K) and transmission electronic spectrum of the same complex (sample/ NaCl disc at 295 K).

III.2. Complexes of Palladium with Chain Quadridentate Ligands

III.2.1. Introduction

The electronic and resonance Raman spectra were obtained of the series of complexes $[\text{PdL}][\text{PdLX}_2](\text{ClO}_4)_4$, where L = 3,7-diazanonane-1,9-diamine (= 2,3,2-tet) or 4,7-diazadecane-1,10-diamine (= 3,2,3-tet) and X = Cl or Br. The ligands L are illustrated in Section I.1.1.

These complexes have the expected linear-chain structure (+2 charge type) and are believed to display the macrocycle-type hydrogen bonding structure (Figure 2). They were prepared by Dr. M. Yamashita according to methods described in Appendix III. Electronic spectra were recorded at room temperature by transmission through pressed discs, as described in Appendix II. Raman/resonance Raman spectra were recorded from pressed discs at 40-80 K as described in Section II.

III.2.2. Results and discussion

The complexes show strong dichroism. Unground, the Cl-bridged complexes are lustrous green (dark green to pale brown in transmitted polarised light), while the Br-bridged complexes are (metallic) golden brown (brown-black to pale brown in transmitted polarised light). When ground to powder the Cl-bridged complexes turn violet and the Br-bridged complexes blue. Electronic spectra are shown in Figure 18 and IVCT band maxima are given in Table 5. As with the analogous Pt complexes, there is no significant difference between results for the two ligands 2,3,2-tet and 3,2,3-tet. However, it is worthwhile to compare the two chloride-bridged cases, $[\text{Pd-2,3,2-tet-Cl-ClO}_4]$ and $[\text{Pd-3,2,3-tet-Cl-ClO}_4]$, with a previously investigated complex $[\text{Pd-en-Cl-ClO}_4]$, for which an IVCT band maximum at $17,800 \text{ cm}^{-1}$ (562 nm) was determined.¹² This is significantly lower than λ_{max} at approximately 20,000

cm⁻¹ (approx. 500 nm) for the currently investigated complexes and may be explained as follows. It has been observed crystallographically²⁸⁻³⁰, that the fewer the hydrogen bonds formed between the diamine hydrogen atoms and the anions alongside the linear chains, the longer is the M^{II}...M^{IV} distance and in consequence (owing to the near constancy of the M^{IV}-X distances) the smaller is the $r(M^{IV}-X)/r(M^{II}-X)$ bond distance ratio. Thus it may be concluded that linear chain complexes with quadridentate ligands, hence fewer hydrogen bonds, have the more localised valences and a higher energy IVCT band. This conclusion is borne out by the comparison of IVCT band maxima above. Further verification of the difference in valence localisation comes from Raman spectroscopy, as shown below.

Resonance Raman spectra of the investigated complexes are shown in Figures 19-22. Each spectrum is dominated by the overtone progression $\nu_1 \nu_1$, extending to $\nu_1=9$ for X=Cl and $\nu_1=4$ for X=Br. Measured values of ν_1 , $\nu_1(\max)$ and $I(2\nu_1)/I(\nu_1)$ and calculated values of harmonic wavenumber ω_1 and anharmonicity x_{11} are given in Table 5, while a full list of wavenumbers and assignments is given in Table 6. This also shows the presence of much weaker progressions $\nu_i + \nu_1 \nu_1$, where ν_i is, for example, ν_2 , the asymmetric (X-Pd^{IV}-X) stretch vibration. As for the analogous Pt complexes, increased valence delocalisation occurs on going from X=Cl to X=Br, with corresponding decreasing electron-phonon interaction and resonance enhancement.^{9,17,61,68,86,92,98}

The ν_1 values for [Pd-2,3,2-tet-Cl-ClO₄] and [Pd-3,2,3-tet-Cl-ClO₄] of 278.0 and 280.4 cm⁻¹ respectively are significantly higher than ν_1 found¹² for [Pd-en-Cl-ClO₄] at 272 cm⁻¹. This result, like that of the higher energy IVCT maxima with quadridentate ligands, is consistent with the greater localisation of the valences for such complexes.

Table 5

Summary of optical results from palladium complexes with linear quadridentate ligands

Complex	Crystal colour	Powder colour	λ_{max}^* / nm	λ_0 / nm	ν_1 / cm^{-1}	ν_1 (max) / cm^{-1}	ω_1 / cm^{-1}	x_{11} / cm^{-1}	$I(2\nu_1) / I(\nu_1)$
[Pd(2,3,2-tet)] [Pd(2,3,2-tet)Cl ₂] (ClO ₄) ₄	Green	Violet	500 ± 10	514.5	278.0	9	278.8 ± 0.5	-0.28 ± 0.05	0.28
[Pd(3,2,3-tet)] [Pd(3,2,3-tet)Cl ₂] (ClO ₄) ₄	Gold-green	Violet	500 ± 10	514.5	280.4	7	281.4 ± 0.5	-0.4 ± 0.1	0.26
[Pd(2,3,2-tet)] [Pd(2,3,2-tet)Br ₂] (ClO ₄) ₄	Gold-brown	Blue	555 ± 10	676.4	151.5	4	153 ± 1	-0.8 ± 0.2	0.20
[Pd(3,2,3-tet)] [Pd(3,2,3-tet)Br ₂] (ClO ₄) ₄	Gold-brown	Blue	560 ± 10	676.4	152.6	3	153 ± 1	-0.5 ± 0.5	0.24

* Spectra obtained by transmission from a pressed disc using the corresponding alkali halide matrix.

Table 6. Wavenumbers $\tilde{\nu}$, relative intensities $I(\tilde{\nu})/I(\nu_1)$, full widths at half maximum $\Delta\tilde{\nu}_{1/2}$ and assignments of bands in the resonance Raman spectra of $[\text{PdL}][\text{PdLX}_2](\text{ClO}_4)_4$, where L = 2,3,2-tet or 3,2,3-tet and X = Cl or Br (excitation wavelengths as specified in Table 5). $\nu_1 = \nu(\text{X-Pd}^{\text{IV}}\text{-X})_{\text{sym}}$ and $\nu_2 = \nu(\text{X-Pd}^{\text{IV}}\text{-X})_{\text{asym}}$.

$\tilde{\nu}/\text{cm}^{-1}$	$I(\tilde{\nu})/I(\nu_1)$	$\Delta\tilde{\nu}_{1/2}/\text{cm}^{-1}$	Assignment
(a) $[\text{Pd}(2,3,2\text{-tet})][\text{Pd}(2,3,2\text{-tet})\text{Cl}_2](\text{ClO}_4)_4$			
278	1.00	17.6	ν_1
347.6	0.02	6	ν_2
556.4	0.28	34	$2\nu_1$
628.4	0.01	14	$\nu_1 + \nu_2$
833.2	0.11	48	$3\nu_1$
908.4	< 0.01	12	$2\nu_1 + \nu_2$
1110	0.05	64	$4\nu_1$
1298	< 0.01	9	
1384	0.02	96	$5\nu_1$
1506	< 0.01	14	
1575	< 0.01	12	
1660	0.01	> 100	$6\nu_1$
1786	< 0.01	14	
1866	< 0.01	17	$6\nu_1 + \delta(\text{N-Pd-N})$
1941	< 0.01	> 100	$7\nu_1$
2146	< 0.01	14	$7\nu_1 + \delta(\text{N-Pd-N})$
2220	< 0.01	> 100	$8\nu_1$
2490	< 0.01	> 100	$9\nu_1$
(b) $[\text{Pd}(3,2,3\text{-tet})][\text{Pd}(3,2,3\text{-tet})\text{Cl}_2](\text{ClO}_4)_4$			
280.4	1.00	11.5	ν_1
390.8	0.02	6	
561.2	0.26	21.5	$2\nu_1$
839.6	0.09	31	$3\nu_1$
1115	0.03	46.2	$4\nu_1$
1324	< 0.01	18	$4\nu_1 + \delta(\text{N-Pd-N})$
1394	0.02	55	$5\nu_1$
1512	< 0.01	25	

Table 6 continued.

$\tilde{\nu}/\text{cm}^{-1}$	$I(\tilde{\nu})/I(\nu_1)$	$\Delta\tilde{\nu}_{1/2}/\text{cm}^{-1}$	Assignment
(b) $[\text{Pd}(3,2,3\text{-tet})][\text{Pd}(3,2,3\text{-tet})\text{Cl}_2](\text{ClO}_4)_4$ contd.			
1605	< 0.01	18	$5\nu_1 + \delta(\text{N-Pd-N})$
1682	0.01	70	$6\nu_1$
1788	< 0.01	25	
1884	< 0.01	18	$6\nu_1 + \delta(\text{N-Pd-N})$
1951	< 0.01		$7\nu_1$
(c) $[\text{Pd}(2,3,2\text{-tet})][\text{Pd}(2,3,2\text{-tet})\text{Br}_2](\text{ClO}_4)_4$			
151.5	1.00	18.3	ν_1
191.5	0.05	9	
227.5	0.01	4	
301.5	0.20	37	$2\nu_1$
349.5	< 0.01	4	
445.5	0.04	60	$3\nu_1$
517.5	< 0.01	4	
579.5	0.01	75	$4\nu_1$
621.5	0.01	6	
951.5	< 0.01	16	
1179	< 0.01	8	
(d) $[\text{Pd}(3,2,3\text{-tet})][\text{Pd}(3,2,3\text{-tet})\text{Br}_2](\text{ClO}_4)_4$			
152.6	1.00	21.2	ν_1
193.2	0.25	20	
264.6	0.07	6	
303.8	0.24	31	$2\nu_1$
350	0.04	12	
390.6	0.02	11	
459.2	0.06	52	$3\nu_1$

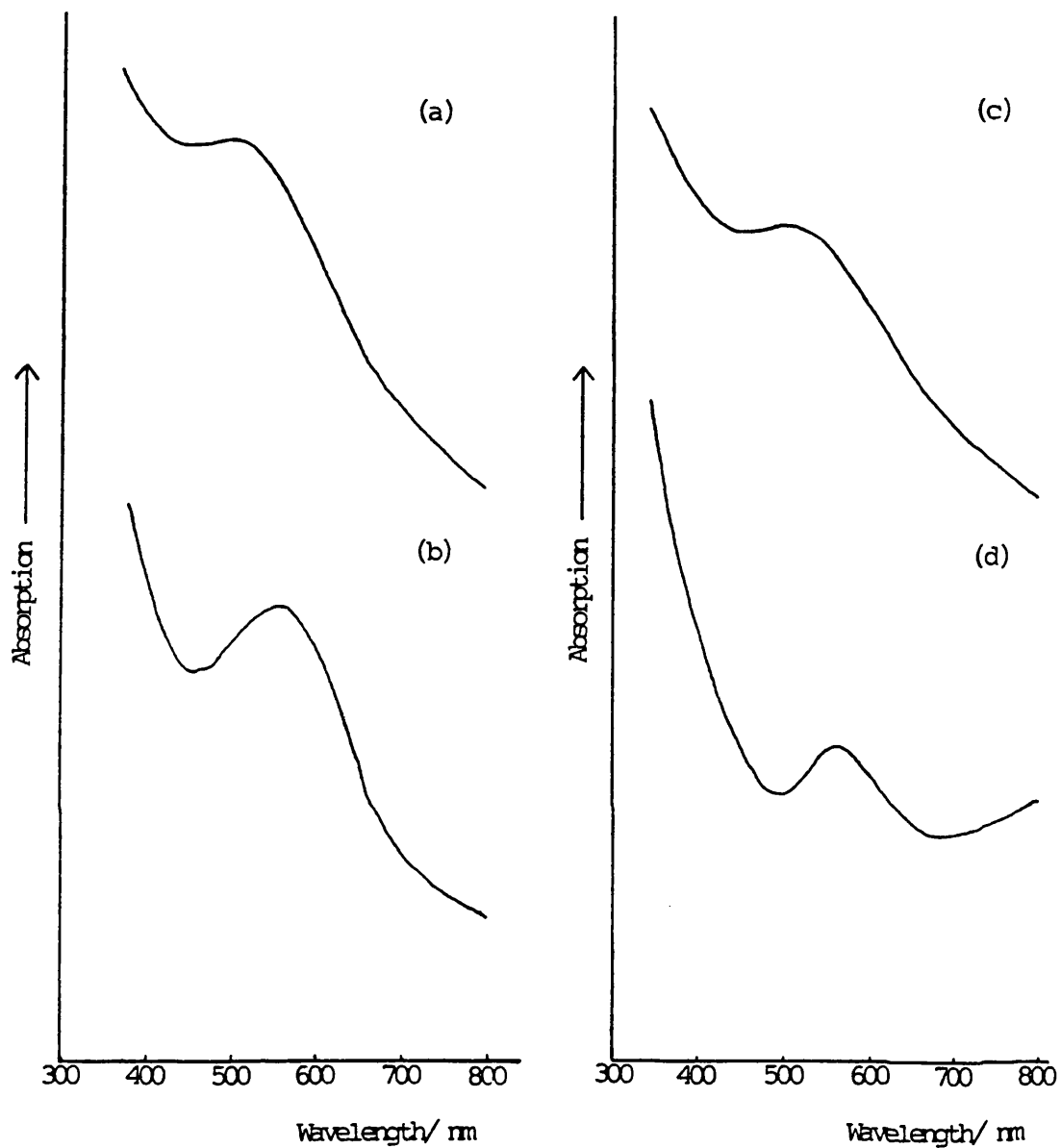


Figure 18. Electronic spectra of $[\text{Pd-L-X-ClO}_4]$, where L = 2,3,2-tet and X = Cl (a) or Br (b), or L = 3,2,3-tet and X = Cl (c) or Br (d). Obtained by transmission from a pressed disc using the corresponding alkali halide matrix.

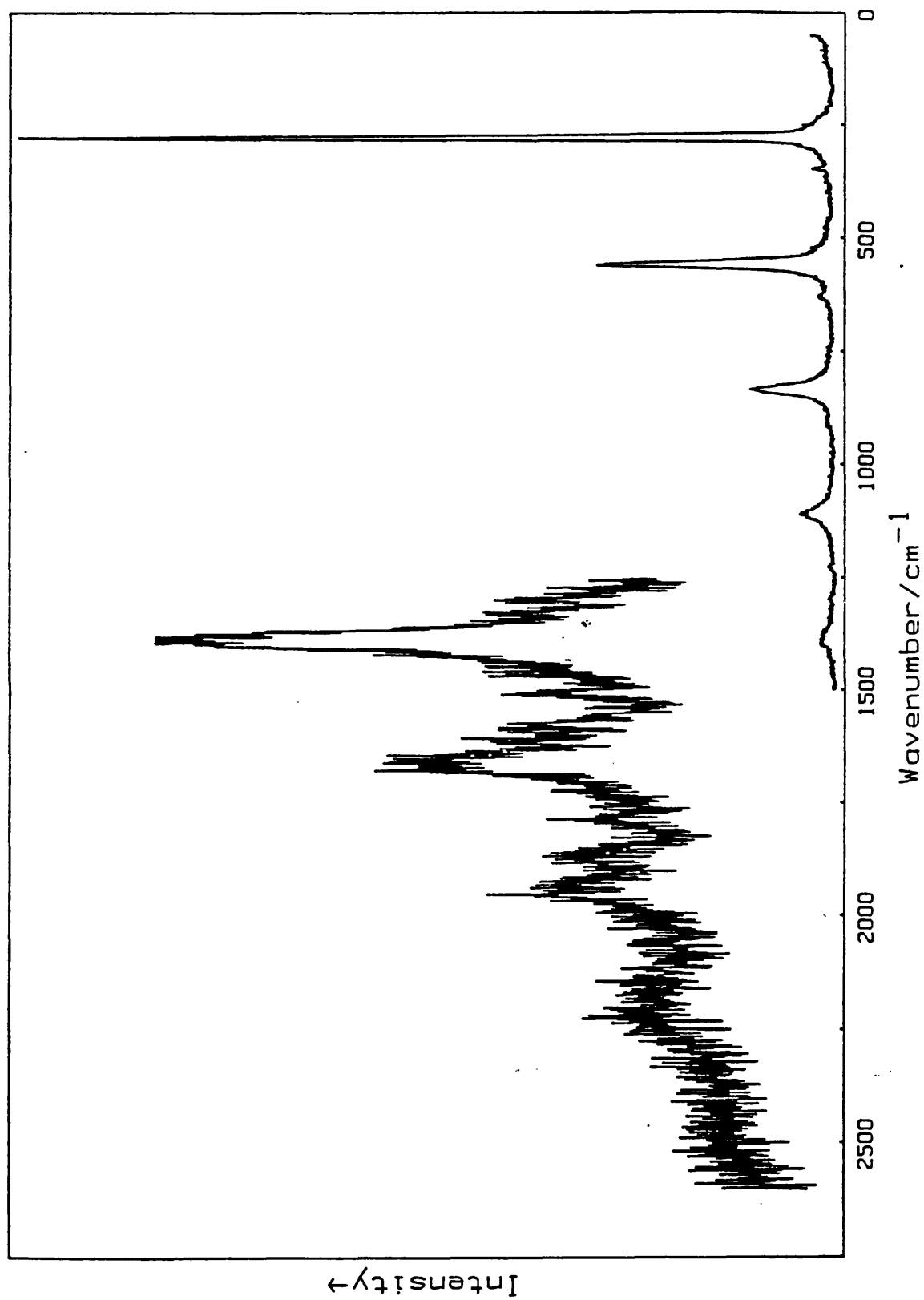


Figure 19. Resonance Raman spectrum of $[\text{Pd}(2,3,2\text{-tet})][\text{Pd}(2,3,2\text{-tet})\text{Cl}_2][\text{ClO}_4]_4$ (pure disc at ca. 80 K, $\lambda_0 = 514.5 \text{ nm}$).

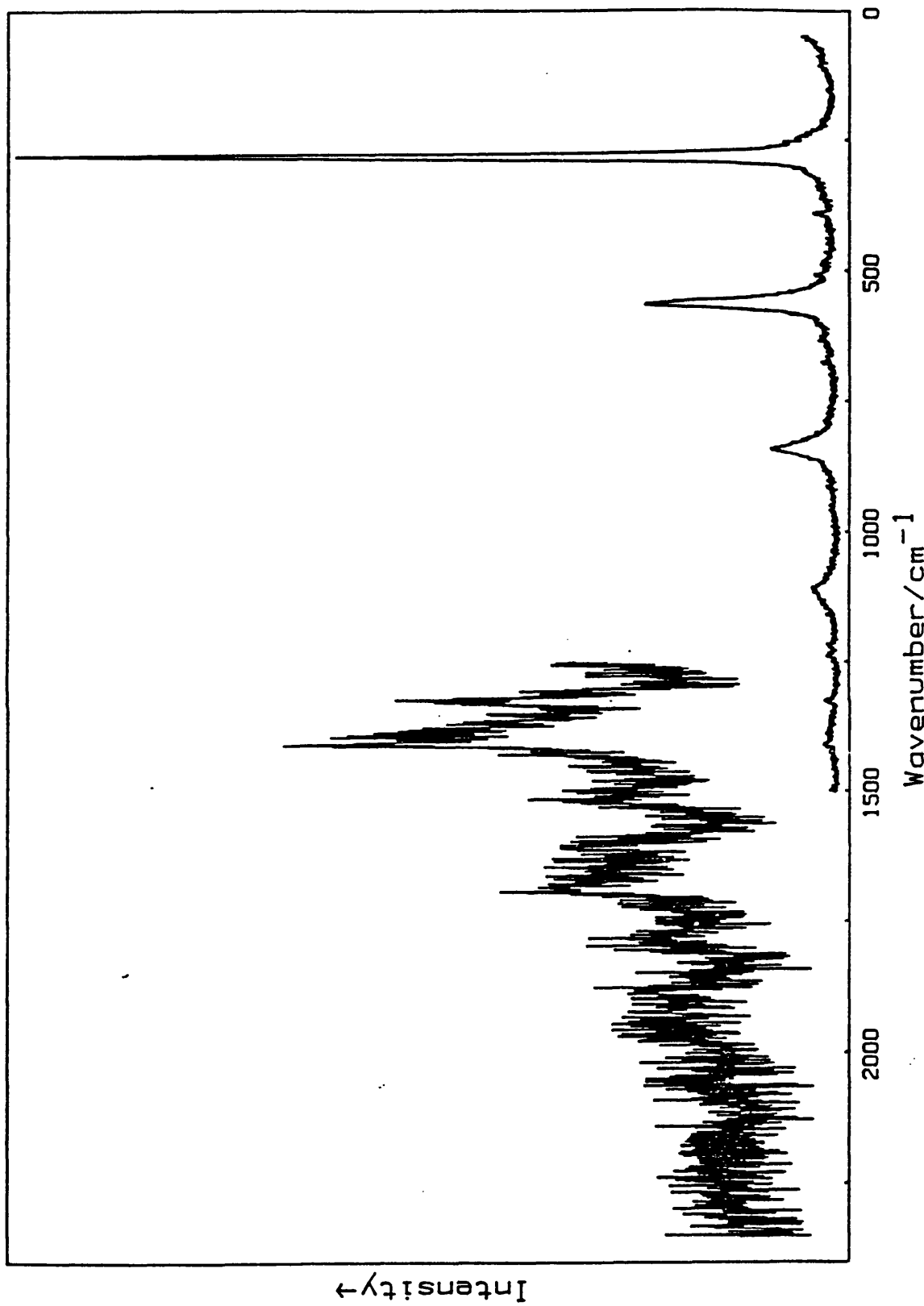


Figure 20. Resonance Raman spectrum of $[\text{Pd}(3,2,2,3\text{-tet})][\text{Pd}(3,2,2,3\text{-tet})\text{Cl}_2][\text{ClO}_4]_4$ (pure disc at ca. 80 K, $\lambda_0 = 514.5 \text{ nm}$).

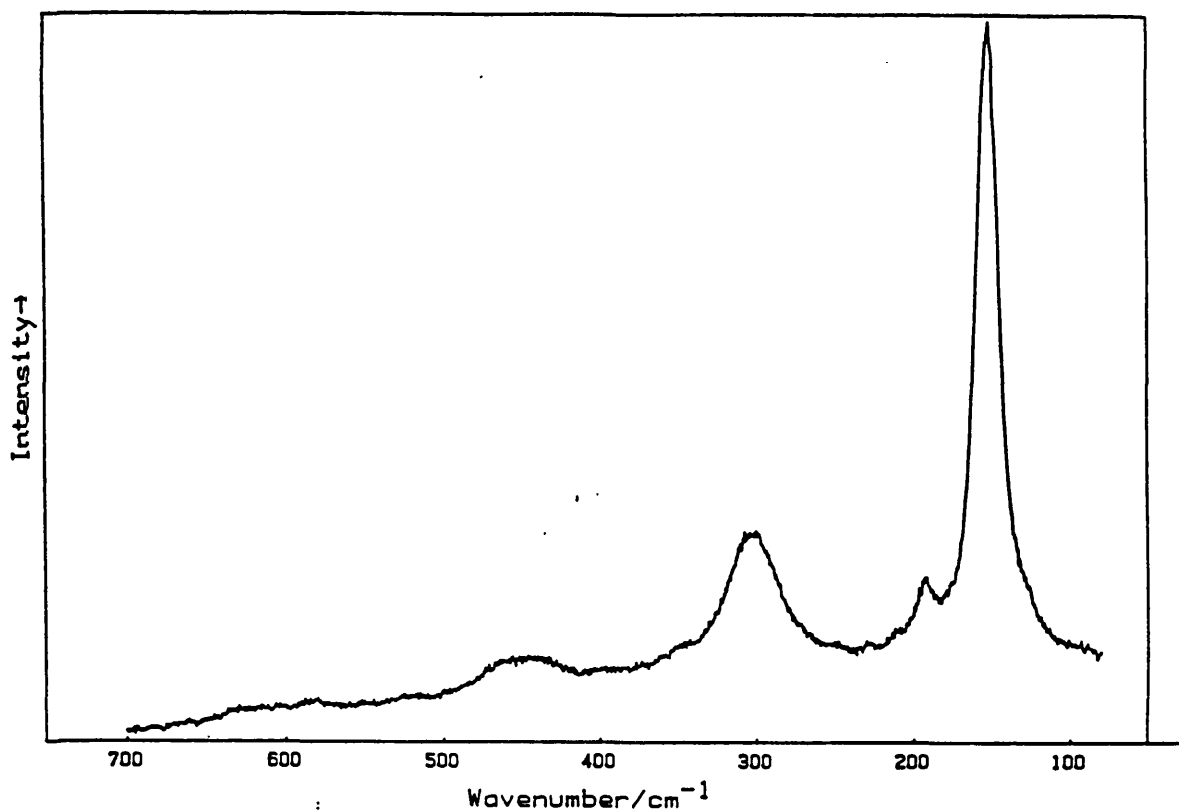


Figure 21. Resonance Raman spectrum of $[\text{Pd}(2,3,2\text{-tet})][\text{Pd}(2,3,2\text{-tet})\text{Br}_2][\text{ClO}_4]_4$ (pure disc at ca. 80 K, $\lambda_0 = 676.4$ nm).

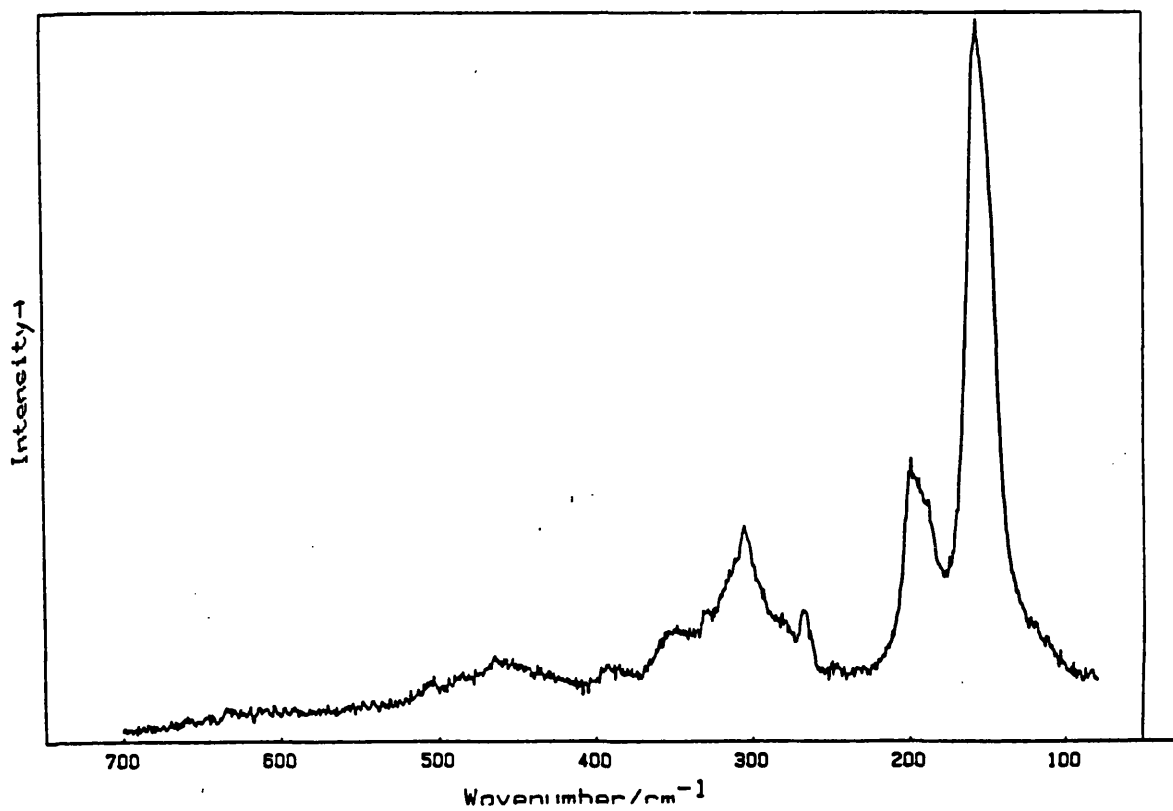
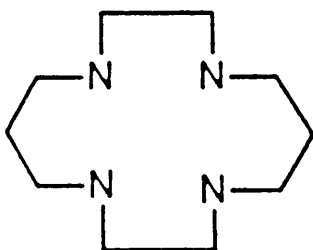


Figure 22. Resonance Raman spectrum of $[\text{Pd}(3,2,3\text{-tet})][\text{Pd}(3,2,3\text{-tet})\text{Br}_2][\text{ClO}_4]_4$ (pure disc at ca. 80 K, $\lambda_0 = 676.4$ nm).

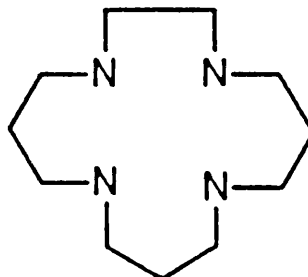
III.3. Complexes of Palladium with Macrocyclic Quadridentate Ligands

III.3.1. Introduction

The electronic and resonance Raman spectra were obtained of the series of complexes $[\text{PdL}][\text{PdLX}_2](\text{ClO}_4)_4$, where L = 1,4,8,11-tetraazacyclotetradecane (henceforth referred to as [14]aneN₄ or cyclam) or 1,4,8,12-tetraazacyclopentadecane (henceforth referred to as [15]aneN₄) and X = Cl or Br. Where L = [14]aneN₄ and X = Cl, different counteranions BF_4^- and PF_6^- were also investigated. In addition, infrared spectra were obtained of $[\text{Pd}([\text{14}] \text{aneN}_4)][\text{Pd}([\text{14}] \text{aneN}_4)\text{Cl}_2]\text{Y}_4$, where Y = ClO_4 or PF_6 . The ligands L are illustrated below.



[14]aneN₄



[15]aneN₄

These complexes have the expected linear chain structure (+2 charge type). They were prepared by Dr. M. Yamashita according to methods described in Appendix III. Electronic spectra were recorded at room temperature by transmission through pressed discs, as described in Appendix II. Raman/resonance Raman spectra were recorded from pressed discs at 40-80 K as described in Section II. Infrared spectra were recorded from pressed discs of sample in a matrix of NaCl, on a Bruker IFS113V evacuable FTIR interferometer, with a liquid nitrogen cooled HgCdTe detector and a Globar source.

III.3.2. Results and discussion

The complexes are strongly dichroic and are similar to

the analogous complexes with linear tetramine ligands. Unground, $[\text{Pd}-[14]\text{aneN}_4-\text{Cl}-\text{ClO}_4]$ and $[\text{Pd}-[14]\text{aneN}_4-\text{Cl}-\text{BF}_4]$ are lustrous green (dark green to pale brown in transmitted polarised light), while $[\text{Pd}-[15]\text{aneN}_4-\text{Cl}-\text{ClO}_4]$ is brown (dark brown to pale brown in transmitted polarised light) and $[\text{Pd}-[14]\text{aneN}_4-\text{Cl}-\text{PF}_6]$ is red (red to yellow in transmitted polarised light). The bromide-bridged complexes are gold-brown or copper-brown (brown-black to pale brown in transmitted polarised light). On grinding, however, the chloride-bridged complexes all turn violet, with the exception of that with the PF_6^- counterion, which is an orange-yellow powder. The powdered bromide-bridged complexes are blue.

Intervalence charge transfer band maxima are given in Table 7. The importance of the counteranion in the chain structure is illustrated by differences in wavenumber of IVCT band maxima observed for $[\text{Pd}-[14]\text{aneN}_4-\text{Cl}-\text{Y}]$. For $\text{Y} = \text{BF}_4$ or ClO_4 , there is not much difference, but for $\text{Y} = \text{PF}_6$, the IVCT maximum occurs approximately 3400 cm^{-1} higher in energy. This may be attributed to increased Peierls distortion for the PF_6^- salt, caused by reduced hydrogen bonding and increased steric effects between the counteranion and the equatorial ligands of adjacent metal centres. The effect of the anion on the strength of the hydrogen bonding along the chain direction is made evident crystallographically as well as spectroscopically. Thus the hydrogen bonding and steric effects on the extent of Peierls distortion are such that the bond distance ratio $r(\text{Pd}^{\text{IV}}-\text{Cl})/r(\text{Pd}^{\text{II}}-\text{Cl})$ for $[\text{Pd}-[14]-\text{Cl}-\text{PF}_6]$ (0.66) is significantly less than that (0.72) for $[\text{Pd}-[14]-\text{Cl}-\text{ClO}_4]$.^{29,30} Further evidence for weakening of the hydrogen bonding on going from the ClO_4 to the PF_6 case comes from infrared spectroscopy. Infrared spectra of $[14]\text{aneN}_4$, $[\text{Pd}-[14]\text{aneN}_4-\text{Cl}-\text{ClO}_4]$ and $[\text{Pd}-[14]\text{aneN}_4-\text{Cl}-\text{PF}_6]$ are shown in Figure 23 and corresponding wavenumbers and assignments of the bands are

given in Table 8. In the spectra of the mixed-valence complexes a doublet of bands is observed at around 3200 cm^{-1} , which is attributed to N-H stretch vibrations of the amine groups around Pd^{II} (higher wavenumber band) and Pd^{IV} . The wavenumbers of the doublet peaks increase on going from ClO_4 (3180 and 3201 cm^{-1}) to PF_6 (3216 and 3257 cm^{-1}) as the counterion. This increase is a result of a weakening of the N-H...counteranion hydrogen bonding. The separation of the doublet peaks in the PF_6 case, at 41 cm^{-1} , is greater than in the ClO_4 case (21 cm^{-1}). This verifies the greater Peierls distortion in the former case than in the latter, the doublet separation being directly related to the difference in oxidation states of the two metal sites (since a correlation exists between the metal oxidation states and the position of the proton in the N-H...Y bonding¹⁰¹). More localised valence in the PF_6^- case is in part also verified by resonance Raman spectroscopy described below.

Resonance Raman spectra of the macrocyclic complexes are shown in Figures 24-28. Each spectrum is dominated by the overtone progression $\nu_1\nu_1$, extending to $\nu_1=9$ for $\text{X}=\text{Cl}$, and $\nu_1=5$ for $\text{X}=\text{Br}$. Measured values of ν_1 , $\nu_1(\text{max})$ and $I(2\nu_1)/I(\nu_1)$ and calculated values of harmonic wavenumber ω_1 and anharmonicity x_{11} are given in Table 7, while a full list of wavenumbers and assignments is given in Table 9. This also shows some much weaker overtone progressions $\nu_1+\nu_1\nu_1$ to be present. Greater resonance enhancement in the majority of Cl-bridged cases than in the Br-bridged case indicates increased electron-phonon interaction and lesser valence delocalisation.^{9,17,61,68,86,92,98}

[Pd-[15]aneN₄-Br-ClO₄] could not be analysed without decomposition of the sample in the laser beam. However, ν_1 is believed to occur at approximately 145 cm^{-1} .

In the case of [Pd-[14]aneN₄-Cl-PF₆], however, the situation is slightly different. As with the IVCT band maximum, ν_1 occurs at substantially higher energy (294

cm^{-1}) than with BF_4 or ClO_4 (277.2 and 281.4 cm^{-1} respectively); this being attributable to reduced hydrogen bonding and increased Peierls distortion. However, the comparatively short progression would appear to be in contradiction to this. It is suggested, therefore, that although electron-phonon interaction is increased through greater Peierls distortion, the intensity of resonance Raman scattering is much reduced through lesser efficiency in intervalence charge transfer, as a result of reduced orbital overlap. This interpretation is verified by the relatively weak dichroic effect and lower intensity of colour in crystals of this complex.

Table 7

Summary of optical results from palladium complexes with macrocyclic quadridentate ligands

Complex	Crystal colour	Powder colour	λ_{max}^* / nm	λ_{D} / nm	ν_{D} / cm ⁻¹	ν_1 (max) / cm ⁻¹	ω_{D} / cm ⁻¹	x_{D} / cm	$I(2\nu_1) / I(\nu_1)$
[Pd([14]janeN ₄)] [Pd([14]janeN ₄)Cl ₂] (ClO ₄) ₄	Green	Violet	490 ± 20	568.2	281.4	9	283.1 ± 0.5	-0.71 ± 0.05	0.30
[Pd([15]janeN ₄)] [Pd([15]janeN ₄)Cl ₂] (ClO ₄) ₄	Brown	Violet	500 ± 10	514.5	284.2	5	285.6 ± 0.5	-0.6 ± 0.1	0.34
[Pd([14]janeN ₄)] [Pd([14]janeN ₄)Br ₂] (ClO ₄) ₄	Gold-brown	Blue	620 ± 40	676.4	154.5	5	155.6 ± 0.5	-0.6 ± 0.1	0.16
[Pd([15]janeN ₄)] [Pd([15]janeN ₄)Br ₂] (ClO ₄) ₄	Copper-brown	Blue	580 ± 10	647.1	ca. 145 (?)	-	-	-	-
[Pd([14]janeN ₄)] [Pd([14]janeN ₄)Cl ₂] (PF ₆) ₄	Green	Violet	530 ± 20	647.1	277.2	7	279.7 ± 0.5	-1.30 ± 0.05	0.25
[Pd([14]janeN ₄)] [Pd([14]janeN ₄)Cl ₂] (PF ₆) ₄	Red	Yellow	420 ± 40	514.5	294.0	3	296 ± 1	-1.5 ± 0.3	0.33

* Spectra obtained by transmission from a pressed disc using the corresponding alkali halide matrix.

Table 8. Wavenumbers $\tilde{\nu}$ and assignments of bands in the 2500-4000 cm^{-1} region of the infrared spectra of $[\text{14}] \text{aneN}_4$ and $[\text{Pd}([\text{14}] \text{aneN}_4)][\text{Pd}([\text{14}] \text{aneN}_4)\text{Cl}_2]\text{Y}_4$, where $\text{Y} = \text{ClO}_4$ and PF_6 . Spectra obtained from sample/alkali halide discs at 295 K.

$\tilde{\nu}/\text{cm}^{-1}$		Assignment
(a) $[\text{14}] \text{aneN}_4$		
2587	w	
2656	m	
2683	w	
2730	m	
2757	w	
2786	m	
2802	s	
2871	s	saturated C-H stretch
2909	w	
2919	s	saturated C-H stretch
2946	w	
2969	w	
3002	m	
3183	s	intramolecular H-bonded N-H stretch
3266	s	free N-H stretch
3407	w	
(b) $[\text{Pd}([\text{14}] \text{aneN}_4)][\text{Pd}([\text{14}] \text{aneN}_4)\text{Cl}_2][\text{ClO}_4]_4$		
2867	m	saturated C-H stretch
2956	m	saturated C-H stretch
3097	w	
3119	w	
3180	m	N-H stretch ($[\text{14}] \text{aneN}_4$ around Pd^{IV})
3201	m	N-H stretch ($[\text{14}] \text{aneN}_4$ around Pd^{II})
3436	m	} H-bonded O-H stretches
3516	m	

Table 8 continued.

 $\tilde{\nu}/\text{cm}^{-1}$

Assignment

(c) $[\text{Pd}([\text{14}] \text{aneN}_4)][\text{Pd}([\text{14}] \text{aneN}_4)\text{Cl}_2][\text{PF}_6]_4$

2865	w	saturated C-H stretch
2956	w	saturated C-H stretch
3216	s	N-H stretch ($[\text{14}] \text{aneN}_4$ around Pd^{IV})
3257	s	N-H stretch ($[\text{14}] \text{aneN}_4$ around Pd^{II})
3460	m	H-bonded O-H stretch

Table 9. Wavenumbers $\tilde{\nu}$, relative intensities $I(\tilde{\nu})/I(\nu_1)$, full widths at half maximum $\Delta\tilde{\nu}_{1/2}$ and assignments of bands in the resonance Raman spectra of $[\text{PdL}][\text{PdLX}_2](\text{ClO}_4)_4$, where L = [14]aneN₄ (X = Cl or Br) or [15]aneN₄ (X = Cl) and of $[\text{Pd}([\text{14}]\text{aneN}_4)][\text{Pd}([\text{14}]\text{aneN}_4)\text{Cl}_2]\text{Y}_4$, where Y = BF₄ or PF₆ (excitation wavelengths as specified in Table 7).
 $\nu_1 = \nu(\text{X-Pd}^{\text{IV}}\text{-X})_{\text{sym}}$ and $\nu_2 = \nu(\text{X-Pd}^{\text{IV}}\text{-X})_{\text{asym}}$.

$\tilde{\nu}/\text{cm}^{-1}$	$I(\tilde{\nu})/I(\nu_1)$	$\Delta\tilde{\nu}_{1/2}/\text{cm}^{-1}$	Assignment
(a) $[\text{Pd}([\text{14}]\text{aneN}_4)][\text{Pd}([\text{14}]\text{aneN}_4)\text{Cl}_2](\text{ClO}_4)_4$			
281.4	1.00	10.3	ν_1
562.2	0.30	20.5	$2\nu_1$
841.8	0.13	31	$3\nu_1$
1118	0.07	41	$4\nu_1$
1395	0.04	51	$5\nu_1$
1671	0.02	72	$6\nu_1$
1942	0.01	> 100	$7\nu_1$
2209	< 0.01	> 100	$8\nu_1$
2468	< 0.01	> 100	$9\nu_1$
(b) $[\text{Pd}([\text{15}]\text{aneN}_4)][\text{Pd}([\text{15}]\text{aneN}_4)\text{Cl}_2](\text{ClO}_4)_4$			
231	0.14	19	
284.2	1.00	15.4	ν_1
568.4	0.34	28	$2\nu_1$
848.4	0.19	43	$3\nu_1$
1134	0.10	55	$4\nu_1$
1404	0.03	77	$5\nu_1$
(c) $[\text{Pd}([\text{14}]\text{aneN}_4)][\text{Pd}([\text{14}]\text{aneN}_4)\text{Br}_2](\text{ClO}_4)_4$			
154.5	1.00	13.8	ν_1
230	0.01	4	
308	0.16	33	$2\nu_1$
457	0.05	52	$3\nu_1$
611	0.02	72	$4\nu_1$
746	< 0.01	100	$5\nu_1$

Table 9 continued.

$\tilde{\nu}/\text{cm}^{-1}$	$I(\tilde{\nu})/I(\nu_1)$	$\Delta\tilde{\nu}_{\frac{1}{2}}/\text{cm}^{-1}$	Assignment
(d) $[\text{Pd}([\text{14}] \text{aneN}_4)][\text{Pd}([\text{14}] \text{aneN}_4)\text{Cl}_2](\text{BF}_4)_4$			
123	0.01	10	
157.2	0.01	10	
205.2	0.06	10	$\delta(\text{N-Pd-N})$
233.4	0.01	10	
277.2	1.00	13	ν_1
378	0.02	5	
482.4	< 0.01	8	$\nu_1 + \delta(\text{N-Pd-N})$
552	0.25	25	$2\nu_1$
823	0.09	38	$3\nu_1$
1093	0.05	55	$4\nu_1$
1226	0.02	8	
1318	0.01	10	
1358	0.02	70	$5\nu_1$
1500	< 0.01	15	
1592	< 0.01	20	
1635	< 0.01	80	$6\nu_1$
1871	< 0.01	25	
1914	< 0.01		$7\nu_1$
2145	< 0.01	30	
(e) $[\text{Pd}([\text{14}] \text{aneN}_4)][\text{Pd}([\text{14}] \text{aneN}_4)\text{Cl}_2](\text{PF}_6)_6$			
294	1.00	15.2	ν_1
584.4	0.33	24	$2\nu_1$
700.8	0.25	10	
874.8	0.12	48	$3\nu_1$

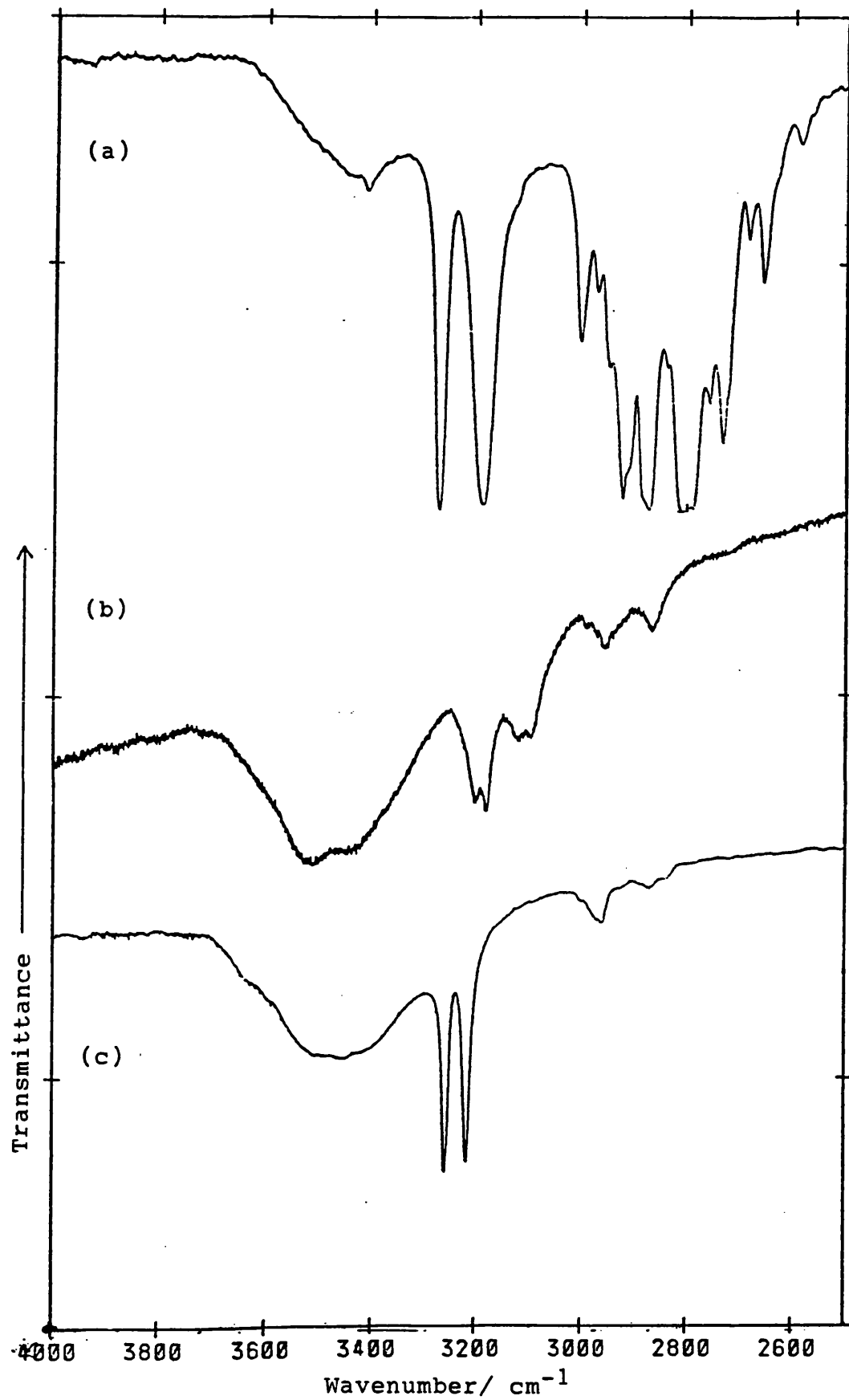


Figure 23. Infrared spectra of [14]aneN₄ (a) and [Pd-[14]aneN₄-Cl-Y₄], where Y = ClO₄ (b) and PF₆ (c). Spectra obtained from sample/KBr discs at 295 K.

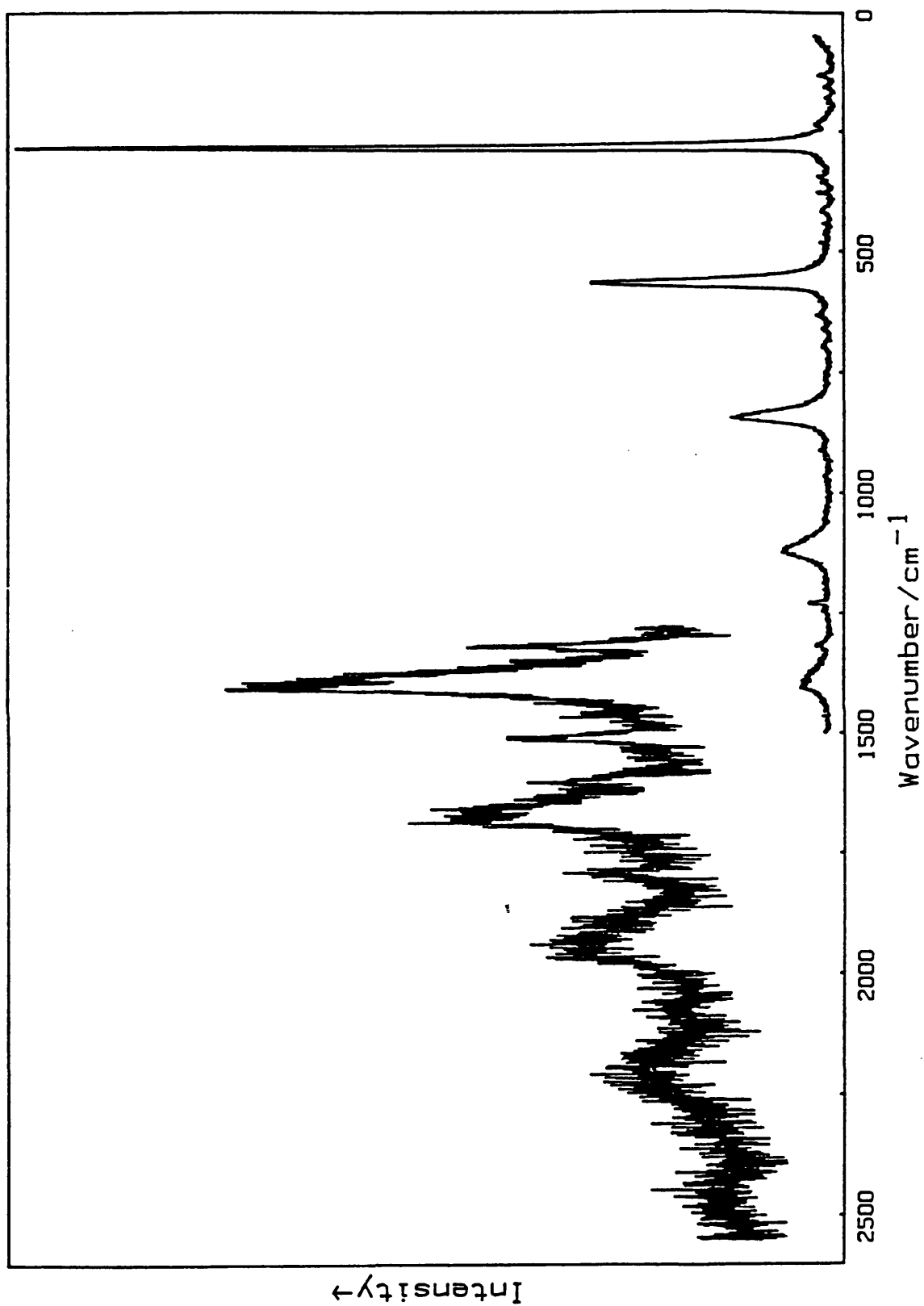


Figure 24. Resonance Raman spectrum of $[\text{Pd}([\text{14}]\text{aneN}_4)][\text{Pd}([\text{14}]\text{aneN}_4)\text{Cl}_2][\text{ClO}_4]_4$ (pure disc at ca. 80 K, $\lambda = 568.2 \text{ nm}$).

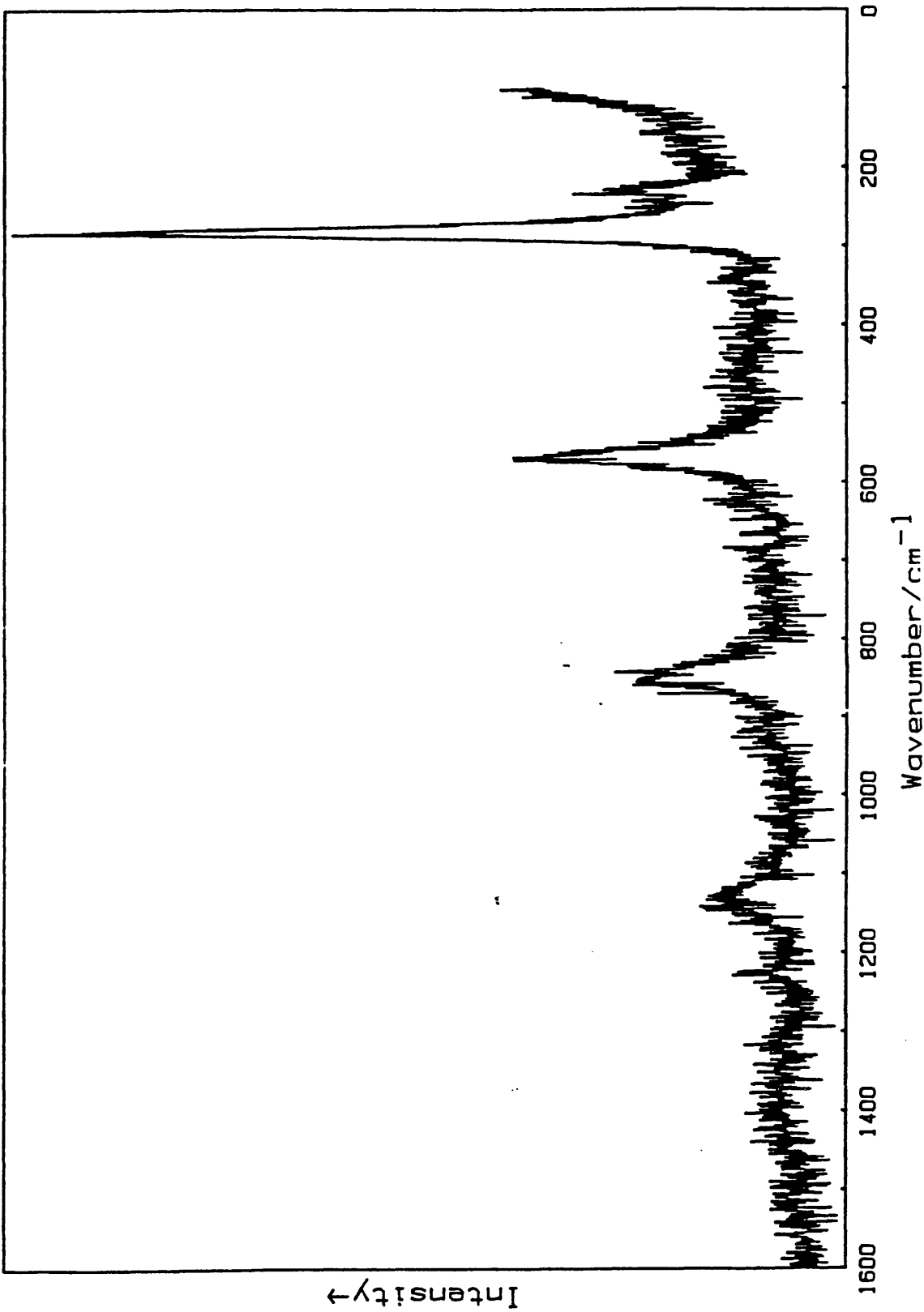


Figure 25. Resonance Raman spectrum of $[\text{Pd}([\text{15}]\text{aneN}_4)][\text{Pd}([\text{15}]\text{aneN}_4)\text{Cl}_2][\text{ClO}_4]_4$ (pure disc at ca. 80 K, $\lambda = 514.5 \text{ nm}$).

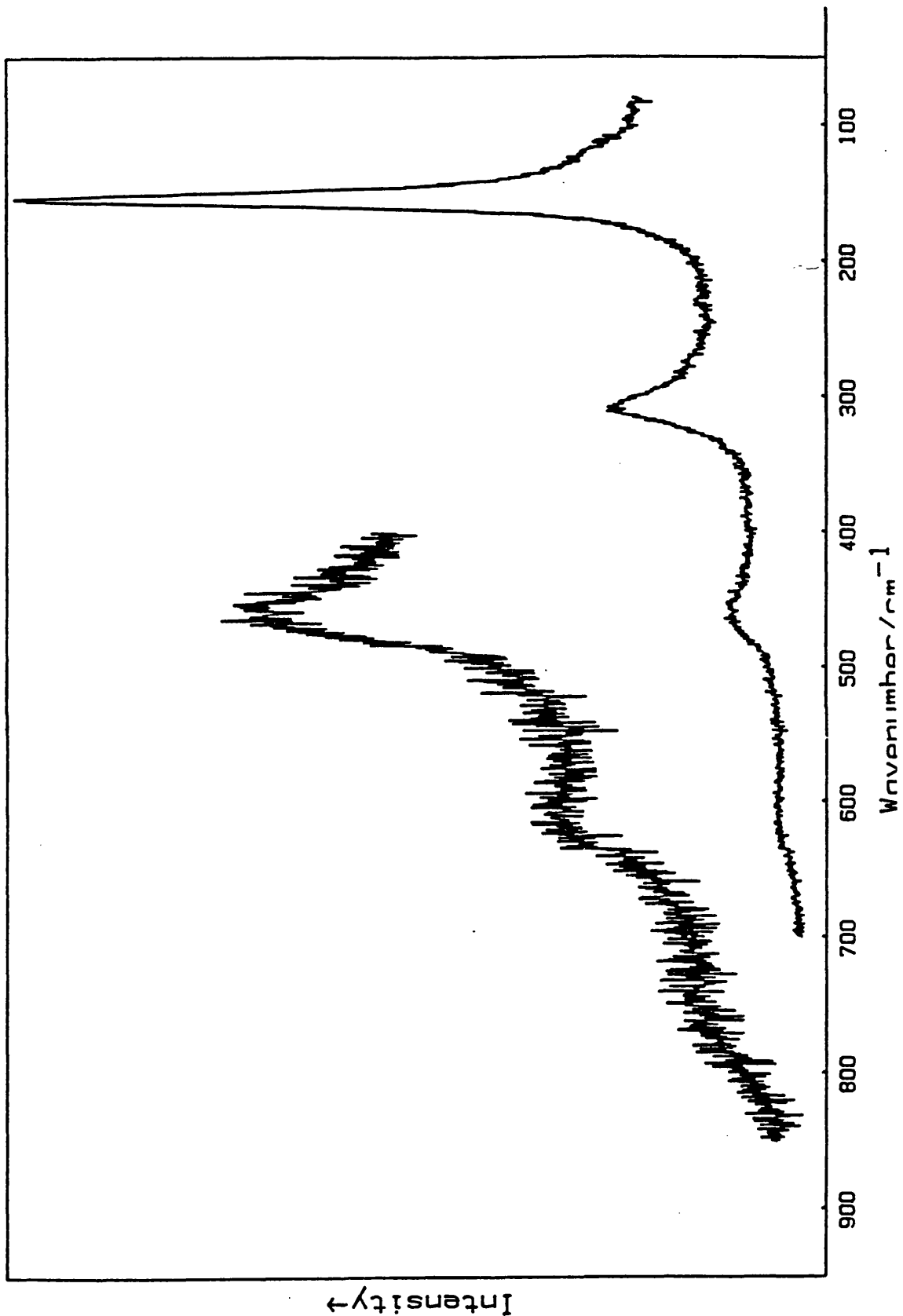


Figure 26. Resonance Raman spectrum of $[\text{Pd}([14]\text{aneN}_4)]\text{Br}_2 \cdot [\text{ClO}_4]_4$ (pure disc at ca. 80 K, $\lambda = 676.4 \text{ nm}$).

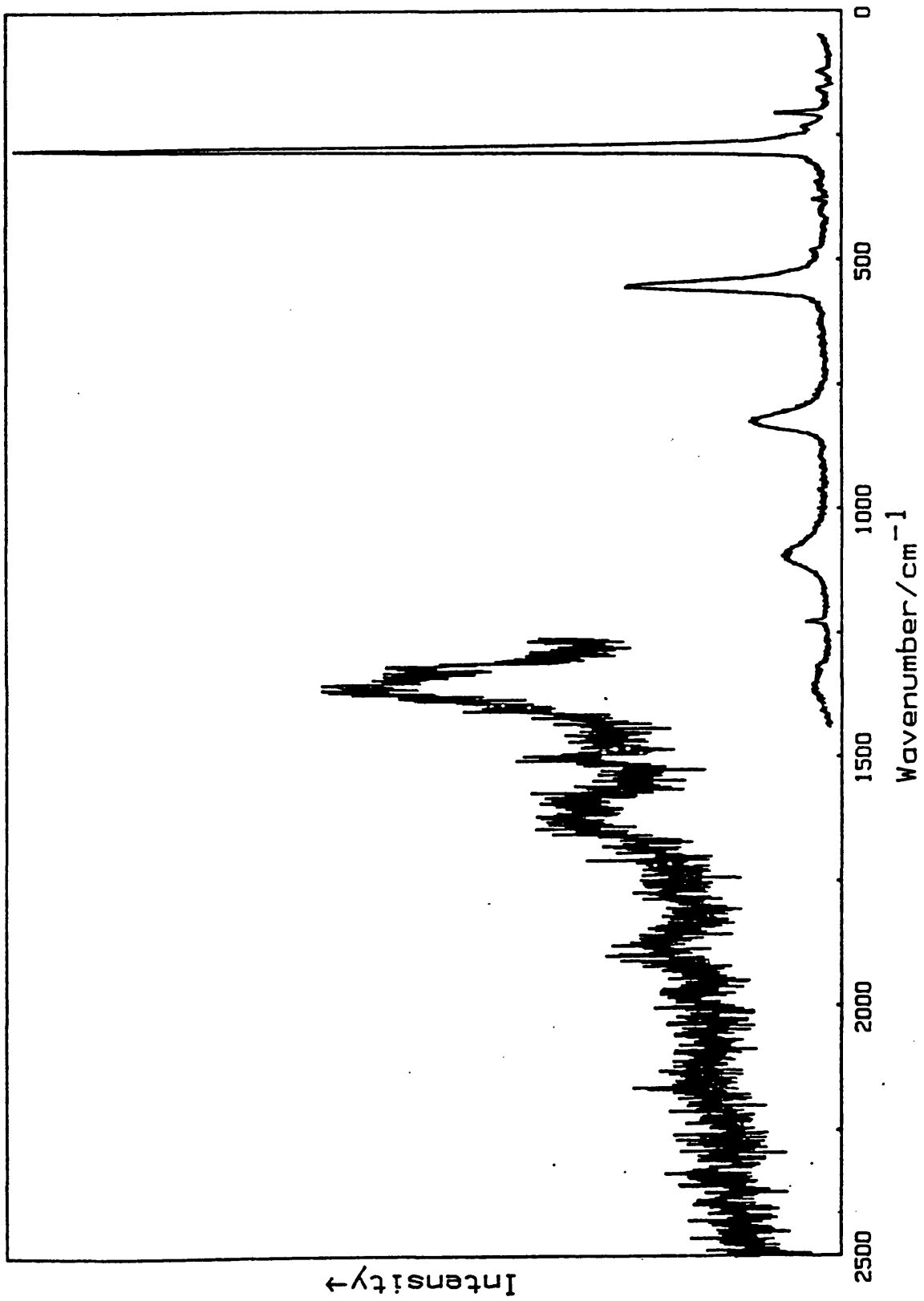


Figure 27. Resonance Raman spectrum of $[\text{Pd}([14]\text{aneN}_4)] [\text{Pd}([14]\text{aneN}_4)\text{Cl}_2][\text{BF}_4]_4$ (pure disc at ca. 80 K, $\lambda = 647.1 \text{ nm}$).

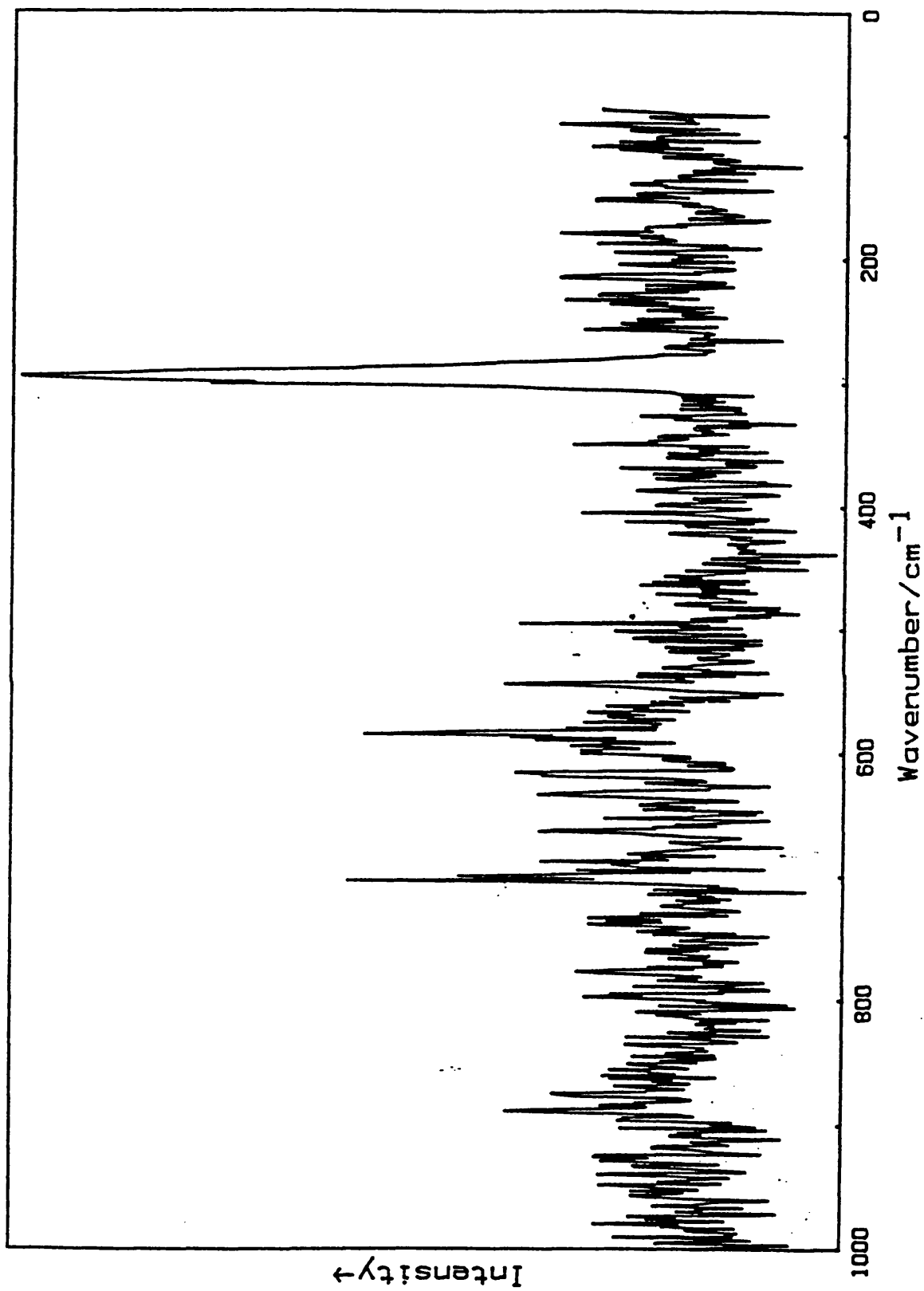


Figure 28. Resonance Raman spectrum of $[\text{Pd}([\text{14Janen}_4)]][\text{Pd}([\text{14Janen}_4)]\text{C}_{12}][\text{PF}_6]_4$ (pure disc at ca. 80 K, $\lambda = 514.5 \text{ nm}$).

IV. HALOGEN-BRIDGED, MIXED-VALENCE AND SINGLE VALENCE COMPLEXES OF NICKEL WITH QUADRIDENTATE AND BIBENTATE LIGANDS

IV.1. Introduction

Resonance Raman spectra have been measured for a number of halogen-bridged complexes of nickel, prepared by Dr. M. Yamashita and Dr. K. Toriumi. They have the Ni^{II}/Ni^{IV} structure and properties,^{17,45,102-6} with the exception of one complex, which differs exceedingly in its conductive, magnetic and optical properties and which is considered to be a Ni^{III}/Ni^{III} structure.^{77,78} The origin of the two types of linear chain in the presence or absence of Peierls distortion has been discussed at length elsewhere (Section I.10.3). Presented here is the Raman/resonance Raman evidence for mixed-valence and non-mixed-valence structures and factors determining such differences are then discussed.

It appears, from this and previous work, that by changing the combination of ligand, bridging halogen and counterion, the oxidation states $+3+\delta$ and $+3-\delta$ of the nickel in the ground state may be tuned over a critical range of values of δ from zero to just greater than zero.

IV.2. Mixed-valence Systems

Two types of Ni^{II}/Ni^{IV} complex have been investigated, which differ in their appearance and in their resonance Raman properties.

IV.2.1. Ni(II)/Ni(IV) Chains with Quadridentate Ligands and Large Complex Counteranions

Resonance Raman spectra were obtained of [NiL][NiLCl₂](BF₄)₄, where L = 3,7-diazanonane-1,9-diamine (= 2,3,2-tet) and 4,7-diazadecane-1,10-diamine (= 3,2,3-tet) and of

[Ni(2,3,2-tet)][Ni(2,3,2-tet)Cl₂](ClO₄)₄. Synthetic methods are given in Appendix III. Spectra were recorded from pressed discs at 40-80 K as described in Section II.

Resonance Raman spectra of the complexes are shown in Figures 29-31 and summarised data are presented in Table 10. These complexes are dark green or dark blue in powdered form and show none of the characteristic lustre of halogen-bridged, mixed-valence metal complexes. As expected, from trends observed with analogous Pt and Pd complexes, resonance enhancement is weak and the overtone progressions are short (wavenumbers and assignments are given in Table 11). This may be explained in terms of increased valence delocalisation, reduced Peierls distortion and lesser electron-phonon interaction, than with Pt or Pd analogues.^{45,67,104} However, variation in wavenumber of proposed ν_1 bands from 213 to 240 cm⁻¹ is considerably greater than is observed with Pt or Pd and illustrates how much more critical, in the case of nickel, is the choice of ligand and counteranion in determining the extent of Peierls distortion. Discussion follows in section IV.4. An infrared spectrum was obtained of [Ni-2,3,2-tet-Cl-BF₄] (using a sample/wax disc), in which no peak was observed at or around 213 cm⁻¹; this verifies that the Raman band at that wavenumber corresponds to a vibration involving no change in dipole moment.

IV.2.2. Ni(II)/Ni(IV) Chains with Bidentate Ligands and Chloride Counteranion

Raman and resonance Raman spectra were obtained of [NiL₂][NiL₂Cl₂]Cl₄, where L = 1,2-diaminopropane (pn) and (-)trans-1,2-diaminocyclohexane (R,R-chxn). Synthetic methods are given in Appendix III. Spectra were recorded from pressed discs at 40-80 K as described in Section II.

Raman and resonance Raman spectra of the complexes are shown in Figures 32-35 and summarised data presented in Table 10. Wavenumbers and assignments are given in Table 12. The resonance Raman spectrum of [Ni-pn-Cl-Cl] (Figure 33) is

in approximate agreement with that obtained by Papavassiliou et al.¹⁰⁶, although a peak reported by the latter at 400 cm^{-1} is absent from the spectrum reported herein. The complexes are dark brown to black and have the characteristic metallic lustre. Resonance enhancement in the Raman spectra is stronger than in the quadridentate cases described above, although still far weaker than for Pt or Pd analogues, as expected from reduced Peierls distortion and electron-phonon interaction.^{45,67,104} Similarly, at approximately 260-265 cm^{-1} , ν_1 is greater than with the quadridentate ligands and oxyanions. Unlike in the quadridentate cases, spectra of the two complexes obtained with red excitation lines show almost a complete absence of resonance enhancement. Bands at 260-265 cm^{-1} were absent from the infrared spectra of the two complexes, obtained from sample/wax discs; the nature of the Raman bands in that wavenumber region was thus verified. Discussion follows in section IV.4.

IV.3. A Ni(III)/Ni(III) System

Raman and resonance Raman spectra were obtained of $\{[\text{Ni}(\text{R},\text{R-chxn})_2\text{Br}]\text{Br}_2\}_\infty$, the first example of a halogen-bridged, linear chain metal complex of the Wolfram's Red Salt type having no Peierls distortion.⁷⁷ This complex, which crystallises in black prisms with no lustre, has a low energy electronic band⁷⁸ at 10300 cm^{-1} , analogous to the IVCT band of the mixed-valence complexes. Although it has not been established what transition this band may correspond to, an obvious possibility is charge transfer in reverse of that of the IVCT, i.e. to give a II/IV state from the III/III state. X-ray, conductive and magnetic data⁷⁸ verify the existence of the III/III state. The synthetic method is given in Appendix III. Raman spectra were recorded from pressed discs at 40-80 K as described in Section II.

Raman and resonance Raman spectra are shown in Figure

36 and summarised data are presented in Table 10. Wavenumbers and assignments are given in Table 13. Peaks occurring in the spectra at 95.5, 132.5, 189.5 and 213 cm^{-1} are only weakly present, if at all, with blue or green excitation, but become quite strongly enhanced on changing the excitation towards the deep red, i.e. on going closer to the maximum of the observed near infra-red electronic transition. Figure 37 shows an excitation profile of the most prominently enhanced band at 213 cm^{-1} , which may correspond to a $\text{Ni}^{\text{III}}\text{-Br}$ stretching vibration. Support for such an assignment comes from work carried out on several complex ions containing Ni-Br bonds, for example those of the type $[\text{LNiX}_3]^-$, where L = triphenylphosphine and X = Cl or Br¹⁰⁷, for which, in the bromide case, it is suggested that (Ni-Br) stretch vibrations occur at 242, 206-12 and 190 cm^{-1} .

IV.4. Discussion

From the above Raman/resonance Raman results it emerges that at least three distinct types of halogen-bridged nickel chain complex may be identified. One of these is the true $\text{Ni}^{\text{III}}/\text{Ni}^{\text{III}}$ chain, as exemplified by $\{[\text{Ni}(\text{R},\text{R-chxn})_2\text{Br}]\text{Br}_2\}_\infty$. This is the only known example of the so-called Mott-Hubbard (undistorted) state of such a complex existing in preference to the Peierls distorted state. The suggested ν_1 band in the Raman spectrum at 213 cm^{-1} , while showing considerable enhancement on going to deep red excitation, is not nearly as strong as ν_1 for most II/IV systems. Resonance enhancement may occur in this case by the excitation of a pair of Ni^{III} sites to the $\text{Ni}^{\text{II}}/\text{Ni}^{\text{IV}}$ state, followed by movement to a Peierls distorted geometry and relaxation to the ground electronic state.

Of the II/IV nickel chains, those with quadridentate ligands and large complex anions show no lustre, considerable variation in the wavenumber of ν_1

(213 - 239 cm^{-1}) and only moderate resonance Raman intensity (a few overtones observed) with all excitation lines used. In this situation, the oxidation state (already close to +3) and Peierls distortion are being significantly altered by a combination of steric and hydrogen-bonding factors. Thus, it is suggested, in [Ni-(3,2,3-tet)-Cl-BF₄] the nickel sites are held slightly closer together than in [Ni-(2,3,2-tet)-Cl-BF₄], so that, for a given absolute displacement of Cl from the bridging position, the Ni^{IV}-Cl distance is shorter (giving the higher ν_1 frequency) and the II/IV potential minimum is closer on the normal coordinate to the III/III potential minimum (giving lesser enhancement). By a similar argument, ν_1 for [Ni-(2,3,2-tet)-Cl-Y] is higher for Y = ClO₄ than for Y = BF₄, as hydrogen bonding is stronger in the former than in the latter.

The II/IV nickel chains with bidentate ligands and halide counterions are lustrous and, with blue excitation, show stronger resonance enhancement than the II/IV nickel complexes discussed above although still far less than in the analogous Pt or Pd cases. Furthermore, ν_1 occurs at a higher wavenumber and there is much less variation with change of ligand than in the II/IV nickel cases above. By analogy with the palladium cases, it is suggested that, although hydrogen bonding in these complexes is probably weaker than with quadridentate ligands, the lesser bulk of the bidentate ligands and halide counterions enables the nickel ions to be closer together; hence valence delocalisation, Peierls distortion and electron-phonon interaction would be correspondingly greater. This would cause ν_1 to occur at higher wavenumber and with greater enhancement.

Table 10

Summary of optical results from nickel complexes

Complex	Powder colour	$\lambda_{\text{max}} / \text{nm}$	λ_0 / nm	$\nu_{11} / \text{cm}^{-1}$	ν_1 (max)
$[\text{Ni}(2,3,2\text{-tet})][\text{Ni}(2,3,2\text{-tet})\text{Cl}_2](\text{BF}_4)_4$	Dark blue	670 ^a	752.5	213.5	4
$[\text{Ni}(3,2,3\text{-tet})][\text{Ni}(3,2,3\text{-tet})\text{Cl}_2](\text{BF}_4)_4$	Dark green		752.5	239.0	2
$[\text{Ni}(2,3,2\text{-tet})][\text{Ni}(2,3,2\text{-tet})\text{Cl}_2](\text{ClO}_4)_4$	Dark green		676.4	230.4	2
$[\text{Ni}(\text{pn})_2][\text{Ni}(\text{pn})_2\text{Cl}_2]\text{Cl}_4$	Dark brown	660 ^b	457.9	266.4	4
$[\text{Ni}(\text{R,R-chn})_2][\text{Ni}(\text{R,R-chn})_2\text{Cl}_2]\text{Cl}_4$	Dark brown		488.0	262.5	4
$[\text{Ni}(\text{R,R-chn})_2\text{Br}]\text{Br}_2$	Black	970 ^c	752.5	213.0	2

a Ref. 17, nujol mull,

b Ref. 102, nujol mull,

c Ref. 78, single crystal reflectivity.

Table 11 . Wavenumbers $\tilde{\nu}$, relative intensities $I(\tilde{\nu})/I(\nu_1)$, full widths at half maximum $\Delta\tilde{\nu}_{\frac{1}{2}}$ and assignments of bands in the Raman/resonance Raman spectra of $[\text{NiL}][\text{NiLCl}_2](\text{BF}_4)_4$, where L = 2,3,2-tet or 3,2,3-tet and of $[\text{Ni}(2,3,2\text{-tet})][\text{Ni}(2,3,2\text{-tet})\text{Cl}_2](\text{ClO}_4)_4$ (conditions as specified in Figures 29-31). $\nu_1 = \nu(\text{Cl-Ni}^{\text{IV}}\text{-Cl})_{\text{sym}}$.

$\tilde{\nu}/\text{cm}^{-1}$	$I(\tilde{\nu})/I(\nu_1)$	$\Delta\tilde{\nu}_{\frac{1}{2}}/\text{cm}^{-1}$	Assignment
(a) $[\text{Ni}(2,3,2\text{-tet})][\text{Ni}(2,3,2\text{-tet})\text{Cl}_2](\text{BF}_4)_4$			
117.5	0.04	17	$\delta(\text{Ni-Cl})$
163.5	0.03	17	
213.5	1.00	13.3	ν_1
233.5	0.13	10	
243.5	0.09	8	
424.5	0.12	32	$2\nu_1$
455.5	0.03	23	
577.5	0.02	17	
638.5	0.04	57	$3\nu_1$
671.5	0.03	20	
819.5	0.03	33	
841.5	0.02	20	
(b) $[\text{Ni}(3,2,3\text{-tet})][\text{Ni}(3,2,3\text{-tet})\text{Cl}_2](\text{BF}_4)_4$			
110.5	0.10	10	$\delta(\text{Ni-Cl})$
191.5	0.11	3	
239	1.00	19.4	ν_1
475	0.09	30	$2\nu_1$
575	0.07	30	
(c) $[\text{Ni}(2,3,2\text{-tet})][\text{Ni}(2,3,2\text{-tet})\text{Cl}_2](\text{ClO}_4)_4$			
115	0.20	16	$\delta(\text{Ni-Cl})$
129	0.16	14	
194.5	0.08	11	
229.5	1.00	17	ν_1
247	0.76	14	

Table 11 continued.

$\tilde{\nu}/\text{cm}^{-1}$	$I(\tilde{\nu})/I(\nu_1)$	$\Delta\tilde{\nu}_{\frac{1}{2}}/\text{cm}^{-1}$	Assignment
(c) $[\text{Ni}(2,3,2\text{-tet})][\text{Ni}(2,3,2\text{-tet})\text{Cl}_2](\text{ClO}_4)_4$			
331	0.09	14	$\nu(\text{Ni-N})$
349.5	0.14	43	
461.6	0.06	29	$2\nu_1$
470.5	0.09	11	
629	0.06	14	

Table 12 . Wavenumbers $\tilde{\nu}$, relative intensities $I(\tilde{\nu})/I(\nu_1)$, full widths at half maximum $\Delta\tilde{\nu}_{\frac{1}{2}}$ and assignments of bands in the resonance Raman spectra of ${}^2[\text{NiL}_2][\text{NiL}_2\text{Cl}_2]\text{Cl}_4$, where L = pn or R,R-chxn (conditions as specified in Figures 33 and 35 respectively). $\nu_1 = \nu(\text{Cl-Ni}^{\text{IV}}-\text{Cl})_{\text{sym}}$.

$\tilde{\nu}/\text{cm}^{-1}$	$I(\tilde{\nu})/I(\nu_1)$	$\Delta\tilde{\nu}_{\frac{1}{2}}/\text{cm}^{-1}$	Assignment
(a) $[\text{Ni}(\text{pn})_2][\text{Ni}(\text{pn})_2\text{Cl}_2]\text{Cl}_4$			
268.5	1.00	29.2	ν_1
313	0.18	10	
542	0.41	37	$2\nu_1$
596	0.08	15	
702	0.07	4	
805	0.13	21	
844	0.05	8	
1050	0.05	21	
1079	0.05	21	
(b) $[\text{Ni}(\text{R,R-chxn})_2][\text{Ni}(\text{R,R-chxn})_2\text{Cl}_2]\text{Cl}_4$			
137	0.12	10	
155.5	0.17	10	
199	0.18	6	
262.2	1.00	33.3	ν_1
296	0.31	6	
378	0.11	6	
437	0.05	6	
519.5	0.24	6	
521	0.24	48	$2\nu_1$
560	0.04	8	
573	0.95	4	
761	0.06	> 50	
803	0.14	17	
1042	0.06	6	
1062	0.06	6	

Table 13 . Wavenumbers $\tilde{\nu}$, relative intensities $I(\tilde{\nu})/I[\nu(\text{Ni-Br})]$, full widths at half maximum $\Delta\tilde{\nu}_{1/2}$ and assignments of bands in the resonance Raman spectrum of $\{[\text{Ni}(\text{R,R-chxn})_2\text{Br}]\text{Br}_2\}_\infty$ (pure disc at ca. 40-50 K, $\lambda_0 = 752.5$ nm).

$\tilde{\nu}/\text{cm}^{-1}$	$I(\tilde{\nu})/I[\nu(\text{Ni-Br})]$	$\Delta\tilde{\nu}_{1/2}/\text{cm}^{-1}$	Assignment
95.5	0.65	9	$\delta(\text{Ni-Br})$
107.5	0.40	3	
132.5	0.25	13	
161	0.10	13	
189.5	0.55	9	
213	1.00	13	$\nu(\text{Ni-Br})$
264.5	0.05	9	
287.5	0.10	4	
310.5	0.15	17	
343	0.10	9	
370	0.15	3	
403	0.05	13	
427	0.10	22	$2\nu(\text{Ni-Br})$
514	0.15	3	
570	0.20	3	

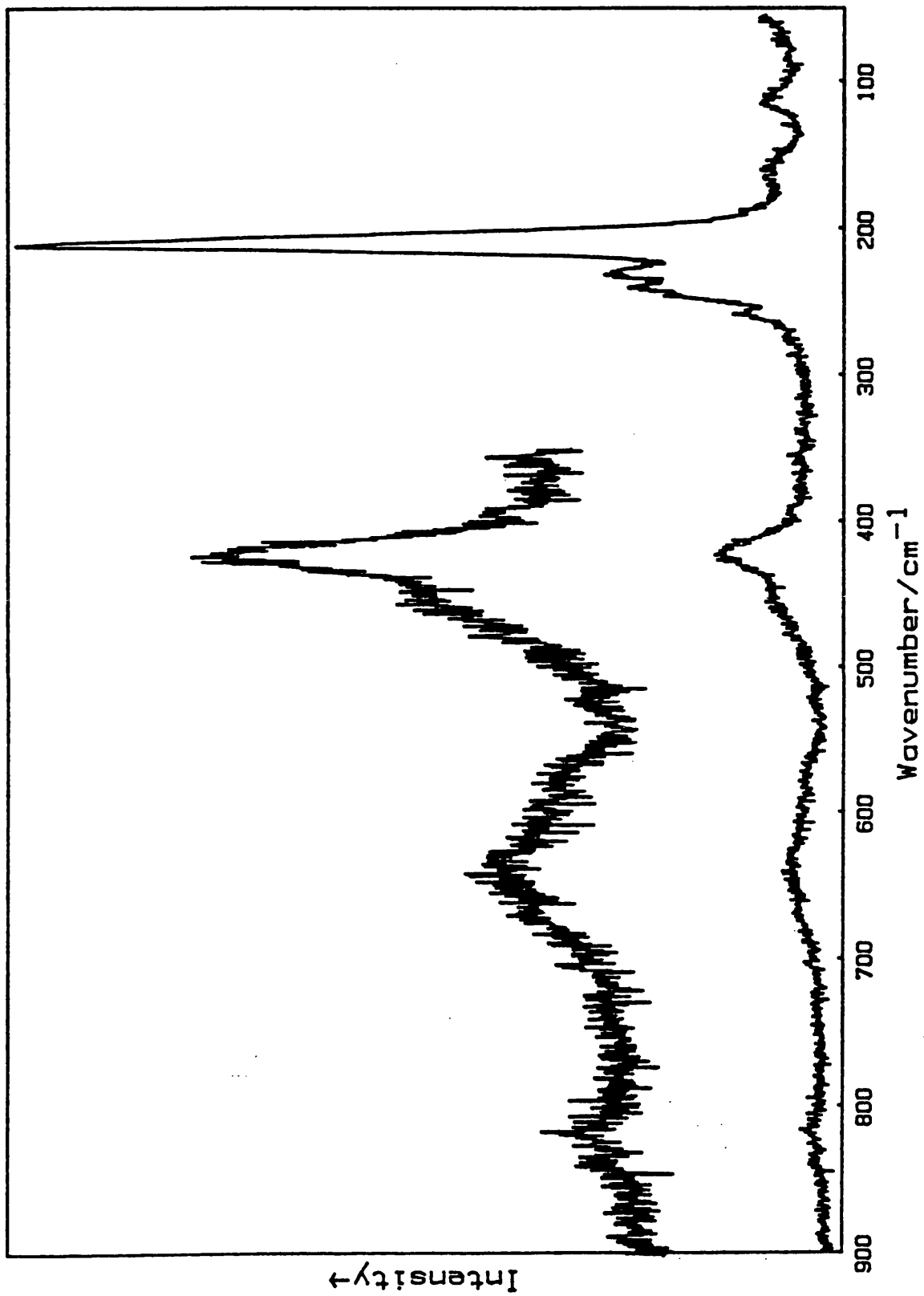


Figure 29. Resonance Raman spectrum of $[\text{Ni}(2,3,2\text{-tet})][\text{Ni}(2,3,2\text{-tet})\text{Cl}_2][\text{BF}_4]_4$ (pure disc at ca. 80 K, $\lambda_0 = 752.5 \text{ nm}$).

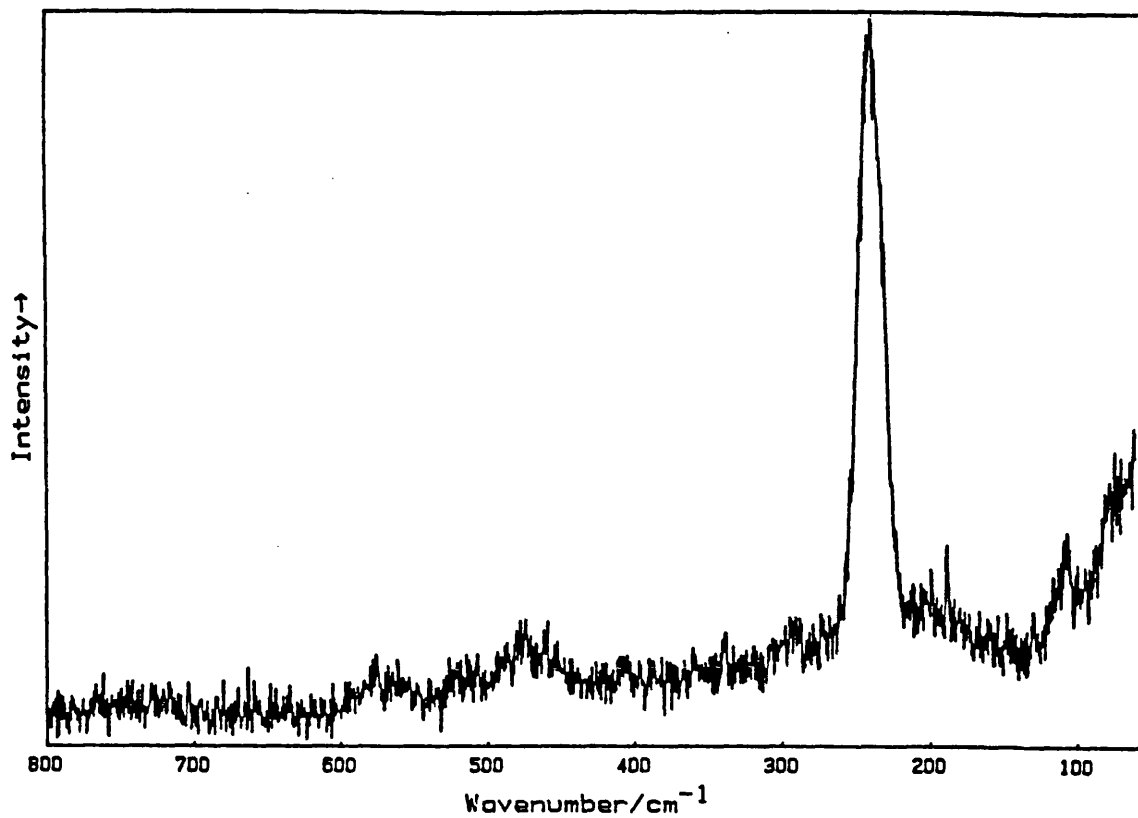


Figure 30. Resonance Raman spectrum of $[\text{Ni}(3,2,3\text{-tet})][\text{Ni}(3,2,3\text{-tet})\text{Cl}_2][\text{BF}_4]_4$ (pure disc at ca. 80 K, $\lambda_0 = 752.5$ nm).

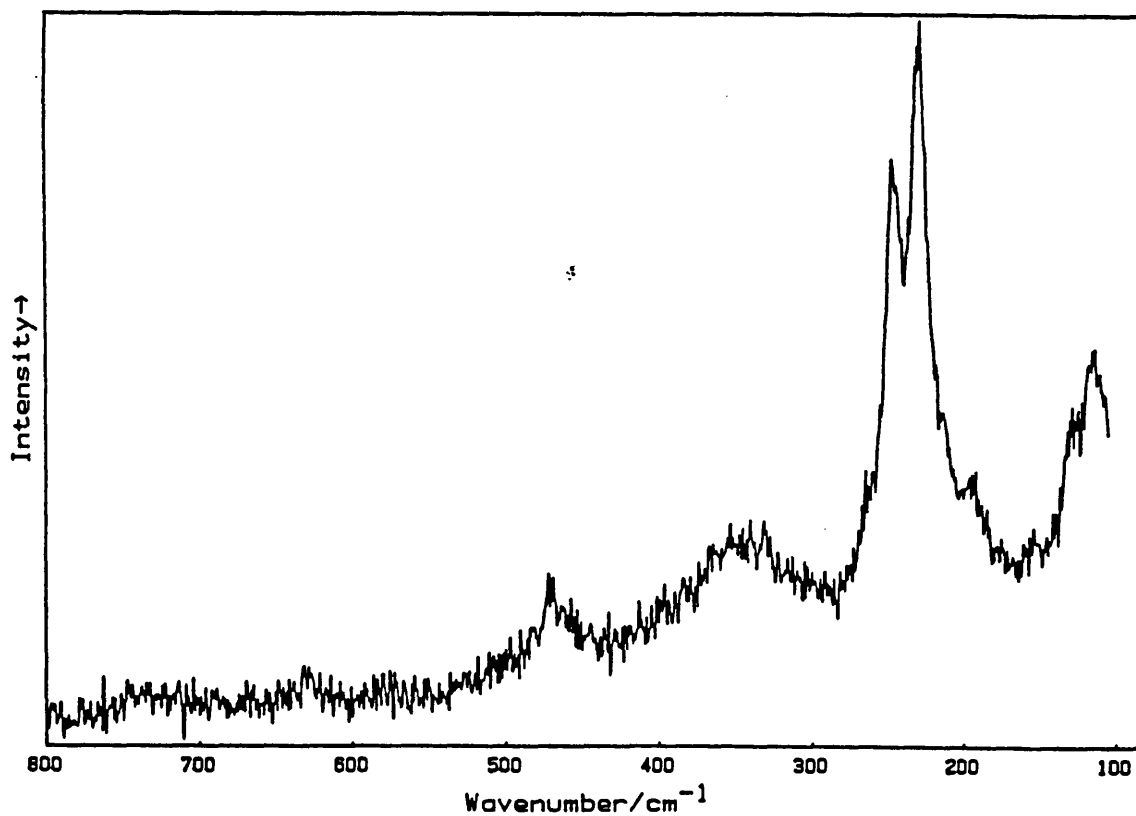


Figure 31. Resonance Raman spectrum of $[\text{Ni}(2,3,2\text{-tet})][\text{Ni}(2,3,2\text{-tet})\text{Cl}_2][\text{ClO}_4]_4$ (pure disc at ca. 80 K, $\lambda_0 = 676.4$ nm).

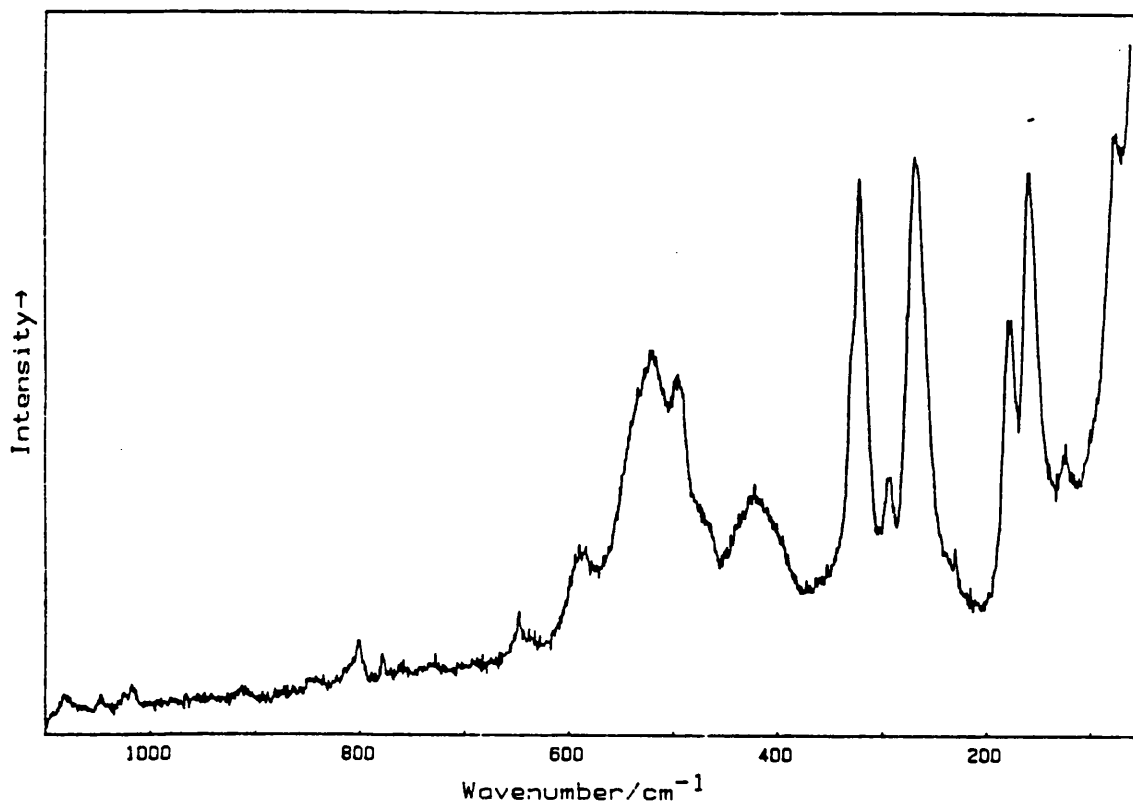


Figure 32. Raman spectrum of $[\text{Ni}(\text{pn})_2][\text{Ni}(\text{pn})_2\text{Cl}_2]\text{Cl}_4$ (pure disc at ca. 80 K, $\lambda_0 = 676.4$ nm).

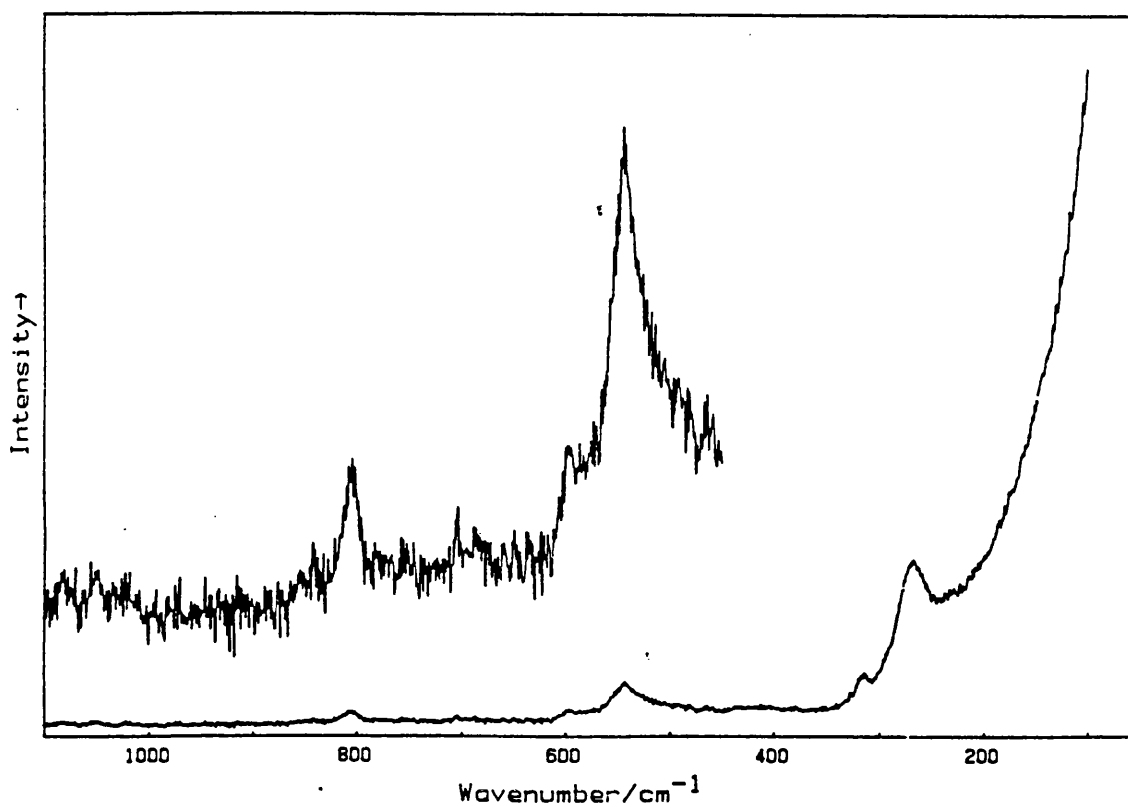


Figure 33. Resonance Raman spectrum of $[\text{Ni}(\text{pn})_2][\text{Ni}(\text{pn})_2\text{Cl}_2]\text{Cl}_4$ (pure disc at ca. 80 K, $\lambda_0 = 457.9$ nm).

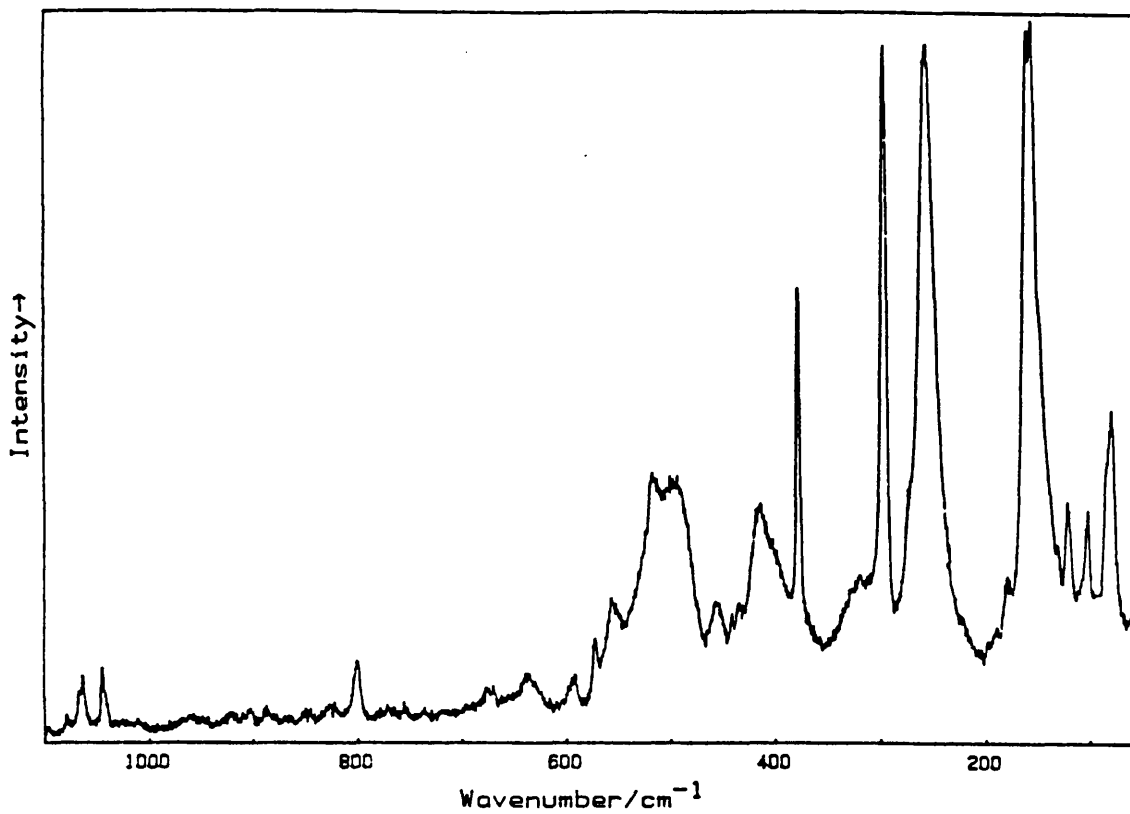


Figure 34. Raman spectrum of $[\text{Ni}(\text{R,R-chxn})_2][\text{Ni}(\text{R,R-chxn})_2\text{Cl}_2]\text{Cl}_4$ (pure disc at ca. 80 K, $\lambda_0 = 647.1$ nm).

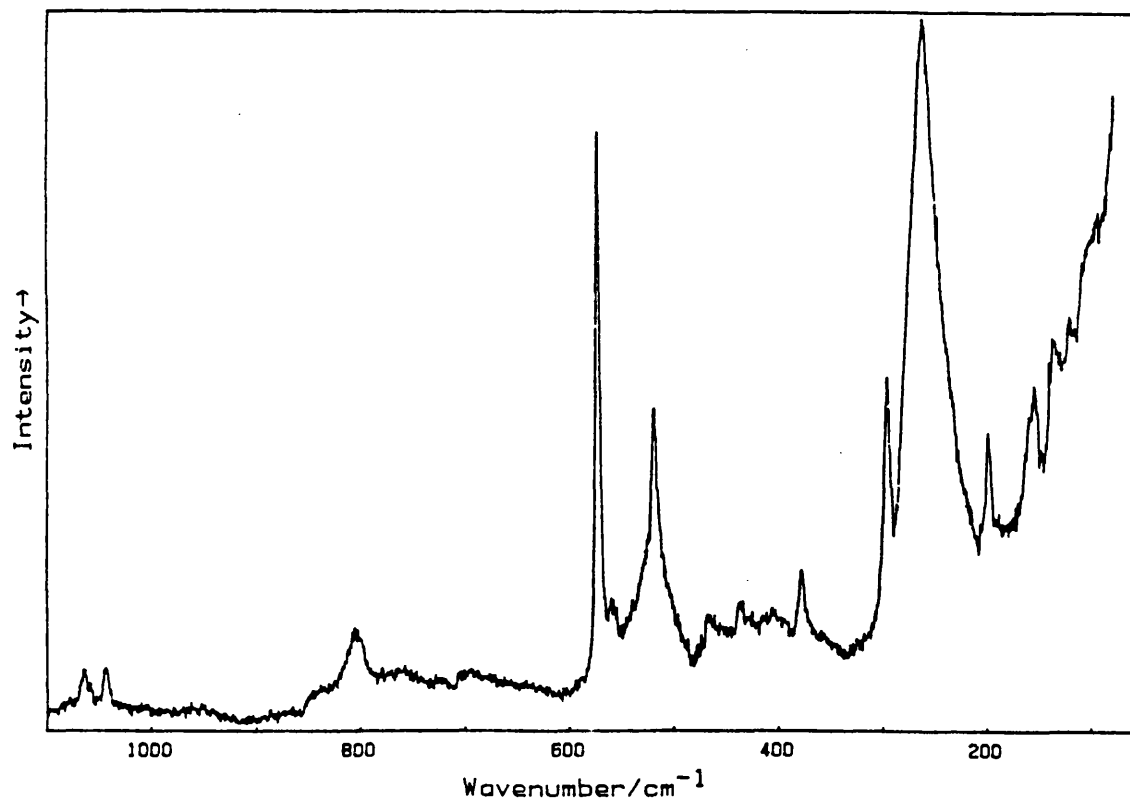


Figure 35. Resonance Raman spectrum of $[\text{Ni}(\text{R,R-chxn})_2][\text{Ni}(\text{R,R-chxn})_2\text{Cl}_2]\text{Cl}_4$ (pure disc at ca. 80 K, $\lambda_0 = 488.0$ nm).

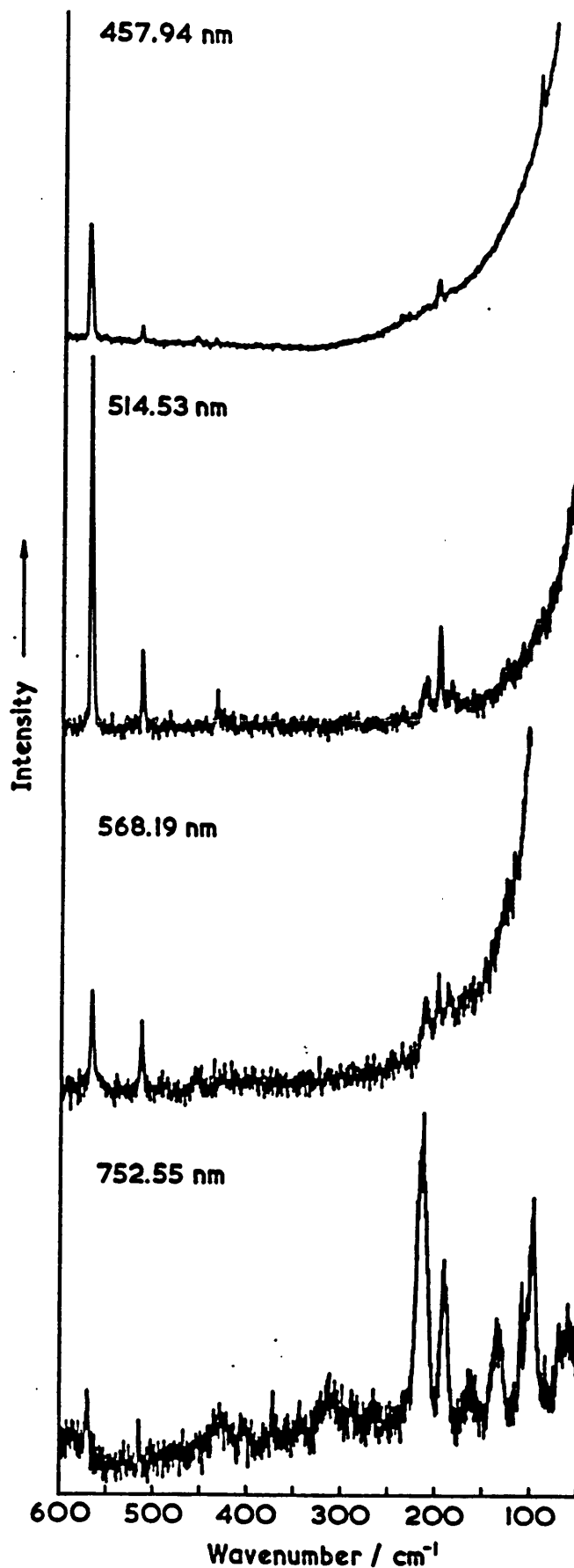


Figure 36. Raman/resonance Raman spectra of $\{[\text{Ni}(\text{R,R-dxvn})_2\text{Br}]\text{Br}_2\}_\infty$ obtained with excitation lines at 457.9, 514.5, 568.2 and 752.5 nm (pure disc at ca. 50 K).

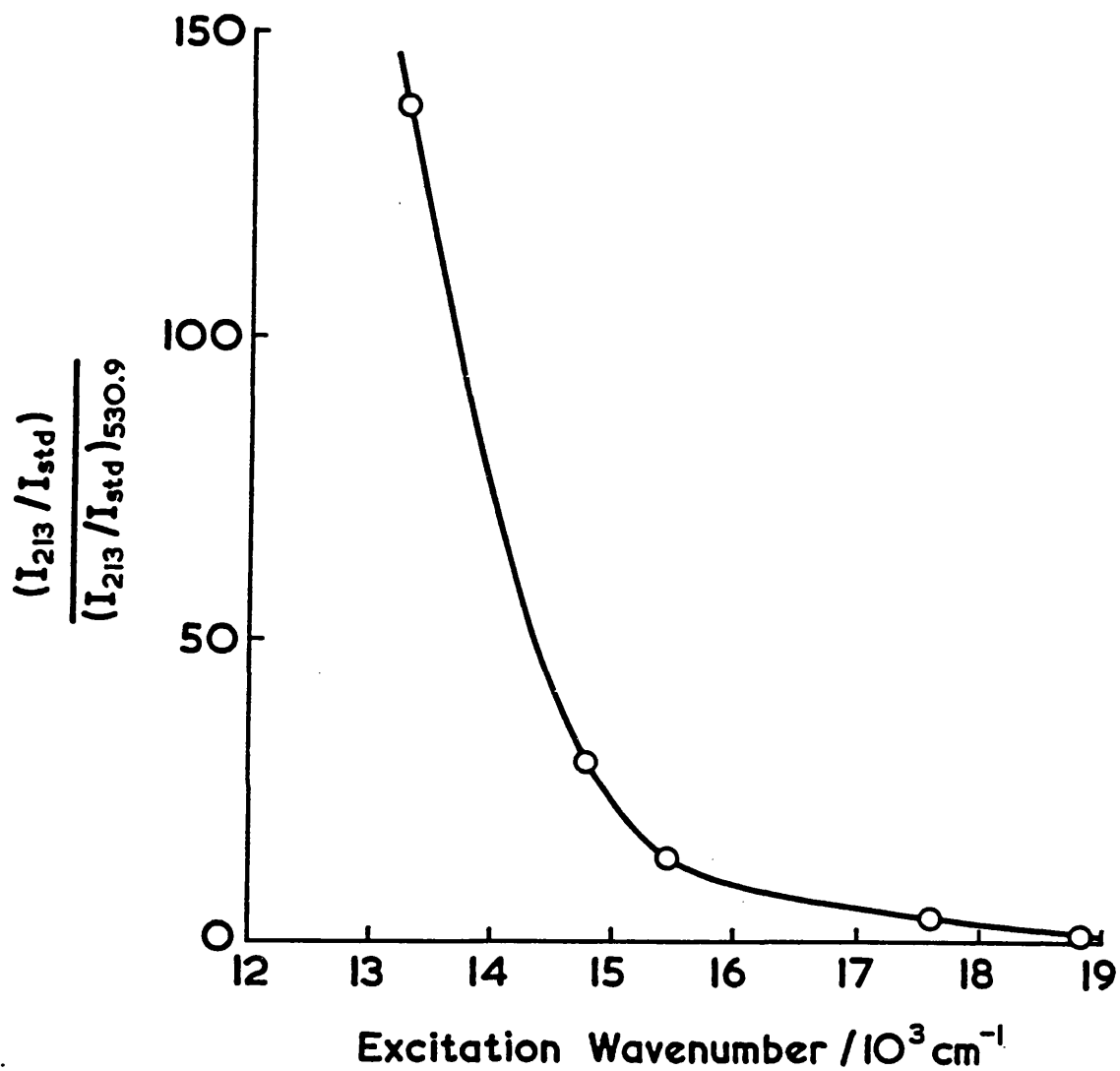


Figure 37. Excitation profile of the 213 cm⁻¹ band of $\{[NI(R,R\text{-chxn})_2Br]Br_2\}_\infty$, obtained from a sample/K₂SO₄ disc at ca. 50 K.

V. A STUDY OF HALOGEN-BRIDGED, MIXED-METAL,
MIXED-VALENCE COMPLEXES OF PLATINUM AND COPPER

V.1. Introduction

Electronic, infrared, Raman and resonance Raman spectra have been measured for $[\text{Cu}_x\text{Pt}_{1-x}(\text{en})_2][\text{Pt}(\text{en})_2\text{Cl}_2][\text{ClO}_4]_4$, with variable copper content ($0 < x < 1$), for comparison with the analogous $\text{Pt}^{\text{II}}/\text{Pt}^{\text{IV}}$ complex. The latter complex contains d^6 and d^8 metal sites, while the copper-platinum complex contains Cu^{II} , which has d^9 , with an unpaired electron in the $d_{x^2-y^2}$ orbital, z being the chain direction.⁷⁵ In spite of this, the $\text{M}^{\text{II}}-\text{Cl}$ and $\text{M}^{\text{IV}}-\text{Cl}$ distances are almost the same in the two complexes (2.318 and 3.085 Å, respectively, in the $\text{Pt}^{\text{II}}/\text{Pt}^{\text{IV}}$ case²³ and 2.313 and 3.081 Å, respectively, in the $\text{Cu}^{\text{II}}/\text{Pt}^{\text{IV}}$ case with $x = 0.89$ ⁷⁵). Nevertheless we might expect significant differences in the optical spectroscopy between the $\text{Pt}^{\text{II}}/\text{Pt}^{\text{IV}}$ and $\text{Cu}^{\text{II}}/\text{Pt}^{\text{IV}}$ cases, as a result of the different electron configurations and nuclear sizes involved. Oshio et al.⁷⁶ reported that, for the complex with a copper:platinum ratio of 0.89:1.11 (i.e. some M^{II} sites were occupied by Pt^{II}), the crystals were highly dichroic with a strong intervalence charge transfer band maximising at 21800 cm^{-1} . They further reported a resonance Raman spectrum showing ν_1 at 313 cm^{-1} , with an intense overtone progression ($\lambda_0 = 514.5 \text{ nm}$). Further investigation is reported here. The bromide-bridged complex $[\text{Cu}_x\text{Pt}_{1-x}(\text{en})_2][\text{Pt}(\text{en})_2\text{Br}_2][\text{ClO}_4]_4$ was also studied.

V.2. Synthesis

The monomeric species $\text{Cu}(\text{en})_2\text{Cl}_2$ and $\text{Pt}(\text{en})_2\text{Cl}_4$ were prepared by standard routes. They were then mixed in aqueous solution in stoichiometric quantities under various conditions of temperature, concentration and excess ClO_4^- counteranion, to obtain crystals of different

known Cu:Pt ratios, the aim being to obtain a ratio of 1. The ratio was estimated by determining the copper content by atomic absorption measurements. Microanalysis yielded, for example, for the sample with $x = 0.99$: C, 10.11; H, 3.32; N, 11.42; Cl, 22.26 %. Calculated for

$C_8H_{32}Cl_6N_8O_{16}Cu_{0.99}Pt_{1.01}$: C, 9.91; H, 3.33; N, 11.57; Cl, 21.95 %.

Copper percentages and calculated Cu:Pt ratios are recorded in Table 14. One powder sample was prepared by rapid precipitation in a large excess of perchlorate counteranion. Owing to perchlorate impurity, a useful copper analysis could not be carried out, but the sample is believed to have a Cu:Pt ratio very close to 1. Attempts were made to prepare likewise the bromide-bridged analogue, by cocrystallisation from aqueous solution of the monomeric species mixed in stoichiometric quantities. Microanalysis and atomic absorption yielded, for example: C, 9.82; H, 3.13; N, 10.89; Br, 10.96; Cl, 13.46; Cu, 6.09 %. Calculated for $C_8H_{32}Br_2Cl_4N_8O_{16}CuPt$: C, 9.09; H, 3.06; N, 10.61; Br, 15.12; Cl, 13.42; Cu, 6.01 %.

Electronic spectra were recorded from single crystals and pressed discs as described in Appendix II and Raman and resonance Raman spectra were obtained from single crystals and pressed discs at 40-80 K as described in Section II. Transmission infrared spectra were recorded on a Perkin-Elmer 337 spectrometer, at 295 K over the range 180-4000 cm^{-1} .

V.3. Results and Discussion

(a) Chloride-bridged Complexes

Electronic spectra are shown in Figure 38 and Raman and resonance Raman spectra in Figures 39-42; the data are summarised in Table 14. Raman band wavenumbers and assignments from a representative spectrum are given in Table 15. Red-brown crystals with a copper percentage of 6.36 (corresponding to a Cu:Pt ratio of 0.97:1.03), i.e. approaching closely the theoretical value of 6.57 % for a

Cu:Pt ratio of 1, were found to be scarcely dichroic, with an electronic band maximum (pressed disc) at around 420 nm (sample independent). Raman spectra of a single crystal from the same preparation (Figures 39-42) show a number of low wavenumber bands not observed for the discrete copper(II) and platinum(IV) constituent complexes. With an excitation wavelength of 676.4 nm, Raman bands at 322 and 341 cm^{-1} occur with approximately equal intensity. On changing to $\lambda_0 = 514.5$ nm, the 322 cm^{-1} band becomes the more enhanced, showing a weak overtone progression, while the 341 cm^{-1} band does not.

Other samples containing greater than 6% copper gave similar results (although the spectra indicate that the sample with 6.48 % Cu gives slightly anomalous results, which are discussed below). It seems likely^{75,76} that the red-brown colour possessed by these crystals arises principally from the $d_{xy} \rightarrow d_{x^2-y^2}$ transition within localised Cu^{II} units and, to a slight extent, from the IVCT absorption of $\text{Pt}^{\text{II}}/\text{Pt}^{\text{IV}}$ domains or chain sections.

On going to a sample containing a smaller copper percentage, the crystals become more intensely coloured and dichroic. Thus, in the case of a crystal with 3.79 % copper (corresponding to a Cu:Pt ratio of 0.58:1.42), the single crystal transmission electronic spectrum shows a strong visible band centred at 490 nm. This band is almost certainly due to intervalence charge transfer between Pt^{II} and Pt^{IV} sites (the IVCT band maximum for the pure $\text{Pt}^{\text{II}}/\text{Pt}^{\text{IV}}$ complex having been previously reported¹⁰ at 500 nm). In the Raman/resonance Raman spectrum the band at the smaller shift, then occurring at 309 cm^{-1} , becomes more intense at the expense of the 341 cm^{-1} band. An overtone progression $\nu_1 \nu_1$ in the 309 cm^{-1} band is observed to extend to $\nu_1 = 16$, with $\lambda_0 = 514.5$ nm. Thus the relative intensities of the two bands may be correlated approximately with the percentage of copper present, i.e. with the Cu:Pt ratio. Excitation profiles were determined for both bands, with excitation wavelengths throughout the

visible region (Figure 38), for a sample with a Cu:Pt ratio of 0.97:1.03. There is no significant enhancement of the 341 cm^{-1} band, but the profile of the 322 cm^{-1} band indicates a strong enhancement maximising at approximately 22000 cm^{-1} .

It seems likely that the band at 322 cm^{-1} should be assigned to $\nu_1(\text{Cl}-\text{Pt}^{\text{IV}}-\text{Cl})$, either from domains of $\text{Pt}^{\text{II}}/\text{Pt}^{\text{IV}}$ chain in $\text{Cu}^{\text{II}}/\text{Pt}^{\text{IV}}$ chains or from chains exclusively of $\text{Pt}^{\text{II}}/\text{Pt}^{\text{IV}}$ interspersed among $\text{Cu}^{\text{II}}/\text{Pt}^{\text{IV}}$ chains. Most probably, domains of all-platinum chain occur along the copper/platinum chains. This would account for both the variation in wavenumber of the ν_1 band at smaller Raman shift with copper content (as the Pt^{II} content increases, so the ν_1 wavenumber approaches that of the all $\text{Pt}^{\text{II}}/\text{Pt}^{\text{IV}}$ case) as well as the observed enhancement of the ν_1 band, which differs somewhat from that observed in the all $\text{Pt}^{\text{II}}/\text{Pt}^{\text{IV}}$ case,¹⁰ for which the maximum in the excitation profile occurs at 17000 cm^{-1} . Anomalous results from the sample with 6.48 % Cu appear to indicate that the proportion of Pt^{II} species present is greater than can be estimated from the copper percentage. They also show the sample to be inhomogeneous, there being substantial scattered intensity both at 309 cm^{-1} (accompanied by strong overtones) and at 322 cm^{-1} .

The band at 341 cm^{-1} may then be assigned to the ν_1' symmetric stretch, $\nu_s(\text{Cl}-\text{Pt}^{\text{IV}}-\text{Cl})$ of the $\text{Cu}^{\text{II}}/\text{Pt}^{\text{IV}}$ chain. The higher wavenumber of ν_1' compared with ν_1 in the $\text{Pt}^{\text{II}}/\text{Pt}^{\text{IV}}$ chain, or in the $\text{Ni}^{\text{II}}/\text{Pt}^{\text{IV}}$ (325 cm^{-1}) or $\text{Pd}^{\text{II}}/\text{Pt}^{\text{IV}}$ (328 cm^{-1}) cases,⁶⁰ is due to lesser valence delocalisation between the metal atom sites, i.e. the platinum is closer to oxidation state +4 in the Cu/Pt complex than in the other analogues mentioned above. ν_1' is, nevertheless, some 6 cm^{-1} lower than ν_1 of the discrete complex $[\text{Pt}(\text{en})_2\text{Cl}_4]$, for which it occurs at 347 cm^{-1} , indicating significant (albeit small) interaction between the Cu and Pt units. The absence of strong colour or dichroism in this complex suggests that

little or no visible intervalence charge transfer occurs and that there is probably little or no electron-phonon interaction. This is borne out by the absence of enhancement to the ν_1' band, using either visible or near uv excitation.

To verify that both the 322 and 341 cm^{-1} bands are due to symmetric (Cl-Pt^{IV}-Cl) stretch vibrations, infrared spectra were obtained of the complexes. There was found to be little variation with sample and typical spectra are shown in Figure 43. Corresponding wavenumbers and assignments are given in Table 16. The most significant feature is the absence of both the 322 and 341 cm^{-1} bands in the low wavenumber part of the spectrum. This indicates that they are both due to symmetric vibrations, in which there is no change of dipole moment with the motion, such as the ν_1 and ν_1' vibrations, to which they have been assigned.

In the Raman spectra it is noteworthy that the ν_1 band of the Pt^{II}/Pt^{IV} sections shows considerable structure (up to 8 components being observable, Figure 40), while the ν_1' band of the Cu^{II}/Pt^{IV} complex shows just an approximate 9:6:1 triplet, in accordance with expectation for an uncoupled (Cl-Pt^{IV}-Cl) symmetric stretching vibration.⁶⁰ The more complicated structure in the ν_1 band has been observed in numerous cases^{88,107,108} and is not yet fully explained (see Section VII). However, it is observed only in cases of strong electron-phonon interaction; its absence from the Raman spectrum of the Cu^{II}/Pt^{IV} complex is further evidence for the absence of such coupling in this complex.

The assignment by Oshio et al.⁷⁶ for the Cu^{II}/Pt^{IV} complex with $x = 0.89$ of an intense, z-polarised, electronic band at 22000 cm^{-1} to the IVCT transition from Cu^{II} to Pt^{IV} is believed to be incorrect. It seems more likely that this band should be attributed to Pt^{II} Pt^{IV} transitions of Pt^{II}/Pt^{IV} sections in the chains. Their assignment of a strongly

enhanced Raman band at 313 cm^{-1} ($\lambda_0 = 514.5 \text{ nm}$) to ν_1' (Cl-Pt^{IV}-Cl) of the Cu^{II}/Pt^{IV} chain is also believed to be erroneous. In the Raman spectrum of Oshio et al. the unenhanced ν_1' band of $[\text{Cu}(\text{en})_2][\text{Pt}(\text{en})_2\text{Cl}_2][\text{ClO}_4]_4$ at approximately 340 cm^{-1} was masked by the much more intense ν_1 band progression of $[\text{Pt}(\text{en})_2][\text{Pt}(\text{en})_2\text{Cl}_2][\text{ClO}_4]_4$, arising from the presence of substantial amounts of that complex.

(b) Bromide-bridged Complexes

Unlike in the chloride-bridged case, the bromide-bridged complexes gave no conclusive results. Different syntheses produced crystals which differed dramatically in appearance. Crystals with the very low copper content of 0.83 %, compared with the theoretical value for $[\text{Cu}(\text{en})_2][\text{Pt}(\text{en})_2\text{Br}_2][\text{ClO}_4]_4$ of 6.01 %, appear lustrous green and dichroic and, when ground, produce a purple powder. Crystals with the very high copper content of 6.09 % appear red-brown and non-dichroic, like the equivalent chloride-bridged complexes. When ground, they give, as in the chloride-bridged case, an orange powder with a weak maximum in the electronic spectrum at approximately 420 nm.

In the case of small copper content there appears to be a high proportion of Pt^{II}/Pt^{IV} complex present, which gives the crystals the characteristics of the pure Pt^{II}/Pt^{IV} complex. With higher copper content these features diminish and the crystals show no substantial intervalence charge transfer, the red-brown colour being, as in the chloride-bridged case, probably due to $d_{xy} \rightarrow d_{x^2-y^2}$ transitions in individual Cu^{II} units.

The above interpretation is not, however, fully supported by the Raman spectroscopic results. For complexes with both low and high copper percentages, the Raman spectrum shows a progression $\nu_1\nu_1'$ in a symmetric (Br-Pt^{IV}-Br) stretching vibration, the fundamental

occurring at 171 to 174 cm^{-1} and the progression extending to $\nu_1 = 7$ ($\lambda_0 = 676.4 \text{ nm}$). Further, weak progressions $\nu_i + \nu_1 \nu_1$ were also observed. These progressions are most likely to be in ν_1 from $\text{Pt}^{\text{II}}/\text{Pt}^{\text{IV}}$ domains in the chains. No bands were observed which were not reported for the pure $\text{Pt}^{\text{II}}/\text{Pt}^{\text{IV}}$ complex. Thus $\nu_1'(\text{Br}-\text{Pt}^{\text{IV}}-\text{Br})$ from the $\text{Cu}^{\text{II}}/\text{Pt}^{\text{IV}}$ complex appeared always to be masked by the strong resonance enhancement of $\nu_1(\text{Br}-\text{Pt}^{\text{IV}}-\text{Br})$ from the $\text{Pt}^{\text{II}}/\text{Pt}^{\text{IV}}$ domains presumed to be present.

Table 14

Summary of optical results from copper-platinum complexes

% Cu in sample	Estimated formula	λ_{max} nm	λ_0 nm	$\nu_1'(\text{Cu}/\text{Pt})$ /cm ⁻¹	$\nu_1(\text{Pt}/\text{Pt})$ /cm ⁻¹	$I(\nu_1')/$ $I(\nu_1)$
3.79	[Cu _{0.58} Pt _{0.42} (en) ₂][Pt(en) ₂ Cl ₂](ClO ₄) ₄	420 ^a 490 ^b	676.5	340	309	0.003
6.36	[Cu _{0.97} Pt _{0.03} (en) ₂][Pt(en) ₂ Cl ₂](ClO ₄) ₄	420 ^a	676.5	341	322.5	0.99 ^c
6.39	[Cu _{0.97} Pt _{0.03} (en) ₂][Pt(en) ₂ Cl ₂](ClO ₄) ₄	420 ^a	676.5	340	322	0.99 ^c
6.48	[Cu _{0.99} Pt _{0.01} (en) ₂][Pt(en) ₂ Cl ₂](ClO ₄) ₄	420 ^a	676.5	340	322	2.26 ^c
Unmeasurable ^e	[Cu(en) ₂][Pt(en) ₂ Cl ₂](ClO ₄) ₄	420 ^a	676.5	342	321	13.87 ^d

a Transmission by pressed disc with NaCl matrix

b Single crystal transmission

c Scattering from single crystal

d Scattering from pressed disc

e Preparation was by fast precipitation with excess perchlorate present

Table 15. Wavenumbers $\tilde{\nu}$, relative intensities $I(\tilde{\nu})/I(\nu_1)$, full widths at half maximum $\Delta\tilde{\nu}_{1/2}$ and assignments of bands in the Raman spectrum of $[\text{Cu}_{0.97}\text{Pt}_{0.03}(\text{en})_2][\text{Pt}(\text{en})_2\text{Cl}_2](\text{ClO}_4)_4$. $\lambda_0 = 514.5$ nm. $\nu'_1 = \nu(\text{Cl-Pt}^{\text{IV}}-\text{Cl})_{\text{sym}}$ in $\text{Cu}^{\text{II}}/\text{Pt}^{\text{IV}}$ bulk, $\nu_1 = \nu(\text{Cl-Pt}^{\text{IV}}-\text{Cl})_{\text{sym}}$ in $\text{Pt}^{\text{II}}/\text{Pt}^{\text{IV}}$ impurity, ν_a is an unassigned enabling mode.

$\tilde{\nu}/\text{cm}^{-1}$	$I(\tilde{\nu})/I(\nu_1)$	$\Delta\tilde{\nu}_{1/2}/\text{cm}^{-1}$	Assignment
188	0.09	14	
291	0.04	6	ν_a
312	0.38	9.5	ν_1' ($^{37}\text{Cl-Pt-}^{37}\text{Cl}$)
316.5	0.67	9.5	ν_1' ($^{37}\text{Cl-Pt-}^{35}\text{Cl}$)
321.5	1.00	9.5	ν_1' ($^{35}\text{Cl-Pt-}^{35}\text{Cl}$)
331	0.09	3.8	ν_1' ($^{37}\text{Cl-Pt-}^{37}\text{Cl}$)
336	0.29	3.8	ν_1' ($^{37}\text{Cl-Pt-}^{35}\text{Cl}$)
341	0.47	3.8	ν_1' ($^{35}\text{Cl-Pt-}^{35}\text{Cl}$)
357.5	0.39	4.8	$\nu_2, \nu(\text{Cl-Pt-Cl})_{\text{asym}}$
521	0.03	3.2	
582	0.03	4.4	$2\nu_a$
622	0.04	6	$\nu_a + \nu_1'$ ($^{37}\text{Cl-Pt-}^{35}\text{Cl}$)
630.5	0.05	6	$\nu_a + \nu_1'$ ($^{35}\text{Cl-Pt-}^{35}\text{Cl}$)
640	0.04	12	$2\nu_1'$ ($^{35}\text{Cl-Pt-}^{35}\text{Cl}$)
671	0.03	6	$2\nu_1'$ ($^{37}\text{Cl-Pt-}^{35}\text{Cl}$)
677	0.03	6	$2\nu_1'$ ($^{35}\text{Cl-Pt-}^{35}\text{Cl}$)
889.5	< 0.01	4	
927	0.02	6	
935	0.03	6	

Table 16. Wavenumbers $\tilde{\nu}$ and assignments of bands in the 180-4000 cm^{-1} region of the infrared spectrum of $[\text{Cu}_{0.97}\text{Pt}_{0.03}(\text{en})_2][\text{Pt}(\text{en})_2\text{Cl}_2](\text{ClO}_4)_4$. Spectra obtained from sample/NaCl and sample/wax pressed discs at 295 K.

$\tilde{\nu}/\text{cm}^{-1}$		Assignment ^a
(a) NaCl disc		
3521	w	$\nu(\text{O-H})$
3319	s	$\nu(\text{N-H})$
3263	s	$\nu(\text{N-H})$
3192	s	$\nu(\text{N-H})$
3104	s	$\nu(\text{N-H})$
2978	w	$\nu(\text{C-H})$
2894	vw	$\nu(\text{C-H})$
1589	s	$\delta(\text{N-H})$
1449	m	
1315	vw	
1303	m	
1282	w	
1261	w	
1178	w	
1073	s	$\nu(\text{C-N})$
1011	w	
990	vw	$\rho(\text{CH}_3)$
974	w	
929	w	
872	vw	
828	w	
712	m	$\rho(\text{NH}_2)$
626	s	$\nu_4(\text{ClO}_4^-)$
(b) Wax disc		
598	vw	
577	w	
555	w	

Table 16 continued.

 $\tilde{\nu} / \text{cm}^{-1}$

Assignment

(b) Wax disc continued.

527	m	ν (Pt-N)
479	w	
422	w	
354	s	$\nu_{\text{as}}(\text{Cl-Pt}^{\text{IV}}-\text{Cl})$
296	s	
238	vw	
232	w	
217	w	
213	w	
203	vw	

a Types of vibration: ν - stretch δ - bend ρ - rock

Captions to the following Figures

Figure 38. Transmission electronic spectra of $[\text{Cu}_x\text{Pt}_{1-x}(\text{en})_2][\text{Pt}(\text{en})_2\text{Cl}_2](\text{ClO}_4)_4$ (baseline refers only to spectrum (a)), and excitation profiles of the ν_1 and ν_1' bands at 322 and 340 cm^{-1} respectively from a sample containing 6.36 % Cu ($x = 0.97$).

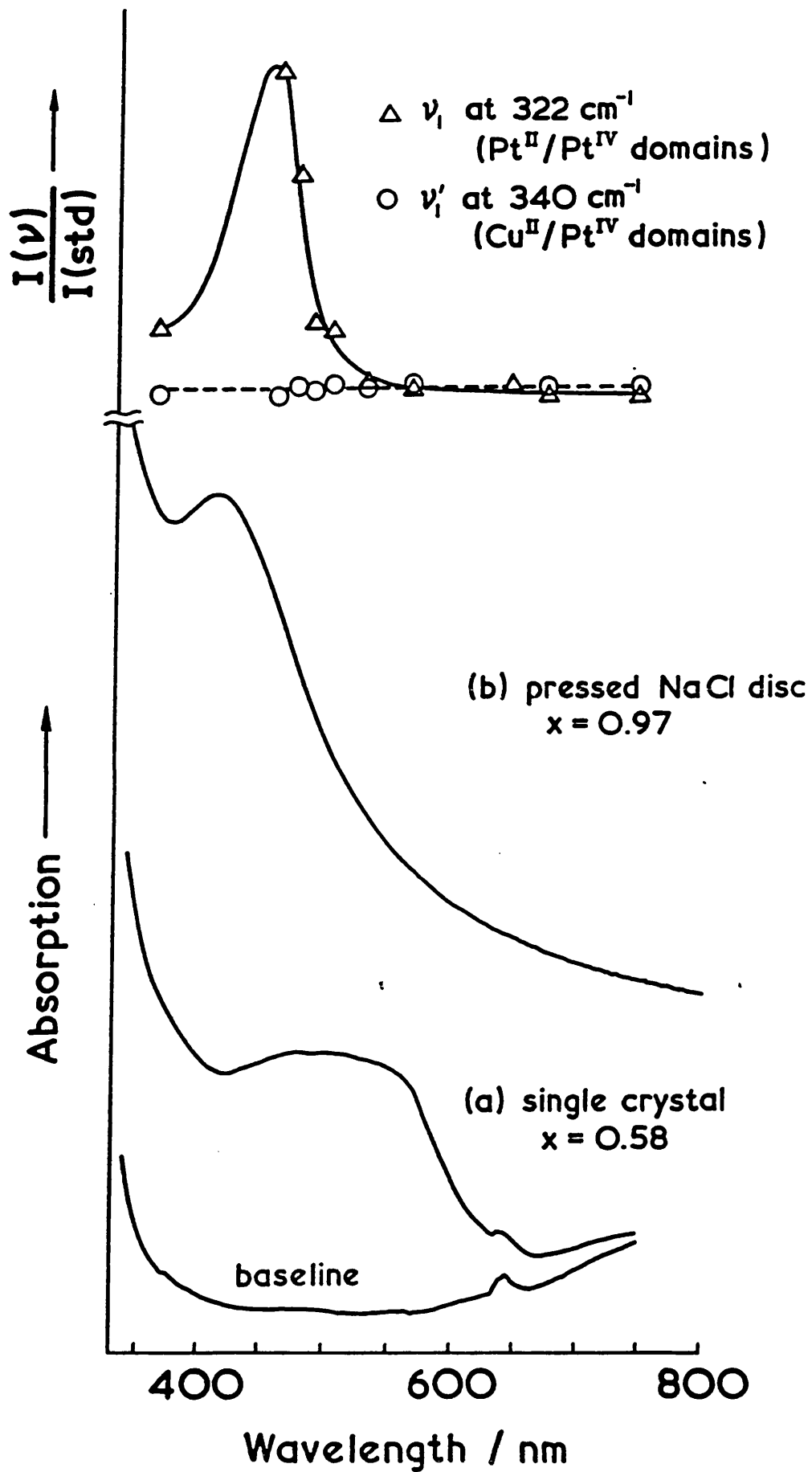
Figure 39. Raman spectra of $[\text{Cu}_x\text{Pt}_{1-x}(\text{en})_2][\text{Pt}(\text{en})_2\text{Cl}_2](\text{ClO}_4)_4$ (pressed disc at ca. 80 K, $\lambda_0 = 676.4$ nm, slitwidth = 400 μm).

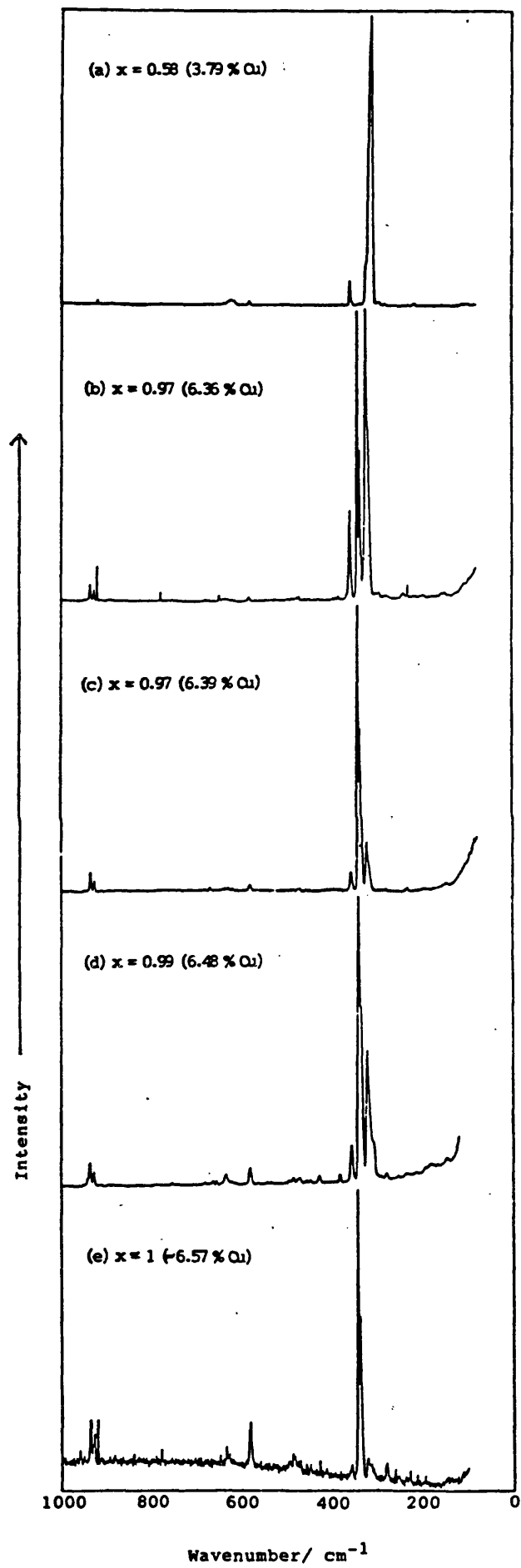
Figure 40. The 295-375 cm^{-1} region of the Raman spectra of $[\text{Cu}_x\text{Pt}_{1-x}(\text{en})_2][\text{Pt}(\text{en})_2\text{Cl}_2](\text{ClO}_4)_4$ (pressed disc at ca. 80 K, $\lambda_0 = 676.4$ nm, slitwidth = 200 μm , (a)-(d) and 400 μm , (e)).

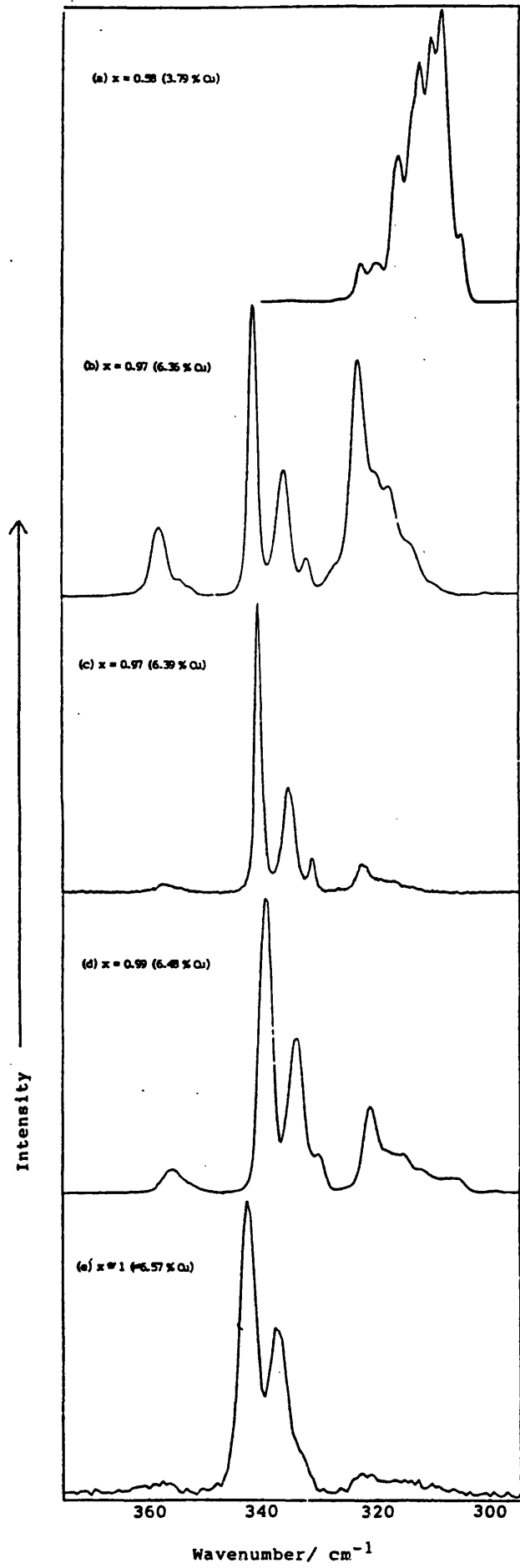
Figure 41. Raman/resonance Raman spectra of $[\text{Cu}_x\text{Pt}_{1-x}(\text{en})_2][\text{Pt}(\text{en})_2\text{Cl}_2](\text{ClO}_4)_4$ (pressed disc at ca. 80 K, $\lambda_0 = 514.5$ nm, slitwidth = 200 μm).

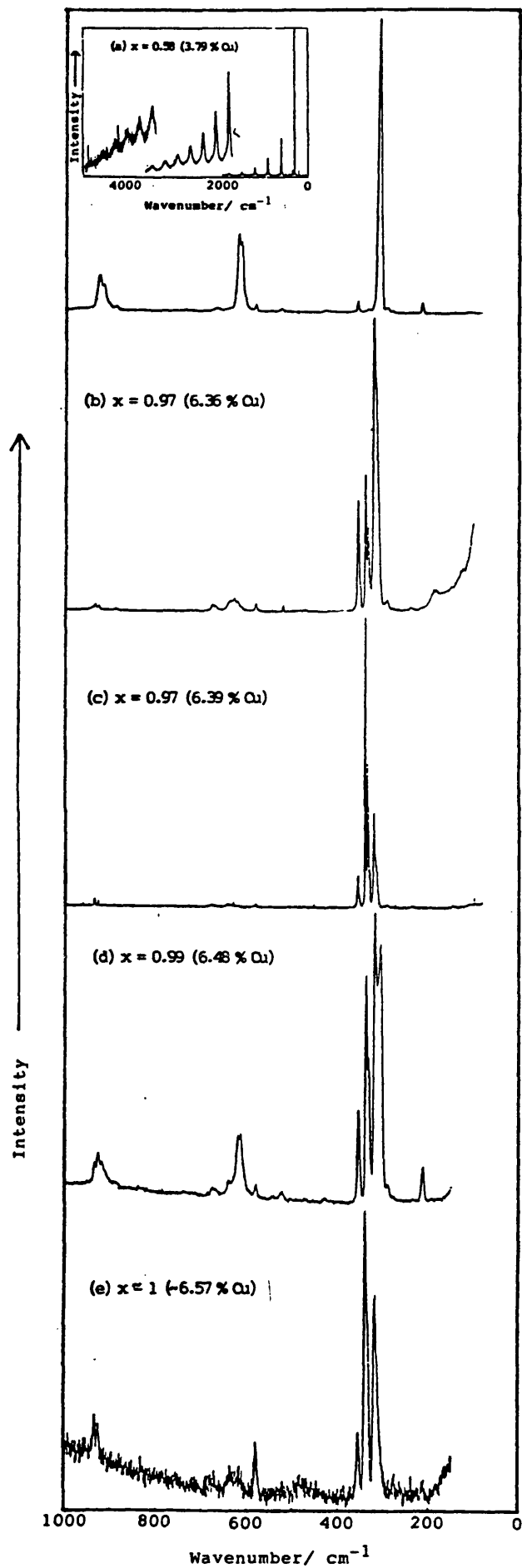
Figure 42. The 295-375 cm^{-1} region of the Raman/resonance Raman spectra of $[\text{Cu}_x\text{Pt}_{1-x}(\text{en})_2][\text{Pt}(\text{en})_2\text{Cl}_2](\text{ClO}_4)_4$ (pressed disc at ca. 80 K, $\lambda_0 = 514.5$ nm, slitwidth = 80 μm , (a)-(d) and 200 μm , (e)).

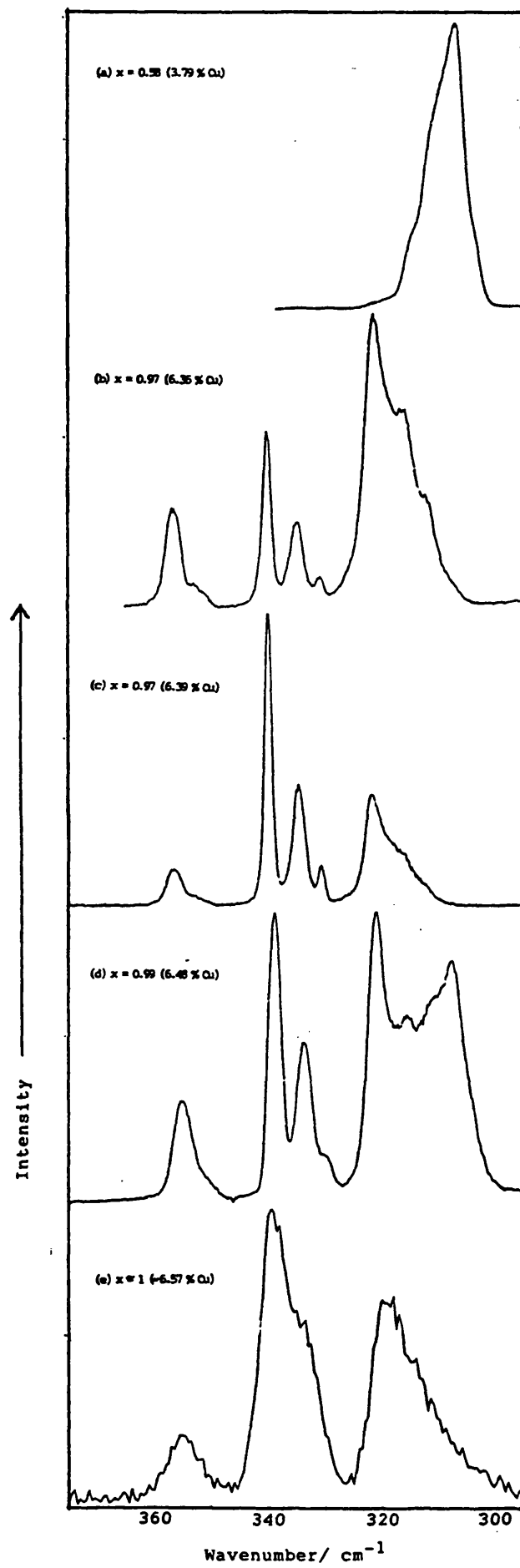
Figure 43. Infrared spectrum of $[\text{Cu}_{0.97}\text{Pt}_{0.03}(\text{en})_2][\text{Pt}(\text{en})_2\text{Cl}_2](\text{ClO}_4)_4$. Spectrum obtained from pressed discs of sample with NaCl, (a) and paraffin wax, (b) at 295 K.

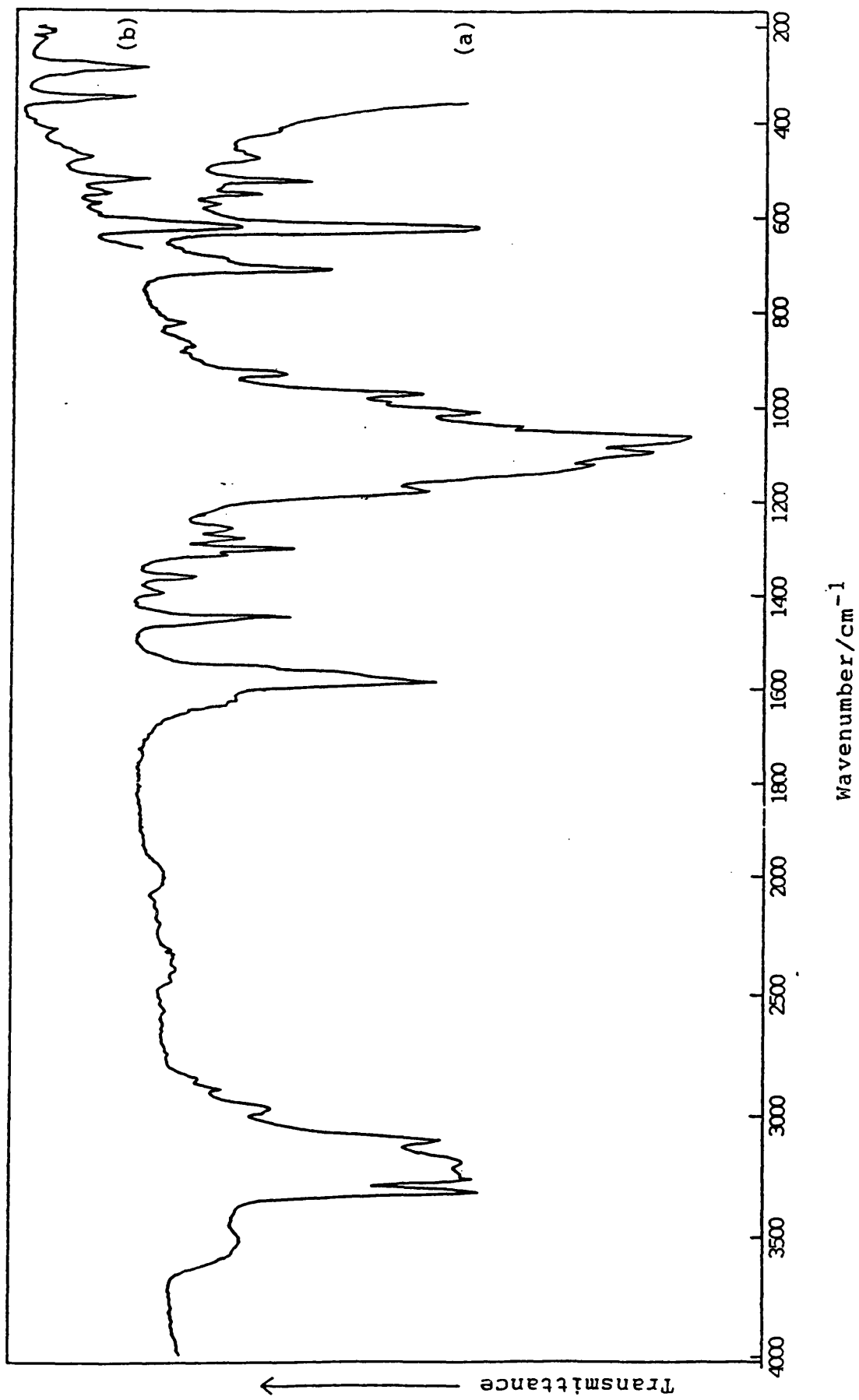












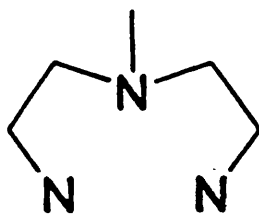
VI. FURTHER STUDIES OF PLATINUM AND PALLADIUM COMPLEXES

VI.1. A Raman Study of the Terdentate Ligand 3-methyl-3-azapentane-1,5-diamine, in its Coordination to Pt(II) and Pt(IV) and in a Mixed-valence Chain

VI.1.1. Introduction

Raman and resonance Raman spectra were obtained of platinum complexes containing the terdentate ligand 3-methyl-3-azapentane-1,5-diamine (abbreviated to 4Me-dien), including the mixed-valence complex $[\text{Pt}(4\text{Me-dien})\text{I}][\text{Pt}(4\text{Me-dien})\text{I}_3]\text{I}_2$. Previous studies have been carried out on the mixed-valence chain complexes $[\text{Pt}(\text{dien})\text{I}][\text{Pt}(\text{dien})\text{I}_3]\text{I}_2$, where dien = 3-azapentane-1,5-diamine, and $[\text{Pt}(\text{lMe-dien})\text{I}][\text{Pt}(\text{lMe-dien})\text{I}_3]\text{I}_2$, where lMe-dien = N-methyl-3-azapentane-1,5-diamine. These complexes are the only examples of the relatively rare +1 charge type yet to have been structurally characterised. They display some interesting structural features. The dien ligands are eclipsed in alternate pairs along the chain; the puckering of the two condensed rings of each ligand makes them slightly concave, the concavity being oriented in the same sense throughout the chain. The deviation from linearity of the iodide-bridged chains (e.g. Pt-I...Pt angles for the dien complex of 153 and 158 degrees¹⁵) is larger than for any other type of chain complex of platinum or palladium (section I.4.1). The methyl substituent of lMe-dien causes further bending of the chain centred on I...Pt^{II}...I junctions, and an overall increase of the Pt^{II}....Pt^{IV} distance.

The effect of introducing a methyl substituent on to the central nitrogen atom of the ligand dien on the ease of formation of the mixed-valence complex and on the Raman spectra thereof has been investigated. The ligand thus produced, 4Me-dien, is depicted below. Syntheses, carried out by Dr. F. P. Fanizzi, were as described in Appendix III. Raman spectra were obtained from pressed discs at 40 - 80 K as described in Section II.



4 Me-dien

VI.1.2. Results and Discussion

The Raman spectrum of the Pt(II) monomeric complex is shown in Figure 44. The corresponding Pt(IV) complex absorbed much of the incident radiation and consequently its Raman spectrum does not show the large number of bands (associated primarily with the 4Me-dien ligand) at higher Raman shift seen in Figure 44. However, the Raman spectrum of $[\text{Pt}(4\text{Me-dien})\text{I}_3]\text{I}$ did show a band at 172 cm^{-1} , which has been assigned to the $\text{Pt}^{\text{IV}}\text{-I}$ stretch vibration.

The Raman spectrum ($\lambda_0 = 647.1\text{ nm}$) of the mixed-valence complex $[\text{Pt}(4\text{Me-dien})\text{I}][\text{Pt}(4\text{Me-dien})\text{I}_3]\text{I}_2$ is shown in Figure 45(a). This spectrum indicates the resonance enhancement of several progressions, some of which become more strongly enhanced on changing the wavelength of the exciting line (Figure 45(b), $\lambda_0 = 799.3\text{ nm}$) towards the deep red (i.e. within the contour of the intervalence charge transfer band). Enhancement occurs for the band at 116.5 cm^{-1} , assigned to the ν_1 symmetric (I-Pt^{IV}-I) stretch vibration, the progression $\nu_1\nu_1$ being observed up to $\nu_1 = 6$. Weaker enhancement occurs for the $\nu_1\nu_1 + \nu_a$ progression up to $\nu_1 = 5$ (where ν_a is an unassigned enabling mode, c.f. a similar band reported by Clark and Kurmoo¹¹⁰), and for $\nu_1\nu_1 + \nu_2$ up to $\nu_1 = 3$ (where ν_2 is $\nu(\text{Pt-I})_{\text{eq}}$). Other progressions detected in the 647.1 nm spectrum include $\nu_1\nu_1 + \nu_3$ up to $\nu_1 = 2$ and $\nu_1\nu_1 + s$ up to $\nu_1 = 3$, where neither of the enabling

modes ν_3 or s could be assigned (although s could be the difference mode $\nu_2 - \nu_a$). Wavenumbers, intensities, halfwidths and band assignments for the spectrum in Figure 45(a) are given in Table 17. The excitation profile of the ν_1 band, which allows for variation in spectral response and intensity dependence on wavenumber and which is normalised (at $\lambda_0 = 647.1$ nm, enhancement factor = 1), is shown in Figure 46. The profile reaches a maximum at ca. 13000 cm^{-1} , suggesting that ν_1 is coupled strongly with the intervalence transition.

The wavenumber of ν_1 , at 116.5 cm^{-1} , is somewhat lower than in the case where dien is the equatorial ligand ($\nu_1 = 120.2\text{ cm}^{-1}$). This is considered to be due to increased steric hindrance from the ligand 4Me-dien to the creation of the linear chain. In all cases except that of the $\text{Pt}^{\text{II}}/\text{Pt}^{\text{IV}}$ linear chain, 4Me-dien takes up the fac (bent) conformation around Pt^{IV} . Iodination of the Pt(II) complex gives the trans iodo- Pt(IV) product, with 4Me-dien in the mer (planar) conformation. Immediate (in situ) crystallisation of this between further Pt(II) complexes to give the linear chain complex causes the 4Me-dien around Pt(IV) to remain mer rather than relaxing to fac. This additional stress on the lattice leads to the $\text{Pt}^{\text{IV}}\text{-I}$ bond being weaker.

Table 17. Wavenumbers $\tilde{\nu}$, relative intensities $I(\tilde{\nu})/I(\nu_1)$, full widths at half maximum $\Delta\tilde{\nu}_{1/2}$ and assignments of bands in the Raman spectrum of $[\text{Pt}(4\text{Me-dien})\text{I}][\text{Pt}(4\text{Me-dien})\text{I}_3]\text{I}_2$. $\lambda_0 = 647.1$ nm. $\nu_1 = \nu(\text{I-Pt}^{\text{IV}}-\text{I})_{\text{sym}}$ and $\nu_2 = \nu(\text{Pt}^{\text{IV}}-\text{I})_{\text{eq}}$.

$\tilde{\nu}/\text{cm}^{-1}\text{a}$	$I(\tilde{\nu})/I(\nu_1)$	$\Delta\tilde{\nu}_{1/2}/\text{cm}^{-1}$	Assignment ^b
72.5	0.03	13	S or $\nu_2 - \nu_a$
94.5	0.88	8.7	ν_a
116.5	1.00	8.7	ν_1
139.0	0.03	13	
167.0	0.57	5.2	ν_2
188.0	0.09	15.2	$\nu_1 + S$
213.5	0.14	26.1	$\nu_1 + \nu_a$
235.5	0.10	26.1	$2\nu_1$
260.5	0.10	13.9	ν_3
285.5	0.08	23.9	$\nu_1 + \nu_2$
305.5	0.03	21.7	$2\nu_1 + S$
333.0	0.07	28	$2\nu_1 + \nu_a$
353.5	0.05	28	$3\nu_1$
378	0.03	26	$\nu_1 + \nu_3$
402	0.02	26	$2\nu_1 + \nu_2$
425	0.02	26	$3\nu_1 + S$
448	0.03	30	$3\nu_1 + \nu_a$
472	0.01	30	$4\nu_1$
495	0.01	26	$2\nu_1 + \nu_3$
521	0.01	-	$3\nu_1 + \nu_2$
529	0.01	-	

a The members of the $\nu_1\nu_1$ progression have, with 799.3 nm excitation, slightly lower wavenumbers (with the exception of ν_1) than with 647.1 nm excitation, as frequently observed for chain complexes^{88,108}; viz. ν_1 , 117.0; $2\nu_1$, 233.0; $3\nu_1$, 348.0; $4\nu_1$, 463; $5\nu_1$, 578; $6\nu_1$, 693 cm^{-1} .

b S (possibly skeletal), ν_a and ν_3 are unassigned enabling modes.

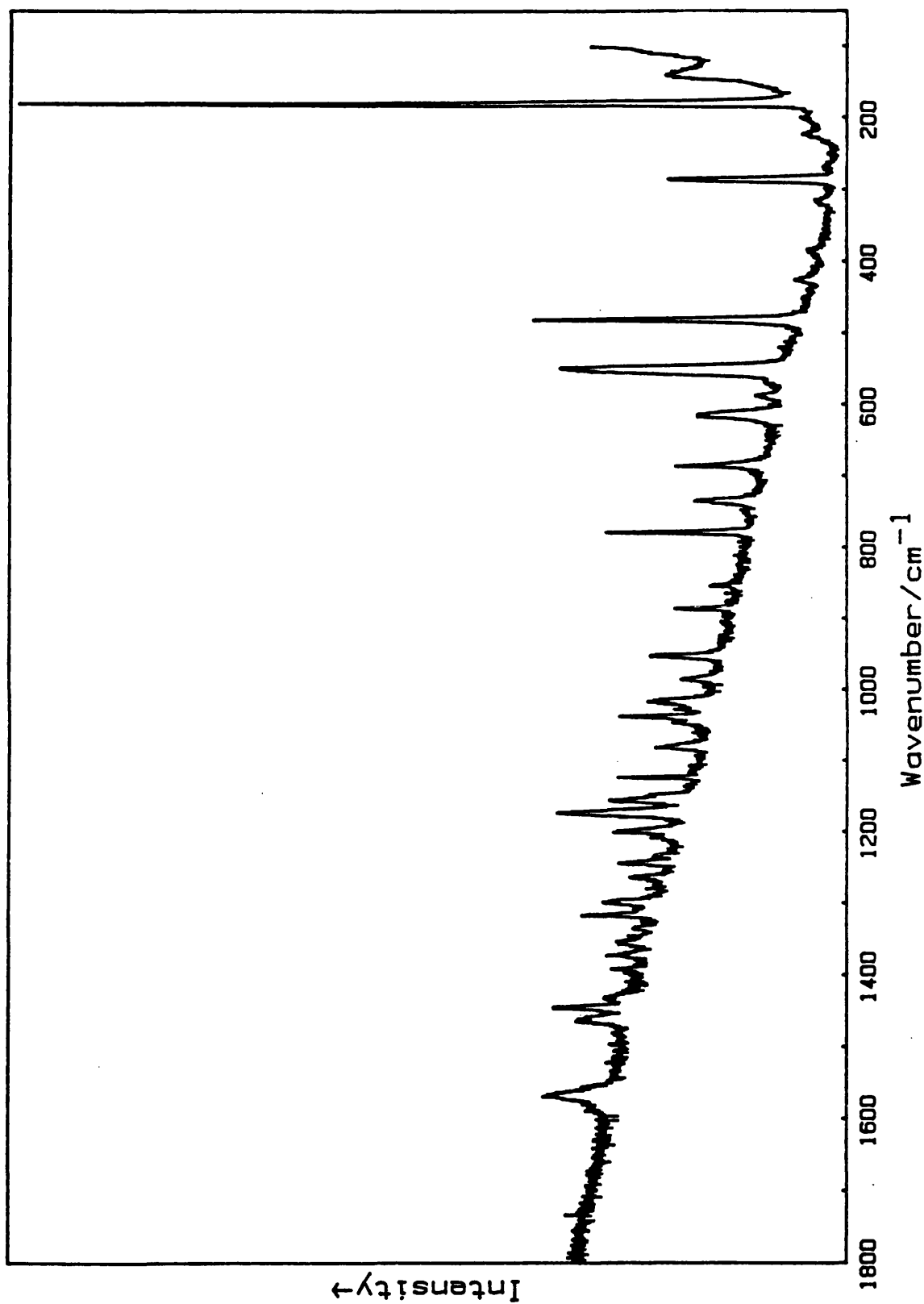


Figure 44. Raman spectrum of [Pt(4Me-dien)I]I (sample/K₂SO₄ pressed disc at ca. 80 K, $\lambda_0 = 514.5$ nm).

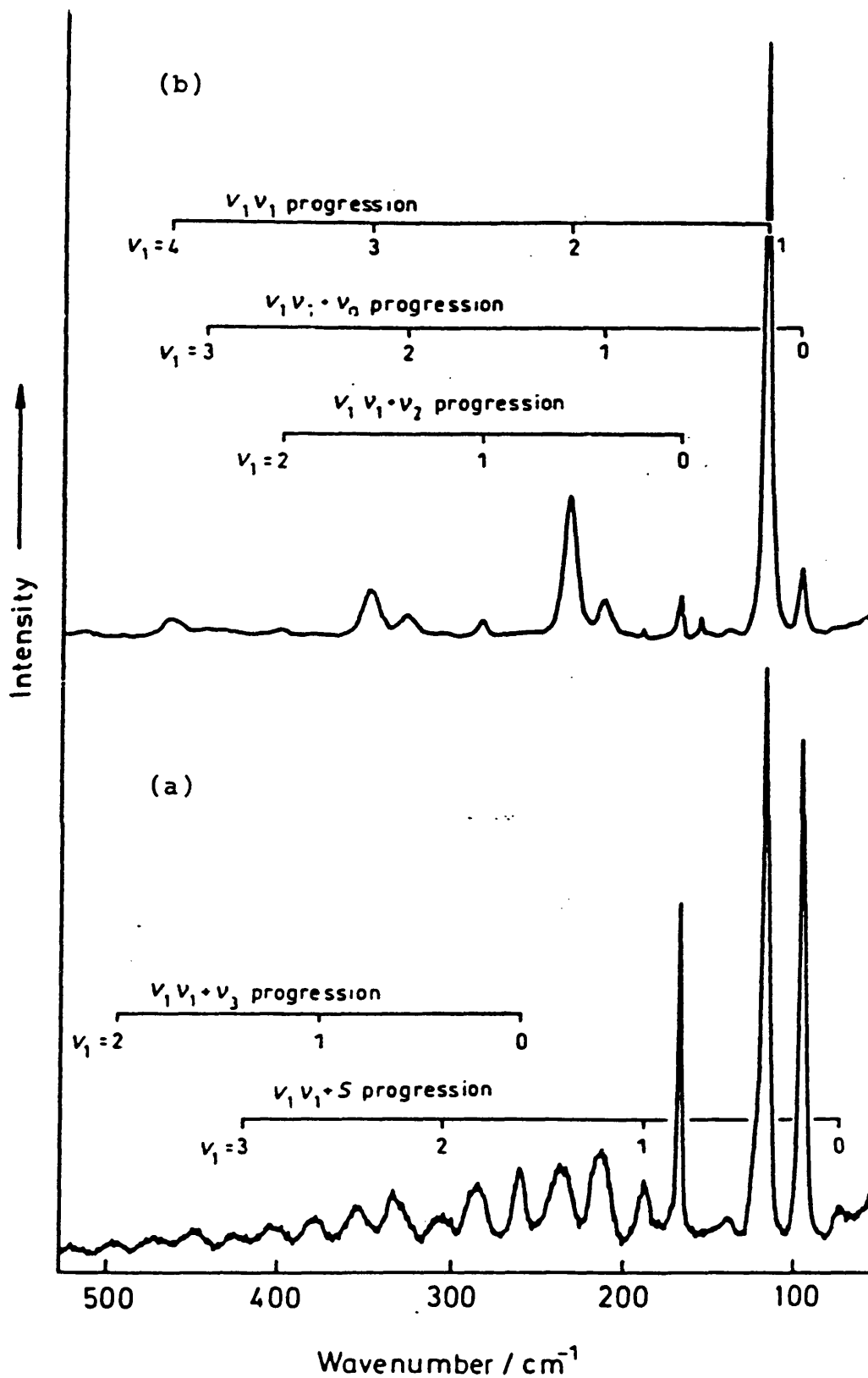


Figure 45. Raman ($\lambda_0 = 647.1$ nm, (a)) and resonance Raman ($\lambda_0 = 799.3$ nm, (b)) spectra of $[\text{Pt}(\text{4Me-dien})\text{I}][\text{Pt}(\text{4Me-dien})\text{I}_3]\text{I}_2$ (sample/ K_2SO_4 pressed disc at ca. 80 K).

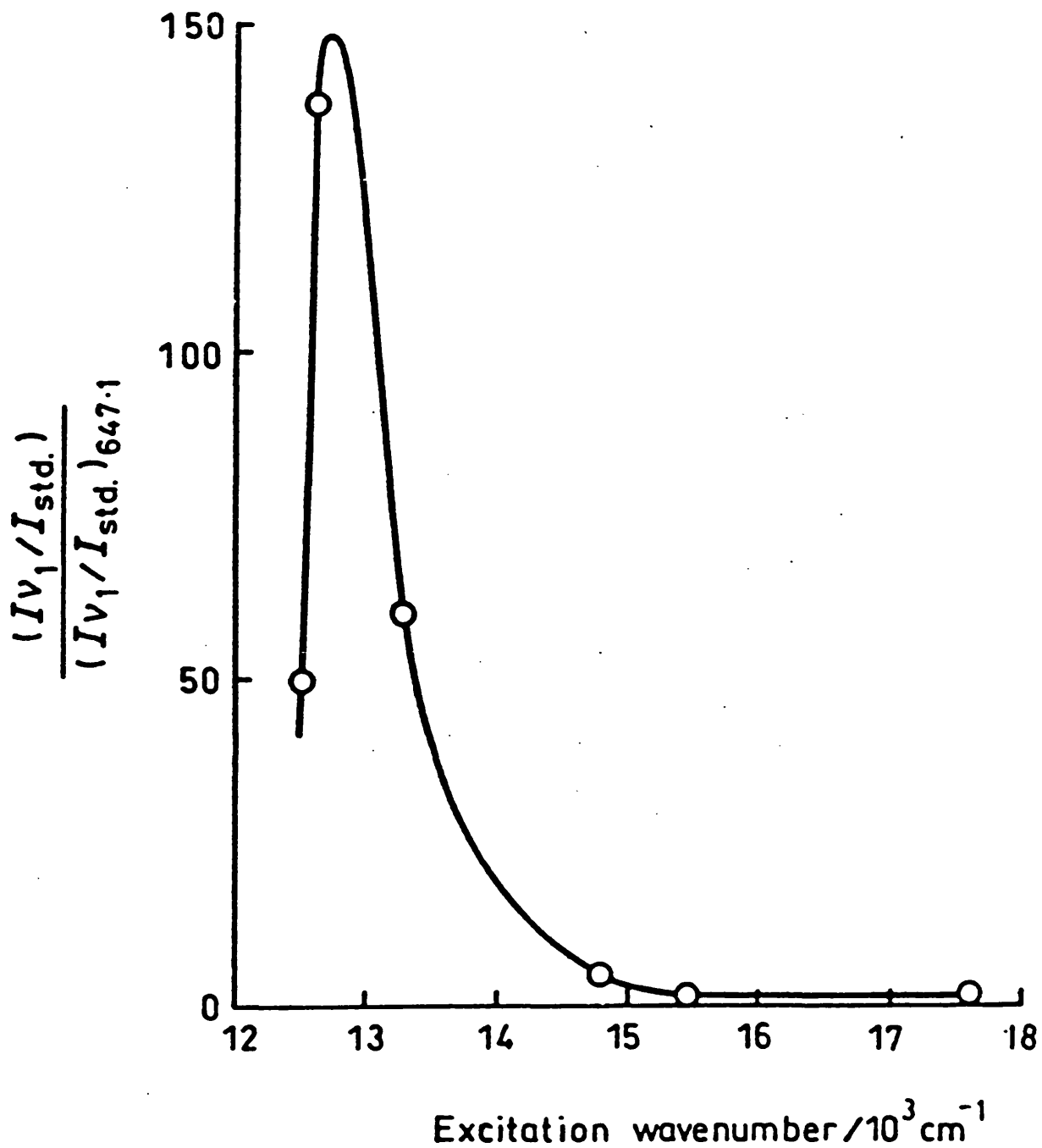


Figure 46. Normalised excitation profile of the ν_1 band of $[\text{Pt}(4\text{Me-dien})\text{I}][\text{Pt}(4\text{Me-dien})\text{I}_3]\text{I}_2$.

VI.2. Raman Spectroscopy of the Bromide-bridged Palladium Complex $[\text{Pd}(-\text{chxn})_2][\text{Pd}(-\text{chxn})_2\text{Br}_2]\text{Br}_4$

VI.2.1. Introduction

The halogen-bridged mixed-valence complex $[\text{Pd}(-\text{chxn})_2][\text{Pd}(-\text{chxn})_2\text{Br}_2]\text{Br}_4$ was studied by means of resonance Raman spectroscopy and found to display unusual features. Previously Toftlund et al.⁸⁶ reported a resonance Raman spectrum of this complex obtained with 514.5 nm excitation radiation. Their spectrum indicated a doublet of ν_1 peaks at 180.5 and 189 cm^{-1} , both of which were resonance enhanced, and overtones coalescing for $\nu_1 \geq 3$. They also reported a specular single crystal reflectance spectrum indicating an IVCT band maximum of $<10000 \text{ cm}^{-1}$. The Raman spectroscopy reported here extends the study to excitation wavelengths ranging from 647.1 to 799.3 nm, i.e. approaching closer to the IVCT band maximum than in the previous work. Raman spectra were obtained from a pressed disc of the pure complex (as supplied by Dr. H. Toftlund) at 80 K as described in Section II.

VI.2.2. Results and Discussion

A full resonance Raman spectrum of $[\text{Pd}(-\text{chxn})_2][\text{Pd}(-\text{chxn})_2\text{Br}_2]\text{Br}_4$, obtained with excitation at 676.4 nm, is shown in Figure 47 and corresponding band wavenumbers, intensities, halfwidths and assignments are given in Table 18. This spectrum shows an intense band at 166 cm^{-1} , assigned to a symmetric (Br-Pd^{IV}-Br) stretch vibration, and an accompanying progression, extending to the sixth harmonic. Examination with other excitation wavelengths reveals further features in the spectroscopy of this complex. Resonance Raman spectra of $[\text{Pd}(-\text{chxn})_2][\text{Pd}(-\text{chxn})_2\text{Br}_2]\text{Br}_4$ in the 100-600 cm^{-1} region, obtained with excitation wavelengths 514.5, 568.2, 647.1, 676.4, 752.5 and 799.3 nm, are shown in Figures 48 and 49. Corresponding data are given in Table 19. Fundamental bands are observed at 155.5 (designated ν_1),

166 (ν_1'), 178 (ν_1'') and 185 cm^{-1} (ν_1'''). While the wavenumbers of these fundamentals do not vary with change of excitation wavelength, their relative intensities and extent of resonance enhancement change greatly. With change of excitation from 799.3 nm through to 514.5 nm, the bands at higher wavenumber successively gain in intensity, at the expense of those at lower wavenumber. Thus, at 799.3 nm, the 155.5 cm^{-1} band is dominant and at 514.5 nm, the 185 cm^{-1} band dominates, while the 166 and 178 cm^{-1} bands are stronger with intermediate wavelengths. In a given spectrum, the relative intensities of the fundamentals are maintained in the overtone bands.

The origin of the four observed bands is unclear. They all show a pronounced resonance enhancement and are therefore all considered to correspond to symmetric stretch vibrations of the $\nu(\text{Br-Pd}^{\text{IV}}\text{-Br})_{\text{sym}}$ type. A similar effect has been observed¹³ in the case of some analogous complexes containing (-chxn). For example, the wavenumber of ν_1 of $[\text{Pd}(-\text{chxn})_2][\text{Pd}(-\text{chxn})_2\text{Cl}_2]\text{Cl}_4$ was observed to show a reversible decrease in wavenumber of 59 cm^{-1} with decreasing excitation energy in the visible region. With higher resolution, this dispersion was seen to be due to changes in relative intensity of component bands of invariant wavenumber. Such apparent dispersion of ν_1 , while widespread in complexes of this type (see section VII), was not observed in the case of $[\text{Pd}(-\text{chxn})\text{-Br-Br}]$, because the components ν_1 , ν_1' , ν_1'' and ν_1''' are so far apart (the average separation of adjacent components being 9.8 cm^{-1}). Weaker, subsidiary bands, such as those assigned by Donohoe et al.¹¹¹ to defect states in the chains, were also not observed. The origin of the components may be, in part, the same as that of apparent ν_1 dispersion in other such complexes (e.g. photoselective enhancement of different chain lengths), although it should be noted that only complexes containing chxn have shown such a high degree of ν_1 band complexity. Where both cis- and trans-chxn are present, or where, for example, trans-chxn is

unresolved, some components may be ascribed to different cis/trans or +/- combinations being present. However, where only (-)trans-chxn is present, the only possible variation is in chelate conformation, which may be $\lambda\lambda$ or $\delta\delta$ (i.e. both conformers around one metal site are either λ or δ). The viability of ascribing ν_1 , ν_1' , ν_1'' and ν_1''' to different conformer combinations in the chain is uncertain.

Table 18. Wavenumbers $\tilde{\nu}$, relative intensities $I(\tilde{\nu})/I(\nu_1')$, full widths at half maximum $\tilde{\nu}_{\frac{1}{2}}$ and assignments of bands in the resonance Raman spectrum of $[\text{Pd}(-\text{chxn})_2][\text{Pd}(-\text{chxn})_2\text{Br}_2]\text{Br}_4$, obtained with excitation at 676.4 nm.

$\tilde{\nu}/\text{cm}^{-1}$	$I(\tilde{\nu})/I(\nu_1')$	$\nu_{\frac{1}{2}}/\text{cm}^{-1}$	Assignment
73	0.19	4	
81	0.09	4	
89	0.03	8	ν_a
122	0.03	15	
156	0.1	6	ν_1
166	1.00	6.1	ν_1'
184	0.08	5.7	ν_1''''
248	0.02	13	
255	0.02	11	$\nu_1' + \nu_a$
306	0.03	5	$2\nu_1$
332	0.23	11.0	$2\nu_1'$
353	0.03	9	$\nu_1' + \nu_1''''$
420	0.02	15	$2\nu_1' + \nu_a$
427	0.02	11	
498	0.07	17.5	$3\nu_1'$
518	0.01	11	$2\nu_1' + \nu_1''''$
588	0.04	6.5	
664	0.03	20.5	$4\nu_1'$
683	0.01	7	$3\nu_1' + \nu_1''''$
755	0.01	10	
828	0.01	35	$5\nu_1'$
920	0.01	25	
992	0.01	40	$6\nu_1'$
1067	0.01	-	

Table 19. Wavenumbers of principal Raman bands of $[\text{Pd}(-\text{chxn})_2][\text{Pd}(-\text{chxn})_2\text{Br}_2]\text{Br}_4$ in the 100 - 850 cm^{-1} region with excitation wavelengths 514.5, 568.2, 647.1, 676.4, 752.5 and 799.3 nm.

514.5 nm	568.2 nm	647.1 nm	676.4 nm	752.5 nm	799.3 nm	Assignment
			73			
		76	81			
91.5	87.5	88	89	90.5	91	ν_a
120.5	123	123	122	123.5	123.5	ν_1
	166		156	155.5	155.5	ν_1'
177.5	178		166	166.5	167	ν_1''
184.5	185		184	185	185	ν_1'''
	215.5					
242.5	243	247	248	249	248	$\nu_1' + \nu_a$
			255	255		$2\nu_1$
			306	310	310.5	$2\nu_1'$
		332	332	333	333	$\nu_1' + \nu_1'''$
357		351	353	352		$2\nu_1''$
363.5	359					$2\nu_1'''$

Table 19 continued.

514.5 nm	568.2 nm	647.1 nm	676.4 nm	752.5 nm	799.3 nm	Assignment
		419	420			$2V_1' + V_a$
427.5			427			
		497	498	464	465	$3V_1$
		516	518	499	498	$3V_1'$
	536					$2V_1' + V_1''''$
545						$3V_1''$
						$3V_1''''$
585	586	589	588	590	589	$V(\text{Pd-N})$
				619	619	$4V_1$
		663	664	664		$4V_1'$
			683			$3V_1' + V_1''''$
		755	755	755		$V_1' + V(\text{Pd-N})$
		823	828			$5V_1'$

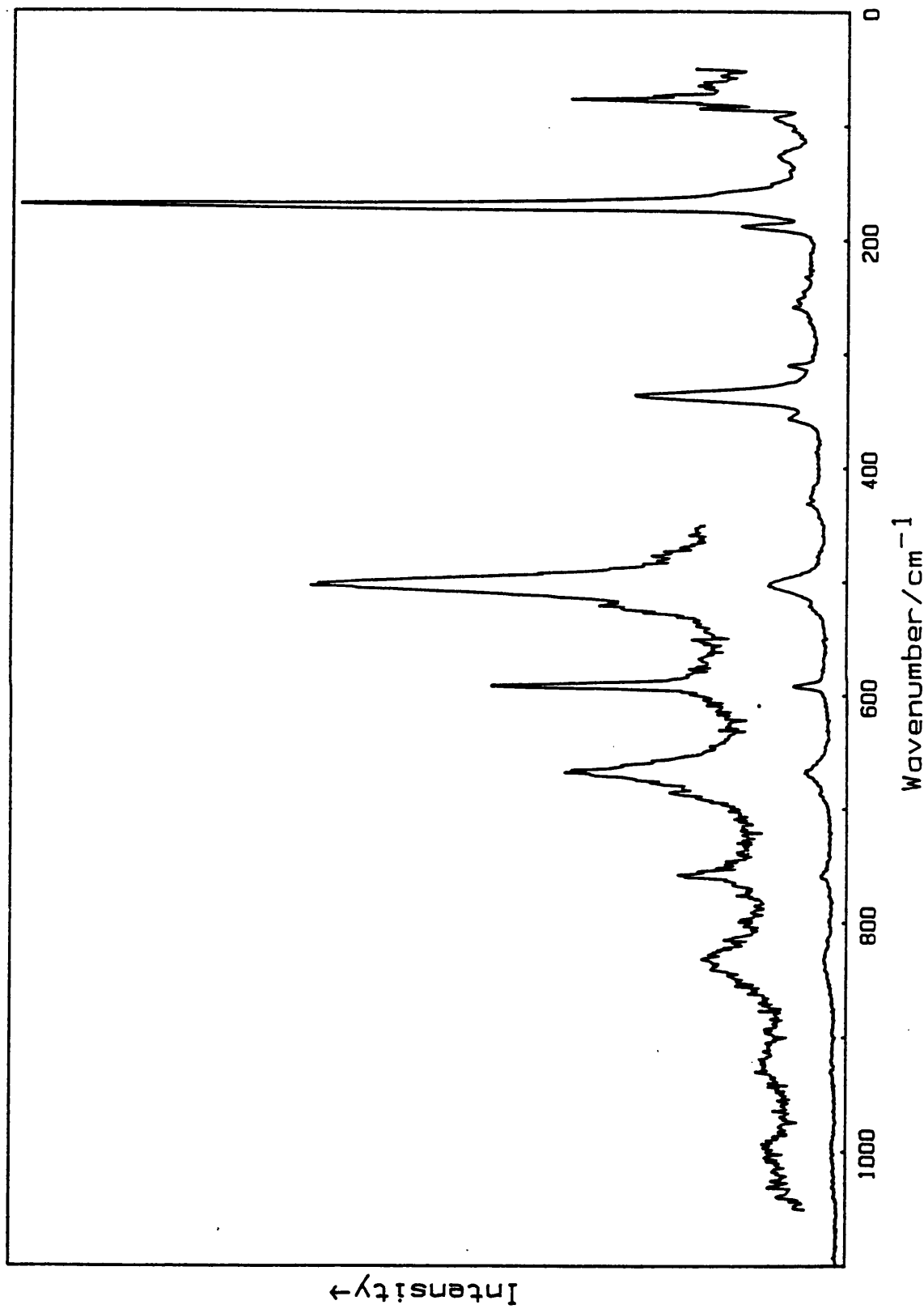


Figure 47. Resonance Raman spectrum of $[\text{Pd}(-\text{chxn})_2][\text{Pd}(-\text{chxn})_2\text{Br}_2]\text{Br}_4$ (pressed disc of pure sample at ca. 80 K, $\lambda_0 = 676.4 \text{ nm}$).

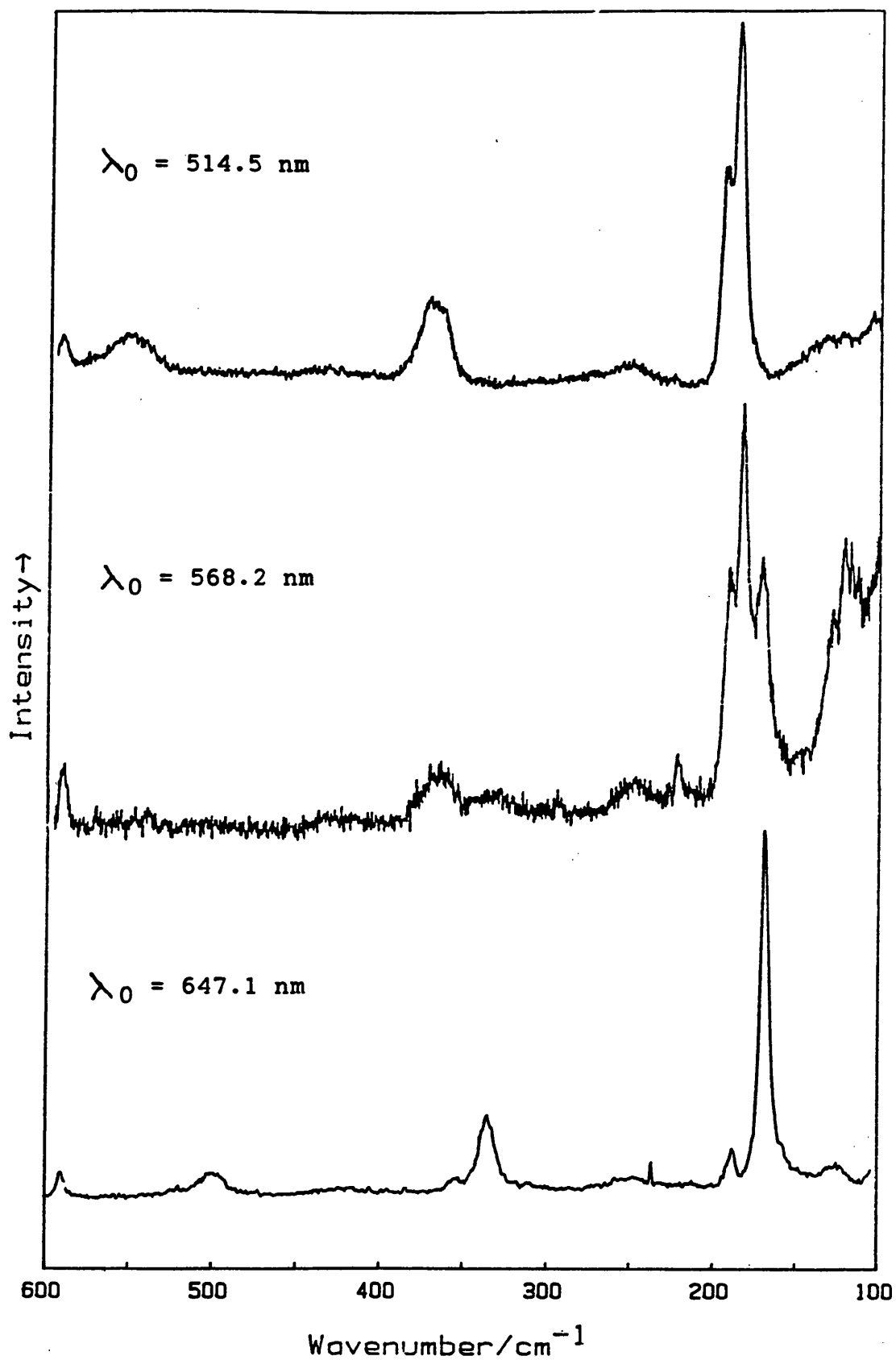


Figure 48. The 100 - 600 cm⁻¹ region of the resonance Raman spectra of $[\text{Pd}(-\text{chxn})_2][\text{Pd}(-\text{chxn})_2\text{Br}_2]\text{Br}_4$, obtained with excitation lines at 514.5, 568.2 and 647.1 nm (pressed disc of pure sample at ca. 80 K).

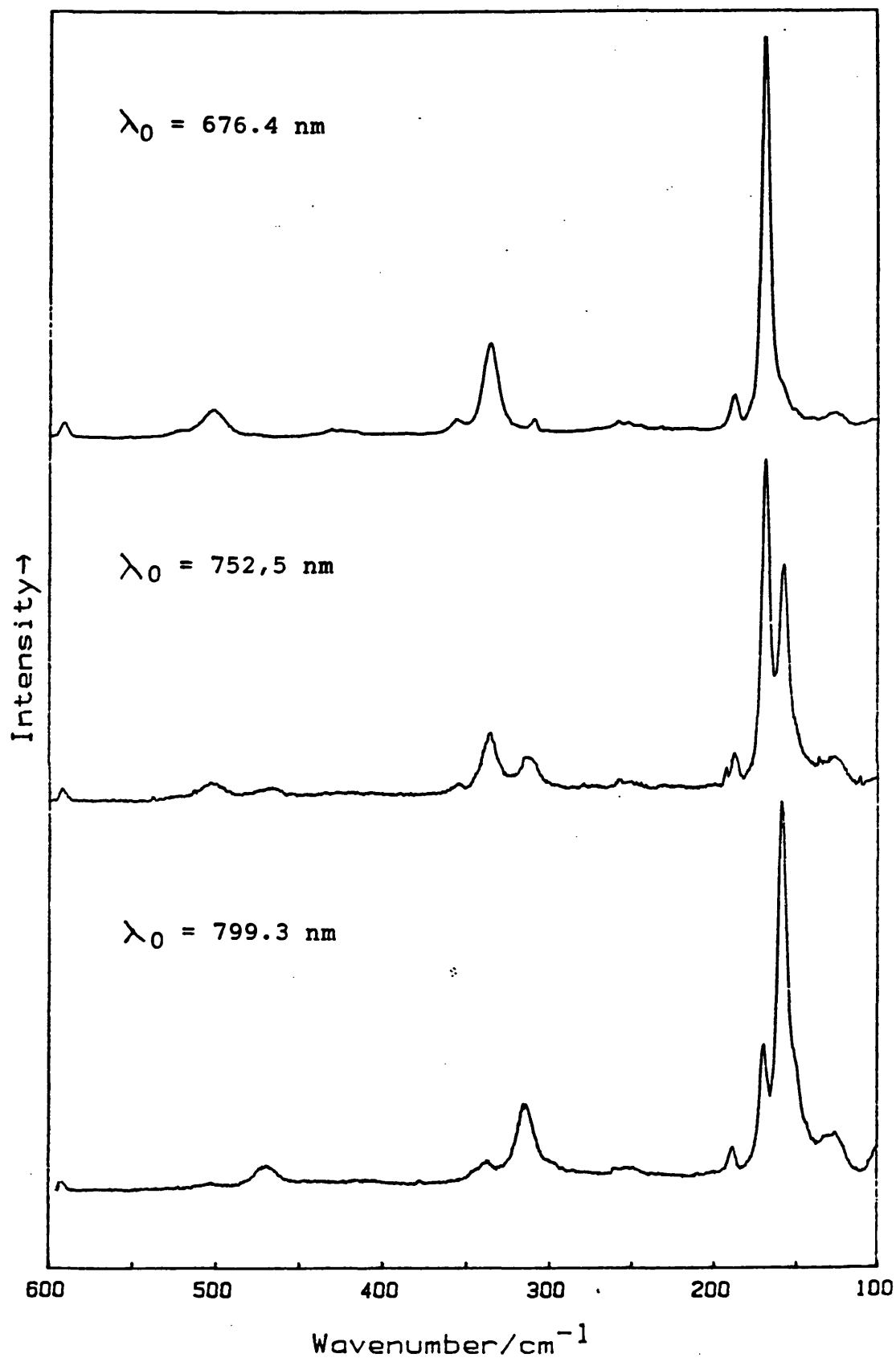


Figure 49. The 100 - 600 cm⁻¹ region of the resonance Raman spectra of [Pd(-chxn)₂][Pd(-chxn)₂Br₂]Br₄, obtained with excitation lines at 676.4, 752.5 and 799.3 nm (pressed disc of pure sample at ca. 80 K).

VII. EXCITATION LINE DEPENDENCE OF THE SYMMETRIC (X-M-X) STRETCH MODE IN THE RAMAN SPECTRA OF HALOGEN-BRIDGED MIXED-VALENCE COMPLEXES

VII.1. Introduction

It was first reported in 1983¹⁰⁸ that, in the resonance Raman spectra of halogen-bridged, mixed-valence linear-chain complexes, the wavenumber of the symmetric X-M^{IV}-X stretch fundamental ν_1 appears to vary with excitation wavenumber ν_0 as follows. For $\nu_0 < E_g$, where E_g is the energy of excitation from the electronic ground state to the IVCT absorption edge, ν_1 appears approximately constant. However, for different ν_0 within the IVCT absorption, ν_1 shows considerable dispersion, increasing approximately linearly with ν_0 . The extent of dispersion increases in the order Cl < Br < I. An example of the effect is given in Figure 50, which illustrates the shift in the wavenumber of ν_1 for [Pd([14]aneN₄)] [Pd([14]aneN₄)Cl₂](ClO₄)₄ from 277.5 to 285.5 cm⁻¹ on changing the excitation wavelength from 752.5 to 514.5 nm. Overtone shifts are correspondingly greater.

In many instances it is seen with sufficiently high resolution that the ν_1 band consists of several components. The number and relative intensities of these components are incompatible with a simple halogen isotope effect. Thus, for example, for a chlorine-bridged complex, the structure exceeds the 9/6/1 triplet structure expected from the various possible halogen isotopic combinations in MCl₂. This effect is considered to be in addition to the more obvious effect observed for complexes containing the ligand 1,2-diaminocyclohexane (e.g. in [Pd(-chxn)₂][Pd(-chxn)₂Br₂]Br₄, section VI.2.), for which several discrete ν_1 bands are observed which vary in relative intensity with different excitation lengths and which may be due to different isomer/enantiomer/conformer combinations around the metal atom sites. The existence of

an additional effect is suggested by, for example, the case of [Pt-en-Cl-ClO₄], for which the ν_1 profile shows up to 17 components,¹¹² and in which there is no possible variation in the isomeric or enantiomeric combination around the metal.

A complete explanation for the observed structure and dispersion in ν_1 is not yet established, although several causes have been proposed.⁸⁸ Certain features of the effect are well established:-

- (a) With increasing wavenumber of ν_0 within the IVCT absorption, the position of strongest scattering in the ν_1 profile shifts to higher wavenumber. As a proportion of the vibrational wavenumber, the apparent dispersion is in general greater for bromide-bridged than for chloride-bridged cases over the same range of ν_0 within the IVCT band, other factors being constant.
- (b) The ν_1 profile is comprised of more than one band.
- (c) The shape of the ν_1 profile changes with ν_0 above the absorption edge.
- (d) The Stokes shifts of components of ν_1 obtained with different excitation lines do not vary.

Thus observing ν_1 at high resolution reveals that the apparent shift with ν_0 within the IVCT absorption is in fact a change in the relative intensities of closely spaced constituent peaks, the Stokes shifts of which are constant. With increasing wavenumber of ν_0 there is a progressive transfer of intensity towards components at greater Stokes shift. It is also observed that, when ν_0 approaches the maximum in the RR excitation profile (i.e. approaches the absorption edge) for a complex, one component in the ν_1 profile is dominantly active over other components.

Tanaka and Kurita¹⁰⁹ have suggested that, by analogy with results from trans-polyacetylene, halogen-bridged, mixed-valence linear chains of different length will have both different IVCT absorption bands and different ν_1 frequencies, i.e. there is photoselective enhancement of

different lengths of conjugated chain. Papavassiliou et al.¹¹³ have reported a shift to higher wavenumber of the IVCT absorption band maximum with shorter chains (indeed this is seen to be likely from colour changes observed on grinding crystals of these complexes). By varying ν_0 within the IVCT absorption band, different chain lengths are excited preferentially and scattering into the corresponding ν_1 bands is observed. This, however, would imply that the ν_1 profile reflects the distribution of chain lengths.

The photoselective enhancement of different chain lengths observed in RR spectra of trans-polyacetylene has been modelled¹¹⁴ in terms of amplitude oscillation of the charge density wave in the trans-polyacetylene chain on interaction with phonons in the chain, which themselves are altered in wavenumber by the interaction. Since a charge density wave also exists in the halogen-bridged complexes, a similar treatment is perhaps feasible in their case.⁸⁸

Variation of ν_1 with length of conjugated chain will depend upon the extent to which vibration of one unit in the chain affects the others. This is not negligible, since ν_1 is considerably reduced relative to ν_1 in the M^{IV} monomer. Clearly, however, there must be a halogen isotope effect occurring, since it is the halogens which move in the vibration. Statistics indicate that, for chloride-bridged complexes beyond a chain length of about twenty units, chains with approximately equal numbers of ^{35}Cl and ^{37}Cl will strongly outweigh other distributions of halogen isotopes. However, the chain length effect on ν_1 is still unknown. An explanation which enlarges on the arguments above is offered in the following section.

VII.2. Further Discussion of the Chain Length Effect

Depending on the level in the valence band from which d electrons are excited and depending on the energy of excitation, different types of free electron-hole pair excitons are produced, which differ in their mean separation

of hole and electron (see Section I.11). When they (ultimately) come to relax to the ground state (and the exciton lifetime will vary with energy of excitation), the number of units in the chain affected by the excitation, i.e. with their geometry changed, and hence influencing the ν_1 wavenumber, will depend on (or even be equivalent to) the mean hole-electron separation. Thus ν_1 would be expected to vary in a discrete manner and the relative intensities of the components would be expected to change with excitation energy ν_0 , both as observed.

Where ν_0 is at the absorption edge E_g , the electron and hole are just free, but they are still associated primarily with two adjacent sites in the chain. Excitation is limited to the lowest few levels of the conduction band and reemission is relatively quick (provided the exciton does not self-trap). ν_1 is also associated mainly with the movement of just two M units in the chain; hence a single component of ν_1 is observed. When ν_0 is increased to greater than E_g , more possibilities are opened up. Starting from a lower level in the valence band, excitation may still only be to the lowest level(s) of the conduction band, in which case ν_1 will be observed as before. If excitation is to higher levels in the conduction band, the mean separation of electron and hole is increased and further M units are significantly affected by the excitation (and change their geometry accordingly); hence, with relaxation to the ground state, ν_1 is at a frequency determined by the geometry of greater than two M units in the chain. Thus more than one component in ν_1 may then be seen.

On going to still higher excitation energy ν_0 , the range of possible mean electron-hole separations in the excited state increases. Hence the range of possible excited state geometry changes is greater and the number of possible values of ν_1 thereby increased.

We can now consider why it is that ν_1 should increase with relaxation from an excited state of increasing mean

electron-hole separation. It is possible that this is due to relaxation occurring to a deeper potential well in the ground state than occurs in the undisturbed chain, the argument being as follows. With higher energy excitation, M units in the vicinity of the electron and hole are, like the latter pair, closer on average to the M^{III} state than with low energy excitation. Given enough time, therefore, the linear chain in the vicinity of the electron and hole will move towards the M^{III} structure. Not only does this entail movement of X towards the midpoint between adjacent M, but the metal ions themselves will move slightly closer together, evidence for this coming from the correlation observed between $M^{II}-M^{IV}$ distances and $r(M^{IV}-X)/r(M^{II}-X)$ ratios, i.e. the extent of valence delocalisation. (Thus, for example, for chloride-bridged platinum chains, the bond length ratio $r(Pt^{IV}-Cl)/r(Pt^{II}-Cl)$ decreases from 0.83 in $[Pt(chxn)_2][Pt(chxn)_2Cl_2]Cl_4$ to 0.71 in $[Pt(NH_3)_4][Pt(NH_3)_4Cl_2][HSO_4]_4$ as the $Pt^{II}-Pt^{IV}$ distance conversely increases from 5.158 to 5.466 Å, there being numerous intermediate cases.) With the eventual electronic relaxation, the chain reaches the ground electronic state with the metal ions closer together than normal; hence the potential well associated with the halogen position is steeper than in the undisturbed ground state and ν_1 slightly higher.

Superimposed on the ν_1 structure created as above is the isotopic splitting. It is suggested that these two factors in combination produce the ν_1 fine structure and the relative intensities observed. Thus, where $\nu_0 \sim E_g$ and only one ν_1 element is produced by the exciton effect, the isotopic structure is most easily observed.

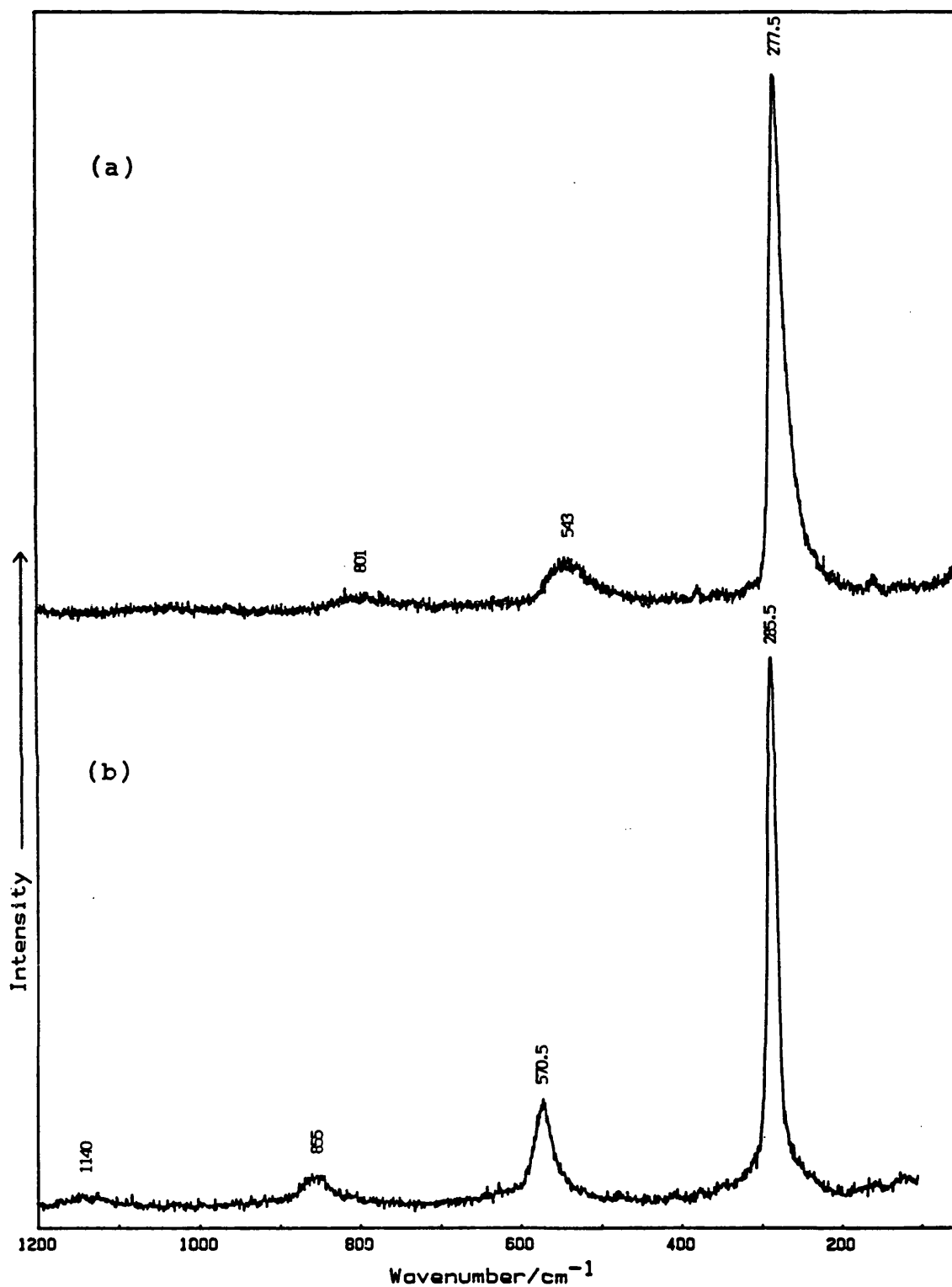


Figure 50. Resonance Raman spectra of $[\text{Pd}([\text{14}]\text{aneN}_4)]-[\text{Pd}([\text{14}]\text{aneN}_4)][\text{ClO}_4]_4$, obtained with excitation lines at 752.5 (a) and 514.5 nm (b) from a pressed disc of pure complex at ca. 80 K.

Intensity and SelectionA.1. Electromagnetic radiation from an oscillating dipole.¹¹⁵

For an electromagnetic wave travelling in, say, the z direction with electric field amplitude E and magnetic field amplitude H, the time-averaged total energy density $\bar{\rho}$ is given by

$$\bar{\rho} = \frac{1}{2}\epsilon_0 E^2 = \frac{1}{2}\mu_0 H^2 \quad (1)$$

where ϵ_0 is the permittivity of free space

and μ_0 is the permeability of free space.

For the irradiance \mathcal{J} of the radiation we multiply $\bar{\rho}$ by the speed of propagation c. In the case of a dipole oscillating harmonically with (circular) frequency ω , the E and H vectors have the following magnitudes.

$$E = (\omega^2 P \sin\theta) / (4\pi\epsilon_0 c^2 r) \quad (2)$$

$$\text{and } H = (\omega^2 P \sin\theta) / (4\pi c r) \quad (3)$$

where P is the magnitude of the dipole,

r is the distance from the dipole

and θ is the angle between the direction of propagation

and the dipole moment vector.

\mathcal{J} is then given by

$$= (\pi^2 c \omega^4 P_0^2 \sin^2\theta) / (2\epsilon_0 r^2) \quad (4)$$

where P_0 is the amplitude of the dipole.

The intensity of radiation is commonly expressed in

terms of radiant intensity, I , which is the ratio of power $d\bar{P}$ radiated within solid angle $d\Omega$ to $d\Omega$. This is closely related to \bar{J} and in the above case is given by

$$I = (\pi^2 c \omega^4 P^2 \sin^2 \theta) / (2 \epsilon_0) \quad (5)$$

To determine the radiant intensity scattered into $d\Omega$ by a scattering molecule at the centre of space-fixed Cartesian coordinates, we require an expression for P_0 . This is considered, for the case of Raman scattering, in the following section.

A.2. Classical derivation of Raman scattering effects. 115

The scattering by a sample of an incident light may be explained classically as the electromagnetic radiation produced by the electric dipole induced in the sample molecules. This interaction between the incoming light and the sample molecules is summarised in the equation for the induced dipole μ_{ind} :

$$\mu_{ind} = \alpha E + \frac{1}{2} \beta E^2 + \frac{1}{6} \gamma E^3 + \dots \quad (6)$$

where α is the polarisability of the molecule, typically $10^{-40} \text{ C V}^{-1} \text{ m}^2$,

β is the hyperpolarisability,

γ is the second hyperpolarisability,

etc.

For the purpose of considering the Raman effect, we need only consider the first term in the series, i.e. the linear induced dipole. Since μ_{ind} and E are vector properties, it

will be seen that α has the properties of a tensor. With some exceptions, α is real and symmetric. Among the exceptions is resonance Raman scattering, which will be considered only in a quantum mechanical model later.

The polarisability α is a measure of the extent to which the electron density throughout the molecule may be deformed under the influence of an external electric field, such as of electromagnetic radiation. It is dependent upon the atomic positions and is therefore time dependent upon the normal coordinates of the molecule. This is represented in the following equation.

$$\alpha = \alpha_0 + \sum_k \alpha'_k Q_k + \frac{1}{2} \sum_{k,l} \alpha''_{k,l} Q_k Q_l + \dots (7)$$

where α_0 is the value of α in the equilibrium configuration,

$Q_k, Q_l \dots$ are normal coordinates of vibration,

$\alpha'_k = \left(\frac{\partial \alpha}{\partial Q_k} \right)_0$, is the rate of change of α with Q_k at the equilibrium configuration,

etc.

On the assumption that changes in α due to activity in one normal mode are unaffected by activity in other modes, we may neglect all but the first two terms of the series (the so-called electrical harmonic approximation).

Henceforth we will consider only one normal vibration coordinate Q_k . Within the harmonic oscillator approximation, this is time dependent as follows:

$$Q_k = Q_{k_0} \cos(\omega_k t + \delta_k) \quad (8)$$

where Q_{k_0} is the normal coordinate amplitude,

ω_k is the frequency of vibration k

and δ_k is a phase factor.

The electric field of the incident light varies with time t :

$$E = E_0 \cos \omega_0 t \quad (9)$$

where E_0 is the amplitude

and ω_0 is the (circular) frequency.

From equations (7)-(9) and the various assumptions made, equation (6) for μ_{ind} may be rewritten as follows:

$$\mu_{\text{ind}} = \alpha_0 E_0 \cos \omega_0 t + \frac{1}{2} Q_k \alpha'_k E_0 \left\{ \cos[(\omega_0 - \omega_k)t - \delta_k] + \cos[(\omega_0 + \omega_k)t + \delta_k] \right\} \quad (10)$$

Thus radiation from the induced dipole may occur at frequencies ω_0 (Rayleigh scattering), $(\omega_0 - \omega_k)$ (Stokes) and $(\omega_0 + \omega_k)$ (anti-Stokes).

While the components of α_0 can only be positive (all molecules are polarisable to some extent), those of α'_k may be positive, negative or zero. This leads to differences in the direction and polarisation characteristics of Rayleigh and Raman scattering. For a given arrangement of illumination and observation and for a given polarisation, the appropriate elements of α'_k and E_0 are combined to give the induced dipole (equation (10)), which, when inserted in equation (5), gives the radiant intensity. Thus the classical selection rule for vibrational Raman activity is that some element of α'_k must be non-zero.

This classical derivation is valid for the prediction of direction and polarisation properties associated with Raman scattering. However, it does not correctly predict the intensities with which scattering may occur. A quantum mechanical model of the scattering must be employed to

replace the classical vibration amplitude Q_{k_0} of normal mode k . The quantum mechanical derivation is lengthy and will not be attempted here. However, a quantum mechanical expression for the radiant intensity is employed in the next section.

A.3. Raman and resonance Raman intensities in a quantum mechanical model.¹¹⁶

For one freely orientable molecule the intensity of light $I(\pi/2)$ scattered at 90 degrees to the incident beam with frequency $\nu_0 \pm \nu_{fi}$, where ν_{fi} is the frequency of the Raman transition between initial state $|i\rangle$ and final state $|f\rangle$ of the molecule, is given by

$$I_{fi}(\pi/2) = \frac{\pi^2 (\nu_0 \pm \nu_{fi})^4}{\epsilon_0^2} \int_0^{\infty} \sum_{\rho\sigma} [\alpha_{\rho\sigma}]_{fi} [\alpha_{\rho\sigma}]_{fi}^* \quad (11)$$

where ν_0 is the frequency of the exciting radiation,

\int_0^{∞} is the irradiance of the incident beam,

ϵ_0 is the permittivity of free space,

$[\alpha_{\rho\sigma}]_{fi}$ is the $\rho\sigma$ element of the transition

polarisability tensor $[\alpha]$, where ρ and σ span Cartesian free space

and * indicates the complex conjugate.

The $[\alpha_{\rho\sigma}]$ elements contain the transition dipole moments upon which the likelihood of the transition occurring depends. In the Kramers-Heisenberg dispersion formula,

$[\alpha_{\rho\sigma}]$ is expressed as follows:

$$[\alpha_{\rho\sigma}]_{fi} = \frac{1}{hc} \sum_r \left\{ \frac{[\mu_\rho]_{fr} [\mu_\sigma]_{ri}}{\nu_{ri} - \nu_0 + i\sqrt{\nu}} + \frac{[\mu_\sigma]_{fr} [\mu_\rho]_{ri}}{\nu_{rf} + \nu_0 + i\sqrt{\nu}} \right\} \quad (12)$$

where \sum_r indicates a sum over all possible intermediate

excited states $|r\rangle$,

$[\mu]$ are transition dipole moments, e.g.

$$[\mu_\rho]_{fr} = \langle f | \hat{\mu}_\rho | r \rangle$$

where $\hat{\mu}_\rho$ is the electric dipole operator,

ν_{ri} is the frequency of transition $|r\rangle \leftarrow |i\rangle$,

ν_{fr} similarly of $|f\rangle \leftarrow |r\rangle$

and Γ_r is a damping term related to the lifetime τ_r of state $|r\rangle$ by $\tau_r = (4\pi c \Gamma_r)^{-1}$.

A.3.1. Raman scattering

For Raman scattering the sum in 12) need not include states $|i\rangle$ and $|f\rangle$. In this non-resonance case we have that $\nu_0 \gg \nu_{fi}$ and also that ν_0 is far removed from the frequency of any electronic transition of the molecule. Using the Born-Oppenheimer approximation we may therefore separate the vibronic wavefunctions $|i\rangle$, $|r\rangle$ and $|f\rangle$ into constituent electronic and vibrational wavefunctions.

$$\begin{aligned} |i\rangle &= |g\rangle |m\rangle \\ |r\rangle &= |e\rangle |v\rangle \\ |f\rangle &= |g\rangle |n\rangle \end{aligned} \quad (13)$$

where $|g\rangle$ and $|e\rangle$ are the electronic wavefunctions of the ground and excited states respectively,

$|v\rangle$ is the vibrational wavefunction of the excited state

and $|m\rangle$ and $|n\rangle$ are vibrational wavefunctions of the ground state.

We can make the following assumptions also:

(a) Under the conditions for which the Born-Oppenheimer approximation is valid, we have that a purely electronic transition moment is usually only slightly dependent on the k normal coordinates Q_k of the system. Thus, for example, in the Taylor series

$$[\mu_r]_{ge} = [\mu_r]_{ge}^0 + \sum_k [\mu_r]_{ge}' Q_k + \dots \quad (14)$$

higher terms are negligible.

(b) The denominators in the expression for $[\alpha]$ are large, so that differences in ν_{ri} or ν_{rf} are negligible.

(c) The closure theorem may be used on the complete orthonormal set of excited state vibrational wavefunctions $|v\rangle$:

$$\sum_v |v\rangle \langle v| = 1$$

(d) $i\Gamma$ is small compared with the rest of each denominator and can be neglected.

Using these approximations, the following expression for the transition polarisability tensor element can be derived.

$$\begin{aligned} [\alpha_{rs}]_{gm, gm} &= \frac{1}{hc} \sum_e \frac{2\nu_e}{(\nu_e^2 - \nu_0^2)} [\mu_r]_{ge}^0 [\mu_\sigma]_{eg}^0 \langle n|m \rangle \\ &+ \frac{1}{hc} \sum_e \sum_k \frac{2\nu_e}{(\nu_e^2 - \nu_0^2)} \left\{ [\mu_r]_{ge}' [\mu_\sigma]_{eg}^0 + [\mu_r]_{ge}^0 [\mu_\sigma]_{eg}' \right\} \langle n|Q_k|m \rangle \quad (15) \\ &+ \frac{1}{hc} \sum_e \sum_{k,k'} \frac{2\nu_e}{(\nu_e^2 - \nu_0^2)} [\mu_r]_{ge}' [\mu_\sigma]_{eg}' \langle n|Q_k Q_{k'}|m \rangle \end{aligned}$$

The first term is non-zero only for $n = m$ and hence contributes only to Rayleigh scattering. The second term is non-zero if $n = m + 1$ and hence contributes to Stokes and anti-Stokes scattering into single quanta of active vibrational modes. The third term is usually relatively small and contributes to first overtones ($k = k'$) or combination modes ($k = k'$).

A.3.2. Resonance Raman scattering

As with Raman scattering, we assume the adiabatic Born-Oppenheimer approximation to be valid. However, we cannot make the further approximations made above. In the situation where ν_0 approaches $\nu_{ev, gm}$, neither the ν dependence nor $i\sqrt{\nu}$ in the denominators of equation (12) can be ignored. We must also consider the effect of vibronic coupling between electronic states on the derivative of the transition dipole moment as defined in equation (14). Taking that into account, the (Taylor) expansion then appears as follows:

$$[\mu_\rho]_{ge} = [\mu_\rho]_{ge}^0 + \sum_s \sum_k [\mu_\rho]_{gs}^0 \frac{h_{es}^k}{\Delta\nu_{es}} Q_k + \dots \quad (16)$$

where $h_{es}^k = \langle e | \frac{\partial \hat{H}}{\partial Q_k} | s \rangle_{Q_k=0}$

where s represents another excited state

and H is the Hamiltonian function

and $\Delta\nu_{es}$ is the frequency of the transition $|e\rangle \leftarrow |s\rangle$.

This expansion is only valid for weak vibronic coupling, i.e. when the adiabatic Born-Oppenheimer approximation is applicable.

In the situation where ν_0 approaches a particular $\nu_{ev, gm}$, that particular excited state will dominate the sum in equation (12). It is then necessary to consider only one or possibly two such electronic transitions to be contributing significantly to the transition polarisability. Thus the transition polarisability may then be expressed as follows.

$$[\alpha_{\rho\sigma}]_{gn, gm} = A + B + C + D \quad (17)$$

$$A = \frac{1}{\hbar c} [\mu_{\rho}]_{ge}^{\circ} [\mu_{\sigma}]_{eg}^{\circ} \sum_{\nu} \frac{\langle n|\nu\rangle\langle\nu|m\rangle}{\nu_{ev, gm} - \nu_0 + i\Gamma_{ev}}$$

$$B = \frac{1}{\hbar^2 c^2} \sum_{s \neq e} [\mu_{\rho}]_{gs}^{\circ} [\mu_{\sigma}]_{es}^{\circ} \frac{\hbar_{es}^k}{\Delta\nu_{se}} \sum_{\nu} \frac{\langle n|Q_k|\nu\rangle\langle\nu|m\rangle}{\nu_{ev, gm} - \nu_0 + i\Gamma_{ev}}$$

$$+ \frac{1}{\hbar^2 c^2} \sum_{s \neq e} [\mu_{\rho}]_{ge}^{\circ} [\mu_{\sigma}]_{s'g}^{\circ} \frac{\hbar_{es'}^k}{\Delta\nu_{es'}} \sum_{\nu} \frac{\langle n|\nu\rangle\langle\nu|Q_k|m\rangle}{\nu_{ev, gm} - \nu_0 + i\Gamma_{ev}}$$

$$C = \frac{1}{\hbar^2 c^2} \sum_{s \neq g} [\mu_{\rho}]_{se}^{\circ} [\mu_{\sigma}]_{eg}^{\circ} \frac{\hbar_{gs}^k}{\Delta\nu_{gs}} \sum_{\nu} \frac{\langle n|Q_k|\nu\rangle\langle\nu|m\rangle}{\nu_{ev, gm} - \nu_0 + i\Gamma_{ev}}$$

$$+ \frac{1}{\hbar^2 c^2} \sum_{s \neq g} [\mu_{\rho}]_{ge}^{\circ} [\mu_{\sigma}]_{es'}^{\circ} \frac{\hbar_{gs'}^k}{\Delta\nu_{gs'}} \sum_{\nu} \frac{\langle n|\nu\rangle\langle\nu|Q_k|m\rangle}{\nu_{ev, gm} - \nu_0 + i\Gamma_{ev}}$$

$$D = \frac{1}{\hbar^3 c^3} \sum_{s, s' \neq e} [\mu_{\rho}]_{gs}^{\circ} [\mu_{\sigma}]_{s'g}^{\circ} \frac{\hbar_{es}^k \hbar_{es'}^k}{\Delta\nu_{es} \Delta\nu_{es'}} \sum_{\nu} \frac{\langle n|Q_k|\nu\rangle\langle\nu|Q_k|m\rangle}{\nu_{ev, gm} - \nu_0 + i\Gamma_{ev}}$$

In general A and B are much greater in magnitude than C and D.

(a) A term

For this to be non-zero, we have that the transition dipole moments $[\mu_{\rho}]_{ge}^{\circ}$ and $[\mu_{\sigma}]_{eg}^{\circ}$ must be non-zero, i.e. the resonant electronic transition must be electric dipole allowed (e.g. charge transfer). We also have that the vibrational overlaps $\langle n|\nu\rangle\langle\nu|m\rangle$ must be non-zero, i.e. the n and v vibrational wavefunctions must be non-orthogonal. This will be the case, for a given normal mode, where the shape of the potential energy surface alters with the excitation and/or where it is shifted (by ΔQ_k) on the normal coordinate. In practice it is found that the former occurs significantly only when the latter occurs also. If the molecular symmetry is unaltered by the excitation, the

latter can occur only for totally symmetric modes. If the molecular symmetry is changed, then the latter can occur only for those modes which are totally symmetric with respect to the subgroup of operations common to the ground and excited states. Thus in general the A term contributes only to totally symmetric mode enhancement. Depending on the magnitude of ΔQ_k , overtones may be observed with considerable intensity.

(b) B term

This contribution arises from vibronic coupling between excited states. For non-zero B, both $|e\rangle \leftarrow |g\rangle$ and $|s\rangle \leftarrow |g\rangle$ must be electric dipole allowed. Under conditions where A is zero the smaller B term becomes significant. In the simple harmonic oscillator approximation the integrals $\langle n|Q_k|v\rangle\langle v|m\rangle$ and $\langle n|v\rangle\langle v|Q_k|m\rangle$ are finite only when $n = m \pm 1$. Thus scattering is observed only for fundamental modes. Activity of a mode depends on the symmetry of $|e\rangle$ and $|s\rangle$. h_{es}^k is finite only if the irreducible representation of mode k is contained in the direct product $\Gamma_s \otimes \Gamma_e$.

(c) C and D terms

These are much smaller than A or B and are rarely significant in an RR spectrum. C is dependent on the extent of vibronic coupling between ground state $|g\rangle$ and excited state $|s\rangle$ (normally negligible). D may give rise to weak first overtones and/or binary combination tones.

In general A is the most significant term in the expression for $[\alpha_{\rho\sigma}]_{ev, gm}$ under resonance conditions and therefore it is usually bands arising from totally symmetric modes which are observed to be enhanced

A.3.3 Resonance Raman scattering involving totally symmetric modes

We will consider a case where there is only one totally symmetric mode, in which case only the diagonal components of the transition polarisability are non-zero. Assuming that only a single resonantly excited state, e , makes a significant contribution and that all molecules are initially in the $m=0$ vibrational level of the ground electronic state, then

$$[\alpha_{\rho\rho}]_{g_n, g_0} = \frac{1}{hc} |[\mu_{\rho}]_{ge}^0|^2 \sum_{\nu} \frac{\langle n_g | \nu_e \rangle \langle \nu_e | 0_g \rangle}{\nu_{ev, g_0} - \nu_0 + i\Gamma_{ev}} \quad (18)$$

Assuming harmonic potentials for $|g\rangle$ and $|e\rangle$, the overlap integrals may be calculated from Manneback's recurrence formulae.¹¹⁷ Substitution of (18) into (11) leads to the following expression for Stokes A-term RR intensities.

$$I_{g_n, g_0}(\pi/2) = K(\nu_0 - \nu_{g_n, g_0})^4 |[\mu_{\rho}]_{ge}^0|^4 \left[\sum_{\nu} \frac{\langle n_g | \nu_e \rangle^2 \langle \nu_e | 0_g \rangle^2}{\mathcal{E}_{\nu}^2 + \Gamma_{\nu}^2} + \sum_{\nu} \sum_{\nu'} \frac{\langle n_g | \nu_e \rangle \langle \nu_e | 0_g \rangle \langle n_g | \nu'_e \rangle \langle \nu'_e | 0_g \rangle [\mathcal{E}_{\nu} \mathcal{E}_{\nu'} + \Gamma_{\nu} \Gamma_{\nu'}]}{(\mathcal{E}_{\nu}^2 + \Gamma_{\nu}^2)(\mathcal{E}_{\nu'}^2 + \Gamma_{\nu'}^2)} \right] \quad (19)$$

where $\mathcal{E}_{\nu} = \nu_{ev, g_0} - \nu_0$ and K incorporates all the constants in equations (11) and (18).

This expression gives us intensities of the fundamental and overtone bands for excitation throughout the resonant absorption, i.e. the excitation profile of each band.

A.4 Overtone Progressions and Anharmonicity^{118,119}

The vibrational term for a polyatomic species is given by the expression

$$G = \sum_j \tilde{\omega}_j \left(\nu_j + \frac{d_j}{2} \right) + \sum_j \sum_{k>j} \tilde{x}_{jk} \left(\nu_j + \frac{d_j}{2} \right) \left(\nu_k + \frac{d_k}{2} \right) \quad (20)$$

where $\tilde{\omega}_j$, v_j and d_j are the harmonic wavenumber, vibrational quantum number and degeneracy, respectively, of the j th fundamental and \tilde{x}_{jk} is an anharmonicity constant. The observed wavenumber $\tilde{\nu}(v_1\nu_1)$ of an overtone of a fundamental ν_1 , is given, for Stokes bands, by the expression

$$\tilde{\nu}(v_1\nu_1) = v_1\tilde{\omega}_1 + v_1\tilde{x}_{11}(2m + d_1 + v_1) + v_1[\tilde{x}_{12}(n + d_2/2) + \tilde{x}_{13}(p + d_3/2) + \dots \tilde{x}_{1j}(j + d_j/2)] \quad (21)$$

where m, n, p, \dots correspond to further fundamentals.

Thus a plot of $\tilde{\nu}(v_1\nu_1)/v_1$ versus v_1 has a slope of \tilde{x}_{11} and an intercept of

$$\tilde{\omega}_1 + \tilde{x}_{11}(2m + d_1) + [\tilde{x}_{12}(n + d_2/2) + \tilde{x}_{13}(p + d_3/2) + \dots \tilde{x}_{1j}(j + d_j/2)]$$

with the terms in the square brackets usually set to zero (as \tilde{x}_{ij} can be positive or negative). For a totally symmetric fundamental $d_1 = 1$ and $m = 0$, in which case the intercept is equal to $\tilde{\omega}_1 + \tilde{x}_{11}$.

If further progressions in ν_1 are observed, based on one or more quanta of another fundamental ν_2 , it is possible, following a similar procedure, to determine a value for the anharmonicity constant \tilde{x}_{12} .

A.5 The Resonance Raman Effect in Crystals

Applying time-dependent perturbation theory to a two-band electronic model for crystals, Loudon and others^{120,121} have shown that the intensity I of the Stokes Raman scattering is given by:

$$I \propto \sum_f \left| \sum_{\alpha, \beta} \frac{\langle f | H_{ER}(\omega_s) | \beta \rangle \langle \beta | H_{EL} | \alpha \rangle \langle \alpha | H_{ER}(\omega_i) | i \rangle}{(\omega_\beta + \omega_0 - \omega_i)(\omega_\alpha - \omega_i)} \right|^2 \times \delta(\omega_i - \omega_s - \omega_0) \quad (22)$$

where $|i\rangle$ is the initial state, $|f\rangle$ the final state, ω_i the frequency of the incident light, ω_s the scattered frequency, ω_0 the frequency of the created phonon, H_{ER} the electron-photon interaction Hamiltonian, H_{EL} the electron-phonon interaction Hamiltonian and δ is the Dirac delta function.

The excited states $|\alpha\rangle$ and $|\beta\rangle$ consist of electron-hole pairs which may be free or correlated. When the incident photon energy or the scattered photon energy approaches that of α or β , the denominator will become small, i.e. an increase in intensity of the phonon band occurs. The Raman scattering efficiency increases steeply as the excitation frequency approaches the absorption edge E_g from below. Above E_g the efficiency of scattering decreases, while the absorption coefficient rises. Hence the excitation profile should reach its maximum at E_g .

A.6 Depolarisation Ratios in Normal Raman Scattering

The depolarisation ratio ρ of Raman scattering excited by linearly polarised incident radiation I_0 is given by:

$$\rho = I_{\perp}/I_{\parallel} \quad (23)$$

where I_{\perp} is the intensity of scattering with polarisation perpendicular to that of I_0

and I_{\parallel} is the intensity of scattering with polarisation parallel to that of I_0 .

For 90° scattering from an assembly of randomly oriented molecules, ρ may be expressed in terms of tensor invariants $\bar{\alpha}$, γ_s and γ_{as} :

$$\rho = (3\gamma_s^2 + 5\gamma_{as}^2)/(45\bar{\alpha}^2 + 4\gamma_s^2) \quad (24)$$

where $\bar{\alpha} = \frac{1}{3}(\alpha_{xx} + \alpha_{yy} + \alpha_{zz})$

$$\gamma_s^2 = \frac{1}{2} \left\{ (\alpha_{xx} - \alpha_{yy})^2 + (\alpha_{yy} - \alpha_{zz})^2 + (\alpha_{zz} - \alpha_{xx})^2 \right. \\ \left. + \frac{3}{2} [(\alpha_{xy} + \alpha_{yx})^2 + (\alpha_{yz} + \alpha_{zy})^2 + (\alpha_{zx} + \alpha_{xz})^2] \right\}$$

and $\gamma_{as}^2 = \frac{3}{4} [(\alpha_{xy} - \alpha_{yx})^2 + (\alpha_{yz} - \alpha_{zy})^2 + (\alpha_{zx} - \alpha_{xz})^2]$

For vibrational normal Raman scattering, γ_{as}^2 is zero and the following behaviour results.

(1) For non-totally symmetric modes $\bar{\alpha} = 0$ and $\rho = \frac{3}{4}$.

(2) For cubic molecules $\alpha_{xx} = \alpha_{yy} = \alpha_{zz}$, hence

$\gamma_s^2 = 0$ for totally symmetric modes and $\rho = 0$. For totally symmetric modes of non-cubic molecules, $0 < \rho < \frac{3}{4}$.

Appendix II. Electronic spectroscopy

Transmission electronic spectra were recorded at 295 K on a Varian 2390 spectrometer. Each sample was prepared as a pressed disc matrix of a corresponding alkali metal halide or of KClO_4 . Reflectance electronic spectra were recorded at 295 K on a Unicam SP1800 spectrometer, for which samples were prepared as powdered mixtures of complex and KClO_4 .

Appendix III. Syntheses of Complexes

A.III.1. Complexes of Platinum and Palladium with Quadridentate Ligands

Platinum complexes of the type $[\text{PtL}][\text{PtLX}_2][\text{ClO}_4]_4$, where L = 3,7-diazanonane-1,9-diamine (2,3,2-tet) or 4,7-diazadecane-1,10-diamine (3,2,3-tet) and X = Cl, Br or I, were prepared according to a standard route²⁴.

Mixed-valence, palladium complexes

$[\text{PdL}][\text{PdLX}_2][\text{ClO}_4]_4$, where L = 2,3,2-tet, 3,2,3-tet, 1,4,8,11-tetraazacyclotetradecane ([14]ane N_4) or 1,4,8,12-tetraazacyclopentadecane ([15]ane N_4) and X = Cl or Br, and $[\text{Pd}([\text{14]aneN}_4)][\text{Pd}([\text{14]aneN}_4)\text{Cl}_2]\text{Y}_4$, where Y = BF_4 or PF_6 , were synthesised as described in reference 16.

A.III.2. Complexes of Nickel

Nickel complexes of the type $[\text{NiL}][\text{NiLCl}_2]\text{Y}_4$, where L = 2,3,2-tet (Y = BF_4 or ClO_4) or 3,2,3-tet (Y = BF_4) were prepared according to or in a similar manner to a previously reported route¹⁷, as were complexes of the type $[\text{NiL}_2][\text{NiL}_2\text{Cl}_2]\text{Cl}_4$, where L = pn or (-)chxn¹⁰² and the Ni(III) complex $\{[\text{Ni}(-\text{chxn})_2\text{Br}]\text{Br}_2\}_\infty$ ⁷⁷

A.III.3. Further complexes of Platinum and Palladium

Complexes containing the ligand 4Me-dien were synthesised as described in reference 18.

$[\text{Pd}(-\text{chxn})_2][\text{Pd}(-\text{chxn})_2\text{Br}_2]\text{Br}_4$ was prepared according to a previously reported route.⁸⁶

References

1. C. V. Raman and V. S. Krishnan, *Nature*, 1928, 121, 501.
2. A. Anderson (ed.), 'The Raman Effect' Vols. 1 & 2, Marcel Dekker Inc. (1971-3).
3. R. J. H. Clark, in 'Vibrational Spectroscopy', eds. A. J. Barnes and W. J. Orville-Thomas, Elsevier, Amsterdam, 1977, p. 121.
4. R. J. H. Clark, in 'Inorganic Chemistry Toward the 21st Century', A. C. S. Symposium Series, No. 211, ed. M. H. Chisholm, 1983, 509.
5. M. B. Robin and P. Day, *Adv. Inorg. Chem. Radiochem.*, 10 (1967), 247.
6. J. S. Miller and A. J. Epstein, *Prog. Inorg. Chem.*, 20 (1976), 1-151.
7. R. J. H. Clark, *Chem. Soc. Rev.*, 19 (1990), 107-31.
8. H. Wolfram, Dissertation, Königsberg, 1900.
9. R. J. H. Clark and P. C. Turtle, *Inorg. Chem.*, 1978, 17(9), 2526.
10. J. R. Campbell, R. J. H. Clark and P. C. Turtle, *Inorg. Chem.*, 1978, 17(12), 3622.
11. R. J. H. Clark and M. Kurmoo, *J. Chem. Soc. Dalton Trans.*, 1983, 761.
12. R. J. H. Clark, V. B. Croud and M. Kurmoo, *Inorg. Chem.*, 1984, 23, 2499.
13. R. J. H. Clark, M. Kurmoo, D. N. Mountney and H. Toftlund, *J. Chem. Soc. Dalton Trans.*, 1982, 1851.
14. R. J. H. Clark and V. B. Croud, *Inorg. Chem.*, 1985, 24, 588.
15. R. J. H. Clark, M. Kurmoo, A. M. R. Galas and M. B. Hursthouse, *J. Chem. Soc. Dalton Trans.*, 1983, 1583.
16. R. J. H. Clark, D. J. Michael and M. Yamashita, *J. Chem. Soc. Dalton Trans.*, 1991, 725.
17. M. Yamashita, I. Murase, I. Ikemoto and T. Ito, *Chem. Lett.*, 1985, 1133.
18. F. P. Fanizzi, G. Natile, M. Lanfranchi, A. Tiripicchio, R. J. H. Clark and D. J. Michael, *J. Chem. Soc. Dalton Trans.*, 1989, 1689.

19. R. J. H. Clark, V. B. Croud and A. R. Khokhar, *Inorg. Chem.*, 1987, 26, 3284.
20. R. J. H. Clark, M. Kurmoo, A. M. R. Galas and M. B. Hursthouse, *Inorg. Chem.*, 1981, 20, 4206.
21. G. Thiele, C. Mrozek, K. Wittman and H. Wirkner, *Naturwiss.*, 1978, 65, 206.
22. K. P. Larsen and H. Toftlund, *Acta Chem. Scand.*, A31 (1977), 182.
23. N. Matsumoto, M. Yamashita, I. Ueda and S. Kida, *Memoirs Fac. Sci. Kyushu University, Ser. C*, 11 (1978), 209.
24. N. Matsumoto, M. Yamashita and S. Kida, *Bull. Chem. Soc. Japan*, 1978, 51, 3514.
25. N. Matsushita, N. Kojima, T. Ban and I. Tsujikawa, *Bull. Chem. Soc. Japan*, 1989, 62, 1785.
26. H. Endres, H. J. Keller, R. Martin and U. Traeger, *Acta Cryst.*, 1979, B35, 2880.
27. H. J. Keller, R. Martin and U. Traeger, *Z. Naturforsch.*, 1978, 33b, 1263.
28. A. L. Beauchamp, D. Layek and T. Theophanides, *Acta Cryst.*, 1982, B38, 1158.
29. M. Yamashita, M. Ito, K. Toriumi and T. Ito, *Inorg. Chem.*, 1983, 22, 1566.
30. K. Toriumi, M. Yamashita, M. Ito and T. Ito, *Acta Cryst.*, 1986, C42, 963.
31. B. M. Craven and D. Hall, *Acta Cryst.*, 1961, 14, 475.
32. P. E. Fanwick and J. L. Huckaby, *Inorg. Chem.*, 1982, 21, 3067.
33. R. J. H. Clark, M. Kurmoo, A. M. R. Galas and M. B. Hursthouse, *J. Chem. Soc. Dalton Trans.*, 1982, 2505.
34. K. L. Brown and D. Hall, *Acta Cryst.*, 1976, B32, 279.
35. H. Endres, H. J. Keller, R. Martin, U. Traeger and N. Novotny, *Acta Cryst.*, 1980, B36, 35.
36. T. D. Ryan and R. E. Rundle, *J. Am. Chem. Soc.*, 1961, 83, 2814.
37. A. L. Beauchamp, D. Layek and T. Theophanides, *Acta Cryst.*, 1982, B38, 1901.
38. H. Endres, H. J. Keller, R. Martin, H. N. Gung and U. Traeger, *Acta Cryst.*, 1979, B35, 1885.

39. N. Matsumoto, M. Yamashita and S. Kida, *Acta Cryst.*, 1979, B35, 1458.
40. H. Breer, H. Endres, H. J. Keller and R. Martin, *Acta Cryst.*, 1978, B34, 2295.
41. L. V. Interrante, K. W. Browall and F. P. Bundy, *Inorg. Chem.*, 1974, 13, 1158.
42. D. Cahen and J. E. Lester, *Chem. Phys. Lett.*, 1973, 18, 108.
43. P. Burroughs, A. Hamnett, J. F. McGilp and A. F. Orchard, *J. Chem. Soc. Faraday II*, 1975, 71, 177.
44. M. Yamashita, N. Matsumoto and S. Kida, *Inorg. Chim. Acta*, 1978, 31, L381.
45. M. Yamashita and T. Ito, *Inorg. Chim. Acta*, 1984, 87, L5.
46. M. Yamashita, I. Murase, T. Ito, Y. Wada, T. Mitani and I. Ikemoto, *Bull. Chem Soc. Jpn.*, 1985, 58, 2336.
47. T. W. Thomas and A. E. Underhill, *J. Chem. Soc. A*, 1971, 512.
48. L. V. Interrante and K. W. Browall, *Inorg. Chem.*, 1974, 13, 1162.
49. Y. Hamaue, R. Aoki, M. Yamashita and S. Kida, *Inorg. Chim. Acta*, 1981, 54, L13.
50. M. Tanaka, S. Kurita, T. Kojima and Y. Yamada, *Chem. Phys.*, 1984, 91, 257.
51. P. Day, in 'Low-dimensional cooperative Phenomena', ed. H. J. Keller, Plenum, New York, 1975, p. 191.
52. Y. Wada, T. Mitani, K. Toriumi and M. Yamashita, *J. Phys. Soc. Jpn.*, 1989, 58, 3013.
53. R. J. H. Clark and V. B. Croud, *Inorg. Chem.*, 1986, 25, 1751.
54. G. C. Papavassiliou, *J. Phys. C*, 1979, 12, L297.
55. G. C. Papavassiliou and A. D. Zdetsis, *J. Chem. Soc. Faraday Trans. II*, 1980, 76, 104.
56. G. C. Papavassiliou and C. S. Jacobsen, *J. Chem. Soc. Faraday Trans. II*, 1981, 77, 191.
57. G. C. Papavassiliou, *Prog. Solid State Chem.*, 1979, 12, 185.
58. G. C. Papavassiliou, T. Theophanides and R.

- Rapsomanikis, J. Raman Spectrosc., 1979, 8, 227.
59. M. Tanaka, S. Kurita, Y. Okada, T. Kojima and Y. Yamada, Chem. Phys., 1985, 96, 343.
60. S. D. Allen, R. J. H. Clark, V. B. Croud and M. Kurmoo, Phil. Trans. R. Soc., 1985, A 314, 131.
61. R. J. H. Clark, in R. J. H. Clark and R. E. Hester (Eds.), Adv. Infrared Raman Spectrosc., 1984, 11, Wiley Chichester, p. 85.
62. G. C. Papavassiliou, D. Layek and T. Theophanides, J. Raman Spectrosc., 1980, 9 (2), 69.
63. R. J. H. Clark, M. Kurmoo, H. J. Keller, B. Keppler and U. Traeger, J. Chem. Soc. Dalton Trans., 1980, 2498.
64. R. Loudon, J. Physique, 1965, 26, 277.
65. A. S. Barker and R. Loudon, Rev. Mod. Phys., 1972, 44, 18.
66. S. Yamada and R. Tsuchida, Bull. Chem. Soc. Jpn., 1956, 29, 894.
67. M. H. Whangbo and M. J. Foshee, Inorg. Chem., 1981, 20, 113.
68. H. Tanino and K. Kobayashi, J. Phys. Soc. Jpn., 1983, 52 (4), 1446.
69. M. Haruki, M. Tanaka and S. Kurita, Synth. Met., 1987, 19, 901.
70. L. Chugayev and I. Chernyaev, Z. Anorg. Allgem. Chem., 1929, 182, 159.
71. Saint Claire Deville and H. Debray, Compt. Rendus, 1878, 86, 927.
72. N. S. Kurnakov, Z. Anorg. Chem., 1898, 17, 207.
73. O Bekaroglu, H. Breer, H. Endres, H. J. Keller and H. N. Gung, Inorg. Chim. Acta, 1977, 21, 183.
74. M. Textor and H. R. Stieger, Z. Anorg. Allgem. Chem., 1976, 423, 185.
75. H. Oshio, K. Toriumi and S. Bandow, Chem. Lett., 1988, 1713.
76. H. Oshio, K. Toriumi, S. Bandow, K. Miyagawa and S. Kurita, J. Chem. Soc. Dalton Trans., 1990, 1013.
77. K. Toriumi, Y. Wada, T. Mitani, S. Bandow, M. Yamashita and Y. Fujii, J. Am. Chem. Soc., 1989, 111, 2341.

78. K. Toriumi, H. Okamoto, T. Mitani, S. Bandow, M. Yamashita, Y. Wada, Y. Fujii, R. J. H. Clark, D. J. Michael, A. J. Edward, D. Watkin, M. Kurmoo and P. Day, *Mol. Cryst. Liq. Cryst.*, 1990, 181, 333.
79. S. Piepho, E. R. Krausz and P. N. Schatz, *J. Am. Chem. Soc.*, 1978, 100, 2996.
80. K. Y. Wong and P. N. Schatz, *Chem. Phys. Lett.*, 1980, 73 (3), 456.
81. K. Prassides, P. N. Schatz, K. Y. Wong and P. Day, *J. Phys. Chem.*, 1986, 90, 5588.
82. M.-H. Whangbo, in 'Crystal Chemistry and Properties of Materials with Quasi-One-Dimensional Structures', ed. J. Rouxel, Reidel, 1986, 27.
83. K. Nasu, *J. Phys. Soc. Jpn.*, 1983, 52(11), 3865.
84. K. Nasu, *J. Phys. Soc. Jpn.*, 1984, 53(1), 302.
85. K. Nasu, *J. Phys. Soc. Jpn.*, 1984, 53(1), 427.
86. H. Toftlund, P. Waage Jensen and C. S. Jacobsen, *Chem. Phys. Lett.*, 1987, 142(3,4), 286.
87. N. Matsushita, N. Kojima, N. Watanabe and T. Ban, *Solid State Comm.*, 1989, 71(4), 253.
88. R. J. H. Clark, D. J. Michael, *J. Mol. Struct.*, 1988, 189, 173.
89. N. Matsushita, N. Kojima, T. Ban and I. Tsujikawa, *J. Phys. Soc. Jpn.*, 1987, 56(11), 3808.
90. S. Kurita, M. Haruki and K. Miyagawa, *J. Phys. Soc. Jpn.*, 1988, 57(5), 1789.
91. A. Mishima and K. Nasu, *Phys. Rev. B*, 1989, 39(9), 5758.
92. N. Kuroda, T. M. Sakai, Y. Nishina, M. Tanaka and S. Kurita, *Phys. Rev. Lett.*, 1987, 58, 2122.
93. M. Haruki and S. Kurita, *Phys. Rev. B*, 1989, 39(9), 5706.
94. S. Kurita and M. Haruki, *Synth. Met.*, 1989, 29, F129.
95. A. Mishima and K. Nasu, *Phys. Rev. B*, 1989, 39(9), 5763.
96. R. J. H. Clark, in R. J. H. Clark and R. E. Hester (Eds.), *Adv. Infrared Raman Spectrosc.*, 1975, 1, Wiley Chichester, p. 143.
97. W. F. Sherman and G. R. Wilkinson, in R. J. H. Clark and R. E. Hester (Eds.), *Adv. Infrared Raman Spectrosc.*,

- 1980, 6, Wiley Chichester, p. 156.
98. Y. Wada, T. Mitani, M. Yamashita and T. Koda, *J. Phys. Soc. Jpn.*, 1985, 54, 3143.
99. R. Loudon, *J. Physique*, 1965, 26, 277.
100. A. S. Barker and R. Loudon, *Rev. Mod. Phys.*, 1972, 44, 18.
101. K. Okaniwa, H. Okamoto, T. Mitani, K. Toriumi and M. Yamashita, *J. Phys. Soc. Japan*, 1991, 60 (3), 997.
102. M. Yamashita, Y. Nonaka, S. Kida, Y. Hamaue and R. Aoki, *Inorg. Chim. Acta*, 1981, 52, 43.
103. M. Yamashita and I. Murase, *Inorg. Chim. Acta*, 1985, 97, L43.
104. K. Toriumi, T. Kanao, Y. Umetsu, A. Ohyoshi, M. Yamashita and T. Ito, *J. Coord. Chem.*, 1988, 19, 209.
105. T. Ito, M. Sugimoto, K. Toriumi and H. Ito, *Chem. Lett.*, 1981, 1477.
106. G. C. Papavassiliou and D. Layek, *Z. Naturforsch.*, 1982, 37b, 1406.
107. J. Bradbury, K. P. Forest, R. H. Nuttall and D. W. A. Stamp, *Spectrochim. Acta*, 1967, 23, A, 2701.
108. R. J. H. Clark and M. Kurmoo, *J. Chem. Soc., Faraday Trans. 2*, 1983, 79, 519.
109. M. Tanaka and S. Kurita, *J. Phys. C: Solid State Phys.*, 1986, 19, 3019.
110. R. J. H. Clark and M. Kurmoo, *J. Chem. Soc., Dalton Trans.*, 1981, 524.
111. R. J. Donohoe, C. D. Tait and B. I. Swanson, *Chem. Mater.*, 1990, 2, 315.
112. R. J. H. Clark and V. B. Croud, in *Organic and Inorganic Low Dimensional Crystalline Materials*, eds. P. Delhaes and M. Drillon, NATO Advanced Research Workshop, Plenum, 1987, p. 341.
113. G. C. Papavassiliou, R. Rapsomanikis, S. Mourikis and C. S. Jacobsen, *J. Chem. Soc., Faraday Trans. 2*, 1982, 78, 17.
114. B. Horowitz, Z. Vardeny, E. Ehrenfreund and O. Brafman, *J. Phys. C: Solid State Phys.*, 1986, 19, 7291.
115. D. A. Long, 'Raman Spectroscopy', McGraw-Hill, New

- York, 1977.
116. R. J. H. Clark and T. J. Dines, *Angew. Chem., Internat. Ed. Engl.*, 1986, 25, 131.
 117. C. Manneback, *Physica*, 1951, 17, 1001.
 118. M. Mingardi and W. Siebrand, *J. Chem. Phys.*, 1975, 62, 1074.
 119. G. Herzberg, 'Infrared and Raman Spectra of Polyatomic Molecules', Van Nostrand, Princeton, 1945, p. 205.
 120. R. Loudon, *Proc. Roy. Soc. (London)*, 1963, A275, 218.
 121. W. Heitler, 'The Quantum Theory of Radiation', Clarendon Press, Oxford, 1954, p. 189.

Syntheses, Crystal Structures, and Raman and Resonance Raman Spectroscopy of Platinum(II), Platinum(IV), and Halogen-bridged Chain Platinum(II,IV) Complexes involving the Terdentate Ligand 3-Methyl-3-azapentane-1,5-diamine (4Me-dien)†

Francesco P. Fanizzi and Giovanni Natile

Dipartimento Farmaco-Chimico dell'Università, via G. Amendola 173, 70126 Bari, Italy

Maurizio Lanfranchi and Antonio Tiripicchio

Istituto di Chimica Generale ed Inorganica dell'Università e Centro di Studio per la Strutturistica

Diffraattometrica del C.N.R., viale delle Scienze, 43100 Parma, Italy

Robin J. H. Clark* and David J. Michael

Christopher Ingold Laboratories, University College London, 20 Gordon Street, London WC1H 0AJ

The effect of introducing a methyl substituent onto the central nitrogen atom of the ligand dien (dien = diethylenetriamine or 3-azapentane-1,5-diamine) on the ease of formation of mixed-valence chain complexes of platinum has been investigated. The chain complex prepared by partial oxidation of $[\text{Pt}(4\text{Me-dien})\text{I}]\text{I}$, viz. $[\text{Pt}(4\text{Me-dien})\text{I}][\text{Pt}(4\text{Me-dien})\text{I}_3]\text{I}_2$ (4) (4Me-dien = 3-methyl-3-azapentane-1,5-diamine), breaks down on recrystallisation to yield separate crystals of $[\text{Pt}(4\text{Me-dien})\text{I}]\text{X}$ [$\text{X} = \text{I}_3^-$ (1) or I^- (2)] and $[\text{Pt}(4\text{Me-dien})\text{I}_3]\text{I}$ (3). X-Ray structural investigation of (1)–(3) and of similar discrete complexes of platinum reported previously indicate that dien coordinates in the planar (pseudo-*mer*) conformation in four-co-ordinate platinum(II) but in the bent (*fac*) conformation in six-co-ordinate platinum(IV) complexes. However, in mixed-valence chain complexes, dien is forced to co-ordinate to the platinum(IV) centre in the *mer* conformation. In the case of 4Me-dien the *mer* conformation around platinum(IV) is severely hindered; hence unless this species is trapped quickly between two platinum(II) entities it isomerises from *mer* to *fac*, thereby preventing the assembly of the mixed-valence chain complex. Complex (4) has a very intense Raman spectrum at resonance with the intervalence band, the principal observed progression being $\nu_1\nu_1$ [ν_1 (116.5 cm^{-1}) is the symmetric stretching mode of the chain, $\nu_{\text{sym}}(\text{I-Pt}^{\text{IV}}-\text{I})$]. The wavenumber of ν_1 found for this complex is lower than that of the analogous species with unsubstituted dien in accord with a lengthening of the $\text{Pt}^{\text{IV}}-\text{I}$ linkage on N-methyl substitution of the ligand. Crystallographic data: (1), monoclinic, space group $P2_1/n$, $a = 15.433(3)$, $b = 7.856(5)$, $c = 13.327(4)$ Å, $\beta = 102.24(2)^\circ$, and $Z = 4$; (2), monoclinic, space group $P2_1/c$, $a = 20.434(7)$, $b = 8.267(2)$, $c = 15.571(1)$ Å, $\beta = 110.67(2)^\circ$, and $Z = 8$; (3), monoclinic, space group $P2_1/m$, $a = 8.960(6)$, $b = 10.561(4)$, $c = 7.651(4)$ Å, $\beta = 103.10(2)^\circ$, and $Z = 2$.

The syntheses, structures, and spectroscopy of mixed-valence chain complexes of platinum containing the terdentate ligands dien and 1Me-dien (dien = diethylenetriamine or 3-azapentane-1,5-diamine, 1Me-dien = *N*-methyl-3-azapentane-1,5-diamine) have been reported.^{1,2} These complexes, $[\text{Pt}(\text{dien})\text{I}][\text{Pt}(\text{dien})\text{I}_3]\text{I}_2$ and $[\text{Pt}(1\text{Me-dien})\text{I}][\text{Pt}(1\text{Me-dien})\text{I}_3]\text{I}_2$, are the only ones of the relatively rare +1 charge type yet to have been structurally characterised³ and they display interesting structural features. The dien ligands are eclipsed in alternate pairs along the chain; the puckering of the two condensed rings of each dien or 1Me-dien makes them slightly concave, the concavity being oriented in the same sense throughout the chain. The deviation from linearity of the iodide-bridged chain is larger than that observed for any other type of chain complex of platinum or palladium. We also observed that the introduction of a methyl substituent onto a terminal nitrogen atom of dien causes yet further bending of the chain centred on the $\text{I}\cdots\text{Pt}^{\text{II}}\cdots\text{I}$ junctions and an overall increase of the $\text{Pt}^{\text{II}}\cdots\text{Pt}^{\text{IV}}$ distance. Moreover the ligands were arranged in such a way as to bring the methyl substituents into staggered rather than eclipsed positions as viewed along the chain direction.

It was considered of value to investigate what structural features would arise by the introduction of a methyl substituent

onto the central rather than a terminal nitrogen atom of the dien ligand. The results of this study are reported herein.

Experimental

Preparation of Complexes.—Commercial reagents were used without further purification. 3-Methyl-3-azapentane-1,5-diamine (4Me-dien) was prepared according to the reported procedure.⁴

$[\text{Pt}(4\text{Me-dien})\text{I}]\text{I}$ (2). The salt $\text{K}_2[\text{PtCl}_4]$ (500 mg, 1.2 mmol) was dissolved in water (7.5 cm^3) and treated with 4Me-dien-3HCl (633 mg, 2.79 mmol). The resulting solution was partially neutralised by addition of KOH (190 mg dissolved in 3 cm^3 of water) and then stirred for 24 h at 60 °C. During this time the colour changed from red to yellow. After being cooled to room temperature the solution was filtered, an excess of NaI (450 mg, 3 mmol) was added, and the solution stirred for 3 h. The brown precipitate which formed was separated and recrystallised from hot water to give pale yellow needles of the

† Supplementary data available: see Instructions for Authors, *J. Chem. Soc., Dalton Trans.*, 1989, Issue 1, pp. xvii–xx.

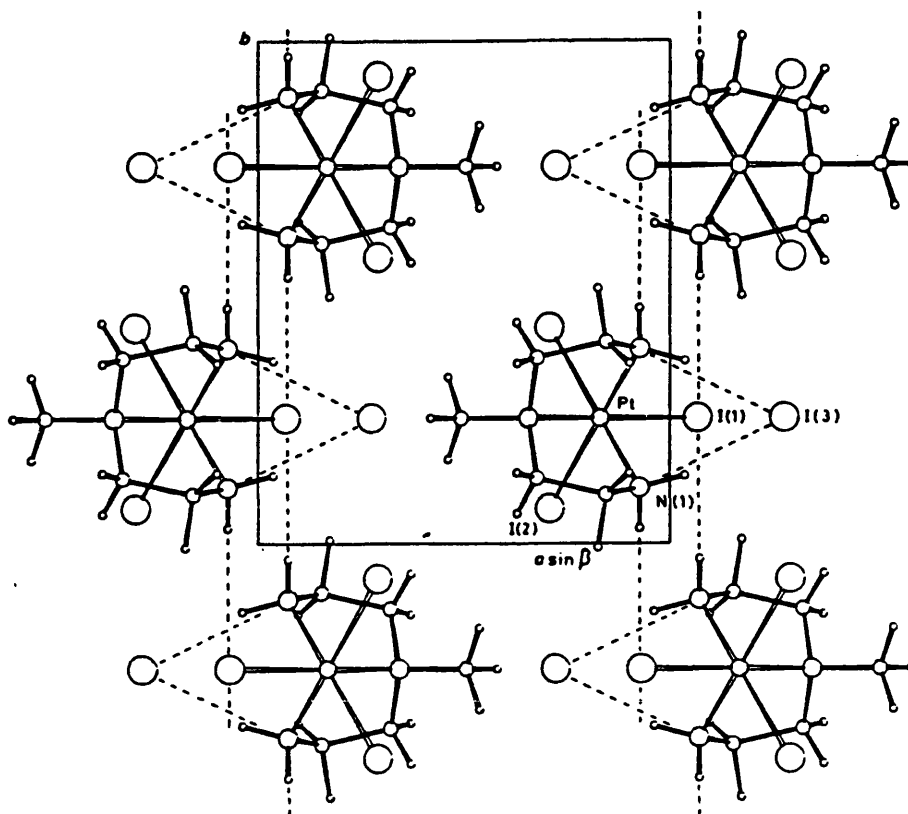


Figure 6. Projection of the structure of complex (3) along the [001] plane

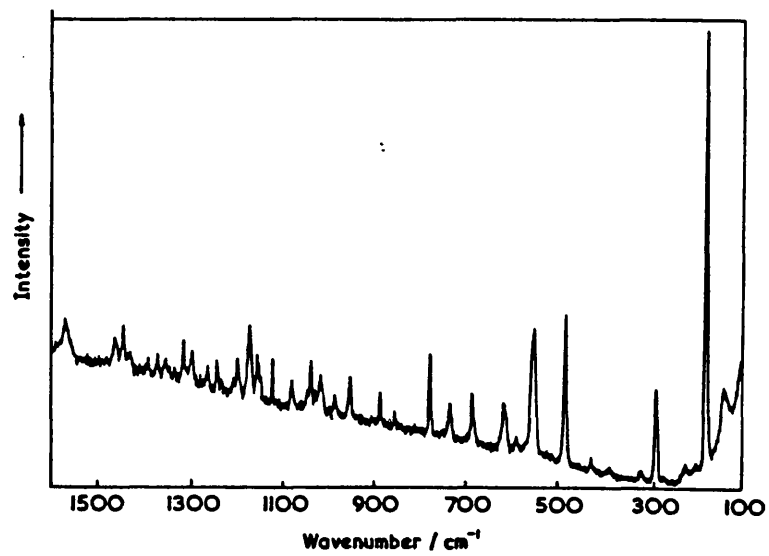


Figure 7. Raman spectrum ($\lambda_0 = 514.5$ nm) of $[\text{Pt}(\text{4Me-dien})\text{I}]\text{I}$, (2), as a K_2SO_4 disc at ca. 80 K

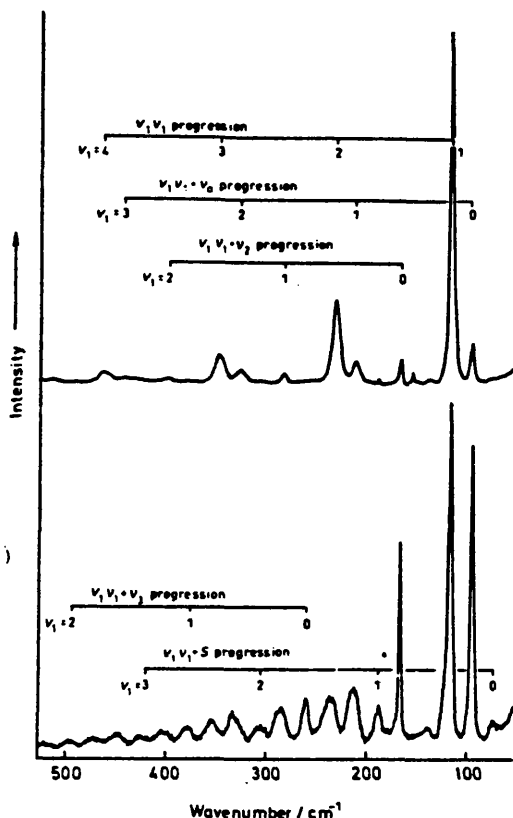


Figure 8. Raman ($\lambda_0 = 647.1$ nm, lower) and resonance Raman ($\lambda_0 = 799.3$ nm, upper) spectra of $[\text{Pt}(4\text{Me-dien})\text{I}][\text{Pt}(4\text{Me-dien})\text{I}_2]_2(4)$, as a K_2SO_4 disc at ca. 80 K

differences appear to have real significance. The I-Pt-I, I-Pt-N, and N-Pt-N angles lie in the range previously reported; however those inside the chelate ring are even smaller (by ca. 3°) than those deduced for complexes (1) and (2), probably as a consequence of the lengthening of the Pt-N bonds. The packing within the crystal is shown in Figure 6. The cations are arranged in chains parallel to the (010) plane. Of the four amine hydrogen atoms of the co-ordinated ligand, two (one from each terminal nitrogen atom) interact with the I^- counter ion and each of the other two with the co-ordinated I(1) atoms of adjacent cations.

Structures of several complexes of the type $[\text{M}(\text{dien})\text{X}_2]^{n+}$ and $[\text{M}(\text{dien})_2]^{n+}$ ($n = 0-3$) have been determined in which the dien ligand can have either a planar (*mer*) or a bent (*fac*) conformation.^{12,13} In the case of platinum(IV) complexes the *mer* conformation has been found only for mixed-valence chain complexes in which the octahedral entity is inserted between two planar platinum(II) entities. By contrast all monomeric platinum(IV) complexes adopt the *fac* conformation.¹ This could indicate that, starting with a platinum(II) species in which the dien ligand is expected to be planar, the first oxidation product has a *mer* conformation; this product would then either crystallise with residual platinum(II) species to give a mixed-valence chain complex or isomerise to the *fac* complex.

The oxidation reaction, carried out on the platinum substrate in which the dien ligand has a methyl substituent on the central nitrogen atom, led initially to the formation of the mixed-

Table 4. Wavenumbers, intensities, and assignments of bands observed in the Raman spectrum of $[\text{Pt}(4\text{Me-dien})\text{I}][\text{Pt}(4\text{Me-dien})\text{I}_2]_2(4)$, $\lambda_0 = 647.1$ nm*

Wavenumber/cm ⁻¹	Intensity	Assignment
72.5	vw	Skeletal (<i>s</i>) or $\nu_2 - \nu_3$
94.5	s	ν_2
116.5	vs	$\nu_1(\text{I}-\text{Pt}^{\text{IV}}-\text{I})$
139.0	vw	
167.0	s	$\nu_2, \nu(\text{Pt}-\text{I})_{\text{as}}$
188.0	w	$\nu_1 + s$
213.5	m	$\nu_1 + \nu_2$
235.5	m	$2\nu_1$
260.5	m	ν_3
285.5	mw	$\nu_1 + \nu_2$
305.5	w	$2\nu_1 + s$
333.0	w	$2\nu_1 + \nu_2$
353.5	w	$3\nu_1$
378	w	$\nu_1 + \nu_3$
402	w	$2\nu_1 + \nu_2$
425	w	$3\nu_1 + s$
448	w	$3\nu_1 + \nu_2$
472	vw	$4\nu_1$
495	vw	$2\nu_1 + \nu_3$
521	vw	$3\nu_1 + \nu_2$
529	vw	

* The members of the ν_1, ν_1 progression have, with 799.3-nm excitation, slightly lower wavenumbers (with the exception of ν_1) than with 647.1-nm excitation as frequently observed for chain complexes (R. J. H. Clark and M. Kurmoo, *J. Chem. Soc., Faraday Trans. 2*, 1983, 519; R. J. H. Clark and D. J. Michael, *J. Mol. Struct.*, 1988, 189, 173); *viz.*: ν_1 , 117.0; $2\nu_1$, 233.0; $3\nu_1$, 348.0; $4\nu_1$, 463; $5\nu_1$, 578; $6\nu_1$, 693 cm^{-1} .

valence chain complex; however all attempts to recrystallise this resulted in the formation of separate crystals of (3) (which cannot give the mixed-valence complex) and (2).

The X-ray investigations have shown that, in cases in which a conformation of the ligand is planar [complexes (1) and (2)], the methyl substituent on the central nitrogen atom extends out of the meridional plane where it would interact strongly with any group in the axial position; for this reason the mixed-valence chain complex is not stable to recrystallisation.

On the other hand for the octahedral species, the isomerisation of the ligand from the *mer* to the *fac* conformation [*cf.* (3)] has moved the methyl substituent from a position in which it was interacting strongly with an axial iodine atom [C(Me)-N-Pt-I torsion angle of 0° and C(methyl)-I distance of ca. 3 Å] to a less-hindered situation [C(Me)-N-Pt-I 45° and C(methyl)-I 3.7 Å]. Therefore the presence of a methyl substituent on the central nitrogen atom of dien has two effects: to destabilise the mixed-valence chain complex and to increase the tendency of the terdentate ligand to assume a bent (*fac*) conformation in the octahedral complex.

Raman Spectroscopy.—The Raman spectrum of the platinum(II) complex (2) is shown in Figure 7. The corresponding platinum(IV) complex (3) absorbed more of the incident radiation than did (2) and consequently its Raman spectrum does not show the large number of bands (associated primarily with the 4Me-dien ligand) at higher Raman shift seen in Figure 7. However, the Raman spectrum of (3) did show a band at 172 cm^{-1} , which is assigned to the $\text{Pt}^{\text{IV}}-\text{I}$ symmetric stretch.

The Raman spectrum ($\lambda_0 = 647.1$ nm) of the mixed-valence complex (4) is shown in Figure 8. This figure also indicates the resonance enhancement of several progressions in the spectrum, features which are clearly observed on changing the wavelength of the exciting line towards the deep red, *i.e.* within the contour of the intervalence band. Enhancement occurs for the ν_1, ν_1

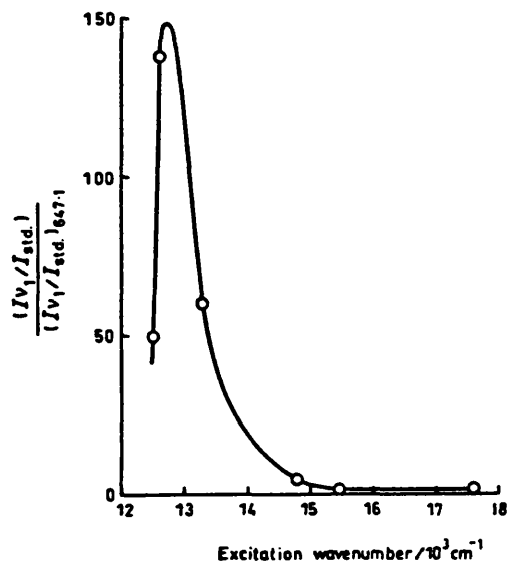


Figure 9. Normalised excitation profile of the ν_1 band of $[\text{Pt}(4\text{Me-dien})\text{I}][\text{Pt}(4\text{Me-dien})\text{I}]_2$ (4)

progression (up to $\nu_1 = 6$ is observed) and weaker enhancement occurs for the $\nu_1\nu_1 + \nu_6$ progression up to $\nu_1 = 5$ (where ν_6 is an unassigned enabling mode, cf. a similar band reported in ref. 14), and $\nu_1\nu_1 + \nu_2$ up to $\nu_1 = 3$ [where ν_2 is $\nu(\text{Pt-I})_{\text{as}}$]. Other progressions detected in the 647.1-nm spectrum include $\nu_1\nu_1 + \nu_3$ up to $\nu_1 = 2$ and $\nu_1\nu_1 + s$ up to $\nu_1 = 3$, where neither of the enabling modes ν_3 or s could be assigned (although s could be the difference mode $\nu_2 - \nu_6$). Peak assignments for the spectrum ($\lambda_0 = 647.1$ nm) in Figure 8 are given in Table 4.

The excitation profile (e.p.), which allows for variation in spectral response and intensity dependence on wavenumber and which is normalised (at $\lambda_0 = 647.1$ nm, enhancement factor = 1), is shown in Figure 9. The e.p. reaches a maximum at ca. $13\,000\text{ cm}^{-1}$, indicating that ν_1 is coupled strongly with the intervalence transition.

Conclusions

This investigation has revealed that a methyl substituent on the dien ligand has a significant effect on the formation and stability of mixed-valence chain complexes. This effect, probably of steric

origin, is connected with the capability of the dien ligand to keep a *mer* conformation without interacting strongly with the apical ligands in an octahedral geometry. In the case of 4Me-dien the interaction between the methyl substituent and an apical iodine atom is estimated to be very strong [$\text{C}(\text{Me}) \cdots \text{I}$ ca. 3.0 \AA]; thus on recrystallisation the chain is destroyed and *mer-to-fac* isomerisation occurs with consequent relief of the steric hindrance [$\text{C}(\text{Me}) \cdots \text{I}$ 3.7 \AA]. The *mer-to-fac* isomerisation of the dien ligands apparently occurs in all discrete platinum(IV) species; only in the chain complexes is the *mer* conformation retained around platinum(IV), because in this case it is 'sandwiched' between platinum(II) species.

Acknowledgements

We thank the S.E.R.C. and N.A.T.O. (grant to R. J. H. C. and G. N.), and the University of London Intercollegiate Research Services, for financial support and Johnson Matthey plc for the loan of chemicals.

References

- R. J. H. Clark, M. Kurmoo, A. M. R. Galas, and M. B. Hursthouse, *J. Chem. Soc., Dalton Trans.*, 1983, 1583.
- F. P. Fanizzi, G. Natile, M. Lanfranchi, A. Tiripicchio, R. J. H. Clark, and M. Kurmoo, *J. Chem. Soc., Dalton Trans.*, 1986, 273.
- R. J. H. Clark, *Chem. Soc. Rev.*, 1984, 13, 219.
- F. G. Mann, *J. Chem. Soc.*, 1934, 3.
- M. S. Lehmann and F. K. Larsen, *Acta Crystallogr., Sect. A*, 1974, 30, 580.
- N. Walker and D. Stuart, *Acta Crystallogr., Sect. A*, 1983, 39, 158.
- F. Uguzzoli, *Comput. Chem.*, 1987, 11, 109.
- G. M. Sheldrick, SHELX System of Crystallographic Computer Programs, University of Cambridge, 1976.
- 'International Tables for X-Ray Crystallography,' Kynoch Press, Birmingham, 1974, vol. 4.
- J. F. Britten, C. J. L. Lock, and W. M. C. Pratt, *Acta Crystallogr., Sect. B*, 1982, 38, 2148.
- R. Melauson, J. Hubert, and F. D. Rochon, *Can. J. Chem.*, 1975, 53, 1139.
- J. F. Britten and C. J. L. Lock, *Acta Crystallogr., Sect. B*, 1980, 36, 2958 and refs therein.
- F. A. Cotton and R. C. Elder, *Inorg. Chem.*, 1964, 3, 397; F. A. Cotton and R. M. Wing, *ibid.*, 1965, 4, 314; F. A. Cotton and D. C. Richardson, *ibid.*, 1966, 5, 1851; F. S. Stephens, *J. Chem. Soc. A*, 1969, 883, 2233, 2493; M. Kobayashi, F. Marumo, and Y. Saito, *Acta Crystallogr., Sect. B*, 1972, 28, 470; M. Konno, F. Marumo, and Y. Saito, *ibid.*, 1973, 29, 739.
- R. J. H. Clark and M. Kurmoo, *J. Chem. Soc., Dalton Trans.*, 1981, 524.

Received 21st November 1988; Paper 8/04627A

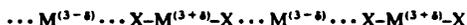
Synthesis and Spectroscopy of Linear-chain Palladium(II,IV) and Platinum(II,IV) Complexes involving Quadridentate Ligands

Robin J. H. Clark,* David J. Michael and Masahiro Yamashita

Christopher Ingold Laboratories, University College London, 20 Gordon Street, London WC1H 0AJ, UK

The effects of the in-plane ligand, the metal atom, the bridging halogen atom and the counter-anion on the electronic structures of a series of linear-chain, halogen-bridged, mixed-valence complexes of platinum and palladium have been investigated. Complexes of the type $[ML][MLX_2]Y_n$, where $M = Pd$ or Pt , $X = Cl, Br$ or I , $L = 3,7$ -diazanonane-1,9-diamine, 4,7-diazadecane-1,10-diamine, 1,4,8,11-tetraazacyclotetradecane or 1,4,8,12-tetraazacyclopentadecane and $Y = BF_4, ClO_4$ or PF_6 , have been examined by means of electronic, Raman and resonance-Raman spectroscopy. The electronic spectra of the complexes each show an intense intervalence charge-transfer band in the visible region, occurring at higher energy, E_p , than it does for analogous bis(ethylenediamine) complexes; this implies greater localisation of valences for the quadridentate than for the bis(ethylenediamine) complexes, in agreement with conclusions drawn from X-ray structural results. Resonance-Raman spectra of the complexes display long progressions in the symmetric chain stretching mode ν_1 , $\nu_{max}(X-M^IV-X)$, corresponding members occurring at higher wavenumbers than for the analogous en complexes. Progressions in ν_1 reach at most to $\nu_1 = 12$ for $X = Cl$, $\nu_1 = 9$ for $X = Br$ and $\nu_1 = 5$ for $X = I$. Both the trends in E_p and also those in ν_1 (max) vary in the order $I < Br < Cl$, $Pd < Pt$ and $BF_4 \leq ClO_4 < PF_6$, implying increased valence localisation to the right in each series.

Halogen-bridged, mixed-valence metal complexes of platinum, palladium and, to a lesser extent, nickel have been synthesised in large numbers and characterised by many techniques.¹ They are all analogues of Wolfram's red salt, $[Pt(NH_2Et)_4][Pt(NH_2Et)_4Cl_2]Cl_4 \cdot 4H_2O$, and contain a linear-chain structure of metal atoms, M , alternately in oxidation states $(3 + \delta)$ and $(3 - \delta)$, bridged by non-equidistant halogen atoms, X , as shown below.



The oxidation states are more usually referred to as IV and II , respectively. This structure is considered to be a Peierls distorted version of a more symmetric one in which trivalent metal ions are bridged by equidistant halogen atoms. The distortion divides the d_{z^2} electronic band of the metal atoms into a lower energy, occupied valence band and a higher energy, vacant conduction band separated by an intervalence charge-transfer (i.v.c.t.) gap of energy E_p .² This band gap, associated with the linear chain (z axis), causes the complexes to behave as one-dimensional semiconductors and to have anisotropic optical properties. Intense visible dichroism is caused by electronic excitation across the z -polarised i.v.c.t. band gap. In terms of orbitals localised on a pair of adjacent metal atoms, the excitation occurs from a ground state M^{II}/M^{IV} pair by the transfer of one electron from a d_{z^2} orbital via the intervening halogen p_z orbital, to form an $M^{III}-M^{III}$ pair. For different combinations of M^{II} and M^{IV} , with other factors the same, E_p increases in the order $Ni^{II}-Ni^{IV} < Pd^{II}-Pd^{IV} < Pt^{II}-Pt^{IV} < Ni^{II}-Pt^{IV} < Pd^{II}-Pt^{IV}$.³ Similarly, with changing halogen, X , E_p increases in the order $I < Br < Cl$,¹ along with the increased Peierls distortion. A strong electron-phonon interaction exists between the i.v.c.t. excitation and the symmetric $(X-M^{IV}-X)$ stretching vibration ν_1 , this being demonstrated by a strong resonance effect in the Raman spectra of Wolfram's red type salts.¹

The amine ligands are co-ordinated equatorially to the metal

centres and may be mono-, bi-, ter- or quadri-dentate (including macrocyclic). Hydrogen bonding between the ligands and the counter-anions has an important role in supporting the one-dimensional structures and has a profound effect on the physical properties of the linear chain by changing the metal-metal distance and the relative positions of the halogen atoms.¹ Two possible types of hydrogen-bonding structure are illustrated in Fig. 1.⁴ The current investigation is concerned with the optical properties of a series of halogen-bridged linear-chain complexes of $Pd^{II}-Pd^{IV}$ and $Pt^{II}-Pt^{IV}$ with quadridentate equatorial ligands. Intervalence charge-transfer energies have been determined by transmission or reflectance electronic spectroscopy while values for ν_1 have been measured from Raman and resonance-Raman spectroscopy. The results are discussed in terms of the effects of changing the metal and halogen atoms, the counterions, and also the equatorial ligands on the ratio of the metal-halogen distances $r(M^{IV}-X)/r(M^{II}-X)$, metal oxidation states and Peierls distortion.

Experimental

Synthesis.—Platinum complexes of the type $[PtL][PtLX_2][ClO_4]_4$, where $L = 3,7$ -diazanonane-1,9-diamine (2,3,2-tet) or 4,7-diazadecane-1,10-diamine (3,2,3-tet) and $X = Cl, Br$ or I , were prepared according to a standard route⁵ by the cocrystallisation of the separately prepared monomeric platinum(II) and platinum(IV) constituents in aqueous solution containing an excess of perchloric acid. Palladium(II) complexes $[PdL][ClO_4]_2$, where $L = 2,3,2$ -tet, 3,2,3-tet, 1,4,8,11-tetraazacyclotetradecane ([14]aneN₄) or 1,4,8,12-tetraazacyclopentadecane ([15]aneN₄), were prepared by mixing palladium(II) acetate with L in equimolar amounts in aqueous solution, followed by an excess of 60% $HClO_4$. Mixed-valence, palladium complexes $[PdL][PdLX_2][ClO_4]_4$, where $X = Cl$ or Br , were prepared by the partial oxidation by halogen of the palladium(II) monomer in aqueous solution containing an excess of $HClO_4$.⁴ The complexes $[Pd([14]aneN_4)][Pd-$

Table 3 Wavenumbers, relative intensities, full widths at half-maximum ($\Delta\tilde{\nu}$) and assignments of bands in the resonance-Raman spectra (excitation wavelengths as specified in Table 1); ν_1 is the symmetric ($X-M^{IV}-X$) stretch and ν_2 the asymmetric ($X-M^{IV}-X$) stretch

$\tilde{\nu}/\text{cm}^{-1}$	$I(\tilde{\nu})/I(\nu_1)$	$\Delta\tilde{\nu}/\text{cm}^{-1}$	Assignment	$\tilde{\nu}/\text{cm}^{-1}$	$I(\tilde{\nu})/I(\nu_1)$	$\Delta\tilde{\nu}/\text{cm}^{-1}$	Assignment
(a) [Pt(2,3,2-tet)][Pt(2,3,2-tet)Cl₂][ClO₄]₄							
182	0.03	9		657	<0.01	11	$\nu_1 + \nu_2$
212	0.06	8	$\delta(\text{N-Pt-N})$	931	0.08	50	$3\nu_1$
226	0.03	9		1109	<0.01	11	
313	1.00	13	ν_1	1232	0.04	61	$4\nu_1$
348.5	0.04	8	ν_2	1402	<0.01	11	
398.5	<0.01	8		1535	0.02	85	$5\nu_1$
422.5	<0.01	11		1833	<0.01	>100	$6\nu_1$
490.5	<0.01	8		2132	<0.01	>100	$7\nu_1$
503.5	<0.01	10		2428	<0.01	>100	$8\nu_1$
540.5	<0.01	11		2708	<0.01	>100	$9\nu_1$
624	0.22	31	$2\nu_1$	2985	<0.01	>100	$10\nu_1$
(b) [Pt(3,2,3-tet)][Pt(3,2,3-tet)Cl₂][ClO₄]₄							
152	<0.01	8		1237	0.07	42	$4\nu_1$
172.5	<0.01	6		1333	<0.01	8	
215.5	<0.01	6		1414	<0.01	8	
267	0.01	8		1541	0.04	69	$5\nu_1$
312.5	1.00	11.5	ν_1	1643	<0.01	11	
347.5	0.01	8	ν_2	1727	<0.01	15	
380.5	<0.01	3		1840	0.02	85	$6\nu_1$
395	<0.01	6		1952	<0.01	15	
408.5	<0.01	6		2040	<0.01	12	
537	0.01	8	$\nu_1 + \delta(\text{N-Pt-N})$	2140	0.01	100	$7\nu_1$
623.5	0.28	23	$2\nu_1$	2432	<0.01	>100	$8\nu_1$
657	<0.01	15	$\nu_1 + \nu_2$	2728	<0.01	>100	$9\nu_1$
849.5	<0.01	15	$2\nu_1 + \delta(\text{N-Pt-N})$	3016	<0.01	>100	$10\nu_1$
931	0.12	35	$3\nu_1$	3288	<0.01	>100	$11\nu_1$
1108	<0.01	11		3572	<0.01	>100	$12\nu_1$
(c) [Pt(2,3,2-tet)][Pt(2,3,2-tet)Br₂][ClO₄]₄							
178.5	1.00	11.8	ν_1	593.5	<0.01	6	
210.5	0.05	7	$\delta(\text{N-Pt-N})$	709.5	0.03	59	$4\nu_1$
242	0.02	7		882.5	0.02	72	$5\nu_1$
304	<0.01	7		1054.5	<0.01	~85	$6\nu_1$
328.5	0.01	7		1236	<0.01	—	$7\nu_1$
356.5	0.25	23	$2\nu_1$	1304	<0.01	10	
388	0.01	10	$\nu_1 + \delta(\text{N-Pt-N})$	1402	<0.01	—	$8\nu_1$
533.5	0.09	35	$3\nu_1$	1580	<0.01	—	$9\nu_1$
(d) [Pt(3,2,3-tet)][Pt(3,2,3-tet)Br₂][ClO₄]₄							
180.5	1.00	18	ν_1	1069	0.01	>100	$6\nu_1$
232	<0.01	4		1241	<0.01	>100	$7\nu_1$
359.5	0.30	37	$2\nu_1$	1333	<0.01	6	
410	<0.01	3		1411	<0.01	>100	$8\nu_1$
536	0.11	53	$3\nu_1$	1515	<0.01	10	
711	0.05	67	$4\nu_1$	1593	<0.01	>100	$9\nu_1$
889	0.02	83	$5\nu_1$				
(e) [Pt(2,3,2-tet)][Pt(2,3,2-tet)I₂][ClO₄]₄							
120	1.00	16.6	ν_1	353	0.04	50	$3\nu_1$
183	<0.01	10		467	<0.01	~75	$4\nu_1$
237.5	0.19	33	$2\nu_1$	580	<0.01	—	$5\nu_1$
(f) [Pt(3,2,3-tet)][Pt(3,2,3-tet)I₂][ClO₄]₄							
119.5	1.00	14.3	ν_1	354.5	0.06	46	$3\nu_1$
238	0.23	28	$2\nu_1$	468.5	0.02	65	$4\nu_1$
(g) [Pd(2,3,2-tet)][Pd(2,3,2-tet)Cl₂][ClO₄]₄							
278	1.00	17.6	ν_1	1506	<0.01	14	
347.6	0.02	6	ν_2	1575	<0.01	12	
556.4	0.28	34	$2\nu_1$	1660	0.01	>100	$6\nu_1$
628.4	0.01	14	$\nu_1 + \nu_2$	1786	<0.01	14	
833.2	0.11	48	$3\nu_1$	1866	<0.01	17	$6\nu_1 + \delta(\text{N-Pd-N})$
908.4	<0.01	12	$2\nu_1 + \nu_2$	1941	<0.01	>100	$7\nu_1$
1110	0.05	64	$4\nu_1$	2146	<0.01	14	$7\nu_1 + \delta(\text{N-Pd-N})$
1298	<0.01	9		2220	<0.01	>100	$8\nu_1$
1384	0.02	96	$5\nu_1$	2490	<0.01	>100	$9\nu_1$

Table 3 (continued)

$\tilde{\nu}/\text{cm}^{-1}$	$I(\tilde{\nu})/I(\nu_1)$	$\Delta\tilde{\nu}_1/\text{cm}^{-1}$	Assignment	$\tilde{\nu}/\text{cm}^{-1}$	$I(\tilde{\nu})/I(\nu_1)$	$\Delta\tilde{\nu}_1/\text{cm}^{-1}$	Assignment
(h) [Pd(3,2,3-tet)][Pd(3,2,3-tet)Cl₂][ClO₄]₄							
280.4	1.00	11.5	ν_1	1512	<0.01	25	
390.8	0.02	6		1605	<0.01	18	$5\nu_1 + \delta(\text{N-Pd-N})$
561.2	0.26	21.5	$2\nu_1$	1682	0.01	~70	$6\nu_1$
839.6	0.09	31	$3\nu_1$	1788	<0.01	25	
1115	0.03	46	$4\nu_1$	1884	<0.01	18	$6\nu_1 + \delta(\text{N-Pd-N})$
1324	<0.01	18	$4\nu_1 + \delta(\text{N-Pd-N})$	1951	<0.01		$7\nu_1$
1394	0.02	~55	$5\nu_1$				
(i) [Pd([14]aneN₄)]₂[Pd([14]aneN₄)Cl₂][ClO₄]₄							
281.4	1.00	10.3	ν_1	1671	0.02	72	$6\nu_1$
562.2	0.30	20.5	$2\nu_1$	1942	0.01	>100	$7\nu_1$
841.8	0.13	31	$3\nu_1$	2209	<0.01	>100	$8\nu_1$
1118	0.07	41	$4\nu_1$	2468	<0.01	>100	$9\nu_1$
1395	0.04	51	$5\nu_1$				
(j) [Pd([15]aneN₄)]₂[Pd([15]aneN₄)Cl₂][ClO₄]₄							
231	0.14	19		848.4	0.19	43	$3\nu_1$
284.2	1.00	15.4	ν_1	1134	0.10	55	$4\nu_1$
568.4	0.34	28	$2\nu_1$	1404	0.03	77	$5\nu_1$
(k) [Pd(2,3,2-tet)][Pd(2,3,2-tet)Br₂][ClO₄]₄							
151.5	1.00	18.3	ν_1	517.5	<0.01	4	
191.5	0.05	9		579.5	~0.01	~75	$4\nu_1$
227.5	0.01	4		621.5	0.01	6	
301.5	0.20	37	$2\nu_1$	951.5	<0.01	16	
349.5	<0.01	4		1179	<0.01	8	
445.5	0.04	60	$3\nu_1$				
(l) [Pd(3,2,3-tet)][Pd(3,2,3-tet)Br₂][ClO₄]₄							
152.6	1.00	21.2	ν_1	350	0.04	12	
193.2	0.25	20		390.6	0.02	11	
264.6	0.07	6		459.2	0.06	52	$3\nu_1$
303.8	0.24	31	$2\nu_1$				
(m) [Pd([14]aneN₄)]₂[Pd([14]aneN₄)Br₂][ClO₄]₄							
154.5	1.00	13.8	ν_1	457	0.05	52	$3\nu_1$
230	0.01	4		611	0.02	72	$4\nu_1$
308	0.16	33	$2\nu_1$	746	<0.01	~100	$5\nu_1$
(n) [Pd([14]aneN₄)]₂[Pd([14]aneN₄)Cl₂][BF₄]₄							
123	0.01	10		1226	0.02	8	
157.2	0.01	10		1318	0.01	10	
205.2	0.06	10	$\delta(\text{N-Pd-N})$	1358	0.02	70	$5\nu_1$
233.4	0.01	10		1500	<0.01	15	
277.2	1.00	13	ν_1	1592	<0.01	~20	
378	0.02	5		1635	<0.01	~80	$6\nu_1$
482.4	<0.01	8	$\nu_1 + \delta(\text{N-Pd-N})$	1871	<0.01	~25	
552	0.25	~25	$2\nu_1$	1914	<0.01		$7\nu_1$
823	0.09	38	$3\nu_1$	2145	<0.01	~30	
1093	0.05	55	$4\nu_1$				
(o) [Pd([14]aneN₄)]₂[Pd([14]aneN₄)Cl₂][PF₆]₄							
294	1.00	15.2	ν_1	700.8	0.25	10	
584.4	0.33	24	$2\nu_1$	874.8	0.12	48	$3\nu_1$

harmonic wavenumber (ω_1) of the symmetric X-M-X stretch, the anharmonicity constant (x_{11}) and the ratio of the intensities of the bands attributed to the first overtone of ν_1 and to ν_1 [$I(2\nu_1)/I(\nu_1)$]. Table 3 includes data on the half-band widths of the members of the ν_1 progression. The assignment of ν_1 is obvious by comparison with data on related complexes as single crystals, subjected extensively to Raman polarisation studies.¹

The effect of changing from platinum to palladium, while keeping other factors constant is shown in Fig. 2, in which the smaller number of overtones for the palladium complexes reflects their lesser degree of electron localisation, Peierls distortion and electron-phonon interaction. In a similar manner, changing the bridging halogen atom from chlorine to

bromine to iodine reduces the extent of Peierls distortion and hence the degree of resonance enhancement to ν_1 and its overtones, as shown in Fig. 3 for [Pt(3,2,3-tet)][Pt(3,2,3-tet)X₂][ClO₄]₄. These results are consistent with the observed decrease in the i.v.c.t. band gap, E_g , in the order Cl > Br > I.

Fig. 4 illustrates the resonance-Raman spectra of chlorine-bridged palladium chains with different equatorial ligands, and shows that the wavenumber of ν_1 is, like that of the i.v.c.t. band maximum, little changed by change of quadridentate ligand. The wavenumber of ν_1 for the complexes [PdL][PdLCl₂][ClO₄]₄, L = quadridentate ligand, are 6–12 cm⁻¹ greater than that (272 cm⁻¹ for λ_0 647.1 nm)⁶ for the complex [Pd(en)₂][Pd(en)₂Cl₂][ClO₄]₄. This result, like that (*vide*

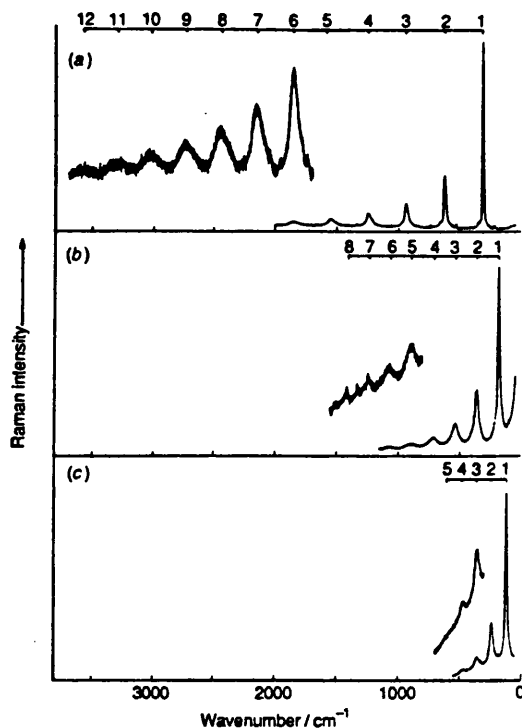


Fig. 3 Resonance-Raman spectra of $[\text{Pt}(3,2,3\text{-tet})][\text{Pt}(3,2,3\text{-tet})\text{X}_2][\text{ClO}_4]_4$, $\text{X} = \text{Cl}$ (a), Br (b) or I (c). Pressed discs of pure salts at ca. 80 K; λ_0/nm 488.0 (a), 488.0 (b) and 676.4 (c)

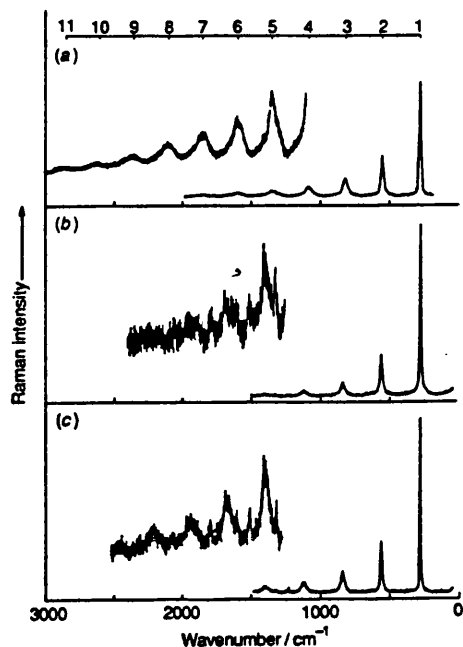


Fig. 4 Resonance-Raman spectra of $[\text{PdL}_2][\text{PdL}_2\text{Cl}_2][\text{ClO}_4]_4$, $\text{L} = \text{en}$ (a) (ref. 6) and $[\text{PdL}][\text{PdLCl}_2][\text{ClO}_4]_4$, $\text{L} = 3,2,3\text{-tet}$ (b) and $[\text{14}] \text{janeN}_4$ (c). Pressed discs of pure material at ca. 80 K; λ_0/nm 647.1 (a), 514.5 (b) and 568.2 (c)

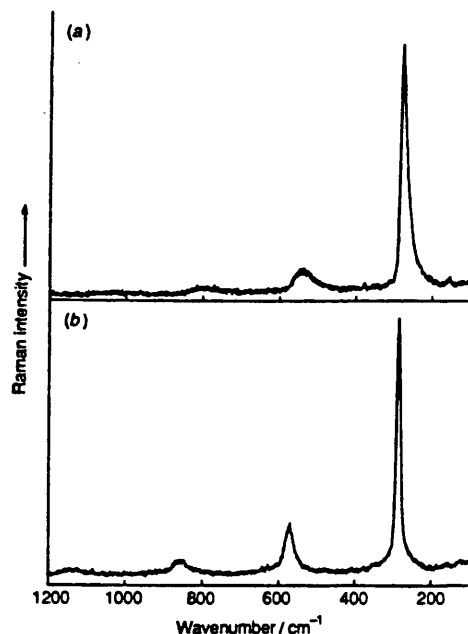


Fig. 5 Resonance-Raman spectra of $[\text{Pd}([\text{14}] \text{janeN}_4)][\text{Pd}([\text{14}] \text{aneN}_4)\text{Cl}_2][\text{ClO}_4]_4$ with λ_0/nm 752.5 (a) and 514.5 (b). Pressed discs of pure material at ca. 80 K

supra) of the higher value for E_g for complexes involving quadridentate ligands, is consistent with greater localisation of the valences for such complexes. The importance of the counter-anion in these structures is illustrated by the differences in E_g values and ν_1 values observed for $[\text{Pd}([\text{14}] \text{janeN}_4)][\text{Pd}([\text{14}] \text{aneN}_4)\text{Cl}_2]\text{Y}_4$, where Y is BF_4 , ClO_4 or PF_6 (Table 1). While E_g and ν_1 are not changed substantially on changing from BF_4^- to ClO_4^- as counterions, in the case of the PF_6^- salt, however, both E_g and ν_1 occur at substantially higher energies. This may once again be attributed to increased Peierls distortion for the PF_6^- salt caused by reduced hydrogen bonding between the counter-anion and the equatorial ligands of adjacent metal centres.^{4,7} Fig. 5 illustrates the shift in the wavenumber of ν_1 for $[\text{Pd}([\text{14}] \text{janeN}_4)][\text{Pd}([\text{14}] \text{aneN}_4)\text{Cl}_2][\text{ClO}_4]_4$ from 277.5 to 285.6 cm^{-1} (the first overtone is shifted from 543 to 570.4 cm^{-1}) on changing the excitation wavelength from 752.5 to 514.5 nm. Such apparent dispersion of the ν_1 band is commonly observed with linear-chain complexes of this type, although not usually to this marked degree. High-resolution studies⁸ have indicated that in general the ν_1 band consists of a number of components and that the apparent dispersion arises from selective enhancement of the components of higher wavenumber with excitation lines of higher wavenumber; under conditions of low resolution, the ν_1 band contour then appears to disperse. The origin of these components (in addition to those attributable to isotopic splitting, in particular for a chlorine-bridged chain⁹) is not well understood but a likely contributory factor is the photosensitive enhancement of different correlation lengths of perfect chains, terminating in defects.^{10,11}

Acknowledgements

The authors thank the SERC for the award of an Advanced Fellowship (to M. Y.) and a CASE Studentship with British Petroleum (to D. J. M.). Johnson-Matthey plc are thanked for the loan of platinum group metals.

References

- 1 R. J. H. Clark, in *Advances in Infrared and Raman Spectroscopy*, eds. R. J. H. Clark and R. E. Hester, Wiley, Chichester, 1984, vol. 11, p. 95; H. Tanino and K. Kobayashi, *J. Phys. Soc. Jpn.*, 1983, **52**, 1446; Y. Wada, T. Mitani, M. Yamashita and T. Koda, *J. Phys. Soc. Jpn.*, 1985, **54**, 3143; N. Kuroda, M. Sakai, Y. Nishina, M. Tanaka and S. Kurita, *Phys. Rev. Lett.*, 1987, **58**, 2122; M. Yamashita, I. Murase, I. Ikemoto and T. Ito, *Chem. Lett.*, 1985, 1133; S. D. Conradson, M. A. Stroud, M. H. Zietlow, B. I. Swanson, D. Baeriswyl and A. R. Bishop, *Solid State Commun.*, 1988, **65**, 723; H. Toftlund, P. W. Jensen and C. S. Jacobsen, *Chem. Phys. Lett.*, 1987, **142**, 286; R. J. H. Clark and V. B. Croud, *J. Chem. Soc., Dalton Trans.*, 1988, 73; R. J. H. Clark and M. Kurmoo, *J. Chem. Soc., Faraday Trans. 2*, 1983, **79**, 519; R. J. H. Clark, M. Kurmoo, A. M. R. Galas and M. B. Hursthouse, *J. Chem. Soc., Dalton Trans.*, 1982, 1851; R. J. H. Clark and P. C. Turtle, *Inorg. Chem.*, 1978, **17**, 2526; R. J. H. Clark, V. B. Croud, R. J. Wills, P. A. Bates, H. M. Dawes and M. B. Hursthouse, *Acta Crystallogr., Sect. B*, 1989, **45**, 147.
- 2 M. H. Whangbo and M. J. Foshee, *Inorg. Chem.*, 1981, **20**, 113; K. Nasu, *J. Phys. Soc. Jpn.*, 1984, **53**, 427.
- 3 M. Yamashita, I. Murase, T. Ito, Y. Wada, T. Mitani and I. Ikemoto, *Bull. Chem. Soc. Jpn.*, 1985, **58**, 2336; Y. Wada, T. Mitani, K. Toriumi and M. Yamashita, *J. Phys. Soc. Jpn.*, 1989, **58**, 3013; R. J. H. Clark and V. B. Croud, *Inorg. Chem.*, 1985, **24**, 588; 1986, **25**, 1751.
- 4 M. Yamashita, M. Ito, K. Toriumi and T. Ito, *Inorg. Chem.*, 1983, **22**, 1566; K. Toriumi, M. Yamashita, M. Ito and T. Ito, *Acta Crystallogr., Sect. C*, 1986, **42**, 963; A. L. Beauchamp, D. Layek and T. Theophanides, *Acta Crystallogr., Sect. B*, 1982, **38**, 1158.
- 5 N. Matsumoto, M. Yamashita and S. Kida, *Bull. Chem. Soc. Jpn.*, 1978, **51**, 2334.
- 6 R. J. H. Clark, V. B. Croud and M. Kurmoo, *Inorg. Chem.*, 1984, **23**, 2499.
- 7 N. Matsumoto, M. Yamashita and S. Kida, *Bull. Chem. Soc. Jpn.*, 1978, **51**, 3514.
- 8 M. Tanaka and S. Kurita, *J. Phys. C*, 1986, **19**, 3019; S. D. Conradson, R. F. Dallinger, B. I. Swanson, R. J. H. Clark and V. B. Croud, *Chem. Phys. Lett.*, 1987, **135**, 463; R. J. H. Clark and D. J. Michael, *J. Mol. Struct.*, 1988, **189**, 173; R. J. H. Clark and V. B. Croud, in *Organic and Inorganic Low Dimensional Crystalline Materials*, eds. P. Delhaes and M. Drillon, NATO Advanced Research Workshop, Plenum, 1987, p. 341.
- 9 S. D. Allen, R. J. H. Clark, V. B. Croud and M. Kurmoo, *Phil. Trans. Roy. Soc. A*, 1985, **314**, 131.
- 10 R. J. H. Clark, *Chem. Soc. Rev.*, 1990, **19**, 107.
- 11 R. J. H. Clark, Plenary lectures, Second European Inorganic Chemistry Seminar, Wiesbaden, Germany, April 1990; NATO Advanced Research Workshop, Aghia Pelaghia, Crete, June 1990.

Received 13th August 1990; Paper 0/03703F